Altered Bone Cell Biology Associated with Type Two Diabetes Mellitus – Consequences for Periodontal Disease

A Thesis Completed in Partial Fulfilment of the Requirements for the Degree of Doctor of Philosophy (Ph.D.)

Cardiff University

2018

Ahmed Makki Abdulrazzaqe Al-Qarakhli, B.D.S, M.Sc.
Oral and Biomedical Sciences
School of Dentistry
Cardiff University
UK

“but overall endued with knowledge is one, the All-Knowing” (The Quran, 12: 76)

Acknowledgements

First and foremost, I praise ALLAH, the almighty for granting me the opportunity, capability and providing me with patience to complete this Thesis. I would like to especially express my sincere gratitude to my principle supervisor, Professor Rachel Waddington for her encouragement, patience, continuous guidance and commitment. Your supervising advice and support made me believe in myself during my study "you can do it". I would like to thank my secondary supervisor Dr. Ryan Moseley for his enthusiasm, tremendous advice, generous support and being friendly along the study time. To Professor Alastair Sloan, my third supervisor, for his shrewdness, kindness and continuous encouragement. Without you all, I would never have completed this study.

I must include thanks to the Ministry of Higher Education and Scientific Research, University of Anbar and College of Dentistry in Iraq, this project would not have been possible at all without your generous financial support.

My praise goes to all the technicians, staff and colleagues in the Oral and Biomedical Department, especially Dr. Sarah Youde who taught me tissue culture and Dr. Maria Stack for assistance in molecular biology. My gratitude goes to Dr. Xiaoqing Wei for his assistance and guidance in Chapter 5 macrophage work.

I would like to extend my thanks to the MTG members for sharing experience and knowledge, co-operation and creating a friendly atmosphere for research. Especially to Dr. Amr Alraies, for his endless assistance, support and companionship along the study, Dr. Wayne Ayre for encouragement and being always ready to help, Paul Battersby for help and assistance, Dr. Norhayati Yusop for generously replying to my inquiries about the cells, for Dr. Abeer Almouallad for being always supportive and Lucy March, you all made my life happy during my study journey.

Compliments go to my cousin Tariq Alhani and his family for being always supportive, endlessly helpful and to his brother Haitham and their brothers in law Muhsin, Saad and their families. Praise goes to Dr. Ghalib Alabid for generous support and continuous fellow-up. To all other unnamed friends, I highly appreciated your support and being a part of my life here in Cardiff.

I would like to dedicate this work to my parents who passed away, but always in thoughts during this journey, they taught me the moral values, perseverance and integrity. I hope that wherever your souls are, you will be proud of this and one day we will meet you again. To my eldest brother Alaa for being as a father all the time and continuous fellow-up and support, to overcome all troubles I faced. To my oldest sister Nidal for her encouragement all the time. To all other family members, you should know that your encouragement and support were worth more than I can express in a paper.

I would like to thank my wife Rawa for standing beside me throughout this stressful period, being a source of my inspiration and motivation for continuing to move my study and career forward. To my wonderful children: Omamah, Hudhaifa and Jumana, for always making me smile, happy and for their understanding and patience on those weekends when I was conducting my experiments and feeding cells instead of being with them. This Thesis would not have been possible without you.

Thesis Summary

Periodontitis is a widely spread disease, affecting about 80% of the worldwide population, resulting in teeth loss, a heavy impact on patients in terms of function and aesthetic. Type 2 Diabetes Mellitus (T2DM) is described to be linked to the exacerbation of periodontitis and delayed healing. This link between these two diseases, however, is not fully evaluated and the mechanisms are yet to be fully elucidated. Osteopontin (OPN) is described to inhibit mineral crystal formation. Herein, it has been hypothesized that increased OPN in diabetic healing bone may be the causative factor of delayed healing in periodontitis and subsequent deterioration, leading to teeth loss. This project aims to gain a greater understanding of the effect of high glucose (HG) levels on mesenchymal stem cells (MSCs) and macrophages, their ability to synthesise OPN and hence, its effects on MSCs to synthesise new bone tissue. Further, the influence of *Porphyromonas gingivalis* lipopolysaccharides (*Pg*-LPS) on these cells was analyzed, in an attempt to create a model to study the healing in the presence of periodontitis and T2DM. Investigating the MSCs isolated from the rat compact bone (CB-MSCs) during the growth in culture, revealed two main populations; a heterogenous population appeared with predominantly mature characteristics at PD15. This population then demonstrated a change in its heterogeneity and became more immature in nature at PD50. These two main populations differed in their growth rate and capability of osteodifferentiation. HG environments exerted significant decreases in osteogenic differentiation on PD15, but not PD50. Addition of *pg*-LPS showed inhibitory effects on osteodifferentiation on PD15 cells more than PD50. Conversely, in the combined presence of HG and *pg*-LPS, PD50 showed a significant decrease in osteodifferentiation. OPN levels demonstrated a gradual decrease in CB-MSCs in both normal and HG conditions. Investigating OPN levels secreted by macrophages, however, revealed interesting results. Synergistic effects of both HG and *pg*-LPS exhibited a significant increase in OPN levels in both pro-inflammatory M1 macrophages and in repair related M2 macrophages. In conclusion, HG was mainly reported to inhibit osteogenic differentiation of the mature cell population, whereas the immature population was found to be affected by combined *pg*-LPS and HG. OPN levels in HG conditions were shown to decrease along the osteodifferentiation period. However, macrophages showed increase secretion of OPN by the synergistic effects of both *pg*-LPS and HG in both M1 and M2 and by *pg*-LPS effects in M2 macrophages. These outcomes as far as we are aware, are novel and disclose a new mechanism of bone resorption in the case of T2DM patients concurrently with periodontal disease.

Abbreviations

α-MEM	Minimum Essential Medium Eagle, Alpha Modifications
AGE	Advanced glycosylation end-products
Arg1	Arginase 1
ALP	Alkaline phosphatase
CB-MSCs	Compact bone mesenchymal stem cells
CFE	Colony forming efficiency
CD	Cluster of differentiation
cDNA	Complementary DNA
Ct	Cross threshold
CO_2	Carbon dioxide
ddH_2O	Double distilled water
DAPI	4'6-Diamidino-2-Phenylindole
Dlx5	Distal-less homeobox 5
DM	Diabetes Mellitus
DMSO	Dimethyl sulfoxide
DNA	Deoxyribonucleic acid
dNTP	Deoxyribonucleotide triphosphate
DSS	Disuccinimidyl Suberate
ECM	Extracellular matrix
EDTA	Ethylenediamine tetra-acetic acid
ELISA	Enzyme-linked immunosorbent assay
EMT	Epithelial-mesenchymal transition
eNOS	Endothelial nitric-oxide synthase
EPC	Endothelial progenitor cells
ESC	Embryonic stem cell

FBS	Foetal bovine serum
FGF	Fibroblast growth factor
FGFR	Fibroblast growth factor receptor
FITC	Fluorescein isothiocyanate
FFA	Free fatty acid
FZD	Frizzled
GAPDH	Glyceraldehyde-3-phosphate dehydrogenase
GDF	Growth differentiation factor
GFAT	Glutamine fructose-6-phosphate aminotransferase
GK	Goto-Kakizaki
GM-CSF	Granulocyte macrophage- colony stimulating factor
GSCs	Germ-line stem cells
GSK3	Synthase kinase 3
HbA1c	Glycated haemoglobin A1c
HBP	Hexosamine biosynthesis pathways
HCL	Hydrochloric acid
HEPES	4-(2-Hydroxyethyl) piperazine-1-ethanesulfonic acid, N-(2-Hydroxyethyl) piperazine-N′-(2-ethanesulfonic acid)
HLA-A	Human leukocyte antigens
hnRNP-A/B	Heterogeneous nuclear ribonucleoprotein A/B
HRP	Horseradish peroxidase
HSCs	Hematopoietic stem cells
IBMX	3-isobutyl-1-methylxanthine
IFNγ	Interferon gamma
IGF	Insulin-like growth factor
IGFR	Insulin-like growth factor receptor
IL	Interleukin

INOS	Inducible nitric oxide synthase
IP	Immunoprecipitation
ISCT	International Society for Cellular Therapy
LPS	Lipopolysaccharides
LRP5/6	Low-density lipoprotein-receptor-related protein 5/6
MAPK	Mitogen-activated protein kinase
MCAM	Melanoma cell adhesion molecule
M-CSF	Macrophage-colony stimulating factor
$MgCl_2$	Magnesium chloride
MI	Myocardial infarction
MMLV	Moloney murine leukaemia virus
MSCs	Mesenchymal stem cells
MMP	Matrix metalloproteinase
MRC1	Macrophages mannose receptor 1
MTT	Thiazolyl blue tetrazolium blue
M1	Macrophage 1
M2	Macrophage 2
NaCl	Sodium chloride
NADH	Nicotinamide adenine dinucleotide (reduced of NAD)
NAFLD	Non-alcoholic fatty liver disease
NaOH	Sodium hydroxide
NFκB	Nuclear factor-κB
NO	Nitric oxide
OCN	Osteocalcin
Oct-4	Octamer-binding transcription factor-4
OPN	Osteopontin
OPG	Osteoprotegerin

$O_2^{\cdot-}$	Superoxide
PAGE	Polyacrylamide gel electrophoresis
PDL	Periodontal ligament
OSX	Osterix
PBS	Phosphate buffer saline
PCR	Polymerase chain reaction
PD	Population doubling
PDGF	Platelet-derived growth factor
PFA	Paraformaldehyde
PG	Proteoglycan
Pg	*Porphyromonas gingivalis*
PGEs	Prostaglandins
***Pg*-LPS**	*Porphyromonas gingivalis*-lipopolysaccharides
PI3K	Phosphatidylinositol 3-kinase
PKC	Protein kinase C
PPARγ	Peroxisomal proliferator-activated receptor gamma
PPi	Inorganic pyrophosphate
qPCR	Quantitative polymerase chain reaction
RAGE	Receptor for AGE
RANK	Receptor activator of nuclear factor kappa-B
RANKL	Receptor activator of nuclear factor kappa-B ligand
Rb	Retinoblastoma protein
RGD	Arginine-glycine-aspartic acid
RLU	Relative luminescence unit
RNA	Ribonucleic acid
ROS	Reactive oxygen species
RT-PCR	Reverse transcription-polymerase chain reaction

Runx2	Runt-related transcription factor 2 (aka Cbfa1)
SA-β-gal	Senescence-associated β-galactosidase activity
SDS	Sodium dodecyl sulphate
SIBLING	Small integrin-binding ligand N-linked glycoprotein
SLRP	Small, leucine-rich proteoglycan
Smad	Sma and Mad Related Family
SOD	Superoxide dismutase enzyme
SOX	SRY (Sex Determining Region Y)-box
SSCs	Somatic stem cells
STELA	Single telomere length analysis
TA	Transit amplifying
TAZ	Tafazzin
TBE	Tris/Borate/EDTA
TBS	Tris buffered saline
TBS-T	Tris buffered saline/0.05% Tween-20
TCA	Tricarboxylic acid cycle
TERT	Telomerase reverse transcriptase
TGF-β	Transforming growth factor-β
TLRs	Toll-Like Receptors
TNAP	Tissue-non-specific alkaline phosphatase isozyme
TNF	Tumour necrosis factor
TR	RNA binding component
TRF	Terminal restriction fragment assay
TTAGGG	A region of repetitive nucleotide sequences
T1DM	Type 1 diabetes mellitus
T2DM	Type 2 diabetes mellitus

UDP-GlcNAc	Uridine 5-diphospho N-acetylglucosamine
UCP	Uncoupling protein
UV	Ultraviolet
VEGF	Vascular endothelial growth factor
Wnt	Wingless associated pathways

Unit of measurement

%	Percentage
bp	Base pairs
^{o}C	Degree Celsius
cm	Centimetre
cm^2	Centimetres squared
g	Gravitational acceleration
g	Gram
h	Hour
kDa	Kilodalton
mA	Milliampere
M	Mole
MΩ	Megaohm
mg	Milligram
min	Minute
mL	Millilitre
mm	Millimetre
mM	Millimole

ng	Nanogram
nm	Nanometre
µg	Microgram
µL	Microlitre
µM	Micromolar
pg	Picogram
RLU	Relative luminescence units
rpm	Revolutions per minute
s	Second
V	Volts
v/v	Volume/volume
w/v	Weight/volume

Table of Contents

Chapter 1: General Introduction

1.1: Background Introduction

Diabetes Mellitus (DM) is a clinically and genetically, heterogeneous group of disorders affecting the metabolism of carbohydrates, lipids and proteins, in which hyperglycemia is the main feature (Graves et al. 2006). There are different forms of diabetes, but the most prevalent one is type 2 diabetes mellitus (T2DM). It forms 90% of all diabetes cases and involves about 382 million people worldwide with this number predicted to rise to 592 million by the year 2035. Moreover, the prevalence rates of T2DM appear to be more among males (8.4%) than females (7.1%). This relatively high percentage has a dramatic impact on the health system, through high morbidity and mortality amongst affected individuals in both western and developing countries (Carnevale et al. 2014).

T2DM is usually associated with insulin resistance. This resistance comes from adipose tissue, in addition to free fatty acid, which is considered as an active regulating hormone. This releases metabolically active molecules that can inhibit the body's ability to respond to insulin. These metabolic disturbances associated with T2DM may lead to high levels of the pro-inflammatory cytokines, such as tumor necrosis factor (TNF-α); and the formation of advanced glycation end products (AGEs), in addition to oxidative stress. Accumulation of these products is proposed to lead to diminished bone formation (Graves et al. 2006). In this situation, the body responds to produce extra insulin, leading to hyperinsulinemic states, to maintain normal blood glucose levels (Dickson and Rhodes 2004).

It has been reported that a long-term hyperglycemic situation can lead to activation of pathways, such as polyol pathways, advanced glycation endproducts (AGEs), high levels of protein kinase C (PKC) activity; and hexosamine bisynthesis pathways, that may exacerbate the diabetic state. The complications can be exemplified by retinopathy, neuropathy, nephropathy, angiopathy, atherosclerosis and periodontitis. In the oral cavity, T2DM alters inflammatory responses of the periodontium to oral pathogens, raising the susceptible risk for periodontal disease two to five fold, compared to non-diabetic patients (Tunes et al. 2010). Examination of human gingival crevicular fluid from diabetic patients has demonstrated higher levels of TNF-α, interleukin-1β (IL-1β) and prostaglandin E2 (PGE2), in comparison to non-diabetics with a similar level of periodontal disease.

Such high levels have been implicated in delayed healing and diminished bone formation. Conversely, this risk may be reduced by better glycemic control (Taylor 2001).

The mineralised tissues have been reported to be affected by T2DM. The harmful effects are proposed to come from, firstly, insulin resistance which results in higher levels of insulin. Initially, this may increase bone mineral density, however, in the long-term, bone turnover will be affected due to an accumulation of AGEs. Secondly, prolonged hyperglycemia results in AGE production, which alters bone quality by affecting osteoblast differentiation (Carnevale et al. 2014). Dysregulation of certain genes, which induce osteoblast proliferation and differentiation is another factor, which may affect the bone tissue. Consequently, deleterious effects and bone damage appear to be associated with T2DM (AI-Aql et al. 2008).

During bone wound healing, progenitor cells are described to be recruited to the injury site by different chemotactic signalling pathways. Several growth factors contribute to the repair process, such as transforming growth factor-β (TGF-β_1), bone morphogenic proteins (BMPs) and platelet-derived growth factors (PDGFs). These growth factors stimulate the proliferation and differentiation of progenitor cells to form osteoblasts that synthesize the mineralised matrix. It has been reported that hyperglycemia, resulting from T2DM, exerts strong effects on specific stages in the bone healing process, including inflammation, clot formation, vascularization, mineralisation, bone matrix synthesis and remodelling (Valero et al. 2007). As a result, this situation leads to alter bone turnover and remodelling. A delay in wound healing is a common condition associated with diabetics.

One of the most important non-collagenous matrix proteins, which has a pivotal role in bone mineralisation and healing is osteopontin (OPN). OPN is synthesized by different cells, such as osteoblasts, macrophages and fibroblasts. It is one of the earliest secreted proteins in the osteogenic process (McKee et al. 2011). OPN binds to mineral crystals to inhibit their growth and consequently, inhibits bone formation. Another function of OPN synthesized by macrophages is that of coating the surface of small particulate mineralised tissue debris, which is generated through some surgical procedures, such as implant placement, acting as an opsonin to facilitate its phagocytosis by macrophages (Pedraza et al. 2008; McKee et al. 2011). A study by Andrews et al. (2012), reported that blocking OPN expression at the site of injury in a murine model showed a reduction in the inflammatory response and subsequent granulation tissue formation. Colombo et al. (2011) showed that there is a delay in bone healing around an implant inserted into diabetic rats, that correlates to

increases in OPN levels. This may perpetuate the inflammation and delay osteocalcin (OCN) synthesis, resulting in delayed bone healing. These studies have demonstrated the importance of OPN secretion in the body homeostasis.

In periodontal disease, bacterial lipopolysaccharides (LPS) play a major role in the disease pathogenesis. LPS is bacterial endotoxins in the form of glycolipids. It is present in the outer cell membrane of all Gram-negative bacteria, such as *Porphyromonas gingivalis, Tannerella forsythia* and *Prevotella intermedia*, which are all associated with sub-gingival periodontal lesions (Tanner et al. 1979; Slots et al. 1986; Moore and Moore 1994; Nakamura et al. 2004). A broad number of studies have proposed that the central periodontopathic agent among these etiological factors is *Porphyromonas gingivalis (P. gingivalis)* (Marcotte and Lavoie 1998; Maiden et al. 2003; Paster et al. 2006; Hajishengallis et al. 2012). *P.gingivalis* comprised 86% of subgingival plaque samples from patients affected by chronic periodontitis (Datta et al. 2008). *P.gingivalis*-LPS (*pg*-LPS) has the ability to activate the host inflammatory responses through cell surface receptors, called Toll-Like Receptor 2 and 4 (TLR-2 and TLR-4) which in turn, induce a production of proinflammatory cytokines, IL-1β, IL-6, IL-8 and TNF-α, disrupting the bone repair process (Jiang et al. 2002; Graves et al. 2011; Herath et al. 2011; Kato et al. 2014). On the other hand, hyperglycemia from T2DM has been reported to alter the host response to bacterial endotoxins through cytokine dysregulation by AGEs, in addition to prolonged TNF-α expression (Graves et al. 2006). Thus, combined effects of hyperglycemia and *pg*-LPS has been described to exacerbate the situation by enhancing more bone resorption, especially when T2DM is associated with periodontal disease.

To date, although there has been scientific research on the effect of the hyperglycemic environment on the cells associated with bone formation, as part of bone remodelling, little is known about the effects of *pg*-LPS derived from periodontal pathogens on this process and the role of OPN. This project will attempt to elucidate further the importance of OPN matrix protein, which we proposed to play a pivotal role in delayed bone healing in a diabetic environment and the role of *pg*-LPS in aggravating this process.

1.2: Periodontal Disease

Periodontitis is a chronic inflammatory disease involving the periodontium. It is characterized by a slowly growing progressive destruction of tooth-supporting structures. If left untreated, this disease can lead to tooth mobility and subsequently tooth loss (Nanci and Bosshardt 2006). It has been reported that periodontal disease is highly prevalent and that severe cases affect 10-12% of adults in most populations, while the moderate form of the disease is more common and involves 40-60% of adults. Periodontal disease has been described to be associated with cardiovascular disease complications, such as myocardial infarction (MI) and ischemic stroke (Mattila et al. 1989; Lu et al. 2008; Holmlund et al. 2017). The disease is always associated with numerous negative impacts on quality of life, in terms of social interactions, confidence and food choices (Fox 1992; Fox et al. 1994; O'Dowd et al. 2010). Periodontal disease classification is very complex, considering the clinical feature, age, the rate of disease progression; and the local and systemic factors that may elevate its risk. The main classification of periodontal disease, includes gingivitis when the inflammation is confined to it. Gingivitis is known to be reversible following proper oral hygiene. The second type is periodontitis, in which the inflammation extends to the deeper part of the periodontium, resulting in tissue and alveolar bone destruction. Consequently, periodontitis leads to a breakdown of the periodontal ligament and formation of largely irreversible periodontal pockets between the tooth and the gingiva. Interestingly, the condition in early stages is asymptomatic and many patients are unaware of its presence. Subsequently, the situation would progress to result in tooth mobility. The alveolar bone resorption occurs in parallel with the progression of attachment loss of the periodontal ligament. Although it is a painless disease, advanced cases of periodontitis are characterized by gingival erythema, swelling, bleeding, recession, tooth mobility, drifting, suppuration from the pockets and eventually tooth loss (Preshaw et al. 2012).

Although the main aim of the host response is to counteract the invading pathogens, it is now regarded to be a major part of the problem of progression of periodontal disease. The invading pathogens can induce periodontal tissue destruction through proteinase enzymes and endotoxins, or indirectly through provoking a strong host response. Leukocyte infiltration can limit the bacterial invasion, but at the same time could be harmful to the tissues. The leukocyte recruitment is promoted by several factors, such as bacterial products, cytokines, chemokines and cross-talk between innate and adaptive immune responses (Page et al. 1997). The resident cells of periodontium, such as fibroblasts, cells of junctional epithelium and vascular endothelium, in addition to leukocytes; can assist in response to the exposure to bacterial products, such as LPS, by secreting cytokines IL-1β,

IL-6, TNF-α and PGE-2. When continually expressed, these are proposed to participate in tissue destruction (Hung et al. 2013; Jiang et al. 2013). In this context, the balance in cytokine secretion can determine whether the tissues maintain homeostasis, or lead to an increase in the severity of the inflammation and tissue destruction (Gemmell et al. 2002).

One of the complexities of periodontal disease, is that the disease is associated with a wide range of pathogenic bacteria, such as *Prevotella intermedia, Tannerella forsythia* and *P. gingivalis*. These specific periodontopathic agents have a prime role in the progression of the tissue destruction (Wang et al. 2013). The critical components of host cells, which respond to the bacterial products is the Toll-Like Receptor family (TLRs). These receptors, when activated by binding to various bacterial components can induce an innate immune response, resulting in more cytokines and chemokines production, which can change the balance towards further tissue destruction (Mahanonda and Pichyangkul 2007).

1.2.1: Bone Repair in Periodontal Disease

Bone repair is a process involving complex biological events, that includes a multitude of intracellular and extracellular molecular signalling pathways, which are coordinated by different cell types to restore the function to normal conditions. This process, however, can be delayed due to different diseases, such as diabetes, osteoporosis and the age of the individual, which can affect signalling events, revascularization and mineral matrix formation (Armas and Recker 2012). In the case of craniofacial tissue, rapid bone healing is the main goal. This is achieved by primary bone healing through intramembranous ossification, where the repair process can be facilitated by revascularization and bone synthesis without micromotion. Excessive micromotion results in secondary bone healing, which consists of a double process, chondrogenesis in regions near the fracture site of periosteum, while an intramembranous ossification at the other site. The bone repair process is divided into several stages; haematoma formation, a reparative phase which leads to the formation of woven bone and finally the remodelling phase whereby woven bone is replaced by lamella bone. Haematoma phase occurs early during tissue damage and may last from 1-3 days. There will be an activation of complement cascade and promotion of platelets accumulation (Kikuchi 2005). The platelets aggregate in a stable fibrin clot, which is provided from plasma fibrinogen and thrombin to form a provisional matrix. This platelet matrix provides an important source of various signalling factors, such as TGFβ_1 and β_2, PDGF, serotonin and histamines, which

trigger chemotactic signalling for neutrophils, monocytes and lymphocytes; and subsequently progenitor cells (Kuzyk and Schemitsch 2011). These inflammatory cells are responsible for secreting the inflammatory mediators, including the proinflammatory cytokines, such as IL-1, IL-6, IL-8, TNF-α and macrophage colony stimulating factors (M-CSF). Despite these inflammatory factors having a chemotactic function to recruit inflammatory cells and amplify further inflammatory events, they are also described to be necessary for extra cellular matrix (ECM) synthesis and bone repair (Gerstenfeld et al. 2001). Angiogenesis generation was reported to start by means of vascular endothelial growth factor (VEGF), together with basic fibroblast growth factor (bFGF) and PDGF. These factors stimulate budding of new vessels (AI-Aql et al. 2008). The second phase of the healing process is the reparative stage, which lasts from 3-50 days, during which granulation tissue and osteoid are formed. The MSCs are recruited to the wound site from the bone marrow and periosteum, by the prominent role of the provisional fibrin matrix, which includes various signalling milieu, such as PDGF and TGF-β_1, β_2 and β_3. Another source of MSCs is the pericytes, cells associated with the endothelial cells of veins and capillaries, which assist in the angiogenesis process. In terms of intramembranous ossification, there are important effects of TGF-β and BMP-2 in inducing osteogenic differentiation of MSCs, via upregulation of Runx2 and Osterix transcription factors. Wnt family of ligand is another pathway that induces osteoinduction, resulting in activation of the canonical β-catenin pathway, as well as osteogenic genes (Clément-Lacroix et al. 2005; Yang et al. 2011). This provisional granulation matrix is subsequently replaced by an unmineralised collagenous matrix, called osteoid; and at the same time, angiogenesis formation takes place to form the Haversian canal system. During osteoblast differentiation, several noncollagenous proteins have been observed to be produced, which have the capability to inhibit crystal growth, such as OPN (McKee et al. 2011); and decorin and biglycan in their dermatan sulphate-conjugated forms (Waddington et al. 2003). OPN attachment to the MSCs or osteoblasts can be performed by its RGD binding sequence (McKee et al. 2011). On completion of osteoid formation, the remodelling process is conducted by removal of these inhibitor proteins and osteoblasts start to synthesize noncollagenous proteins, which facilitate the deposition of hydroxyapatite crystals along the collagen fibril framework to form bone. In this mineralisation stage, the chondroitin sulphate-conjugated forms of decorin and biglycan, are expressed together with OCN and osteonectin. Herein, some of the osteoblasts become entrapped inside the mineralised matrix and form osteocytes. Alternatively, other osteoblasts undergo apoptosis to arrest further bone synthesis. Importantly, the growth factors become embedded within the bone matrix and to be

released in case of matrix is resorbed, as a sequence of the remodelling process. Osteoblasts also secrete osteoprotegerin (OPG), which acts to prevent binding of RANKL to the osteoclast cell surface receptor, RANK; to control osteoclastic activities. MSCs of bone marrow and pericytes origin subsequently differentiate into osteoblasts to replace the lost bone in sequences similar to the reparative stage. The remodelling process, however, is much slower than the reparative stage, lasting from approximately 6 months up to 4 years to replace the woven bone (Kwong and Harris 2008).

The late remodelling of woven bone occurs around 2 months later, which requires the activation of osteoclasts for bone removal (Kwong and Harris 2008). This process is non-inflammatory in general and it is strongly controlled by MSCs and osteoclasts, which produce RANKL and M-CSF cytokines, facilitating monocyte cells recruitment, differentiation and activation of osteoclasts that capable of bone matrix degradation (Edwards and Mundy 2011).

In the periodontium, this process is more complicated, depending on the tissue and cells that contribute to this healing process. It is required a new attachment of principle fibres to the root surface cementum occurs, which has been previously affected by periodontal pathogens. In order to obtain healing in periodontium, there should be organized events taking place, the progenitor periodontal ligament cells should migrate to the root surface, to form a new attachment apparatus. Likewise, osteoprogenitor cells must also migrate, mature and conjunct with periodontal ligaments to achieve tissue regeneration. In this context, there is a requirement to healthy cells and precise coordination, in terms of spatial and temporal events, to ensure the availability of the appropriate cells of periodontal regeneration. Clinically, this is difficult to achieve and hence total regeneration is often minimal. In addition, the profile of periodontal disease demonstrates a cyclic nature, commencing as a period of aggressive alveolar bone destruction, followed by a period of remission and then wound repair. This repair period was proposed to be insufficient to replace the lost bone especially, when another cycle of bone destruction begins, due to loss of the balance between bone formation and bone resorption (Zeichner-David 2006; Chen and Jin 2010).

1.3: Growth Signalling Factors

1.3.1: Transforming Growth Factor-β (TGF-β)

TGF-β is part of a large family growth factors encompassing several isoforms, ranging from TGF-β_1 to TGF-β_5, BMPs, growth differentiation factors (GDFs), inhibins, activins and anti-Mullerian hormones (Dimitriou et al. 2005). This large family contributes to various systemic regulation and cell functions; namely proliferation, differentiation and ECM synthesis. Different TGF-β isoforms coordinate with specific heterodimer receptor complex, that are comprised of two distinct proteins termed as TGF-β receptor I (TGF-β1R) and TGF-β receptor II (TGF-β2R). These two receptors belong to the serine/threonine kinase receptors, which activate a broad complex range of intracellular signaling pathways (Janssens et al. 2005). While Type III receptor was reported not to be directly associated with TGF-β signalling and may have a pronounced binding effects of TGF-β to receptor III (Pfeilschifter et al. 1998). In bone healing, TGF-β has been described to have a positive effect by inducing *in vitro* cell growth via IGF-I activation, causing a significant increase in osteogenic differentiation of primary human osteoblasts (Viereck et al. 2002). It has a role in controlling MSCs proliferation by means of other factors, such as extracellular environment, its concentration at the healing site and ligand-receptor that interacts with other growth factors. Thus, the role of TGF-β in bone healing is more modulatory rather than stimulatory (Pfeilschifter et al. 1998). Furthermore, TGF-β was proposed to play an important role in bone remodelling by contributing to reduce bone resorption through inducing apoptosis of osteoclasts and suppressing their activity (Ehnert et al. 2010).

In the early inflammatory stage (days 1-3), TGF-β_1 has been described to be increased, whereas TGF-β_1, β_2 and β_3 have been reported to increase in the reparative stage (days 3-50) and remodelling stage (2-9 months) (Cho et al. 2006; Würgler-Hauri et al. 2007). It has been found that higher levels of TGF-β_1 in the early stage of healing tissues could be associated with excessive scar formation (Tsubone et al. 2006). In diabetic healing bone, TGF-β_1 was found to be delayed expression until week 9, when high level was observed (Colombo et al. 2011). It has been also found to stimulate migration of monocytes in the hyperglycemic microenvironment, by induction of p38 pathways and ALK5 kinase via phosphoinositide 3-kinase (PI3K) (Olieslagers et al. 2011). These pieces of evidence may refer to the potential capacity of TGF-β_1 to induce altered bone healing in hyperglycemic environments.

1.3.2: Bone Morphogenic Proteins (BMPs)

Bone morphogenic proteins are the most important growth factors of the TGF-β superfamily. BMPs play a critical role in regulating differentiation and apoptosis of various cell types, such as osteoblasts, chondroblasts, neural and epithelial cells. Their regulatory effects differ according to the phenotype of targeted cells, the stage of cell differentiation, as well as interactions with various circulatory factors (Sakou 1998). MSCs, osteoprogenitor cells, osteoblasts, in addition to chondrocytes within the ECM, are all reported to contribute to the production of BMPs. There are four members of the BMP family, based on their amino acid sequences. The first group consists of BMP-2 and BMP-4. Another group encompasses BMP-5, BMP-6 and BMP-7. The third group includes BMP-12, BMP-13 and BMP-14, whereas the last group includes BMP-3 (osteogenin) and BMP-3b (GDF-6) (Tsiridis et al. 2007). Each BMP has a unique function and a distinct expression pattern during fracture healing, although they are structurally and functionally related to each other. It has been observed that knockout mice for BMP-5, BMP-7 and BMP-11, showed localized bone abnormalities (Luo et al. 1995). Chen et al. (2004) suggested after a series of analysis of the osteogenic activities to numbers of BMPs, that there is a hierarchical model of BMPs. BMP-2, BMP-6 and BMP-9 are the most potent BMPs in terms of inducing differentiation of mesenchymal progenitor cells into osteoblasts. Furthermore, BMPs may stimulate the production and secretion of other bone growth factors, for example, insulin growth factor (IGF) and vascular endothelial growth factor (VEGF) (Tsiridis et al. 2007).

1.3.3: Wnts

Wnts (Wingless) are a group of more than 19 secreted proteins that bound to receptors, known as membrane-spanning frizzled (FZD). These are implicated in various cellular activities, namely the recruitment of progenitor cells and their differentiation into osteoblasts; and apoptosis. Wnt signalling occurs by the canonical and non-canonical pathways. The canonical pathway includes different Wnt proteins, FZD as well as low-density receptors LRP5 and LRP6 (Arvidson et al. 2011). Strong evidence proposes that the canonical pathway had a critical role in bone synthesis and is involved in the expression of osteoblast specific markers (Westendorf et al. 2004; Jackson et al. 2005). It has been reported that Wnt binding to FZD and LRP5/6 complexes inhibits glycogen synthase kinase 3 (GSK3) activity, resulting in the blocked phosphorylation of β-catenin by preventing its ubiquitin-degradation, which can cause β-catenin translocation to the nucleus and interact with T-cell factor/lymphoid enhancer factor, leading to activation of transcription factors of

target genes (Fujita and Janz 2007). β-catenin protein levels are known to be elevated in osteoblast precursors, while inactivation of β-catenin, leads to chondrocyte differentiation of MSCs (Day et al. 2005). Levasseur et al. (2005), reported that loss of function mutations in LRP5 results in osteoporosis-pseudoglioma syndrome. On the contrary, functional mutations in LRP5 cause increased bone density, associated with upregulation of bone marker formation, such as OCN (Boyden et al. 2002). It has also been observed that there is a high bone mass, as well as an increase in Runx-2 and OCN expression, in the case of an over-expression of Wnts in transgenic mouse models. This suggests that Wnts signalling might contribute to osteoblast differentiation (Gaur et al. 2005). However, the exact role of Wnt signalling in osteoblastogenesis is still not conclusive (Luo 2004).

1.3.4: Platelet Derived Growth Factor (PDGF)

PDGFs are a family of growth factors that act as strong chemotactic signals, which stimulate inflammatory cells, mesenchymal and osteoprogenitor cells, to migrate to injury sites (Tsiridis et al. 2007). PDGFs consist of three isoforms; first, homodimers consist of polypeptide chains PDGF-A (PDGF-AA), second, PDGF-B (PDGF-BB) and third, a heterodimer (PDGF-AB) (Heldin and Westermark 1999). The primary PDGF signals commence through PDGF receptor α (PDGFRα), while the predominant PDGF signals are via PDGF receptor β (PDGFRβ). Signals are mainly through the MAPK pathway (Donovan et al. 2013). It has been found that deletion of PDGFRβ resulted in MSC differentiation into osteoblasts and upregulation of Runx2 and OCN (Tokunaga et al. 2008). Inhibition of PDGF-BB receptor in human MSCs, however, demonstrated a decrease in cell proliferation but has no influence on osteo-differentiation (Kumar et al. 2010).

1.3.5: Fibroblast Growth Factor (FGF)

FGF family members contain twenty-three monomeric polypeptides. The action of FGFs is through binding to tyrosine kinase receptors (FGFR1-FGFR4) (Tsiridis et al. 2007). FGFs are produced by monocytes, macrophages, MSCs, chondrocytes and osteoblasts. Simultaneously, FGFs promote the growth and differentiation of different cells, such as fibroblasts, osteoblasts, chondrocytes and myocytes. It has been reported that FGFs play a pivotal role in angiogenesis, in addition to MSC mitogenesis at the early phases of bone healing. The role of fibroblast growth factor 1 or α (FGF-1 or FGF-α), is mainly in regulation of chondrocyte proliferation and possibly maturation, while in general, osteoblasts express FGF-2 or FGF-β, which is more potent than FGF-1 (Lieberman et al. 2002). In a study using a canine tibial osteotomy model, it has been reported that FGF-2 was

accompanied with an early increase in callus formation (Nakamura et al. 1998). Conversely, FGF-2 knockdown in mice showed a decrease in bone mass, compared to normal mice. Additionally, there is a lower expression of Runx-2 and decreased bone nodule formation in cultured bone marrow stromal cells (Naganawa et al. 2008). Over-expression of FGF-2 leads to an increase in apoptosis in a transgenic mouse model (Mansukhani et al. 2000). FGF-2 addition to bone marrow progenitor cells appears to improve their proliferation and differentiation potential (Delorme et al. 2009). FGF-2 also stimulates epithelial to mesenchymal transition, which is of importance during development and tissue healing (Shirakihara et al. 2011). FGF-18 is expressed in mesenchymal cells and assists in the differentiation of osteoblasts, in addition to inducing osteogenic differentiation of MSCs. This process is achieved by activation of MAPK and P13K signalling, after activation of FGFR-1 and FGFR-2 (Naganawa et al. 2008).

1.3.6: Insulin-Like Growth Factors (IGFs)

IGF family members mainly consist of two forms, IGF-I (somatomedin-C) and IGF-II (skeletal growth factor). The sources of IGFs are the bone matrix, osteoblasts, endothelial cells and chondrocytes. Growth hormone regulates the serum concentration of IGF-I, which in turn promotes the formation of the bone matrix, such as type I collagen and non-collagenous matrix proteins. This is achieved by enhancing fully-differentiated osteoblasts. The second type is IGF-II, which is less potent than IGF-I and it acts at a later phase of endochondral bone formation, in addition to stimulation of type I collagen synthesis, matrix production and cellular proliferation (Tsiridis et al. 2007). IGFs have been observed to have a synergistic function with other growth factors, such as BMP-2. There is an increase in the expression of IGF-I and II in rat calvaria cell cultures when treated with BMP-2 (Canalis and Gabbitas 1994). Another study has reported that TGF-β_1 increases IGF-I and II expression in human osteoblast cultures (Okazaki et al. 1995). Taniguchi et al. (2006) postulated that IGF-1R possibly had the same homological structure of insulin receptors, which may give the possibility that IGF-1 would have the affinity to bind to the insulin receptor. In experimental studies, there is an elevation in osteoblastic activity, cell proliferation and higher expression of alkaline phosphatase (ALP), due to insulin application. Based on this outcome, administration of insulin could possibly bind to IGF receptor, activating cell proliferation and stimulating certain growth factor receptors (Gandhi et al. 2005). This assumption, however, is expected to be different in T2DM, because of insulin resistance, based on this physiological disorder, which may never respond to IGF stimulation.

It is worth stating that despite this information, there is lack of full understanding of the synergy of signalling pathways.

1.4: Stem Cells and Their Role in Bone Repair

Stem cells are unspecialized cells, which can differentiate into other types of cells during development and bone repair. They are also capable of self-renewal by means of signalling pathways, which are believed to be controlled by certain growth factors, existing within the stem cell niche. Almost all connective tissues have a stem cell population, that is believed to have an important role in tissue injury and repair (Lin et al. 2008). According to their ability to differentiate into other types of cells, there is some evidence that they may play a pivotal role in the future cell therapy (Denham et al. 2005). In respect to stem cells differentiation capacity, the cells can be identified according to their differentiation potency. There are currently five identified phenotypes, stem cells which are Toti-, Pluri-, Multi-, Oligo- and Uni-potent following a reverse hierarchy. Going down through this hierarchy pattern, the cells show lower capacity for differentiation. Totipotent cells can differentiate into all types of cells of a body organism including membranes, placenta and extra-embryonic tissues. Zygotes and their immediate descendants in the morula of developing embryo are considered as a true Totipotent cell (Seydoux and Braun 2006). Pluripotent cells can differentiate into different phenotypes from various germ layers. Multipotent cells can only differentiate into a specific type of cells, similar to their tissues, such as MSCs. Oligopotent cells can differentiate into a few descendent phenotypes namely, lymphoid and myeloid cells, in addition to mammalian ocular surface cells (Hombach-Klonisch et al. 2008; Majo et al. 2008). Unipotent cells can only differentiate into a mature cell closely related phenotype within a single tissue; a typical example for them is the committed osteoprogenitor cells. Additionally, there is another classification of stem cells into 3 main classes; germ-line stem cells (GSCs), embryonic stem cells (ESCs) and adult (somatic) stem cells (SSCs). Germ-line and embryonic stem cells are described as pluri-potent cells; these exist and contribute to growth events in the earlier stage of embryonic development. They are derived from the inner cell mass of the 5-6 day old human blastocyst (Bongso and Lee 2005). Adult/somatic stem cells (SSCs) are described as multi-potent cells which are present in different body tissues, such as bone, the blood stream, cornea and retina, skeletal muscle, liver, skin, gastrointestinal tract, pancreas, spinal cord and brain. SSCs generate intermediate cell types called progenitor cells, that have a commitment to their tissues and contributing to body homeostasis (Verstappen et al. 2009). These cells have the capability for differentiation into specific tissues, depending on the site and specific signals from their niche (Gafni et al. 2004; Lin et al. 2008). There

are several types of adult stem cells and their classification is mostly according to their location in a body organ.

1.4.1: Mesenchymal Stem Cells (MSCs)

MSCs were first described by Friedenstein et al. (1968) in bone marrow, defining them as osteogenic stem cells. Nevertheless, Caplan (1991) was the first person who called MSCs by this name. Their morphology is mononuclear with a fibroblastic shape (Mareschi et al. 2001). MSCs have the capability to differentiate into different types of cells *in vitro*, such as osteoblasts (Rickard et al. 1996), adipocytes (Bennett et al. 1991), chondrocytes (Ashton et al. 1980) and myoblasts (Wakitani et al. 1995). Furthermore, other studies have shown their ability to differentiate into bone and cartilage *in vivo* during implants via ceramic carriers (Friedenstein et al. 1987; Goshima et al. 1991). Because of the wide diversity of these cells in differentiation into osteoblasts, chondrocytes and adipocytes, in addition to ease of handling, this makes MSCs a "gold standard" for tissue engineering and regenerative medicine. Differentiation of MSCs is controlled by different signals and growth factors, such as TGF-β, BMP and TNF-α (Kratchmarova et al. 2005).

1.4.2: Hierarchy Model of MSCs

The pattern of stem cell division consists of two types, symmetrical and asymmetrical cell division. Symmetrical cell division produces two identical cells. However, asymmetrical division produces a cell identical to the mother and another cell more able to proliferate and differentiate. In terms of stem cells, division is achieved by asymmetrical division of mother cell, to give rise to a daughter cell, which assists to retain self-renewal ability, that is identical to the mother cell. This mother stem cell has a long-lifespan and it is proposed to maintain its ‘slow’ division mechanism to minimize the possibility of DNA replication mutations (Reya et al. 2001; Riquelme et al. 2008). The second cell derived is a rapidly proliferative daughter cell, which is proposed to form a transit amplifying (TA) cell after frequent proliferations. TA cells were described to form large colonies, exhibiting the highest proliferative capacity, as well as highest multipotency (Figure 1.1). As cell division continues, TA cells exhibited a decreased proliferative potential and smaller colonies. During this period, TA cells commence transformation into lineage-restricted MSCs. These lineages demonstrated tri-, bi- and uni-potentiality (Chan et al. 2004; Phinney 2012). Thus, the population of MSCs is a heterogeneous mixture and differs in their stage of lineage commitment and ranges of differentiation. These lineages have different potency to differentiate into bone, cartilage and adipose tissue (Sarugaser et al. 2009), or could be bi-potent for only two of these lineages. The uni-potent cells, however, are committed to only one cell phenotype (Lee et al. 2010). It has been

reported that tri-potent MSCs had a high ability to proliferate and in colony forming efficiency. However, in bi-potent and uni-potent cell lineages, this ability has been reported to be decreased (Russell et al. 2010). For many years, MSCs and CFU-fibroblasts have been considered as identical cells, however, more recently, Shipounova et al. (2013), proved that there are marked differences between them and they reported that increased levels of FGFR2, VEGF and BMP4 in MSCs, may indicate the more immature nature of these cells. This hierarchy model elucidates the described cellular phenotype regarding MSC populations derived from compact bone and bone marrow.

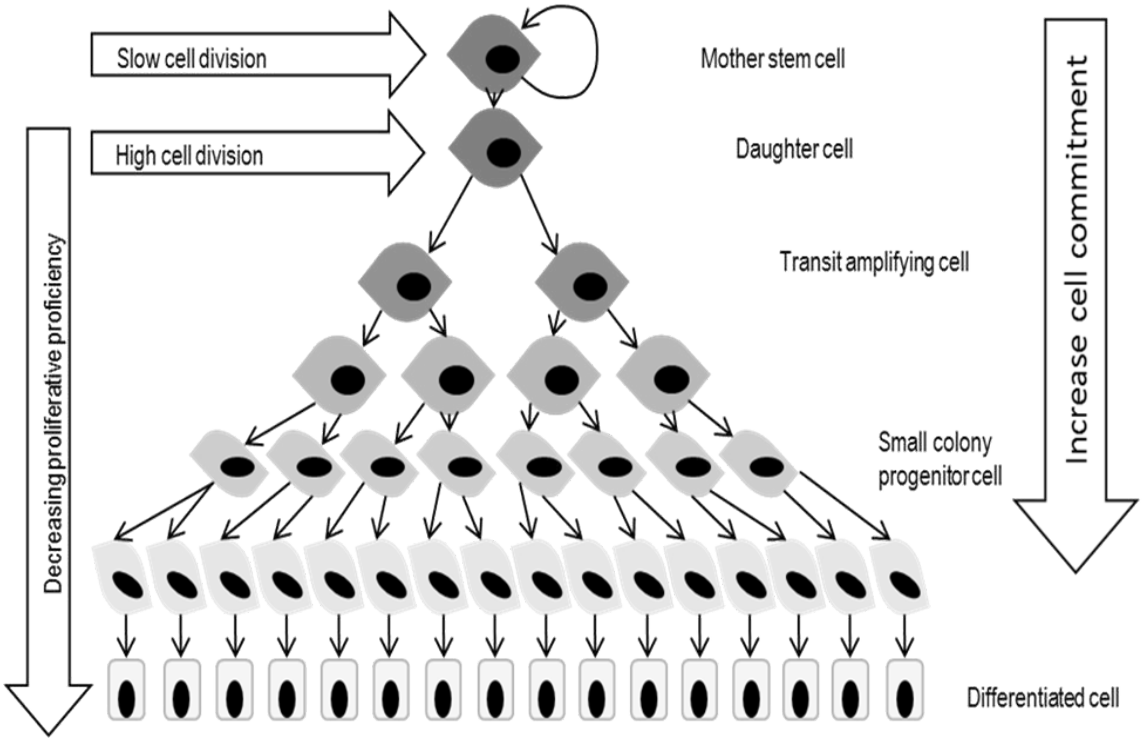

Figure 1.1: Hierarchy model of stem cells division (Adapted from Chan et al. 2004).

1.4.3: Mesenchymal Stem Cell Characterization

Recently, MSCs have generated considerable interest through their therapeutic potential in biomedical disciplines, tissue engineering and regenerative medicine. However, the literature has reported a wide range of different methodologies utilised for their isolation and expansion; and varied approaches for their characterization. These different approaches have created some issues and hampered progress in the field, in terms of comparisons amongst studies. In addition, the heterogeneity in morphology and function provides evidence regarding the difficulty in identifying an ideal phenotypic fingerprint of MSCs (Bianco 2014). The International Society for Cellular Therapy (ISCT) states the minimal criteria to define MSCs (Dominici et al. 2006). These criteria consist of three requirements which are, first, that the cells should adhere to plastic in standard culture conditions; secondly, their expression of specific surface antigens and lastly, the cells should be able to differentiate into somatic cells. The property of plastic adherence is well-described, when MSCs are maintained in tissue culture in the presence of standard culture conditions (Colter et al. 2000). The second criterion is ≥ 95% of MSCs must express the specific surface antigens, ecto 5'ectonucleotidase (CD73), Thy1 (CD90) and endoglin (CD105). Simultaneously, MSCs should lack expression of hematopoietic antigens CD45; pan-leukocyte marker, CD34; primitive hematopoietic progenitors and endothelial cells; CD14 and CD11, which are related to monocytes and macrophages; CD79α and CD19β cell markers and HLA-DR, which do not express on MSCs, unless stimulated by interferon-γ (IFN-γ). The third and the final criterion for MSCs is that they must be capable of differentiating into osteoblasts, chondroblasts and adipocytes, by using standard protocols and tissues culture conditions (Dominici et al. 2006).

It has been found that these criteria, however, do not meet the characterization requirements for all MSCs, because of several critical shortcomings. Firstly, ISCT criteria lack a unique marker that can be universally shared among all species. Secondly, it emphasized on the positive expression of CD105, CD90, CD73, however, none of these markers are expressed by all human and animal species (Boxall and Jones 2012). Thirdly, the criteria refer to the ability to differentiate into three independent cell phenotypes; osteoblasts, chondrocytes and adipocytes, while it lacked the multiple differentiation pathway, including the immature MSCs, which have been described to have the ability to differentiate into the majority of cells in the body (Abdalla and Kassem 2008; Samsonraj et al. 2015). The plastic adherence, nonetheless, is reported to be shared by the majority of stem cell populations, thus it is not such a unique MSC marker itself. Moreover, these classical markers are

observed to be upregulated or downregulated with increasing culture expansion (Jones et al. 2010; Halfon et al. 2011; Harrington et al. 2014). In addition to the markers that been described by ISCT, there are other surface markers that have also been identified such as, STRO-1, HLA-A, HLA-B, HLA-C, HLA-DR, HLA-1, Oct4, Oct 4A, Nanog, Sox-2, telomerase (TERT); and others (Mafi et al. 2011). STRO-1 is molecule attributed to be highly specific for MSCs (Simmons and Torok-Storb 1991). It has been observed that STRO-1 expression is down-regulated during extended culture. The effect of STRO-1 on MSCs remains widely unknown. One study has shown that expanding STRO -1^{+} MSCs has a better homing capacity in comparison to STRO-1^{-} MSCs, suggesting it has a strong role in migration and attachment of MSCs to the ECM (Bensidhoum et al. 2004). Gronthos et al. (2003) added CD106 (VCAM-1) as another MSCs marker. Similar to STRO -1, CD106 expression has been reported to decline with prolonged culture (Jones et al. 2010; Jung et al. 2011). FGFR1 (CD331) is another marker, which is important in organizing epithelial-mesenchymal transition (EMT) and mesoderm morphogenesis, which assists in cell migration and patterning, which can be achieved by controlling Snail1 expression (Eghbali-Fatourechi et al. 2005). It has been reported that absence of FGFR1 and Snail1 during development, leads to craniofacial abnormalities, namely cleft palate (Goncharova et al. 2012). In conclusion, it is difficult to conclude that all MSCs resident in various tissues and organs have the same markers. More research is needed to obtain a wide range of knowledge about cell phenotype and gene expression profile of MSCs *in vitro* and in their original niche *in vivo* study, with continued search for novel markers, which can be shared among all MSCs phenotypes and would undoubtedly assist in developing an improved methodology for characterization (Boxall and Jones 2012).

1.4.4: Senescence of MSCs

Senescence is a limited ability of the cells to proliferate. It was firstly described by Hayflick and his colleagues, when they reported that human diploid fibroblasts had a limited proliferative ability in culture (Hayflick and Moorhead 1961). *In vivo*, however, this process consequently ends by cell death and may negatively impact bone healing and repair process (Campisi and d'Adda di Fagagna 2007). It was reported that the mitotically-competent cells may respond to various stresses and undergo cellular senescence or so-called "end replication problem", which subsequently, leads to cell-cycle arrest. Examples of these stresses involve dysfunctional telomeres, disorders that affects the chromatin organization, DNA damage, in addition to strong mitogenic signals (Turinetto et al. 2016). At the end of each chromosome, there is a repetitive region of DNA called the telomere, which comprises of tandem chromatin TTAGGG. During cell division and proliferation activities,

the process is usually accompanied by telomere shortening. Telomerase is an enzyme, which preserves telomeres from shortening, encoding by the telomerase reverse transcriptase, TERT, with a template of telomerase RNA component (TERC) (Blasco 2005). Despite this telomere preserving activity, it has been reported that after each cell division, the telomere becomes shorter and loses 50-200 base pairs of telomeric DNA, because of incomplete chromosomal replication by DNA polymerases (Wagner et al. 2008). It has been reported that these enzymes are associated with immortal (cancer cells) and embryonic cells in high levels and are at lower levels in human adult stem cells (Zimmermann et al. 2003). On the other hand, telomerase was described to be expressed at high levels in mouse stem cells (Hiyama and Hiyama 2007). Senescent cells face irreversible growth arrest. However, they continue to be metabolically active and develop a flat, large morphology and disclose some characteristic changes in their gene expression. Senescent cells have been described to typically exhibit a senescence-associated β-galactosidase (SA-β-gal) activity, reveal a persistent DNA damage nuclear foci (PDDF) that contain DNA damage response proteins, such as γH2AX and 53BP1(Rodier et al. 2011). In addition to the features above, there is an accumulation of heterochromatin structure called senescence-associated heterochromatin foci. Furthermore, the senescent cells secrete a number of cytokines, growth factors and proteases, that have potent autocrine and paracrine activities (Acosta et al. 2008; Coppé et al. 2010; Turinetto et al. 2016). At a molecular level, it has been found that senescence is induced by the retinoblastoma protein (Rb) or p53 pathways, which in turn activates the cyclin-dependent kinase inhibitor, p16 and p21, pathways. Importantly, these pathways can act on each other to induce senescence after blocking the cell cycle to sustain growth arrest (Bargonetti and Manfredi 2002; Chau and Wang 2003; Turinetto et al. 2016).

1.4.5: Osteogenic Differentiation Pathway of MSCs

Osteogenic differentiation into osteoblasts is a complex process, required for the formation of bone tissue. Various signalling molecules and transcription factors have been described to be involved in this sophisticated process, for example runt-related transcription factor-2 (Runx2), Tafazzin (Taz), Osterix, and Distal-Less Homebox5 (Dlx5). Runx2 is considered as a master gene to achieve osteogenic differentiation. It is also known as core-binding factor subunit α (Cbfa1). In cases where Runx2 has been knocked out, it has been reported that this leads to loss in the ability to differentiate to osteoblasts (Otto et al. 1997). Runx2 has been found to regulate the expression of OCN, bone sialoprotein (BSP), OPN, collagen type I and some other signalling molecules (Ducy et al. 1997; Javed 2001). Despite the pivotal role of Runx2, its transcriptive action has been reported to be

inhibited by TNF-α (Abbas et al. 2003). Taz is another transcription factor that activates Runx2 expression through FGF2, to enhance osteoblast differentiation (Cui et al. 2003; Byun et al. 2014). Taz is proposed to provide a prime role in inhibiting adipogenesis by repressing peroxisomal proliferator-activated receptor gamma (PPAR-ϒ) gene expression. Therefore, Taz has been suggested to control the fate of multipotent MSCs and determine the switching between osteogenesis and adipogenesis (Hong et al. 2005). Osterix transcription factor is proposed to act downstream to Runx2, expressed in all developing bone and thus holds an important role in bone biomineralisation. Nakashima et al. (2002) have revealed that knockout of Runx2 in mice showed no Osterix expression. Osterix activation enhances pre-osteoblasts to mature into osteoblasts. This is observed by upregulating the expression of mature osteoblast markers OCN, BSP and type I collagen (Komori 2006; Choi et al. 2011). Dlx5 is another important bone-inducing transcription factor, assisting in osteoblasts differentiation. Its major role is to induce BMP-2 downstream to transcription factor Runx2 leading to induce Osterix expression (Lee et al. 2003). Increased expression of Dlx5 is proposed to be associated with upregulation of OCN expression and gives an indication of mineralised matrix formation in culture (Tadic et al. 2002).

1.5: Non-Collagenous Extracellular Matrix Proteins

There are a number of non-collagenous extracellular matrix proteins (NCPs) in bone, which have vital roles in the regulation and direction of the construction and maintenance of the ECM. These proteins may only comprise about 2% of total bone weight, however, they play critical roles in development and embryogenesis, in addition to regulating the formation of collagen fibrils, signalling pathways and mineralisation control. These proteins are divided into several classes. In this review, the focus will be placed on OPN, due to its diverse functions in bone injury and healing.

1.5.1: Osteopontin (OPN)

OPN is also called secreted phosphoprotein. It was first identified in 1985 as sialoprotein (component of mineralised tissues, such as bone, calcified cartilage, dentin and cementum), derived from the bovine bone matrix (Franzén and Heinegård 1985). The name, OPN, is composed of 'osteon' that means bone in Greek and 'pons' the Latin word for bridge, which refers to OPN function as a linking factor (Reinholt et al. 1990). OPN is considered as a member of the Small Integrin-Binding Ligand N-linked Glycoprotein (SIBLING), of mineralised tissue-associated proteins (Fisher and Fedarko 2003). It is secreted by osteoblasts in the early phases of osteogenesis. It acts as an inhibitor for mineral formation and crystal growth. It is found in regions of reduced

mineralisation, such as bone cement lines, in addition to the periodontal ligament and root cementum. (Junaid et al. 2007) have suggested that OPN is also found in the cytoplasm and the nucleus of cells, which is called intracellular OPN and has a different function from that of secreted OPN. It is found in various cells, namely pre-osteoblasts, osteoblasts, chondrocytes, fibroblasts, macrophages, smooth and skeletal muscle cells and endothelial cells. OPN functions have been reported to be highly regulated because of post-translational modifications (Kazanecki et al. 2007; Boskey et al. 2013). Transglutaminase 2 enzyme can introduce a conformational change in cross-linking with OPN (Kaartinen et al. 2002; Nishimichi et al. 2009). Other enzymes, for example, thrombin, plasmin and matrix metalloproteases-3, -7 and -9, can induce functional motifs for cell attachment and migration (Agnihotri et al. 2001; Christensen et al. 2010; Lindsey 2015), and acts as a potent regulator of bone mineralisation (Boskey 1995; Pampena et al. 2004). OPN has also been reported to play an important role in chronic inflammatory diseases, such as Crohn's disease and multiple sclerosis, in addition to cardiovascular diseases and several types of cancer (Kahles et al. 2014). In contrast, OPN upregulates mineralisation at sites of pathological calcification, namely vascular calcification, renal crystals formation and gallstones (Imano et al. 2010; Hirose et al. 2012; Berezin and Kremzer 2013). Moreover, OPN has proposed to play a critical role in the development of adipose tissue and insulin resistance in diabetes in mice (Nomiyama et al. 2007).

1.5.1.1: OPN Role in Bone Biomineralisation and Remodelling

Recently, it is well-recognized that the critical physiological function of OPN is the control of the biomineralisation process. After an injury or surgical procedure, OPN acts as a secreted chemokine-like protein. It acts as a chemoattractant and an inflammatory amplification signal for neutrophil and macrophage recruitment to the site of trauma or injury (Cooper et al. 2005). OPN has also been reported as one of the earlier secreted proteins at the site of biomineralisation by pre-osteoblasts/osteoblasts or macrophages; and it is reported to be accumulated at the margins of the resorbed bone surfaces forming what is called “OPN-rich cement line” (Pedraza et al. 2008; McKee et al. 2011). OPN has been described to act through adhesion and also via cell signalling, to recruit the maturing osteoblasts to the bone surface area, regulating early steps of bone mineralisation and assisting in the bonding of new bone to current bone forming an OPN cement line (Pedraza et al. 2008; McKee et al. 2011). OPN has been described to have a high proportion of acidic amino acids and many phosphorylation sites distributed along the full-length of the protein. These kinds of properties allow for protein peptides to bind tightly to apatite crystals, acting as an opsonin to inhibit

their formation and assist in the bone remodelling process (Hunter et al. 1996; Addison et al. 2007; Hunter 2013). Bone remodelling is the physiological activity by which old bone is removed by means of osteoclasts, followed by bone formation by osteoblasts. The role of OPN in bone homeostasis not only involves inhibiting new mineral formation, but also by promoting osteoclast differentiation and enhancing its activities (Standal et al. 2004). Interestingly, knockdown of OPN was found to impair bone remodelling (Asou et al. 2001).

1.5.1.2: The Role of OPN in Obesity and Type 2 Diabetes Mellitus

Obesity is considered as a chief risk factor for insulin resistance development, which subsequently leads to T2DM and its complications. In obesity, there is a chronic low-grade inflammation which has been described as a substantial part of the expansion of adipose tissue. This inflamed adipose tissue has the ability to enhance the secretion of cytokines, which specifically recruit macrophages (Ahlqvist et al. 2013). These cytokines including resistin, visfatin, apelin, omentin, chemerin, IL-6, monocyte chemoattractant protein-1 (MCP-1) and TNF-α have a role of linking obesity to the development of insulin resistance (Gualillo et al. 2007). It has been observed that in mouse models, there is an elevated OPN expression in macrophages recruited to adipose tissue, following administration of a high-fat diet. In contrast, there is a significant reduction in adipose tissue expression of IL-6, TNF-α, MCP-1 and inducible nitric oxide synthase (iNOS) in the mice that lack the OPN gene. Interestingly, OPN reduction not only leads to decrease in adipose tissue inflammation, but also improves total body glucose tolerance as well as reduced insulin resistance in mice (Nomiyama et al. 2007). To date, the mechanism by which OPN is upregulated in inflamed adipose tissue remains unclear, despite OPN expression being enhanced by various cytokines and growth factors (Kahles et al. 2014). Some studies have indicated that after the analysis of adipose tissue cellular components, macrophages within adipose tissue are the main source of OPN in both human and murine genetic, in addition to diet-induced, obesity (Nomiyama et al. 2007; Kiefer et al. 2008). Of note, obesity and T2DM are strongly associated with hepatic disorders known as a non-alcoholic fatty liver disease (NAFLD). This is proposed to range from simple hepatic steatosis to non-alcoholic steatosis, in addition to steatofibrosis, eventually leading to liver cirrhosis and hepatocellular carcinoma, when OPN is upregulated. It has been noticed that OPN expression is also upregulated in the liver during obesity and hepatic OPN levels correlate with hepatic triglyceride content levels (Bertola et al. 2009).

1.5.1.3: The Role of Osteopontin in the Periodontium

OPN is known to regulate the mineralisation in both *in vitro* and *in vivo* study models, in both normal and pathological situations (Hunter et al. 1996; Boskey et al. 2002; Wesson et al. 2003; Erik Holm et al. 2014). It has been reported that OPN is one of the constituents of the ECM of both dental cementum and alveolar bone, within the periodontium (Bronckers et al. 1994; Mckee et al. 1996; Bosshardt et al. 1998; Foster 2012). Foster et al. (2018), have reported an important role of OPN in mineral regulation in the periodontium. They have suggested that OPN may influence the property of tissue density of the periodontal ligament, alveolar bone and cellular cementum. However, it does not affect the apposition of acellular cementum. Lack of OPN was reported to promote increasing bone volume and mineral tissue in mandibular bone in mice (Foster et al. 2018). Similarly, the formation of dentin and cellular cementum were also observed to be rapidly increased in absence of OPN, suggesting that OPN may regulate the pace of dentinogenesis and control the matrix mineralisation of the alveolar bone (Erik Holm et al. 2014; Foster et al. 2018).

There are contradictory findings between reports about the phosphorylated status of OPN (Neame and Butler 1996; Salih et al. 1996; Sodek et al. 2000; Qin et al. 2004). Dephosphorylation of OPN was described to render it less effective in biomineral regulation (Addison et al. 2007; Narisawa et al. 2013). The periodontium was proposed to be extremely rich in tissue-non-specific alkaline phosphatase isozyme (TNAP); an enzyme that hydrolyzes inorganic pyrophosphate (PPi) and potent inhibitor of the mineralisation process, expressed by skeletal and dental cells (Millán and Whyte 2016), where there is high activity of TNAP/ALP (Groeneveld et al. 1995; Bos and Beertsen 1999; Mckee et al. 2013). Therefore, Foster et al. (2018) have suggested that OPN in this area is relatively in a dephosphorylated state. This raises the possibility that the function of OPN may be more about cell attachment and signalling activities (Christensen et al. 2012). This piece of knowledge is valuable to be further studied in case of increased OPN levels in diabetes and whether its function here is for biomineral regulation or more for chemoattractant and signalling activities.

1.6: Macrophages

Macrophages have the prime role in response to pathogens by both innate and adaptive immunity. They control tissue homeostasis by secreting certain inflammatory mediators and regulate different steps of wound healing through secretion of cytokines and chemokines. Researchers have recently categorized macrophages into two main groups, residents and circulating macrophages. The resident macrophages are described to be derived from hematopoiesis of yolk sac of the embryo and reside in all tissue of mammals in uterus (Schulz et al. 2012; Sieweke and Allen 2013). Resident macrophages have been proposed to be heterogeneous and have the capacity of self-renewal. They can differentiate into macrophages in their 'home' tissue and take different nomenclatures according to the host tissue, such as osteoclasts in the bone, Kupffer cell in the liver and microglia in the brain. These unique classes of macrophage populations have been described to have various transcription profiles (Gautier et al. 2012).

The circulating macrophages have been reported to derive from monocytes which originate from hematopoietic stem cells (HSCs) in bone marrow and consequently may differentiate into macrophages (Akashi et al. 2000; Fogg et al. 2005; Liu et al. 2009; Hettinger et al. 2013). These macrophages can display two different phenotypes, the development of which is dependent upon the nature of stimulating factors, such as granulocyte-macrophage colony stimulating factor (GM-CSF) or macrophage colony stimulating factor (M-CSF). The former stimulating factor would trigger the cells to form macrophages specific for pro-inflammatory conditions and phagocytosis activities, in case of pathogenic stimulus and are called M1 macrophages, whereas the latter would drive the cells to display anti-inflammatory action by certain cytokines to repress the inflammation, remove the dead tissue and commence the repair process and are called M2 macrophages (Tushinski et al. 1982; Bartocci et al. 1987; Hamilton 2008; Yang et al. 2017). The function of the circulating and resident macrophage phenotypes is the same in all tissues. Nevertheless, circulating macrophages, which are described to stay for short periods (1-2 days) in the circulation, support the function of resident macrophage phenotypes according to the severity of the pathogen. In cases where they have not been recruited to face pathogens, they undergo apoptosis (Italiani and Boraschi 2014; Yang et al. 2017). M1 macrophages have been reported to produce chemokines in response to the presence of high levels of the pro-inflammatory cytokines of the inflamed area, such as TNF-α, and IFN-γ, IL-1β and IL-6, to help perform their phagocytotic activity (Sima and Glogauer 2013). On the other hand, M2 macrophages can be primed by IL-4 and IL-13; and exhibit anti-inflammatory markers, for example arginase 1 (Arg-1), IL-10, CD163 and CD206 (Sima and Glogauer 2013). This

classification, however, cannot reflect the *in vivo* environment, in which various cytokines can be secreted by other cells and may interact differently compared to *in vitro* state (Wynn et al. 2013).

1.7: Diabetes Mellitus (DM)

DM is a heterogeneous metabolic disease, associated with hyperglycemia due to insulin resistance. It constitutes a modern epidemic issue, affecting 382 million people according to the International Public Diabetic Federation in 2014. This number is expected to rise to 592 million by 2035. Interestingly, 90% of this number is T2DM. Thus, this review focuses on T2DM, due to its heavy societal burden. In 2012, the global mortality rate associated with T2DM was 4.8 million. Furthermore, the high level of the expenditure for its treatment was estimated at $471 billion. The normal blood glucose level is indicated as 5.5mM, for fasting plasma glucose. The increase in blood glucose above this level means that diabetes occurs (reviewed by Carnevale et al. 2014). For information, T1DM is an auto-immune disease, resulting from the destruction of β-cells of the pancreas, owing to a cellular mediated immune reaction. This leads to a total loss of insulin secretion (Graves et al. 2007). There are genetic and environmental factors involved in the disease progression. It has been reported that there is a rising trend of T1DM in children (Aathira and Jain 2014). Notably, the present study in going to investigate the pathological disorder of T2DM on bone repair.

1.7.1: Type 2 Diabetes Mellitus (T2DM)

T2DM is also formally known as ‘non-insulin-dependent diabetes’. The main pathology is the resistance to insulin, combined with a failure to provide enough additional insulin to compensate for this insulin resistance. T2DM is commonly accompanied by obesity, which enhances insulin resistance (Kahn and Flier 2000). Increase in adipose tissue can release metabolically active molecules, which are reported to inhibit cellular ability to respond to insulin, resulting in insulin resistance (Greenberg and Obin 2006). In two-third of obese individuals, insulin resistance can be overcome by increasing insulin production, identified by an increase in β-cell number. However, in one-third of those obese individuals, there has been found a marked decrease in β-cell numbers, due to apoptosis. This condition renders β-cells incapable of compensating for this insulin resistance and then, T2DM develops (Dickson and Rhodes 2004).

1.7.2: Signalling Pathways Involved in Hyperglycemic Complications

Hyperglycemia is reported to cause several perturbations associated with some metabolic pathways, which are considered to have significant roles in the etiology of diabetic complications. These pathways include; polyol pathways, AGEs, high levels of PKC activity and hexosamine biosynthesis pathways. Disturbances in each of these signalling pathways may affect the important cellular molecular activities, resulting in pathological changes (Vlassara 1997; Koya and King 1998; Asnaghi et al. 2003).

The polyol pathway has been found to be activated by hyperglycemia, which leads to enhancing formation of sorbitol and fructose by activation of aldose reductase and sorbitol dehydrogenase (Gabbay 1973; Greeneand and Stevens 1996). This pathway was reported to contribute to diabetic microvascular complications and sorbitol accumulation inside cells, which could cause cellular damage. In addition, D'Souza et al. (2009), have suggested that Runx2 activation during diabetic bone healing is regulated by the polyol pathway.

AGEs are non-enzymatic fragments of glucose molecules which bind to proteins. The number of glucose molecules that bind proteins is governed by the exposure time and the glucose concentrations. Thus, AGEs form and accumulate due to age, as well as in hyperglycemic conditions as in diabetes. They appear to have various deleterious effects on wound healing by different mechanisms, such as enhancing and prolonging inflammation, inducing cells apoptosis and affecting production, repairing and remodelling of the ECM (Owen et al. 1998; Vlassara and Palace 2002). It has been found that the blocking of AGEs improved the rate of wound healing in a diabetic mouse model. Likewise, down-regulation of pro-inflammatory cytokines, TNF-α, IL-6 and matrix metalloproteinase activity, subsequently improves matrix formation (Lalla et al. 2000). The effect of AGEs was also proposed to alter the bone metabolism, through the decreased expression of genes that enhance osteoblast differentiation, diminish growth factor production and lead to a reduction in ECM (Bouillon 1991; Lu et al. 2003). Despite AGE detrimental effects, a basal level of them has been reported to be required to maintain cell proliferation and osteogenic differentiation (Autréaux and Toledano 2007; Byon et al. 2008; Atashi et al. 2015).

PKC expression is reported to be increased by hyperglycemia. PKC is activated by a lipid second messenger diacylglycerol protein (Kingand and Brownlee 1996; Koyaand and King 1998; Hiramatsu et al. 2002). It is also enhanced by the increasing nicotinamide adenine dinucleotide /nicotinamide adenine dinucleotide reduced (NAD^+/ NADH) ratio (Kingand and Brownlee 1996; Good et al. 1998). Increased PKC expression has been suggested to stimulate reactive oxygen species (ROS) production, which in turn found to activate NADPH oxidase in endothelial cells, resulting in the progression of atherosclerosis in diabetic patients (Inoguchi et al. 2000).

Hyperglycemia can also activate and trigger hexosamine biosynthesis pathways (HBP). This leads to producing excessive flux of free fatty acids (FFA) and uridine 5-diphospho N-acetylglucosamine (UDP-GlcNAc) into the circulation and developing of insulin resistance (Hebert et al. 1996; Buse 2006). The activation of HBP and glutamine fructose-6-phosphate aminotransferase (GFAT), in addition to O-GlcNAclation revealed different pathological perturbations, which are proposed to directly participate in micro- and macro-vasculature complications, for example insulin resistance (Buse 2006), increased NF-κB-dependent promoter activation (James et al. 2002), in addition to developing of hyperlipidemia and obesity (Veerababu et al. 2000) (Figure 1.2).

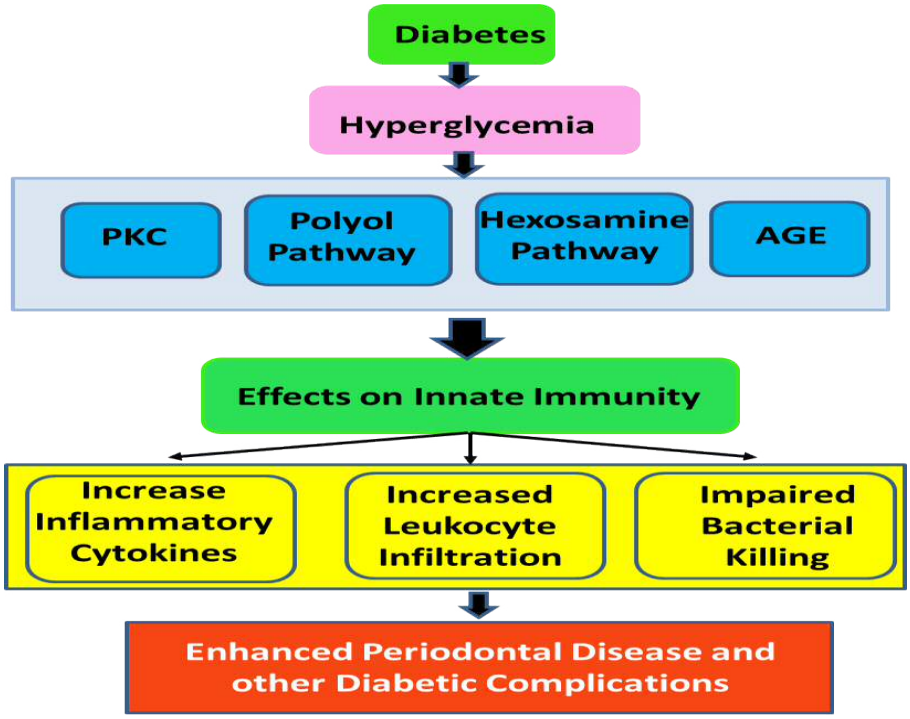

Figure 1.2: Signalling pathways proposed in diabetic complications (Adapted from Graves and Kayal 2011).

1.7.3: Cell and Tissue Damage Induced by Hyperglycemia

Hyperglycemia is known to be mostly accompanied by high ROS production and this induces oxidative stress in various tissue, which negatively affects cellular functions. Where ROS production exceeds levels of the endogenous antioxidants, this will result in a state of oxidative stress. In the absence of regulation of endogenous antioxidant within the body system, this will exert harmful effects on cells and their tissues (Rolo and Palmeira 2006; Fenga et al. 2013). Soardo et al. (2011) have revealed that FFA may act as a pivotal role in activating the oxidative stress in human hepatocyte cell culture. It has been also reported that a massive level of ROS may result in depolymerization of proteins, lipid and even DNA (Waddington et al. 2000; Moseley et al. 2004).

Glucose metabolism in the normal physiological state is performed through the tricarboxylic acid cycle (TCA cycle). This will activate electron pump channels to move the electrons across the mitochondrial membrane and produce the energy. High glucose concentrations in the environment, however, leads to increase in the voltage across the membrane and produces superoxide ($O_2^{\cdot -}$) by means of NADPH oxidases (Brownlee 2005). $O_2^{\cdot -}$ is considered as important ROS products and has a central role in the vasculature. Thereafter, $O_2^{\cdot -}$ undergoes a dismutation by superoxide dismutase enzyme (SOD) and form more stable ROS, namely hydrogen peroxide (H_2O_2), (Figure 1.3). H_2O_2 is then turned into H_2O and oxygen by the catalase enzyme (Taniyama and Griendling 2003). Notably, catalase has been reported as reduced and sometimes absent in diabetic tissues (Góth 2008; Waddington et al. 2011). The imbalance of these antioxidant molecules leads to accelerating cellular damage (Waddington et al. 2000). Nitric oxide has been also observed to be lower in diabetic patient, which affected the endothelial progenitor cells in term of number and functionality, causing an impairment of vascularization in a diabetic healing bone (Hamed et al. 2010).

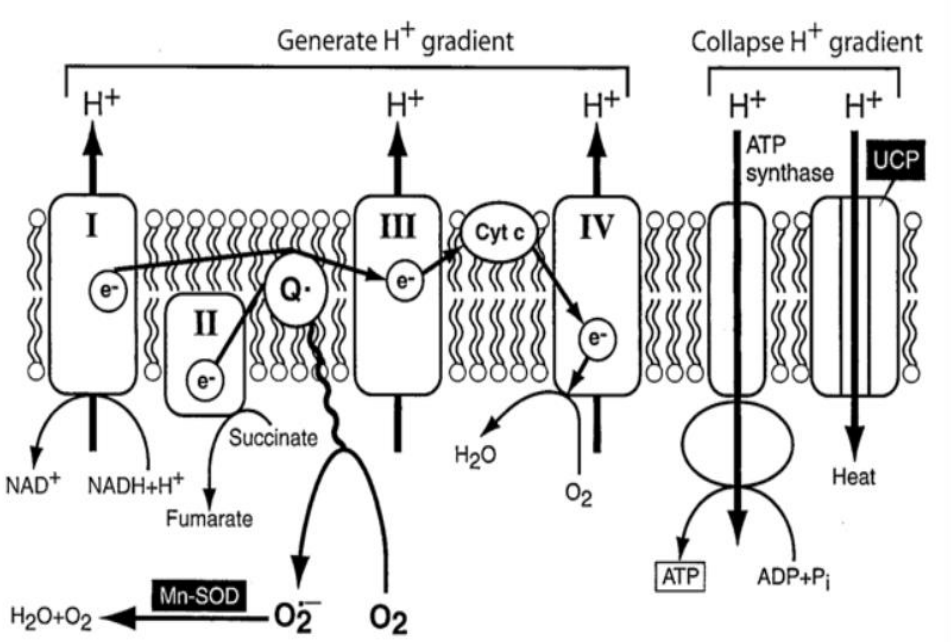

Figure 1.3: Diagram elucidates how hyperglycemia enhanced $O_2^{\cdot-}$ production occurs via the mitochondrial electron transport chain (Adapted from Brownlee 2005).

1.7.4: Diabetic Impact on Bone and Tissue Healing

Wound healing is a sophisticated process encompassing inflammation, granulation tissue formation and tissue repair and remodelling. Hyperglycemic environments due to diabetes have been found to have deleterious effects, resulting in impairment of wound and bone healing, such as a reduction in bone matrix formation (Suzuki et al. 2005; Kwon et al. 2008; Wang et al. 2010b). A broad number of studies have been conducted *in vitro* and *in vivo,* in order investigate the mechanisms by which hyperglycemia impairs bone healing. Evans et al. (2002), stated that this impairment may be due to possible alterations to some steps in the healing process. For example, the influx of progenitor cells, such as bone marrow and endothelial progenitor cells (EPCs) has been demonstrated to be delayed, which consequently results in decreased osteogenesis and angiogenesis (Fiorina et al. 2010). Moreover, hyperglycemia has been reported to reduce the proliferation and differentiation capacity of these cells (Albiero et al. 2011). In diabetic mice, EPCs were reported to possess decreased mobility in the circulation, due to impaired activation of endothelial nitric oxide synthase (eNOS) (Gallagher et al. 2007). The decrease in cell migration, in the pro-inflammatory cells, to the site of injury or fracture, may be another mechanism of impairment of diabetic wound healing. In case of inflammation, activation of macrophages, fibroblasts, endothelial cells and platelets results in triggering the release of essential cytokines and growth factors for maintaining the healing process

(Brem and Tomic-Canic 2007). In a diabetic environment, it has been proposed that the chemotactic ability to recruit the inflammatory cells to the wound healing site is lower than that in the normoglycemic environment. Fewer cytokines and growth factors also lead to reduced angiogenesis and bone repair (Medina et al. 2005). This alteration in the inflammatory profile and decrease in cellular immune response has been associated with higher levels of infectious complications in cases of uncontrolled diabetic rats (Blondet and Beilman 2007). The role of growth factors, such as TGF-β, IGF, VEGF and others, in bone matrix formation has also been found to be altered in diabetes. Dysregulation of these factors results in impairments of neovascularization and consequently, a reduction of oxygen and nutrient supply (Maruyama et al. 2007). AGEs stimulate TNF-α expression and matrix metalloproteinase enzymes, leading to reduced collagen deposition within the matrix. When associated with chronic inflammation, this tends to decrease ECM capacity to support growth factor activities, which delays the healing process (Al-Zube et al. 2009). Hyperglycemia has been found to induce 71 genes in diabetic animal models, that promote apoptosis and enhance caspase activity (caspase-3, caspase-8 and caspase-9), which have been reported to reduce the fibroblast density and affect collagen synthesis, resulting in lower matrix formation (Al-Mashat et al. 2006). Moreover, diabetes has been reported to drive progenitor cells into adipogenesis rather than osteogenesis, by means of PPARγ, which exacerbate the condition and delay bone healing (Botolin et al. 2005; Botolin and Mccabe 2007; Wang et al. 2010a). Such harmful effects on bone formation are also confirmed by the reduction of OCN concentration, which is an important biomarker for osteogenesis. In diabetic individuals, it has been reported that osteocytes have secreted a substance into circulation called sclerostin, which is an antagonist of osteoinductive Wnt/β-catenin (canonical) pathway, essential for osteogenesis (Gaudio et al. 2012; Carnevale et al. 2014).

1.7.5: Type 2 Diabetes Mellitus and Inflammation

Elevations in the levels of inflammatory systemic markers is a common feature of diabetes. It has been reported that the serum levels of TNF-α, IL-1 and IL-6 are increased (Senn et al. 2002; Borst 2004). This condition has serious implications which lead to micro- and macro-vascular complications. One major complication is the cardiovascular disease that contributes to the death of 80% of individuals with T2DM (Chiquette and Chilton 2002).

Diabetes has also been described to affect oral health, involving an altered inflammatory response to bacterial plaque. It has been reported that gingival crevicular fluid from diabetic individuals with

periodontal disease contained higher IL-1β and PGE_2 levels, compared with nondiabetic individuals with the same periodontal disease levels (Salvi et al. 1997). Naguib et al. (2004) investigated the inflammatory response of T2DM mouse to *P.gingivalis,* when inoculated into the connective tissues. The inflammatory response of both control and diabetes was similar after 1 day. At day 3, however, the inflammatory cells infiltrate was reduced in control, while it remained high in diabetic mice. Importantly, the bacterial killing mechanism was similar in both control and diabetic groups. However, the persistent inflammation exemplified by the prolonged high level of TNF-α can exacerbate the situation. Interestingly, knocking out TNF-α with etanercept, a recombinant TNF-α receptor, was reported to relieve the inflammation (Naguib et al. 2004). Thus, prolonged TNF-α presence and the dysregulation of cytokine signalling may be considered as important mechanisms by which diabetes might alter the host response to a pathogenic challenge (Naguib et al. 2004; Graves et al. 2007).

1.7.6: Diabetes and Cell Apoptosis

Apoptosis is a programed cell death that can be induced by several signaling pathways. By this mechanism, the body can remove unwanted cells during the developmental process, in addition to infected cells or those susceptible to be tumorigenic. Despite the low percentage of apoptotic cells at any given time, the cumulative effects of a one-day period in diabetic patient are considered to be quite high (Graves et al. 2006). It has been observed that apoptosis acts a pivotal role in several diabetic complications, namely nephropathy and myocardial apoptosis (Cai et al. 2002). Diabetes is usually associated with the formation of ROS, pro-apoptotic factors, AGEs and TNF-α. These factors have a different potency in apoptosis induction. Intriguingly, AGEs induce nuclear factor-kB activation, which acts as anti-apoptotic in most cell types (Cai et al. 2002). In other words, AGEs and the pro-apoptotic molecules, stimulate both anti- and pro-apoptotic factors; and the overall balance between them produce the net result (Alikhani et al. 2005). Therefore, increasing their levels in diabetic individuals tends to increase in apoptotic activities.

1.7.7: Diabetes Impact on Periodontal Disease

Diabetes has been undoubtedly confirmed as a prime risk factor for periodontal disease (Khader et al. 2006; Salvi et al. 2008; Chavarry et al. 2009). Diabetes increases the susceptibility of individuals to periodontal disease by twofold to fivefold. In addition, there is a well-established relationship between the hyperglycemic degree and the severity of periodontal disease (Preshaw 2009). The association between these two conditions, however, is not completely understood. The situation

between the two diseases involves various aspects, such as the immune function, cytokine biology and neutrophil activity. It is postulated by the United State National Health Examination Survey that adults with 9% Glycated haemoglobin A1c (HbA1c) level or more for diabetes, had significantly higher prevalence of severe conditions of periodontal disease, compared with those without diabetes (Tsai et al. 2002; Preshaw 2009).

There are several mechanisms proposed to elucidate how diabetes affects periodontitis, however, recently, more studies have focused on the established host response in periodontitis (Kornman et al. 1997; Preshaw 2009). The immune response to subgingival microflora reported being increased in diabetic individuals (Senn et al. 2002; Borst 2004). These include an increase in systemic markers, such as TNF-α and IL-6, prostaglandins and matrix metalloproteinases. The increase and dysregulated production of these immune mediators, altering and exaggerating the host response to bacteria, result in attachment loss, pocket formation and alveolar bone destruction (Preshaw 2009).

Impaired neutrophil function is another mechanism that may explain the diabetic impact on periodontal disease. Chemotaxis, adherence and neutrophil function have reported being impaired, in addition to delayed apoptosis activity in diabetic individuals (Darby et al. 1997; Rai et al. 2005; Graves et al. 2007). Neutrophils are the key defensive factors against periodontal plaque bacteria. However, delayed apoptosis may result in neutrophil retention in the periodontal tissues, which in turn, could elevate tissue destruction due to excessive release of destructive enzymes by neutrophils, such as matrix metalloproteinases and ROS (Preshaw 2009).

AGEs have been proposed as a further mechanism that link diabetes to periodontal disease. In hyperglycemic conditions, glycosylation of proteins, as well as matrix molecules, take place leading to AGE formation. The formation of these products is irreversible, which in turn, increased cross-linking to collagen molecules, contributing to various diabetic complications, decreasing blood vessels elasticity and contributing to periodontal tissue destruction. AGEs can trigger monocytes through surface receptor of AGEs, called RAGEs, resulting in the release of numbers of pro-inflammatory mediators, such as TNF-α, IL-1β and IL-6, which increase tissue damage (Lalla et al. 2001). Interestingly, Lalla et al. (2000) have demonstrated that blocking AGEs down-regulates matrix metalloproteinase activity, which may assist in the matrix formation. Taken collectively, this

evidence leads to conclude that diabetes appeared to increase the risk and exaggerate periodontal disease in comparison to non-diabetic individuals.

1.7.8: Periodontal Disease Impact on Diabetes

Recently, the fact that diabetes is considered as a risk factor to periodontal disease has now changed and recently, the focus on a new hypothesis 'two-way' relationship between the two diseases, where periodontitis could demonstrate negative effects on glycemic control (Preshaw et al. 2012). It has been found that severe periodontitis was accompanied by an increased risk of hyperglycemia in individuals with HbA1c > 9 % at a minimum of 2-years follow-up. This finding suggests that severe periodontal disease may be considered as a risk factor to enhance diabetes (Taylor et al. 1996; Costa et al. 2017). Another longitudinal study assessed the impact of periodontitis on the HbA1c levels of 2,973 non-diabetic subjects (Demmer et al. 2010). The participants who had advanced periodontal disease at baseline, exhibited an approximately fivefold increase in HbA1c during the 5 years of fellow-up, compared to those with no periodontal disease. This result predicts that periodontitis leads to progress HbA1c levels among non-diabetic individuals. The study is continuing to identify if these subclinical changes in HbA1c levels might progress into increasing the risk of diabetic incidence at 10 years. Meta-analyses of different studies indicated that there were reductions by around 0.4% of HbA1c in diabetic individuals, after effective treatment of periodontitis (Preshaw et al. 2012). Although this is considered as a relatively small change, it still demonstrates the impact of periodontitis on diabetes, however, more studies are needed to support this concept.

1.7.9: Macrophages Role in Obesity and Type 2 Diabetes Mellitus

Obesity was reported to induce a chronic state of low-grade inflammation (Kammoun et al. 2014). This inflammation was described not to be resolved as in acute inflammation, but results in certain implications, such as atherosclerosis and T2DM (Osborn and Olefsky 2012; Noto et al. 2013). The primary effectors of this inflammation are the immune cells through innate and adaptive immune systems. In adipose tissue, macrophages infiltrate and comprise the major effector type of immune cells (Okabe and Medzhitov 2014). M1 macrophage phenotype numbers were described to correlate with enhancing insulin resistance in obese rodents (Fujisaka et al. 2009). Patsouris et al. (2008), demonstrated that ablation of the M1 phenotype from the obese mouse by targeting diphtheria-sense CD11c+ cells, resulted in improved glucose tolerance. On the other hand, it has been suggested that M2 macrophages had positive effects by strongly promoting pancreatic β-cell proliferation (Xiao et al. 2014).

Macrophages were found to dynamically switch from one phenotype to the other, in response to their environmental conditions. In diabetes, M2 has been reported to transform to M1, resulting in loss of M1/M2 balance. Increase in M1 in the tissue is associated with more cytokines production, concurrently with a decrease in M2 cytokines. This will result in adipose tissue dysfunction and insulin resistance through impaired glucose tolerance. Of interest, PPARγ transcriptive factor has been proposed to play a major role in switching M2 to M1 cells (Shi et al. 2006; Davis et al. 2008; Kraakman et al. 2014).

1.8: Macrophages Role in Periodontal Disease

The chronic periodontal disease is known to affect the periodontium, due to dysregulated interactions between the subgingival bacterial biofilms and their host immune system (Pihlstrom et al. 2005). Macrophages are described to play an important role in fighting periodontal pathogens, resulting in periodontal inflammation (Poole et al. 2013). As a response to periodontopathic bacteria, the epithelial cells of gingiva, resident macrophages and other dendritic cells secrete cytokines and chemokines, such as IFN-γ, IL-1β, IL-6 and IL-8, that result in vasodilation to recruit neutrophils, which are considered as the first line of defence (Sima and Glogauer 2013). In addition, further circulating macrophages migrate to the area of infection and become active M1 macrophages. In this situation, the clinical symptoms of periodontitis have appeared (Yang et al. 2017). The increase in M1 cells and imbalance between M1 and M2 macrophages are likely to exacerbate inflammatory conditions. Interestingly, the immune system can control the infection in some individuals, which remains confined to gingiva during gingivitis. However, in other cases, when macrophages are activated to be more M1 rather than M2, inflammation is exacerbated, extending down to involve periodontal ligament tissue and the alveolar bone, resulting in periodontal tissue destruction (Yu et al. 2016).

1.9: Aims and Objectives

The aim of this Thesis is to elucidate the effects of a hyperglycemic environment on MSCs derived from compact bone (CB-MSCs), during expansion in culture; and in terms of osteogenic and adipogenic differentiation. This may demonstrate the detrimental effects of hyperglycemia on repair processes. OPN is profoundly investigated to determine its effects on bone

mineralisation and subsequently on the healing process, as it is proposed to be increased in hyperglycemic conditions. In addition, the role of LPS derived from *P. gingivalis* (*Pg*-LPS) in exacerbation of the inflammatory conditions associated with periodontal disease, was also investigated under normal and high glucose conditions. This will underpin the development of a solid knowledge, assisting in the successful management of periodontally-involved, patients with T2DM. The aims of this Thesis were achieved through the following objectives:

Chapter 2: Characterization of CB-MSCs at PD15, PD50, PD100 and PD200, in respect to the expression of a range of MSC markers, proliferative capacity, cell morphology and ageing. In addition, investigation of the hyperglycemic influence on these cells during long expansion in culture and the heterogenous profile of CB-MSC populations will be investigated.

Chapter 3: Investigation of the ability of CB-MSC populations to differentiate into osteogenic and adipogenic lineages. The influence of hyperglycemia on these populations, as well as the differentiation process was also assessed. The influence of hyperglycemia on OPN expression by these cells *in vitro,* was analyzed, in order to further understanding it's *in vivo* effects, which is proposed to hamper mineral formation and osteogenesis.

Chapter 4: Investigation of the effects of *Pg*-LPS on the osteogenesis of PD15 and PD50 populations of CB-MSCs (committed and immature), under normal and hyperglycemic conditions. The effects of *Pg*-LPS on OPN levels were also analysed in an attempt to understand the extensive bone destruction in periodontally-involved patients with T2DM.

Chapter 5: Investigation of the influence of hyperglycemia and *Pg*-LPS on M1/M2 macrophages and the role of M1/M2 macrophages on the expression and secretion of OPN upon exposure to the aforementioned factors alone and both together. That was in an attempt to imitate periodontitis and explore OPN detrimental effects on the healing in case of periodontitis complicated by T2DM.

Chapter 6 Summary of the main outcomes obtained from this Thesis.

Chapter 2: Characterization of Compact Bone Derived from Mesenchymal Stem Cells of Rat Femur

2.1: Introduction

Mesenchymal stem cells (MSCs) are considered to play pivotal roles in bone regeneration and repair, due to their ability to differentiate into osteogenic tissue, complemented by their self-renewal capacity (Caplan 1991; da Silva et al. 2006). The primary sources of MSCs during bone repair come from different sites, namely the bone marrow, periosteum and the endosteal surface of bones (Knight and Hankenson 2013). It has been reported through *in vitro* studies, that the osteoprogenitor cells involved in the healing of cortical (direct) fractures come from a perivascular source, with few from the endosteal niche (Pittenger et al. 1999; Bari et al. 2001; Noth et al. 2002; Bari et al. 2006). By contrast, it has been proposed during *in vivo* studies during secondary (indirect) fracture healing, that both intramembranous and endochondral ossification are required, involving the endosteal niche to provide MSCs for osteodifferentiation and bone repair (Zhang et al. 2005; Bielby et al. 2007). However, in all of these study cases, tracking of MSCs in terms of their migration and differentiation in order to participate in tissue formation, has been impeded by the lack of a consensus and a clear definition of the MSC phenotype (Bielby et al. 2007).

MSCs are proposed to consist of two types of cell niches. First, the perivascular niche, comprised around sinusoidal endothelial cells (Kiel et al. 2005; Sugiyama et al. 2006). This cell niche also contains the active hematopoietic stem cells (HSCs) involved in renewing the hematopoietic system (Wilson et al. 2008; Levesque and Winkler 2011). The perivascular/subendosteal niche is also described to have uncommitted MSCs (Balduino et al. 2012). Second is the endosteal niche, which is organized around pre-osteoblasts and osteoblasts from lining cells of endosteal bone surfaces (Kohler et al. 2009; Xie et al. 2009). This cell niche has, thus, been described to have more committed osteoblasts, which have been found to have greater involvement in bone repair (Balduino et al. 2012). Macrophages have also been described to be found adjacent to MSCs and osteoblasts necessary for supporting the functional integrity of these cell niches. Within this well-arranged endosteal cell niche, macrophages have been proposed to have a prime role in supporting hematopoietic cell activities (Chow et al. 2010; Winkler et al. 2010).

Isolation of MSCs from various tissues by different methods and approaches, has demonstrated inconsistencies in study outcomes (Muraglia et al. 2000; Peister et al. 2004). Subsequently, the characterization of cells has been difficult, due to the heterogeneous nature of MSCs and a lack of standardized criteria to define various MSCs isolated from different tissue

(Dominici et al. 2006). This led the International Society for Cellular Therapy (ISCT) to propose minimal criteria for MSCs identification. These criteria are firstly, MSCs should have plastic adherence by standard culture conditions. Secondly, the cells should express endoglin (CD105), 5'-ectonucleotidase (CD73) and Thy-1 (CD90) and at the same time, should lack expression of hematopoietic stem cell markers CD45, CD34 and CD14. Thirdly, these cells should be capable of differentiating into osteoblasts, adipocytes, and chondrocytes *in vitro* (Dominici et al. 2006).

These criteria, however, do not match the characterization requirements for all MSCs owing to several critical shortcomings. First, ISCT criteria lack a unique marker that can be universally shared between all organisms. The criteria emphasize on the positive expression of CD105, CD90, CD73, despite none of these markers being expressed by all human and animal species (Boxall and Jones 2012). Thirdly, the criteria refer to the ability of MSCs to differentiate into three independent lineages; osteoblasts, chondrocytes and adipocytes, whereas it did not refer to the multiple differentiation capacity, including the immature MSCs, which have been described to have the ability to differentiate into the majority of cells in the body (Abdalla and Kassem 2008; Samsonraj et al. 2015). It has been found that he plastic adherence can be shared by the majority of stem cell populations; thus, it is not such a unique MSC marker itself. Furthermore, these classical markers are seen to be upregulated or downregulated with increasing passage in culture (Jones et al. 2010; Halfon et al. 2011; Harrington et al. 2014). Eventually, it is very necessary to identify unique MSC markers, can presumably be found among both animals and human.

One of the prime characteristic features of MSCs is the hierarchy model that describes MSC heterogeneity. In this model, transit amplifying cells (TA) are proposed to be derived from mother stem cells after frequent proliferation and exhibit the greatest potential to form large colonies, demonstrating a higher proliferative capacity and highest multipotentiality. As cell division continues, TA cells demonstrate a decreased proliferative potential with smaller colonies and transform into lineage-restricted MSCs, exhibiting tri-, bi- and uni-potentiality (Chan et al. 2004; Phinney 2012). This hierarchy model might explain the described phenotypic and cellular differences, regarding MSC populations derived from bone marrow and compact bone.

Hyperglycaemia exhibits a great negative impact on bone healing and repair. High glucose affects all steps of bone healing. It has been found to interfere with cell migration and proliferation (Kim et al. 2013; Salabei et al. 2016). In addition, a high number of studies have shown that high glucose affects bone matrix formation by reducing the stem cells ability to differentiate into matrix

production cells (osteoblasts); and through apoptotic effects on these cells by oxidative stress and AGEs (Kwon et al. 2008; Fiorina et al. 2017). Consequently, high glucose directly impairs MSCs contribution to the healing process (Albiero et al. 2011). In addition to all of the above, ageing effects are important consequences, which subsequently lead to cell death. As cells divide, they undergo telomere shortening in each single division until the cells reach the Hayflick limit, when cells reach a limited point in their replication. Subsequently, the cells suffer from senescence but remain viable, although they are no longer able to proliferate (Hayflick and Moorhead 1961; Serakinci et al. 2008; Wagner et al. 2008). It has been found that MSCs in high glucose microenvironment demonstrate shorter telomere lengths with a decline in telomerase activity, due to the effects of oxidative stress, leading to premature cell senescence and ageing (Salpea and Humphries 2010).

This Chapter aims to provide a detailed characterisation of MSCs derived from the endosteal niche of the compact bone and how extensive culture expansion influences the heterogeneous phenotype of the MSC population within. MSCs are characterized with respect to the expression and retention of a range of MSC markers, including immature MSC markers; proliferative capacity, cell morphology and ageing characteristics. In addition, this Chapter has investigated how high glucose influences these cells during culture expansion with respect to ageing and the heterogeneous profile of the MSC population.

2.2: Materials and Methods

2.2.1: Isolation and Culture of Mesenchymal Cells from Compact Bone (CB-MSCs)

The cells used in this study were previously isolated by Dr. Norhayati Yusop, a PhD student at the Mineralised Tissue Group (MTG), School of Dentistry, Cardiff University. Cells were isolated from the femur and humerus of 28-day-old male Wistar rats by flushing the bone marrow using a 21-G needle and syringe filled with isolation medium (IM) [Minimal Essential Medium, (α-MEM), (Gibco, ThermoFisher Scientific, UK), 1% antibiotics-antimycotics (Sigma-Aldrich, UK)] to remove the bone marrow stromal cells. Bone diaphysis was cut into fragments (1-3mm^3) and the fragments were digested with 3mg/mL collagenase II (Sigma-Aldrich), in isolation media for 2h at 37ºC with agitation. After 2h, the digestion media with the released cells was removed and the bone chips were washed three times with 5mL of basal media [IM and 20% Fetus Bovine Serum (FBS) (ThermoFisher Scientific)]. The digested bone chips were incubated with basal media at 37ºC in a 5% CO_2 incubator. At day 3, the bone chips and the non-adherent cells were removed; and the remaining adherent cells were cultured to allow for expansion. At day 12, adherent cells were harvested using Accutase (Sigma-Aldrich) for 10-15min. This passage was considered as passage 0. Cells were then re-suspended in 1mL of basal media and 10µL of the re-suspended cells was mixed with 10µL of 0.4% trypan blue vitality stain; and cells were then counted using Neubauer hemocytometer with a light microscope (Nikon Eclipse TS100, Japan). Cells were reseeded and culture expanded in basal media. Culture media were changed every two or three days. Once the cells reached 80% confluence, further passages were performed and cell population doublings were determined. After each passage, a defined number of the cells were frozen in cryovials using Bambanker (Bambanker, serum-free freezing medium cryoprotectant, Alpha Labs, UK).

2.2.2: Determination of Cell Population Doubling Levels

Cell population doubling analysis was conducted to monitor cell expansion during the long-term culture period. This was determined by counting the total number of cells obtained, following accutase treatment and by calculating the total number of re-seeded cells; to establish the population doubling levels by the following formula:

$$PD = \frac{\log_{10}(\text{total cell counts obtained}) - \log_{10}(\text{total cell counts re-seeded})}{\log_{10}(2)}$$

2.2.3: Mycoplasma Testing of Cell Cultures

Mycoplasma testing was conducted using a VenorGeM Mycoplasma Detection Kit for conventional Polymerase Chain Reaction (PCR) (Cambio, UK), using 100µL of the supernatant sample taken from approximately 90% confluence cell cultures. Mycoplasma testing was routinely conducted every month for each culture. If found positive, cell cultures were treated with 10µg/mL BM-cyclin 1 and 5µg/mL BM-Cyclin 2 (Roche, UK), for 2 weeks with a repeated dose for 1 week until negative results were obtained.

2.2.4: Cryopreservation and Defrosting of Cells

Cryopreservation of cultured cells was performed by re-suspending the cells in Bambanker solution (Alpha Labs) at a concentration of $1x10^6$/mL. The vials were transferred into Mr. Frosty containers with isopropanol; and kept overnight at -80°C before being transferred into liquid nitrogen for long-term storage. Defrosting of cells was performed by quickly thawing the vial and washing the cells with working media, by applying the universal tube into the centrifuge at 400 g for 5 min.

2.2.5: Characterisation of CB-MSCs

All subsequent analyses were performed on CB-MSCs at PD15, PD50, PD100 and PD200 in normal glucose (5.5mM) and high glucose (25mM) conditions.

2.2.5.1: Gene Expression for CB-MSCs Markers

2.2.5.1.1: RNA Extraction and cDNA Reverse Transcription

Cells were seeded at 4,000 cells/cm^2 in three wells of 6 well-plates and cultured to 90% confluence. Total RNA was extracted using the RNeasy® Mini Kit (Qiagen, UK), as follows. The medium was aspirated from the well and cells were washed 3 times with phosphate buffered saline (PBS), before adding 600µL of lysis buffer [1mL of RLT buffer with 10µL of β-mercaptoethanol (Sigma Aldrich)], to the well for 1min. Cells were harvested and centrifuged with a QIAshredder tube for 2min at 10,000g (QIAShredder Kit), to homogenize the samples. The cell lysates were mixed with an equal volume of 70% (V/V) absolute ethanol (Sigma Aldrich), transferred to RNA Mini Kit columns and centrifuged for 15s at 8,000g. The flow-through was discarded from the columns and the remaining cell lysate solutions were washed with 350µL of RW1 buffer for 15s at 8,000g. The flow-through was discarded, 10µL of RNase-free DNase was mixed with 70µL of RDD Buffer (Qiagen, UK), and added to the column membranes for 15min. The columns were washed with 350µL of RW1 Buffer

and centrifuged for 2min. Two further column washes were conducted with 500µL of RPE Buffer, centrifuged for 15s and 2min, for the first and the second washes, respectively. The flow-through was discarded after each wash. The columns were transferred to sterile RNase-free, 1.5mL micro-centrifuge tubes (Eppendorf, UK), 30µL of RNase-free water was added to the columns and centrifuged for 2min. Obtained total RNA was quantified using NanoVue™ (GE Healthcare, UK) spectrophotometry. RNA purity was determined by A260/A280 absorbance, with values around 2 indicating good purity. RNA was directly stored at -80°C for use in reverse transcription reactions. cDNA was synthesized using 1µg of the total RNA sample by converting them to the equivalent volume, adding 1µL random primer (Promega, UK); and made the volume up to 15µL with nuclease-free water. This mix was applied to PCR machine (G-Storm™ GSI Thermal Cycler Software 45 V3.3.0.0), (Genetic Research Instrumentation Ltd., Braintree, UK); and set at 70ºC for 5 min. Meanwhile, the reaction master mix was prepared, containing 5µL 5X Moloney Murine Leukemia Virus Reverse Transcriptase (MMLV) reaction buffer, 1.25µL deoxynucleotide triphosphates (dNTPs), 0.6µL RNasin and 1µL MMLV enzyme, added to RNA-free water to 10µL. 15µL of random primer/RNA and nuclease-free water was added to the reaction mix to produce a final volume of 25µL cDNA. The final 25µL volume was applied to the PCR machine and set at 37°C for 1h. The negative control (RT negative) for each cDNA sample was tested, by adding 1µL of nuclease-free water to the RT master mix, followed by the same procedure above.

2.2.5.1.2: **Polymerase Chain Reaction (PCR)**

PCR was conducted using reagents obtained from Promega, UK. For each reaction, 1µL of cDNA sample was used with 5µL 5x buffer, 0.5µL (10mM) deoxyribonucleotide triphosphate (dNTP), 1.25µL forward and reverse primers, as shown in Table 2.1, 1µL (25mM) magnesium chloride, 0.25µL Taq polymerase; and 14.75µL RNA-free water, to a total volume of 25µL. Primer sequences were obtained from various related studies that fulfill the standards of the National Centre for Biotechnology Information (NCBI) Primer-BLAST software. Reactions were performed in a Thermal Cycler (G-Storm™ GSI), under the following conditions, one initial denaturation at 95ºC for 4min and thirty-five cycles of annealing and extension at 95ºC for 1min, primer-specific annealing temperature 55ºC for 1min; 72ºC for 1min, and a final cycle extension at 72ºC for 10 min. For the specificity of the reaction, negative controls, RT-negative (1µL of RT negative added to the PCR master mix) and PCR-negative (1µL of nuclease-free water added to the PCR master mix), were used. β-actin was used as an endogenous reference gene. PCR products were stored at -20°C.

2.2.5.1.3: Agarose Gel Electrophoresis for PCR Products

A 2% agarose gel was prepared by adding 1.4g of agarose powder (AGTC Bioproducts, USA) to 70mL of 0.5x tris/borate/ ethylenediamine tetra-acetic acid EDTA (TBE) buffer (89mM trizma base, 89mM boric acid and 2mM EDTA (Sigma-Aldrich). The solution was heated using a microwave, until the agarose had dissolved. The solution was cooled slightly, prior to mixing with 7µL of Safeview DNA stain (NBS Biological Ltd., UK). The mixture was poured into a casting tray, assembled with a well comb and left to set at room temperature. The gel was transferred to an electrophoresis tank filled with 0.5x TBE. 5µL of 100bp DNA ladder (Promega, UK) was added to the first well and 10µL of PCR samples/controls for analysis were added to subsequent wells. The samples were separated at 90V for approximately 50min. The band visualisation was performed using a GelDoc™ Scanner and Doc™ EZ Imaging System with Image Lab™ Version 5 (Bio-Rad Laboratories Ltd., UK).

Table 2.1: Primer sequences and product sizes of selected MSCs markers for RT-PCR analysis.

Gene	Primer Sequence Forward (F)& Reverse(R)	Product Length (b p)	Annealing Temperatue°C	Source
CD105	F: CGGTCTCCAGCTGCGGTGGTGGGCTCC R: CACTGCCACCACGGGCTCCCGCTTGCT	896	62	(Harrington et al. 2014)
CD 90	F: CCTGACCCGAGAGAAGAA R: TGAAGTTGGCTAGAGTAAGGA	125	55	(Harrington et al. 2014)
CD 73	F: TCCCGCGGCTGCTACGGCACCCAAGTG R: ACCTTGGTGAAGAGCCGGGCCACGCCG	204	62	(Scherer et al. 2012)
CD 45	F: AGCAATACCAGTTCCTCTATGA R: TCCGTCCACTTCGTTATGA	113	55	(L. Wang et al. 2010)
CD106	F: TCCACACTGACGCTGAGCCCTGTGGGTG R: CTCCGGCATCCTGCAGCTGTGCCTTGCG	898	55	(Harrington et al. 2014)
CD146	F: GCAGCGCCACGGGTGTGCCAGGAGAGG	900	62	(Harrington et al. 2014)

	R: CCCCACTGTGGTGCTTCTGGGCGGGCT			
Snail	F: GCGAGCTGCAGGACGCGTGTGTGGAGT R: CGGCAAAGGCACGGTTGCAGTGGGAGC	597	62	(Harrington et al. 2014)
Slug	F: CACTCCCCTCTGCCCAGCGGCCTTTCT R: GGCATGGGGGTCTGAAAGCTTGGGCTG	171	62	Lee CP PhD thesis (Cardiff University)
Oct4	F: GCCCACCTTCCCCATGGCTGGACACCT R: GCAGGGCCTCGAAGCGGCAGATGGTTG	563	62	Lee CP PhD thesis (Cardiff University)
Nanog	F: GGGGATTCCTCGCCGATGCCTGCCGTT R: GGGATACTCCACCGGCGCTGAGCCCTT	477	62	(Harrington et al. 2014)
TERT	F: GCTCCGGTTACACAGCAGCCCCTGGCA R: GGTCCAGAGCACGCACACGCAGCACGA	752	62	Lee CP PhD thesis (Cardiff University)
TR Terc	F: CTCCGCCCGCTGTTTTTCTCGCTGACT R: GCCACCGAACTCAGGGACCAGTTCCGT	300	62	Lee CP PhD thesis (Cardiff University)
β-actin	F: TGAAGATCAAGATCATTGCTCCTCC R: CTAGAAGCATTTGCGGTGGACGATG	155	55	(Gatto et al. 2008)

2.2.6: Cell Morphology

24-well plates were used and a 13mm glass coverslip (Coverslip, round 13mm, VWR, UK) was immersed in 70% alcohol for aseptic purposes, then rinsed in PBS and inserted into each well. Cells were cultured at seeding densities of 4,000/cm^2 and incubated for 24h at 37ºC in 5% CO_2 incubator. On the second day, the medium was aspirated and the cells were washed 3 times with α-MEM and fixed with 4% paraformaldehyde (Santa Cruz, USA) for 30min. The 4% paraformaldehyde was then aspirated and the cells were washed 3 times with tris buffered saline (TBS). Cells were permeabilized with filtered 1% Triton X-100 (Sigma-Aldrich) for 30min at room temperature and washed again three times with TBS, before blocking the non-specific binding sites with 1% Normal Horse Serum (Vector Laboratories, UK), in TBS for 1h at room temperature. Normal Horse Serum was removed and the freshly prepared phalloidin stain (phalloidin fluorescein isothiocyanate labeled, Sigma-Aldrich) (diluted 1:50 in TBS), was applied to the cells for 40min at room temperature. Cells were washed 3 times with TBS and left for 5min to dry. The cover slips in each

well were gently removed and mounted on the slide using 10µL of DAPI (Vectashield Hard Set, Vector Laboratories, UK). Images were taken by an AX70 Olympus Provis microscope with UV light, at 20X and 40X magnifications.

2.2.7: Colony Forming Efficiency (CFE)

Cells were reseeded in 6-well plates at 100 cells/well and cultured in the basal media, at 37ºC in 5% CO_2 incubator, for up to 5 days. The cells were viewed by light microscopy (Nikon Eclipse TS100, Japan) every 24h and the number of colonies (colony defined by Jones and Watt 1993, representing greater than 32 cells) were identified and recorded, using a marker pen on the underside of the culture well.

2.2.8: qPCR for Cell Cycle Marker (p53, p21 ^{waf1} and p16 ^{INK4a}) Expression

Expression of cell cycle markers (p53, $p21^{waf1}$ and $p16^{INK4a}$) was investigated using quantitative real-time polymerase chain reaction (q-PCR)**.** RNA was extracted and cDNA was prepared, as described previously (Sections 2.2.5.1.1). 1µg of the obtained cDNA was diluted 1:10 with nuclease-free water (Promega). For each q-PCR reaction, 2µL of 3µM primers (forward and reverse sequences, detailed in Table 2.2), were mixed with 10µL of 2x Precision FAST q-PCR Master Mix (Primer Design, UK); and 1µL of nuclease-free water. 5µL of diluted cDNA was applied in triplicate into white 96-well q-PCR plates (Primer Design), followed by 15µL of pre-prepared Master Mix. Plates were covered with adhesive optical seals (Primer Design); and centrifuged at 500*g* for 5min. q-PCR analysis was conducted in a QuantStudio™ 6 Flex Real-Time PCR System machine (ThermoFisher Scientific, USA), using QuantStudio™ Real-Time PCR Software (v1.0). Reaction conditions were as follows: one initial denaturation at 95°C for 20s, forty cycles of denaturation for 1s and annealing for 20s. After cycling was completed, melt curve analysis was performed as follows: 95°C denaturation for 15s, 60°C dissociation for 1min and 95°C denaturation for 15s. GAPDH was used as an internal reference control for data normalisation. The quantitative analysis of the gene expression was calculated using the ΔCt method, through expression the gene as a percentage of the GAPDH. Error bars represent standard error of the mean (SEM).

Table 2.2: Primer sequences, product sizes and the annealing temperature of the selected MSCs cell cycle markers for q-PCR analysis.

Gene	Primer sequence Forward (F), Reverse (R)	Product Length (b p)	Annealing Temperature °C	Source
$p16^{INK4a}$	F: TGCAGATAGACTAGCCAGGGC R: CTCGCAGTTCGAATCTGCAC	184	55	Author (Ahmed Al-Qarakhli)
p53	F: ACAGCGTGGTGGTACCGTAT R: GGAGCTGTTGCACATGTACT	83	55	P.Battersby (Cardiff University)
$p21^{waf1}$	F: TCTTGCACTCTGGTGTCTCA R: GGGCTTTCTCTTGCAGAAG	147	55	Author (Ahmed Al-Qarakhli)

2.2.9: Measurement of Cell Telomere Length

2.2.9.1: DNA Extraction for Telomere Restriction Fragment (TRF) Assay

DNA was extracted using QIAmp kits (Qiagen). Cells were seeded at 4,000/cm^2 in 6-well plates and cultured until 90% confluent. Cells were detached from the plate using accutase and centrifuged at 1,800rpm for 5min. The supernatant was discarded and the pellets re-suspended in 200µL PBS, mixed with 20µL proteinase K and 200µL of AL lysis buffer, both provided within the Kit. Samples were incubated at 56ºC for 10min and mixed by pulse-vortex for 15s. 200µL of 100% ethanol was added to each sample and mixed by pulse-vortex for 15s. Samples were transferred to QIAamp mini spin columns, setting in a 2-mL collection tube and centrifuged at 6,000g for 1min. The flow-through was discarded and the columns placed in a new 2mL collective tubes. 500µL Buffer AW1 was added to each column and centrifuged at 6,000g for 1min. The collection tubes were discarded and the columns placed in a new 2mL collective tubes. 500µL of buffer AW2 was added to each column and centrifuged at a full speed 20,000g for 3min. The columns were placed in a new 1.5mL micro-centrifuge tube, 200µL of buffer AE provided with the Kit was applied to the column, left for 1min at a room temperature and centrifuged at 6,000g for 1min. The obtained DNA concentration was quantified by spectrophotometry (NanoVue) and stored at -20ºC.

2.2.9.2: Measurement of Cell Telomere Length by (TRF) Assay

The telomere lengths of each DNA sample were determined using Telo-TAGGG Telomere length Assay Kit (Roche, UK), according to manufacturer's instructions. Each sample of DNA (1µg) was digested with Hinf1/Rsa (1µL) and 10X digestion buffer (2µL), to a final volume of 20µL with nuclease-free water. The samples were incubated at 37ºC for 2h. The reactions were terminated by 5µL gel electrophoresis loading buffer. Gel electrophoresis was conducted using 0.8% highly pure, nucleic acid grade agarose-agarose MP (Geneflow, UK) in 1X Tris-acetate-EDTA (0.04M Tris-acetate, 0.001M EDTA, 1X TAE). Digested DNA samples were loaded as following; 1µg of DNA digest equal to 20µL were loaded onto wells, in addition to 10µL of diluted DIG molecular weight marker (4µL DIG molecular weight markers, 12µL of nuclease free-water and 4µL loading buffer), in the wells on both side of the gel to ensure accurate length measurement and set at 20V overnight, until the bromophenol blue separated to about 10cm from the starting wells. The gels were transferred to a tank and submerged in a 0.25 M hydrochloric acid solution for 10min at room temperature. Gels were rinsed twice with distilled water before being submerged in 2X denaturation solution (0.5M sodium hydroxide, 1.5M sodium chloride) for 15min at room temperature and again, rinsed twice with distilled water. The gels were then submerged in 2X neutralization solution (0.5M Tris-HCl, 3M sodium chloride, pH 7.5), for 15min at room temperature. Washing steps were all performed with gentle agitation.

Southern blotting was conducted using a blotting unit (BIOS, UK). The tank within the blotting unit was filled with 2X standard sodium citrate buffer (SSC) (3M sodium chloride, 0.3M sodium citrate, pH 7.0). Four pieces of 3mm Whatman paper (Sigma-Aldrich) were placed on the platform of the blotting unit. The gel was applied over these papers. A positively charged nylon membrane (Roche, UK), was customized and applied on the gel surface to transfer the DNA signal. Four pieces of Whatman paper soaked in 20X SSC were placed over the nylon membrane, to enable the 2X SSC buffer in the tank to move through the nylon membrane to assist in the transfer of DNA. Finally, 10cm of dry paper towels was applied on the apparatus to assist in capillary movement; and topped with 2kg weight. The whole apparatus was covered with Saran Wrap, to prevent any evaporation and left overnight at room temperature to allow for proper transfer. On the morning of the second day, the 2kg weight was removed, the nylon membrane was taken, fixed twice for 10s, using UV-crosslinker (Stratalinker, USA) to make sure good DNA signal stickiness to the membrane. Hybridization steps were achieved in a hybridization oven (VWR, UK). The membrane was placed side up (DNA signal side) in the hybridization bottle and rotated gently on a rotisserie with 25mL

of DIG Easy Hyb (reconstitute the granules (bottle-9-kit from the Kit) with 64mL of autoclaved distilled water, incubated for 1h at 42ºC. This solution was replaced with 10mL pre-warmed hybridization solution mixed with 2µL of telomere probe and incubated at 42ºC for 3h. The membrane was washed with 25mL of 2X Stringent Wash Buffer I (2X SSC, 0.1% sodium dodecyl sulfate) for 5min at room temperature. Another wash was performed with 25mL of 2X Stringent Wash Buffer II (0.2 X SSC, 0.1% sodium dodecyl sulphate) for 20min at 50ºC and then a wash with 25ml of washing buffer for 5min at room temperature. After that, the membrane was incubated for 30min in 25ml of [1X blocking solution (dilution 10X (bottle 13 from the Kit), 1:10 with malic acid buffer)] and washed with 25mL washing buffer for 30min at room temperature. The membrane then incubated with 25mL [anti-DIG-AP working solution (Dilute bottle 14) 1:10,000 with blocking solution), and 1X detection buffer (Dilute 10X (bottle 15), 1:10 with autoclaved distilled water] for 15min, followed by a final wash for 5min with autoclaved distilled water at room temperature.

The membrane was removed from the hybridization bottle and incubated for 5min in substrate solution at room temperature and wrapped with Saran Wrap. The membrane was laid in a cassette (Hypercassette, UK), exposed to a high-performance Chemiluminescence Film (GE Healthcare) for 1, 2 and 5min, respectively. The film was developed using CURIX 60 Auto-Developer (AGFA, Belgium).

2.2.9.3: Densitometry Analysis

To calculate the telomere length, the chemiluminescence film containing the telomeric-specific smear of the Southern blot was scanned at 300 resolution. The image was opened in ImageJ software, rotated to align vertically to enable the analysis through converting the telomere-specific signal into mean TRF. To measure the optical density, 33 rectangular even size boxes were overlaid on each specific smear sample (Figure 2.1). The software then converted this optical density into numbers on an excel spread sheet. The background density was calculated using the average density of three boxes that did not contain a telomere-specific signal and subtracted from each box of the lane that contained the sample. The mean density (ODi) of each box containing DNA and the corresponding length (Li) according to the molecular weight ladders (measured in kbp) localized at the midpoint of the box were calculated and applied to the formula $\sum$ (ODi) / $\sum$ (ODi) /Li). Finally, the mean TRF was obtained (Kimura et al. 2010).

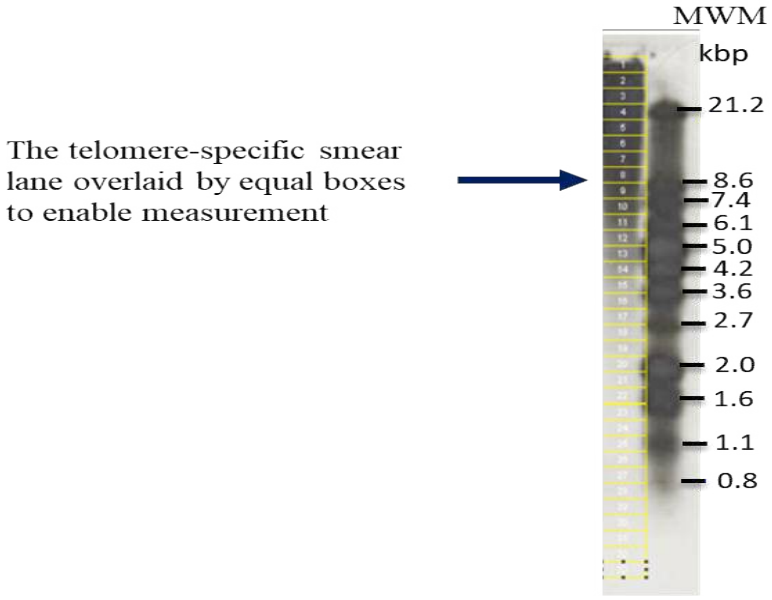

Figure 2.1: Southern blot image showing the boxes overlaid on the telomeric specific smear layer to calculate the mean of the telomere length, using ImageJ software.

2.2.10: Senescent Associated β-galactosidase (SA β-gal) Assay

A Senescence Cell Histochemical Kit (Sigma-Aldrich) was utilised to detect senescent associated β-galactosidase activity in senescent cells. In accordance with the manufacturer's instructions, cells were seeded in 6-well plates at 4,000/cm^2 and cultured in the basal medium at 37^{0}C, 5% CO_2, for 24h. The culture medium was aspirated and the cells washed 3 times with PBS, diluted 1:10 in ultrapure water. Fixation buffer was diluted 1:10 in ultrapure water (18.2MΩ H2O) and added to the cells (1.5 mL/well) for 7min at room temperature. Fixation solution was removed from each well and cells were rinsed 3 times with PBS (1mL/well). 1mL of pre-prepared staining mixture was added to each well and incubated at 37ºC at 5% CO_2 overnight. The staining mixture was removed and the wells were filled with 2mL PBS and sealed with parafilm to prevent dryness. 5 Images were taken by a light microscope (Nikon Eclipse TS100) for each well and then positive blue-stained cells were counted. Finally, the percentage of cells expressing β-galactosidase activity was calculated. Three repeats experiments were conducted.

2.2.11: Statistical Analyses

Statistical analyses were performed using One-Way ANOVA with a post-hoc Tukey test to determine the statistical differences between sample groups, using the software GraphPad InStat 3 (v3.06). Statistical significance of differences was defined as significant (*, $p<0.05$), very significant (**, $p<0.01$) or highly significant (***, $p<0.001$).

2.3: Results

2.3.1: CB-MSC Population Doublings (PDs)

CB-MSCs were cultured and PDs calculated for each passage (Figure 2.2). Cells reached 300PDs at about day 350 in both the normal physiological medium (5.5mM glucose, N) and the high glucose medium (25mM glucose, G). The cells in both media demonstrated a lag phase until about PD10 before the growth continued and PDs rose with time to PD300 at about day 350, without any signs of slowing growth rates.

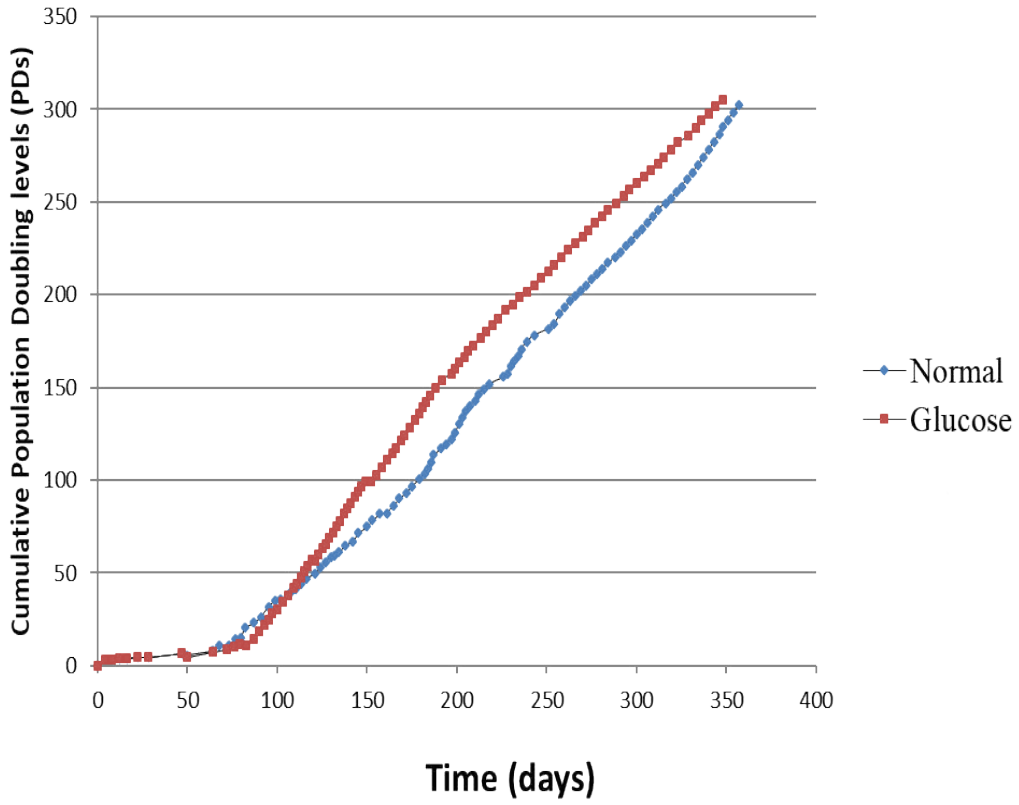

Figure 2.2: Population doublings for CB-MSCs represented by normal (5.5mM blue line) and high glucose media (25mM red line). Cells growing initially showed a lag phase for both groups. Seeding density was 10,000 cells/cm^2. Cell passage was always performed, when cultures reached 80% confluence.

2.3.2: Characterization of CB-MSCs

RT-PCR analysis of gene expression for CB-MSCs to identify the minimally defined gene expression markers for MSCs, CD105, CD90 and CD73. These markers were positively expressed in all sample groups (Figure 2.3). β-actin was used as a reference gene marker and consistently expressed throughout culture for all PDs in normal and glucose media. Hematopoietic marker expression CD45 was negative, whereas CD34 exhibited very low expression. CD146 was expressed in all samples, but exhibited low expression at PD200, in high glucose. There was no expression of CD106 or the pluripotent stem cell markers, Nanog and Oct4. Embryonic markers, Slug and Snail, had an even expression in all groups. In the case of the telomere maintenance markers, Tert and TR, Tert was expressed at PD15 N and PD100 N, whereas only trace levels PD50 N. In glucose exposed cells, Tert expressed at a high level at PD15 and showed a gradual decrease in expression at PD50 and PD100. Tert had no expression in PD200 for both normal and high glucose conditions. TR was expressed in both normal and high glucose conditions at PD15, PD50 and PD100, while showing faint expression in PD200 N, with no signal in PD200 G (Figure 2.3).

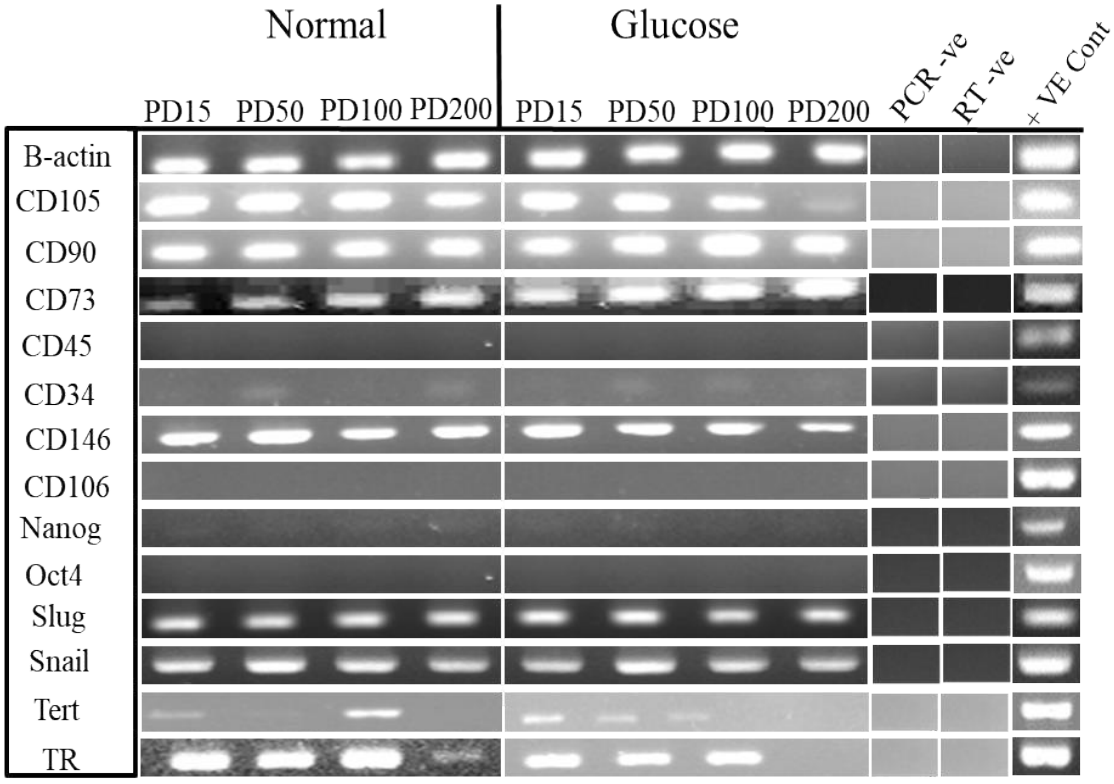

Figure 2.3: Expression of CB-MSC gene markers using RT-PCR, showed the mRNA expression profile of the classical MSC markers, CD105, CD90 and CD73. No expression of hematopoietic endothelial marker CD45 with very low expression CD34. There was also detectable expression of CD146, Slug, Snail and no expression of CD106 and Oct4, with trace expression of Nanog. Tert and TR were expressed in all populations except at PD200. TR showed faint expression at PD200 normal and glucose conditions.

2.3.3: Cell Morphology and Surface Area

Cells exhibited heterogenous morphology at PD15, with spindle, fibroblast-like and stellate shapes. PD50, PD100 and PD200 had more stellate-shape cells, with a typical feature of MSCs (Figure 2.4A). Cells were treated with FITC-phalloidin stain and digital images were taken using a fluorescence microscope (Figure 2.4B). PD15 N and G demonstrated significantly higher cell surface areas among all PDs (*** = p<0.001), with various shapes and sizes; both spindle and stellate. Some cells had stressed actin fibers, which appeared brighter under fluorescence (Figure 2.4A). PD50 cells exhibited more stellate shapes, and the cell surface area became significantly smaller than at PD15 (*** = p<0.001). PD50 G was significantly (*** = p<0.001) larger than PD50 N (Figure 2.4 C). PD100 cells were smaller and again maintained the same stellate shape, with the

cell surface area being the smallest of all PDs assessed (*** = $p<0.001$), PD100 G was smaller compared to PD100 N (*** = $p<0.001$) (Figure 2.4C). PD200 had stellate-shape with cells significantly larger than these under high glucose conditions (* = $p<0.05$) (Figure 2.4C).

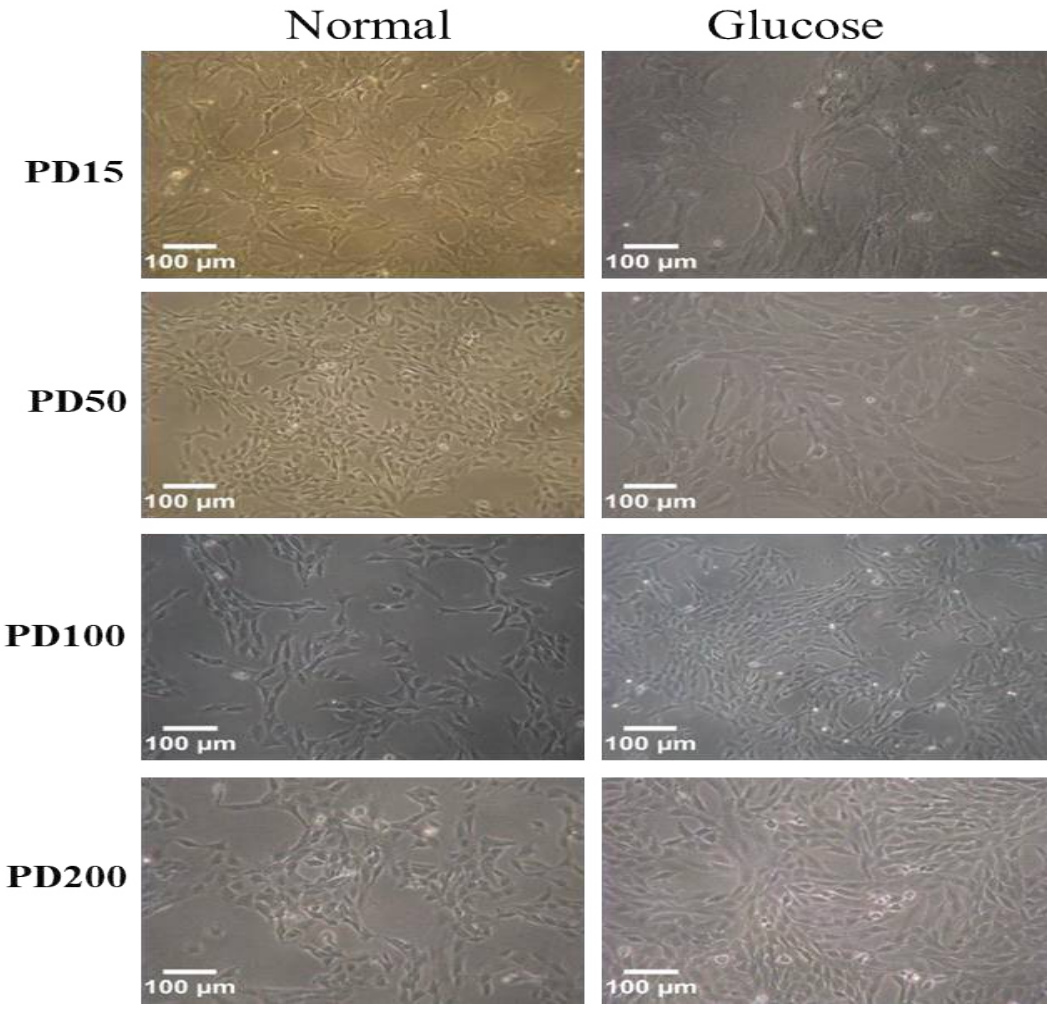

Figure 2.4: CB-MSCs morphology and measured the cell surface areas. **A**. Cells grown in normal (5.5mM) and glucose (25mM) conditions, showed heterogeneous morphologies. Cells at PD15 showed predominantly fibroblast-like shapes. Whereas cells at PD50, PD100 and PD200 exhibited more stellate morphologies. X10 magnification, scale bar 100µm.

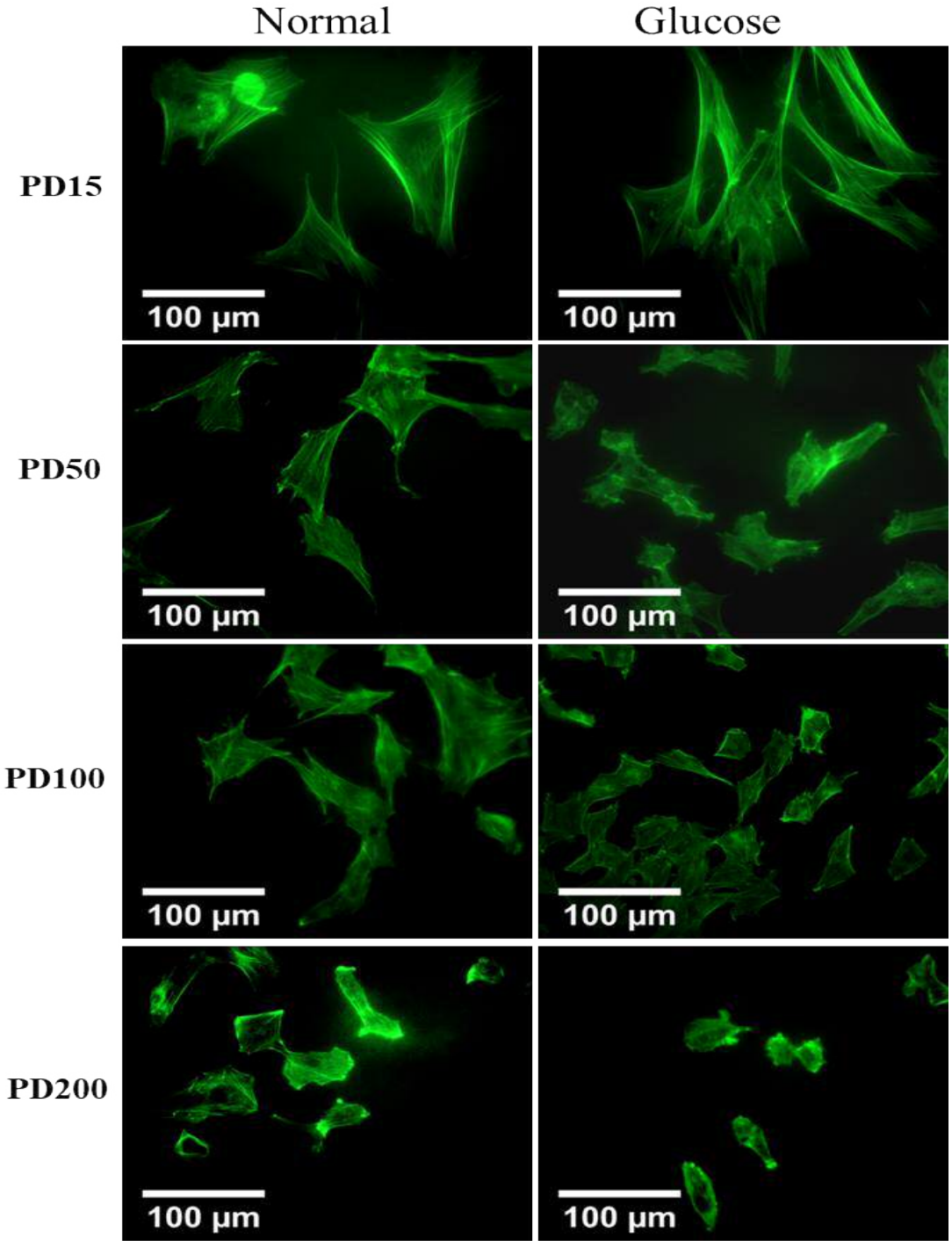

B. CB-MSCs were treated with FITC-phalloidin staining to examine the cell shape and measure the cell surface area. Digital images were taken at X40 magnification and the scale bar was 100µm.

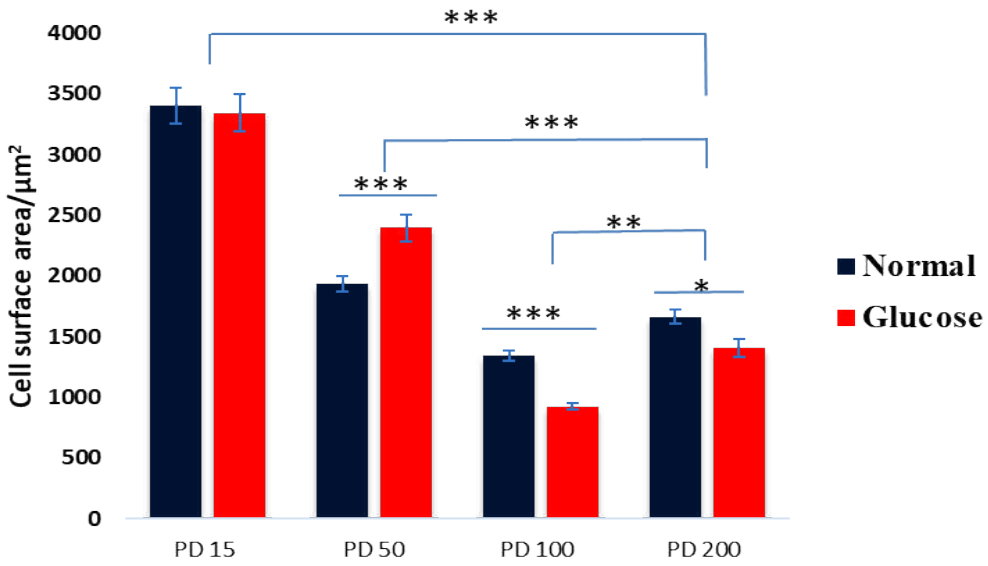

C. The bar chart demonstrated CB-MSCs mean of cell surface area. PD15 was the largest surface area. Cells became smaller with continuing expansion in culture. PD100 N and PD200 N cells were significantly larger than G groups. Error bar represents standard error of mean, * = $p<0.05$, *** = $p<0.001$.

2.3.4: Colony Forming Efficiency (CFE)

Colonies started to appear at day 3 in all groups, as at day 1 and day 2, the number of the cells were still less than 32 cells to be considered as a colony. PD15 showed very low colonies and significantly fewer numbers, compared to PD50, PD100 and PD200 (*** = $p<0.001$). PD50 and PD100 demonstrated increase in CFEs, however, there were no significant differences between them. PD200 G exhibited significant decrease in CFE formation at day 5, compared to PD100 G at day 5 (** = $p<0.01$). In contrast, PD200 N was significantly increased (* = $p<0.05$), compared to PD100 N at day 4 and day 5. PD15 demonstrated no significant differences between normal and high glucose conditions. PD50 and PD100 showed a significant increase in CFE in glucose, compared to normal conditions at day 3, day 4 and day 5 (* = $p<0.05$). PD200 exhibited significant decrease in CFEs under high glucose conditions at day 4 (* = $p<0.05$) and day 5 (*** = $p<0.001$) compared to normal conditions (Figure 2.5).

A)

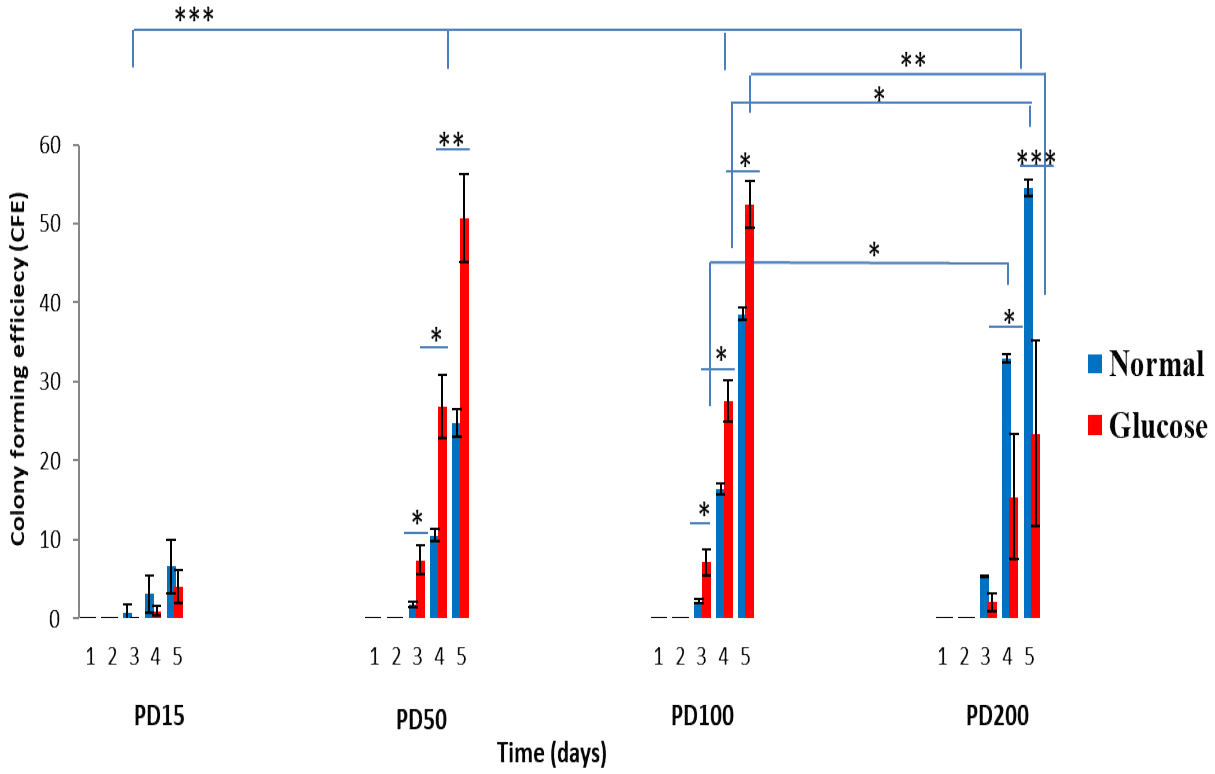

B)

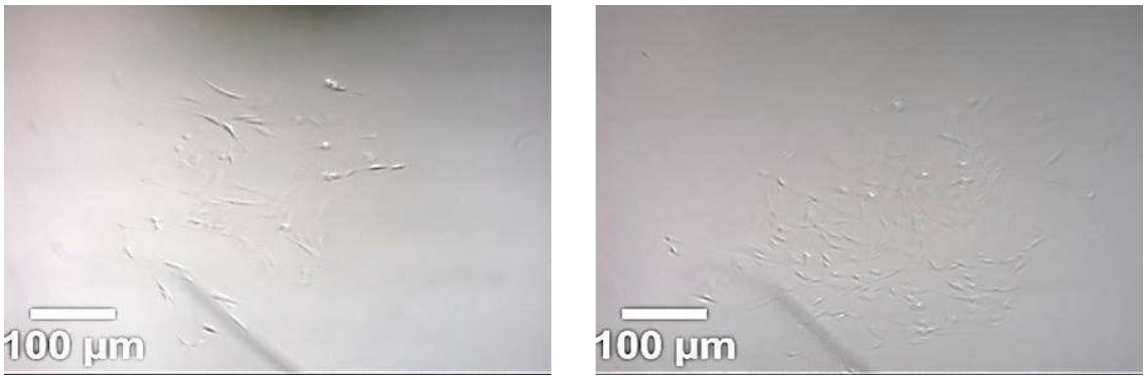

Figure 2.5: A. CFE capacity of CB-MSCs varied at different PDs. More committed cells (PD15) showed a lower number of CFEs, whereas more immature cells (PD50) exhibited gradual increases in CFEs. PD100 demonstrated the same trend as PD50. High glucose conditions at PD50 and PD100 significantly increased CFEs. Subsequently, PD200 showed a significant decrease in CFEs under high glucose. Error bar represents standard error of mean, * = $p<0.05$, *** = $p<0.001$. **B.** Image demonstrated one cell that proliferated to form a single CFE under normal glucose conditions (magnification 5X).

2.3.5: Cell Cycle Marker (p53, p21 ^{waf1} and p16 ^{INK4a}) Expression

Cell cycle marker (p16^{INK4a}, p53, and p21^{waf1}) expression by CB-MSCs, was investigated, using qPCR (Figure 2.6). p16^{INKA4a} gene expression, in general, was low in all groups. PD15 N and G demonstrated the highest expression of p16^{INK4a}, while differing significantly (p<0.05) compared to PD50 G and PD100 N. p21^{waf1} exhibited very low expression in all groups. p53 demonstrated a steady increase in gene expression from PD15 onwards until PD200. There were significant differences (p<0.05) in mRNA gene expression between PD15, PD50 and PD100 N. PD100 G exhibited significantly higher p53 expression, compared to PD100 N (p<0.05). PD200 N and G demonstrated significant gene expression, in comparison to PD50 N and G (p<0.05); and PD15 N and G (p<0.01) (Figure 2.6).

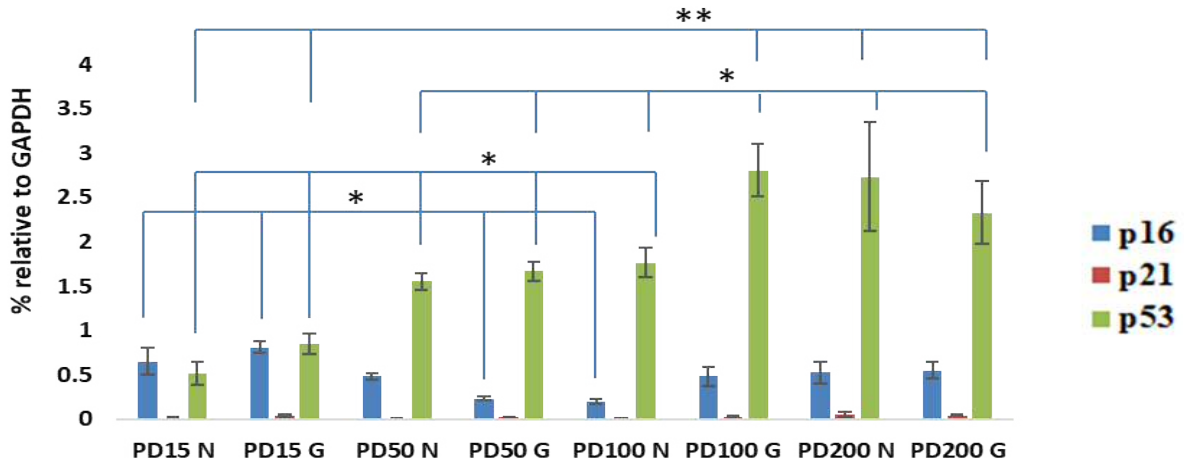

Figure 2.6: Detection of the cell cycle marker gene expression using qPCR. p16 ^{INK4a} gene demonstrated the highest expression level at PD15 N and G, whereas the lowest expression was in PD50 G and PD100 N (p<0.05). p21^{waf1} gene exhibited very low expression levels. p53 gene showed a gradual increase in gene expression from PD15 to PD200. (* = p<0.05, ** = p<0.01).

2.3.6: Terminal Restriction Fragment Assay (TRF)

The average telomere length of PD15 N was demonstrated as significantly shorter compared to PD50 and PD200 N (p<0.01) (Figure 2.7). PD15 had almost the same telomere length in N (20.4 kbp) and G (18.1 kbp) samples. PD50 and PD200 exhibited a significant increase in telomere length in N (p<0.01), which had average values 28.4-29.7 kbp respectively. In addition, these groups

showed significant decreases in telomere length in G compared to N (p<0.001). PD100 demonstrated the shortest telomere length in both N (14.4 kbp) and G (11.9 kbp) groups (p<0.001) (Figure 2.7).

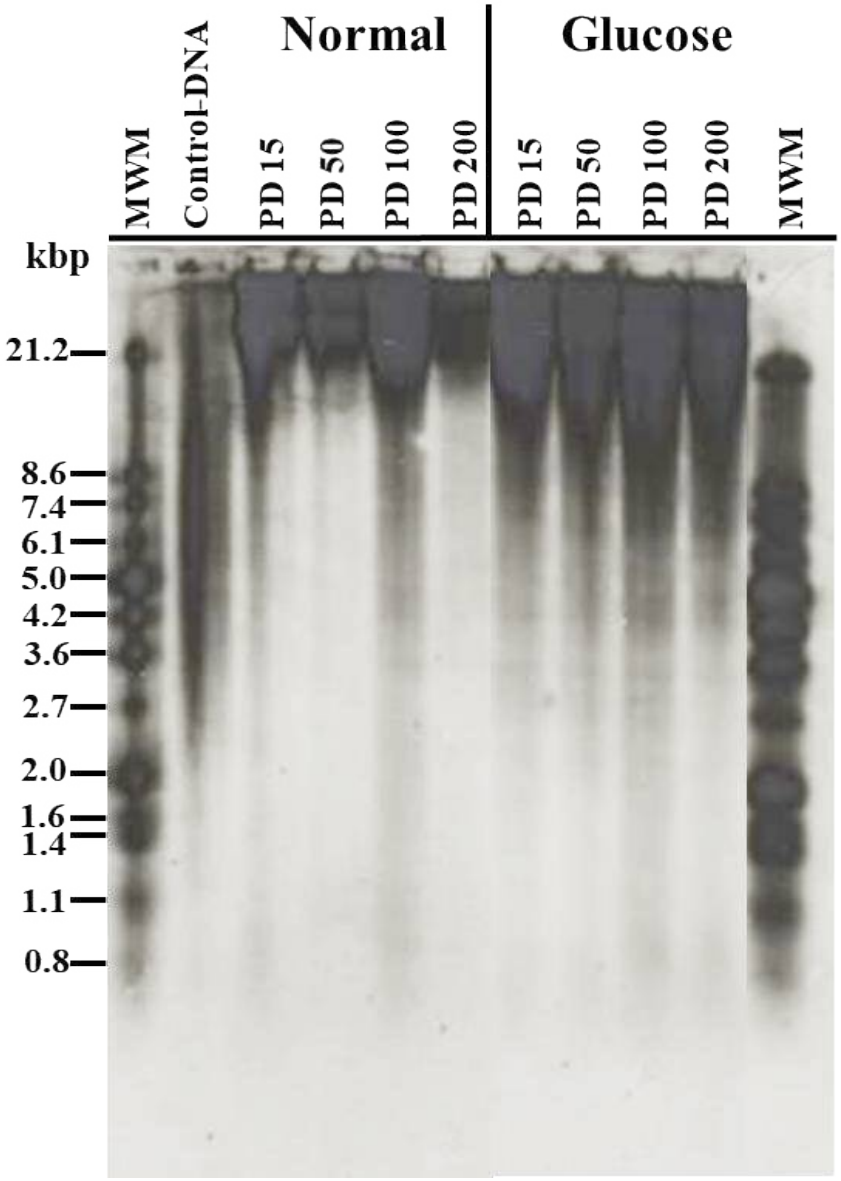

Figure 2.7: A. Southern blot to measure the average telomere length of the CB-MSCs exhibited the DNA telomere-specific smear of sample groups both N and G samples. Molecular weight marker contains the standard size ranging from 21.2kbp to 0.8 kbp. High glucose samples demonstrated significantly shorter telomere lengths expressed by the dark smear extended with their lanes (Southern blot were repeated three times).

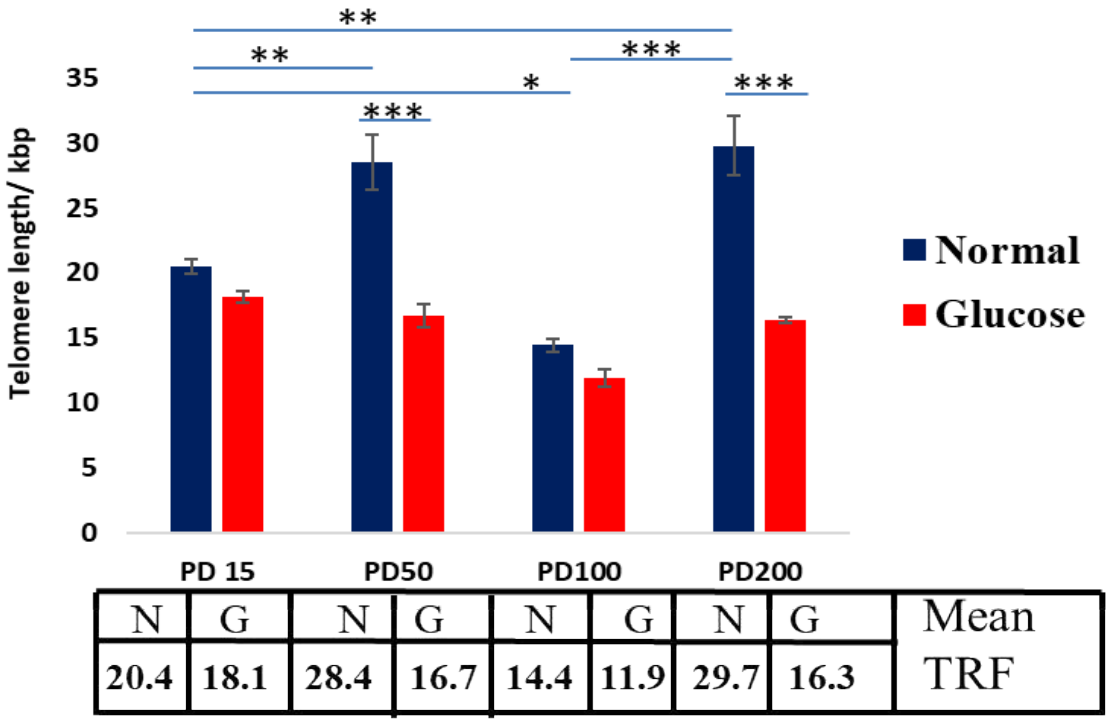

N	G	N	G	N	G	N	G	Mean
20.4	18.1	28.4	16.7	14.4	11.9	29.7	16.3	TRF

B. Bar chart demonstrates the terminal restriction fragment for sample groups of CB-MSCs telomere length. There were significant decreases in telomere lengths of G samples. PD100 was the significantly shortest telomere lengths for both N and G groups. Error bar represents Standard error of mean, (* = $p<0.05$, ** = $p<0.01$, *** = $p<0.001$).

2.3.7: Senescence Associated β-galactosidase Staining

Cells were treated with SA β-gal staining to visualize senescent cells. The overall number of senescent cells were low in all experimental groups. Although, the highest percentage of senescent cells were seen in the PD50 N and G. PD15 G demonstrated a higher number of senescent cells, compared to PD15 N, with significant differences (* = $p<0.05$). PD100 and PD200 exhibited the lowest number of senescent cells and were significant different to PD50 G (** = $p<0.01$) (Figure 2.8).

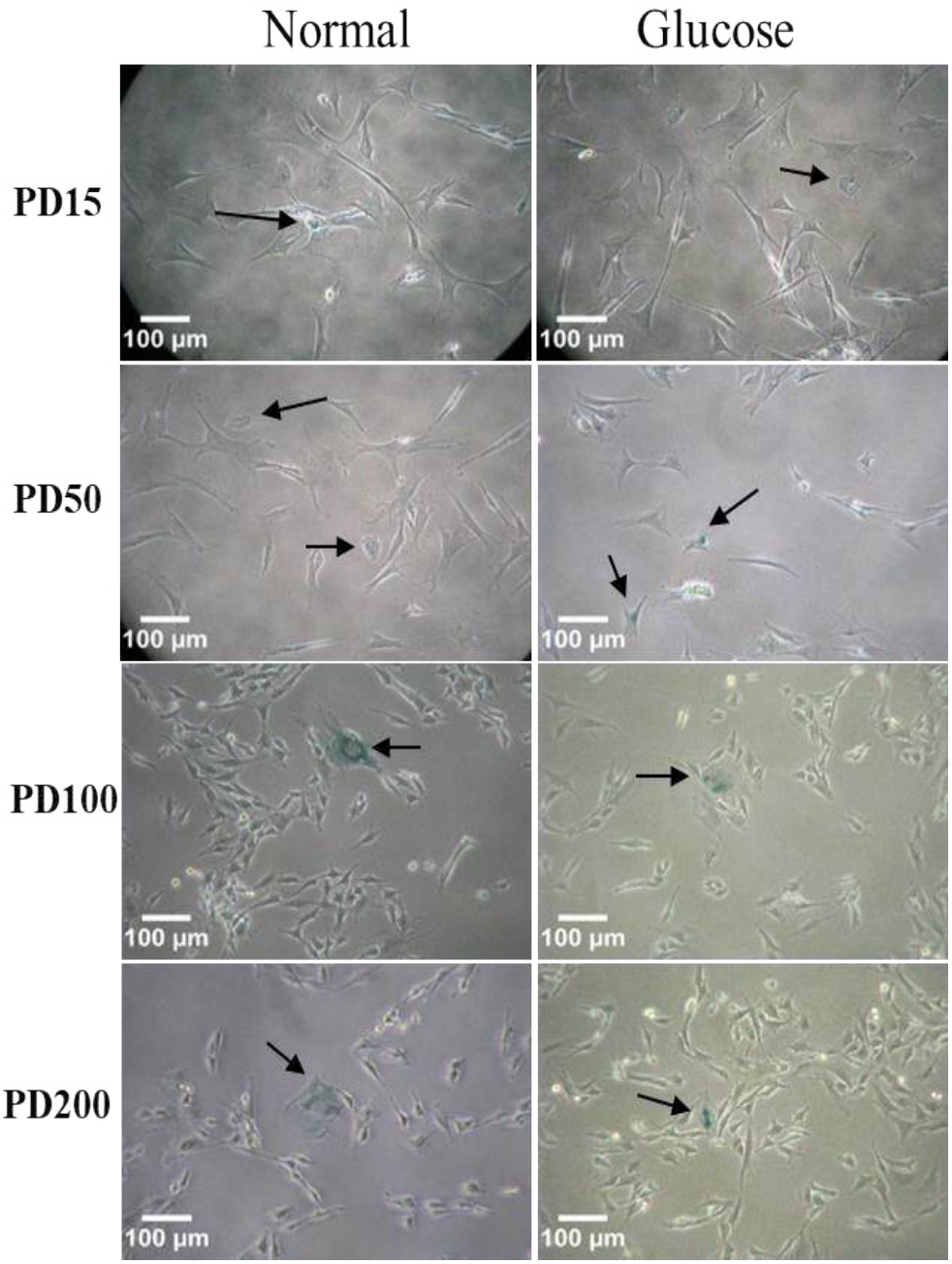

Figure 2.8: A. SA β-galactosidase staining of CB-MSCs to identify senescent cells. Images showed senescent cells were larger compared to normal cells with blue colour, pointed by black arrows.

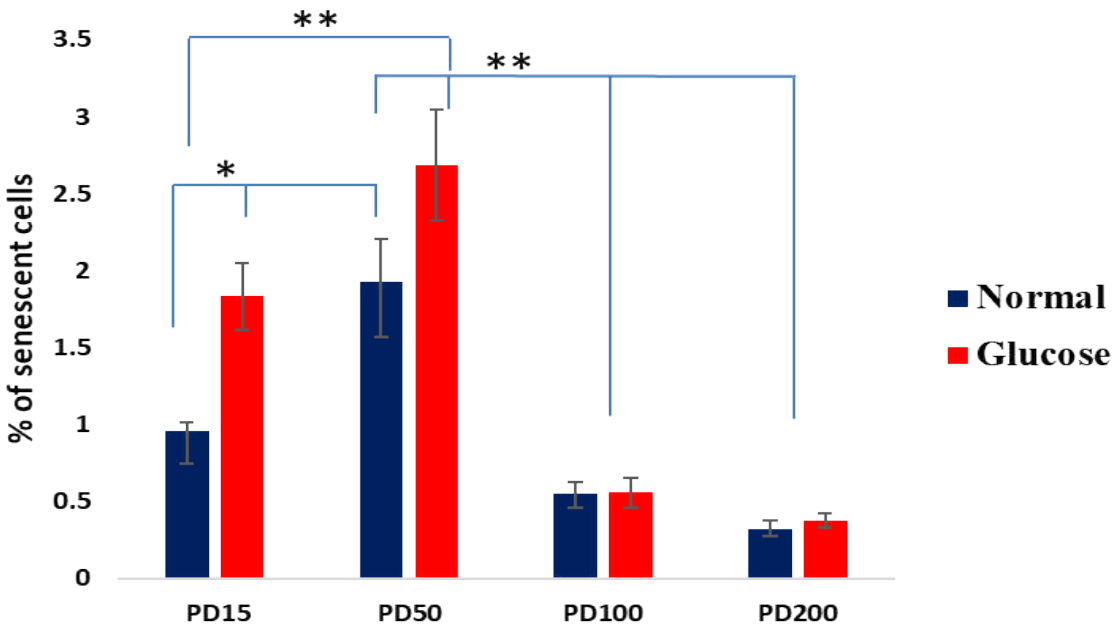

B. The bar chart demonstrated general low percentages of senescent cells overall. PD15 and PD50 demonstrated the highest percentage of senescent cells among all sample groups. PD50 in both N and G were higher than PD15, however, percentages of senescent cells decreased in PD100 and PD200. Error bar represents Standard error of mean. n=3. (* = $p<0.05$, ** = $p<0.01$).

2.4: Discussion

This Chapter showed a pronounced change in the heterogenous profile of CB-MSC phenotypes during extensive culture expansion. Hyperglycemia also exhibited distinctive effects on this change, linked to fasten regenerative rates, which then declined at late PDs and steadily decreased telomere length. These results would suggest that certain CB-MSC subpopulations have lost during culture expansion. High glucose demonstrates more detrimental effects by decreasing telomere lengths, which accelerated these changes.

At the beginning of *in vitro* culture expansion, MSCs demonstrated a slow-growing lag phase until around PD10. This trend has also been reported by (Harrington et al. 2014; Lee et al. 2015). This lag phase period may reflect low numbers of highly proliferative MSCs, concomitant with predominant committed cells; and/or the MSCs trying to adapt to the new culture environment, which is obviously different from the original *in vivo* niche environment. The cells then continued to proliferate gradually in a faster manner in both types of media.

During the cell expansion period, characterization procedures at PD15, PD50, PD100 and PD200, proposed to prove the criteria of ISCT and may underpin that these cells are pure MSC populations. However, this was not enough to further understanding of the heterogenous profile of these CB-MSCs. Extended characterization investigated a set of other markers to gain a wider knowledge. $CD146^{+}$ (Melanoma Cell Adhesion Molecule, MCAM) was expressed in all samples and is considered as an indicator of the ability of MSCs to differentiate into osteoblasts, chondrocytes and adipocytes. In addition, Russell et al. (2010), considered CD146 as a marker of multipotency. This leads to predict that CB-MSCs might be able to differentiate into another type of cell, however, this needs further studies to be proven. CD146 has also described to assist in cell proliferation (Sacchetti et al. 2007; Baker et al. 2014), that may be linked to the continuing CB-MSCs proliferation *in vitro* culture. CD106 (Vascular Cell Adhesion Molecule-1, VCAM-1) is reported as a positive on some of MSC surfaces (Liu et al. 2012); and has distinct roles in cell attachment, migration and cell signal transduction (Meirelles et al. 2006). Within CB-MSCs, CD106 was absent at all PDs. This result is in agreement with Mafi et al. (2011), who demonstrated its absence on a number of MSC surfaces and was observed to decline with prolonged cell culture. Embryonic pluripotent marker (Nanog and Oct4) expression is thought to be a key factor in maintaining pluripotency and self-renewal. Nanog had a very trace expression, while Oct4 had no expression. This lack of expression for Nanog and

Oct4 is similar to the outcomes of the rodent dental pulp (Kerkis et al. 2006). Furthermore, this would suggest that these CB-MSCs are more mature and multipotent, than being pluripotent cells.

To further extend characterization, Snail and Slug neural crest markers were investigated and found to be expressed at all PDs. These markers are implicated in epithelial-mesenchymal transition (EMT) (Aybar et al. 2003, Kokudo et al. 2008). They are described to promote commitment to a mesenchymal lineage and activation of a mesenchymal promotor (Solanas et al. 2008; Batlle et al. 2013). Expression of Snail and Slug within CB-MSCs would suggest a level of immaturity of some subpopulations and possibly having multipotent capacity rather than being tri-potent MSCs. Such a novel finding needs further investigation. Telomerase (TERT) and the RNA binding component (TR) were the last investigated markers, which demonstrated a decrease in their expression with long-term culture. These findings, however, did not perfectly relate to the mean telomere length results (TRF) which, for example, demonstrated an increase in mean telomere length at PD200. This may be linked to the heterogenous nature of CB-MSCs, which might have an immature subpopulation, possibly assists in increased mean telomere length. Furthermore, adult MSCs are unlike embryonic stem cells (ESCs), which exhibited a high level of telomerase activity (Hiyama and Hiyama 2007; Saretzki et al. 2010).

PD15 exhibited a heterogeneous cell morphology with varied shape phenotypes, such as large spindle, stellate and flat-shaped cells. In terms of CFE, this PD demonstrated cells with low ability rates. It is described that each clonal colony would proliferate at a rate controlled by its mother cell. So, when there is a low ability for colony forming, this may reflect that the mother cell has either reached a committed stage or approaching a terminal proliferative stage. This cell profile and colony forming ability trend, however, was found to be changed at PD50. Furthermore, at PD15 the average telomere length was shorter and cell morphology showed brighter actin stress fibers in some large cells treated by phalloidin staining, which would suggest that some of the subpopulation cells have a signs of a senescence (Asumda and Chase 2011). Taken all together, these characteristic features proposed that PD15 consisted of a heterogenous population and subpopulations of more committed cells and another possible population of immature cells. Herein, the $p16^{INK4a}$ cell cycle marker, which is proposed to be involved in cell growth arrest may support the notion that its presence may represent a subpopulation of mature osteoblasts differentiated from MC3T3 cells (Zhang et al. 2010). This marker was seen to be elevated at PD15. Cell cycle markers, $p21^{waf1}$ and p53, are known to act in a dependent and independent way to arrest the progression of the cell cycle at G1/S phase

to regulate cell proliferation and also acting as tumour suppressors (Macleod et al. 1995). Herein, $p21^{waf1}$ expression was very low in all PDs, which is reported to be upregulated when cells enter G0 (quiescent phase) (Spencer et al. 2013). This suggests the expression of $p21^{waf1}$ and p53 would come from the active proliferative subpopulation within CB-MSCs.

This heterogenous nature of the PD15 population might 'suffer' from senescence and was noticed to have changed at PD50, when the spindle-like cells disappeared leaving MSCs with smaller cell surface areas, demonstrated by predominant stellate-like cells. This would link to the large cells seen at PD15, as a committed large cell lineage is proposed to be lost during the expansive culture, leaving a subpopulation of immature cells. This speculation may be inferred, due to a marked longer mean of telomere length, highly proliferative capacity within this population; and the significantly declined mean cell surface areas, compared to PD15, may be attributed to the loss of the large spindle cells. SA β-gal stain, however, demonstrated low percentages number of senescent cells. This stain is known to be active only in senescent cells not in quiescent, pre-senescent or differentiated cells (Dimri et al. 1995), due to increasing lysosomal mass through long cellular replication (Lee et al. 2006). This may explain the low number of SA β-gal stained cells. Looking to a low expression level of cell cycle markers, $p21^{waf1}$ and p53, in addition to the $p16^{INK4a}$ cell cycle inhibitor, this would reflect the active proliferative rates at PD50 of CB-MSCs during expansion period in culture (Spencer et al. 2013).

Investigation of CB-MSCs at PD100 during continued culture expansion suggested an important senescent change. The main difference here was the significant decrease in mean telomere lengths. It is well-documented that shortening of telomeres is associated with cell ageing and senescence (Hiyama and Hiyama 2007; Salpea and Humphries 2010). CB-MSCs, however, exhibited no decline in the proliferation nor in the colony forming ability; and they again showed a decline in cell surface area. This may lead to expect a presence of a high proliferative subpopulation within the heterogenous populations of CB-MSCs. Upregulation of p53 expression was seen here, which refers to ageing effects specifically in the high glucose group. Whereas expression of $p16^{INK4a}$ may be linked to the process of shortening of the telomere, although some studies reported no link between the two processes (Rayess et al. 2012). Furthermore, other studies find the expression of $p16^{INK4a}$ is due to the accumulation of reactive oxygen species in bad culture environment (Ramirez et al. 2001).

At PD200, CB-MSCs continued growing and actively expanding in culture. Intriguingly, the pivotal changes here, were significant reduction in colony forming ability in high glucose and some of MSC markers disappeared. Reduced CFE capacity in glucose group would be as a result of the long-term effects of hyperglycemia on regenerative capacity on CB-MSCs (Albiero et al. 2011). While loss expression of CD105, TERT and TR was reported due to long-term expansive culture (Russell et al. 2011). Herein, telomere lengths recorded significant increases, which could come from a growing immature high proliferative population within the heterogenous population. Expression of a high level of p53 and a low level of $p21^{waf1}$ suggest a low level of DNA damage and thus, means a healthy cell cycle although with a trace expression of $p16^{INK4a}$ (Rayess et al. 2012). Investigation of population changes, however, require further confirmation by a more sophisticated approach to track the cells to provide evidence to elucidate how these changes in subpopulations happen.

Worthy of remark within this study, high glucose has shown significant effects on CB-MSCs, in terms of regenerative capacity of this heterogenous population. Telomere length reduction was reported to be associated with an increased level of oxidative stress and advanced glycation end products (AGEs), come from high glucose, which in turn induce oxidative telomeric DNA damage and eventually shortened telomeres. Ultimately this leads to premature cell senescence (Salpea et al. 2010; Salpea and Humphries 2010). Interestingly, the CFE data demonstrated significant increases at PD50 and PD100. These findings are in disagreement with that of Li et al. (2007) and Stolzing et al. (2011), however, they both were using cell-lines and Li was using telomerase immortalized cells, which may differ from the CB-MSCs. Subsequently, the probable cumulative effects of high glucose demonstrated a significant decline in CFE at PD200. This may reflect the long-term detrimental effects of glucose on the regenerative capacity of MSCs, when ultimately leads to delay the healing ability (Li et al. 2007; Albiero et al. 2011; Stolzing et al. 2012). Another ageing and detrimental effect, which may be attributed to high glucose is significant increase in p53 expression when CB-MSCs underwent long-term culture at PD100 and PD200 (Stolzing et al. 2011), whereas a low expression of $p21^{waf1}$ indicates continued growth in culture (Spencer et al. 2013). It is also observed that increased $p16^{INK4a}$ expression may be linked to DNA damage (Giacinti and Giordano 2006). On the other hand, MSCs became smaller in surface area, which was reported with increased cell proliferative capacity and telomere length according to Samsonraj et al. (2015). Taken together, these findings reveal pronounced harmful effects of high glucose on the heterogenous population of CB-MSCs during an expansive culture period, which may reflect that one of the subpopulations could be affected more than the other, for example, immature and committed mature populations.

Understanding this valuable part of high glucose effects would open the door for deeper knowledge, which is still vague and requires further investigations.

One limitation of this study related to the measurement of telomere lengths, which needs to be considered. In this study, telomere length was measured by terminal restriction fragment assay (TRF). Although TRF has been a widely-used method, there are certain limitations, such as measuring the mean telomere length of all subpopulations. Thus, this technique is less sensitive in the heterogeneous population, when there are different cell phenotypes (Aubert et al. 2013). However, such a technique was only available to be used in our laboratory and would uncover a general insight about the change in telomere length in CB-MSCs populations and the effects of high glucose. Alternatively, the recommended technique to be considered for future work is the single telomere length analysis (STELA), using picogram range of DNA to individually evaluate cells (Baird et al. 2003).

Overall, results from this Chapter suggested that the isolated CB-MSCs have heterogeneous populations with different proliferative capacities and susceptibility to prolonged culture expansion and high glucose exposure. There was a change in this heterogeneity at PD50 confirmed by an increase in CFE, smaller cell surface area and longer telomere length that infers to the presence of more immature cells. Long-term cell expansion in culture demonstrated no effects on various MSC surface markers. High glucose exhibited a reduction in MSCs regenerative capacity as the CFE decreased; and a marked shortening of the telomere length. However, both normal and glucose groups have successfully continued expansion in culture. Further investigations to prove the ability of CB-MSCs to bi-potent capacity; differentiate into osteogenic and adipogenic lineages will be shown with the forthcoming experiments.

Chapter 3: Effects of High Glucose on the Bi-differentiation of CB-MSCs Osteogenic and Adipogenic Lineages

3.1: Introduction

MSCs have been demonstrated to possess the ability to differentiate into various cell phenotypes, such as osteoblasts, chondrocytes, adipocytes and neural cells (Sharma et al. 2014). MSCs derived from bone are the main source of proliferative osteoprogenitor cells, which can be induced to differentiate into pre-osteoblasts and then into osteoblasts (Walsh et al. 2001; Porter et al. 2003).This process can be achieved through series of complex steps; proliferation, differentiation, matrix deposition and mineralisation; and eventually obtaining a mature osteocyte. This process has been found to be affected by the tissue microenvironment, such as during hyperglycemia (Juncheng et al. 2013). Consequently, this could impair bone repair and regeneration processes. However, the exact mechanisms involved in hyperglycemic-induced bone loss remain unclear.

Although glucose is a central source of energy for all cells, it has been noted that a hyperglycemic microenvironment in rat MSCs, affects self-renewal, proliferation, and differentiation, in addition to enhancing early premature cell senescence and apoptosis (Albiero et al. 2011 Kim et al. 2013; Salabei et al. 2016). Impairment of MSC proliferation and differentiation has been attributed to a chronic exposure to advanced glycation end products (AGEs) and reactive oxygen species (ROS), which are found increased in the circulation during hyperglycemia (Denu and Hematti 2016). Although detrimental effects are associated with these products, a normal physiological level of them have been reported to be required to maintain cell proliferation and osteogenic differentiation (Autréaux and Toledano 2007; Byon et al. 2008; Atashi et al. 2015). Increased levels of oxidative stress are proposed to activated various cell signalling pathways, such as PI3K/Akt and cAMP/protein kinase A (PKA)/extracellular signal-regulated kinase (ERK) pathways, that not only inhibits osteogenic differentiation, but stimulates adipogenic differentiation, leading to osteoporosis, abnormal bone healing and repair (Botolin et al. 2005; Botolin and Mccabe 2007; Wang et al. 2010a).

A number of studies have investigated the effects of high glucose on MSCs. As far as it is being aware, however, most of these studies do not specify whether the detrimental effects of high glucose are on mature MSCs, immature cells, transit amplifying TA or on osteoprogenitor cells. Obtaining

this piece of knowledge would assist in more understanding the healing ability in case of the hyperglycemic microenvironment.

Different concentrations of high glucose have been studied to investigate its effects on heterogenous populations of MSC proliferation, differentiation and function. These investigations have shown contradictory results. García-Hernández et al. (2012) and Liu et al. (2015) have respectively shown that 15.5mM and 24 mM glucose concentrations increased cell proliferation and biomineralisation process by activating the PI3K/Akt pathway, while elevated glucose concentrations from 25mM to 35mM had a negative impact on cell proliferation and osteogenic ability, which appeared to gradually decline. On the contrary, Li et al. (2007) demonstrated MSCs are more resistant to high (25mM) toxicity during short (several days) and long-term exposure (4 weeks), depending on the stemness of the MSCs, as effects of high glucose on the transit amplifying compartment of MSCs may differ from the mature cells, although this is still yet to be proven. However, they reported that 40mM glucose affected both cell proliferation and osteodifferentiation. These discrepant findings may be due to varying experimental protocols and different sources of cell lines, so further studies are needed to uncover the molecular mechanism of high glucose resistance in various MSC phenotypes.

One of the important extracellular proteins, playing a pivotal role in bone healing, remodelling and bone repair is osteopontin (OPN). OPN is one of the earlier secreted proteins by pre-osteoblasts and it accumulates against resorbed bone surfaces forming what is called OPN-rich cement line (Pedraza et al. 2008; McKee et al. 2011). Here, it is reported to act as an adhesion and cell signaling protein for recruiting mature osteoblasts to the bone surface, regulating early stages of mineralisation and assisting in the bonding of old bone to new bone evident as an OPN cement line. However, OPN binding to mineral crystals inhibits their growth aiding in bone remodelling; and therefore increased expression would inhibit bone formation (Pedraza et al. 2008; McKee et al. 2011). OPN has been reported to act as a substrate for the covalent cross-linking activity of transglutaminase 2 (Kaartinen et al. 2002), proposed to contain several integrin-binding motifs (Lund et al. 2009) and acts as a potent regulator of mineralisation (Boskey 1995; Pampena et al. 2004).

Interestingly, within MTG, Colombo et al. (2011) have found an increase in expression of OPN in the extracellular matrix of rat diabetic healing bone, compared to normal bone healing. This would

have detrimental effects and might be linked to the inhibition of bone formation. Therefore, this study also focussed on this protein in high glucose microenvironment in order to investigate its action on osteogenic differentiation process.

This Chapter aimed to investigate the ability of various CB-MSC population doublings during on-going expansion in culture, to differentiate into osteogenic and adipogenic lineages. In the previous Chapter of this thesis, experiments identified that culture expansion of CB-MSC populations led to a change in the heterogeneous profile of the MSCs. At early population doublings (PDs), a cell population containing a high proportion of committed osteoblasts along with immature cells was identified. At PD50, the committed osteoblasts were no longer the dominant cell population. Using this knowledge, the current Chapter investigated the influence of high glucose concentrations on differentiation potential of the different heterogeneous cell populations. Pertinently, this work was designed to continue to understand the *in vitro* influence of high glucose on OPN expression of these cells, which is hypothesized to be increased in high glucose healing bone *in vivo* and proposed to impede osteogenesis.

3.2: Materials and Methods

The population doubling of CB-MSCs at PD15, PD50, PD100 and PD200 were investigated in normal (5.5mM) and high (25mM) glucose conditions.

3.2.1: Investigation of MSCs Differentiation Capacity into Osteogenic and Adipogenic Lineages

CB-MSCs bi-potential differentiation capacity was assessed by inducing differentiation into osteogenic and adipogenic lineages until day 28 and day 21, respectively. During this period, various specific differentiation markers and transcription factors of MSCs were investigated, both at a gene and protein levels.

3.2.1.1: Osteogenic Induction

Cells were seeded at $4x10^3/cm^2$ in a 6-well plate, with culture medium (CM) [(αMEM) with ribonucleosides and deoxyribonuclosides (Gibco, ThermoFisher Scientific), supplemented with 10% Fetal Bovine Serum (FBS) (ThermoFisher Scientific, UK), 1% antibiotics-antimycotics (Sigma-Aldrich, UK)] for 24h and then replaced with osteogenic medium comprised of CM, 10nM dexamethasone and 10 mM β-glycerolphosphate (both from Sigma-Aldrich), incubated at 37ºC and 5% CO_2 for 28 days. Media were changed every two days, cells were collected on day 2, 7, 14, 21 and 28 for a total RNA extraction, reverse transcription for cDNA and then qPCR analysis. Osteogenic marker expressions investigated mRNA levels of osterix (OSX), osteopontin (OPN) and osteocalcin (OCN), (Table 3.1). To conduct a negative control, cells were cultured in CM only. Osteogenic differentiation analyses were performed in triplicate on three separate occasions.

3.2.1.2: Alizarin Red S Staining and Mineral Quantification

2% Alizarin Red S solution (w/v in distilled water) was prepared and pH was adjusted to between 4.1-4.3 with ammonium hydroxide, prior to being filtered through a 0.22μm syringe filter (Millipore, USA) and then the stain was stored in darkness. At day 28, media were removed from cells, washed 3 times with phosphate buffer saline (PBS), followed by 30min fixation with 4% paraformaldehyde solution (PFA) (Santa Cruz, USA) at room temperature. The PFA was then removed and the fixed cells were washed 3 times with PBS. 200 μL of Alizarin Red S solution was added to each well and gently agitated for 20min. The excess staining solution was removed and washed with distilled

water. Wells were left to dry at room temperature. Images were taken by digital cameras (Canon PC1234 UK Ltd., UK), while viewing under light microscopy (Nikon Eclipse TS100).

The mineral formation of PDs was quantified according to Gregory et al. (2004). 800µL of 10% (v/v) acetic acid was added to each well and incubated at room temperature for 30min with shaking. The cell monolayer was removed using a cell scraper and transferred to a 1.5mL Eppendorf tube using a stripette to obtain all the insoluble materials. Eppendorf tubes were vortexed for 30s, wrapped with parafilm to prevent evaporation when heated to 85ºC for 10min in a heat block and then immediately transferred onto the ice for 5min to cool down. The samples were centrifuged at 20,000xg for 15min at 4ºC. 500µL of the supernatant was transferred to a new 1.5 mL Eppendorf tube. 150µL aliquots of the supernatant were read in triplicate at 405nm in a 96-well plate, using a SPECTROstar Omega Plate Reader (BMG Labtech, Germany).

3.2.1.3: Adipogenic Induction

Cells were seeded at $1x10^4/cm^2$ and cultured with CM until 90% confluent. CM was then replaced with adipogenic induction medium consisting of 10% FBS, 1% antibiotic-antimycotic, 1µM dexamethasone (Sigma-Aldrich) which dissolved in ethanol (ThermoFisher Scientific, UK). 100µM 3-isobutyl-1-methylxanthine (IBMX) dissolved in dimethyl sulfoxide (DMSO), 10µg/mL insulin (all from Sigma-Aldrich) dissolved in 1M hydrochloric acid (HCl) (ThermoFisher Scientific); and 100µM indomethacin (Sigma-Aldrich) dissolved in methanol (ThermoFisher Scientific), at 37ºC, 5% CO_2 for 6 days, with media changed every 3 days. At day 7 media were removed and replaced with adipogenic maintenance medium consisted of 10% FBS, 1% antibiotic-antimycotic, in αMEM and supplemented with 10µg/mL insulin for 2 days. Adipogenic differentiation was conducted for a total of 21 days. Media were changed during this period as follows: induction at day 1 and 4, maintenance at day 7, induction at day 9 and 12, maintenance at day 15 and induction at day 17. The pre-prepared as stock solutions were vortexed to give a precipitate-free solution, and filtered with 0.22µm filter and stored at -20ºC until use. Media were prepared for each change by thawing adipogenic components, mixing and adding 10% FBS and vortexing for thorough dissolution. Negative control samples were cultured with CM for 21 days (non-adipogenic). Total RNA was extracted on day 0 and day 21. cDNA was obtained for each sample to visualize adipogenic expression markers (adiponectin and PPARγ) using qPCR (Table 3.1).

Table 3.1: Primer sequences and product sizes of selected osteogenic and adipogenic markers for qPCR analysis.

Gene	Primer sequence Forward (F) and Reverse(R)	Product length (bp)	Annealing Temperature (°C)	Source
GAPDH	F: GCA AGA GAG AGG CCC TCA G R: TGT GAG GGA GAT GCT CAG TG	74	55	(Xing et al. 2009)
OSX	F: GCT TTT CTG TGG CAA GAG GTT C R: CTG ATG TTT GCT CAA GTG GTC G	136	55	(Georgiou et al. 2012)
OPN	F: AAG CAA GAA ACT CTT CCA AGC AA R: GTG AGA TTC GTC AGA TTC ATC CG	132	55	Dr. Wayne Ayre (Cardiff University)
OCN	F: AAG CCC AGC GAC TCT GAG TCT R: CCG GAG TCT ATT CAC CAC CTT ACT	75	55	(Korkalainen et al. 2009)
Adiponectin	F: GAATCATTATGACGGCAGCAC R: CTTGGAGCCAGACTTGGTCTC	224	55	(Ding et al. 2013)
PPARɣ	F: GGAAGCCCTTTGGTGACTTTATGG R: GCAGCAGGTTGTCTTGGATGTC	174	55	(Ji et al. 2009)
β-actin	F: TGAAGATCAAGATCATTGCTCCTCC R:CTAGAAGCATTTGCGGTGGACGATG	108	55	Sigma-Aldrich, Centre.

3.2.1.4: Neutral Lipid Detection (Lipid Tox™ Green)

Cells were cultured in adipogenic and control conditions to perform neutral lipid analysis in BD Falcon™ glass chamber slides (BD Biosciences, UK). As described above, at day 21, cells were fixed and stained using HCS Lipid TOX™ Green neutral lipid stain according to manufacturer's protocol (Invitrogen, UK). Briefly, cells were washed twice with PBS, fixed with 4% PFA for 10min at room temperature, washed twice with PBS, and stained with Lipid TOX™ diluted 1:200 in PBS, for 30min. The slide chambers were removed, cells on the slides were stained with DAPI Vectashield Hard-Set Mounting Medium (Vector Labs, UK) and covered with cover slips (ThermoFisher Scientific). Nuclear DAPI and green-lipid fluorescence were observed using Olympus Provis AX70 microscope with Nikon ACT-1 v.2.63 software.

3.2.1.5: Quantitative Real-Time Polymerase Chain Reaction (qPCR) to Examine Osteogenic and Adipogenic-Specific Markers

qPCR was used to assess the osteogenic and adipogenic gene markers, as described in Chapter 2, section (2.2.8). Reverse and forward primers used and annealing temperatures are given in (Table 3.1).

3.2.2: Protein Extraction and Quantification

In this study, protein investigation focused on CB-MSC populations of PD15 and PD50. Protein was investigated in two ways. Firstly, by examining the total protein in cells and extracellular matrix by analyzing the cell lysate extracts. Secondly, by detecting the protein released into the cell culture medium. Cells were seeded at 4,000 cells/cm^2 in T75 tissue culture flasks, cultured in 10mL osteogenic induction medium and incubated at 37°C in 5% CO_2. The medium was changed every 2 days on a regular basis. At day 7, 14 and 21, culture media were collected and the cell monolayer was washed twice with ice-cold PBS, and treated with 1mL of extraction RIPA buffer [(ThermoFisher Scientific) supplemented with Complete™ Protease Inhibitor Cocktail with a ratio of one tablet in 50mL of RIPA buffer (Roche, UK)] to each T75 flask for 5min, while incubated onto ice at 4ºC. The cell lysate and matrix were removed using a cell scraper, collected into a universal tube and kept at 4ºC (on ice), then sonicated by cell sonicator for 20s (on ice) and centrifuged for 15min at 1500 rpm at 4ºC to sediment particulate material. The culture media supernatants were exhaustively dialyzed using 25mm width cellulose dialysis tubing membrane, 12,000Da molecular weight cut-off (MWCO) (Sigma-Aldrich). Dialysis was performed for 5 days against deionized distilled water containing protease inhibitor solutions (0.5mM iodoacetic acid,

0.5mM benzamidine, and 0.1mM N-ethylmaleimide, all from Sigma-Aldrich) at 4°C with a magnetic stirrer in a continuous agitation. Dialysis solution was changed every day. Protein was recovered by lyophilization (Edwards Freeze-dryer Modulyo, UK) and kept at -20ºC.

3.2.2.1: Bicinchoninic Acid Protein Assay (BCA)

Lyophilized protein was re-suspended in 1mL of tris-buffered saline (TBS; 50mM Tris, pH 7.4 and 0.15 M NaCl), until completely dissolved. Protein concentration was analyzed using BCA Protein Assay Kit, according to the manufacturer's protocol instructions (Pierce® Thermo Scientific). Briefly, 25µL of each standard and protein sample was added to 96 well-plate in triplicate. 200µL working reagent [reagent A: bicinchoninic acid in 0.1M sodium hydroxide and reagent B: 4% (w/v) cupric sulfate, (50:1, reagent A: B)] was added to each well in triplicate and mixed thoroughly on a plate shaker for 30s. The plate was incubated at 37ºC for 30min. Colorimetric absorbance was read at 562 nm using a SPECTROstar Omega Plate Reader (BMG Labtech). Absorbance readings were corrected and averaged using empty wells. Protein concentrations were calculated using the standard curve and polynomial equation with Microsoft® Excel® 2016 package.

3.2.2.2: Western Blot (WB) for Protein Electroblotting

20µg of protein samples (determined above) were diluted 1:1 with 1X Laemmli buffer (Bio-Rad, USA). Samples were heated to 95ºC for 5min and 18µL loaded on 4-15% Mini- Protean® TGX™ Precast Gels (Bio-Rad) along with 8µL Kaleidoscope™ Prestained Standard Markers (Bio-Rad). Gels were placed into Mini-PROTEAN® Tetra Vertical Electrophoresis Cell (BioRad Laboratories, UK) in 1x sodium dodecyl sulphate-polyacrylamide gel-electrophoresis (SDS-PAGE) running buffer [1.92M glycine (ThermoFisher Scientific), 250mM tris-base (Sigma-Aldrich), 1% SDS, pH 8.3). Protein samples were separated by gel-electrophoresis at 200V, for 40min in Mini-PROTEAN® Tetra Vertical Electrophoresis Cell, (BioRad). Gels were removed from the cast and soaked in a transfer buffer (192mM glycine, 25mM tris-base, 20% (v/v) methanol, pH8.3) for 10min. Meanwhile, the electroblot 'sandwich' components were prepared by soaking 2 electroblot sponges, 2 sheets of thick blot filter paper (BioRad) and cut to size piece of nitrocellulose membrane (GE Healthcare, UK) in a transfer buffer for 5min. One of the electroblot sponge was laid onto a plate of the blotting device, followed by a sheet of filter paper, the gel containing the proteins separated by electrophoresis, nitrocellulose membrane, then another sheet of the filter paper and lastly the second electroblot sponge. The electroblot sandwich was placed into the Mini-PROTEAN® Tetra Vertical Electrophoresis Cell at 75volt and the electrical current passed across the membrane for 1h. Protein

transfer was confirmed by staining the nitrocellulose membrane with Ponceau Red stain for 5min and de-staining by washing with TBS.

3.2.2.3: Protein Detection by Immunoblotting

Membranes were blocked overnight at 4ºC with 5% (w/v) non-fat milk (Tesco, UK) in TBS-T [(TBS supplemented with 0.05% Tween-20 (Sigma-Aldrich)] with a gentle agitation. Membranes were transferred to blocking buffer solution supplemented with primary antibody of goat polyclonal IgG osteopontin (Insight Biotechnology, UK) (dilution 1:500) for 1h at a room temperature. Membranes were washed 3 times for 5min each in TBS-T, transferred to a blocking buffer supplemented with rabbit anti-goat horseradish peroxidase (HRP)-conjugated secondary antibody at 1:30,000 dilution (Insight Biotechnology) and incubated for 1h at room temperature. Membranes were washed 3 times for 5min each in TBS-T, with two additional washes for 5min in TBS only, to reduce a high background. Negative controls were performed to confirm the specificity of OPN antibody. OPN primary antibody was incubated with a 10X excess of the respective OPN blocking peptide (Santa Cruz) for 1h at room temperature. The nitrocellulose membrane was incubated in ECL™ Prime Detection Reagent (GE Healthcare) for 2min. Chemiluminescence was detected by exposing the membrane to Hyperfilm™ (GE Healthcare) and developed using an Auto-developer machine (Curix 60, AGFA, Belgium).

3.2.2.4: Immunoprecipitation (IP) of Osteopontin from Cell Medium

Total protein was obtained from medium supernatant of cells, as previously described in Section 3.2.2. Immunoprecipitation (IP) of OPN was conducted using a Pierce® Crosslink IP Kit (Thermo Fisher Scientific), according to the manufacturer's protocol. Experimental steps were performed at 4ºC, unless otherwise stated. The centrifugation was conducted at 1,000g for 1min. Each protein sample was performed in a separate Pierce spin column. 20µL of Pierce protein A/G plus agarose was applied into a spin column, then centrifuged and the flow-through discarded. The resin was washed twice with 100µL of couple buffer. The column base was tapped onto a paper towel and then sealed with a bottom plug. 10µg of OPN antibody goat polyclonal IgG osteopontin (Insight Biotechnology) was added to 5µL of 20x couple buffer and the total volume was adjusted to 100µL with ultrapure water (18.2MΩ H_2O). OPN antibody solution was added to the resin-containing spin columns, sealed and incubated for 1h at room temperature. The spin columns were centrifuged, washed once with 100µL of couple buffer and twice with 300µL of couple buffer and the flow-through discarded in each time. To cross link OPN antibody to the resin, 2.5µL of 20x couple buffer, 9µL of 2.5mM Disuccinimidyl suberate (DSS) and 38.5µL of 18.2MΩ H_2O were added to each column and incubated for 1h at room temperature with gentle agitation. The spin columns were centrifuged and washed by adding 50µL of elution buffer, followed by 2 washes with 100µL of elution buffer; and then 2 washes with 200µL of IP lysis/wash buffer. The spin columns were sealed and stored until further use at 4ºC after pipetting 200µL of IP lysis/wash buffer into each column. For pre-clearing the samples, 80µL of the control agarose resin slurry (40µL of settled resin) was applied into the fresh spin columns and centrifuged and washed with 100µL couple buffer. 1mg of total protein was reconstituted in 1mL of TBS, while the final volume was adjusted to 1.2mL. Protein concentrations were determined according to Section 3.2.2.1. 600µL of protein solution was added to each spin column which already containing 40µL of settled resin. Spin columns were sealed with a top plug and incubated for 1h with gentle end-over-end mixing. The columns were centrifugated and the flow-through kept for the IP confirming procedures. The spin columns containing immobilised antibodies were washed twice with 100µL of TBS and sealed with a bottom plug. 600µL of total protein solution was added to each column. The columns were then sealed and incubated overnight with gentle end-over-end mixing at 4ºC. The spin columns were centrifuged and retained the flow-through. Columns then washed, by adding 200µL of IP lysis/wash buffer and centrifuged. The columns were then washed twice with 200µL of IP lysis/wash buffer and then once with 100µL of conditioning buffer. The spin columns were placed into a new 1.5mL collection tube

provided with 5µL of 1M tris-base at pH of 9.5. 10µL of Elution Buffer was pipetted into each column and centrifuged. 50µL of elution buffer was added to the resin in each spin column and incubated for 5min at room temperature. The spin columns were centrifuged and flow-through retained for confirmation IP procedures. The spin column was centrifuged and the samples were collected and loaded on a gel to perform SDS-PAGE to confirm the purified OPN at the right molecular weight. The amount of obtained protein was estimated by BCA protein assay. Volumes for OPN depleted flow-through and enriched elution pools utilised in forthcoming experiments were proportional, relative to the total volume of depleted elution.

3.2.2.5: Enzyme Linked-Immunosorbent Assay (ELISA) of Rat Osteopontin in Supernatant Culture Media

CB-MSCs were cultured for 21 days in osteogenic conditioning media in normal and high glucose conditions. Samples were collected at day 7, 14 and 21. The secreted OPN from the supernatant was quantified using Osteopontin (Rodent) ELISA kit (Enzo Life Science, UK). The 96-well plate provided within the kit was pre-coated with a monoclonal antibody specific for OPN. According to the manufacturer's instructions, 2 wells of this plate were left empty; in addition, 2 wells were loaded with 50µL of assay buffer. Protein standard was loaded into nominated wells in duplicate in a descending way (100 - 3.13 ng/mL). 50µL of each pre-diluted purified OPN sample in assay buffer were loaded to each well in duplicate and incubated for 1h with a constant agitation at room temperature. Supernatant was decanted from the well. Each well was washed four times with ELISA washing buffer. Wells were gently tapped on a tissue to make sure complete dryness of the wells. 50 µL of biotinylated polyclonal antibody specific for OPN was added to each well except the blank ones and incubated for 1h on a mixer at room temperature. Wells were evacuated and washed as above, then adding 50µL of streptavidin conjugated to horseradish peroxidase antibody specific for OPN and incubated for 30min on a mixer at room temperature. Wells were washed as above and then 50µL of substrate solution was added to each well including the two blank wells and left on a mixer for 30min at room temperature. The enzyme activities were stopped by applying 50µL of stop solution, to each well including the blanks. Absorbance was measured using a spectrophotometry plate reader at 450nm. The amount of OPN was quantified by plotting the standard samples as a reference standard curve. The experiment was performed in triplicate and the results were expressed in ng/mL/1mg protein.

3.2.3: Detection of Phosphorylated Osteopontin by Anti-Phosphoserine Antibody

Fractions of purified OPN which are proportionally equal to 10µg from 1mg of total protein was electrophoretically separated by SDS-PAGE and protein components electroblotted onto nitrocellulose membranes, as described in Section 3.2.2.2 and 3.2.2.3. Fractions were probed with (1:250) diluted anti-phosphoserine primary antibody (Abcam, UK) in 5% bovine serum albumin (BSA) with 0.1% (w/v) gelatin (Sigma-Aldrich). Three washes were performed by TBS-T, then probing for 1h with goat anti-rabbit horseradish peroxidase (HRP)-conjugated secondary antibody at a dilution of 1:30,000 (Insight Biotechnology), at room temperature. Three washes were repeated by TBS-T 5min each and the fourth with TBS only for reducing a high background. Membranes were probed by ECL^{TM} Prime Detection Reagent and visualized by developer machine, as described previously in Section 3.2.2.3.

3.2.4: Statistical Analyses

Statistical analyses were performed using One-Way ANOVA with a post-hoc Tukey test to determine the statistical differences between sample groups, using the software GraphPad InStat 3 (v3.06). Statistical significance of differences was defined as significant (*, $p<0.05$), very significant (**, $p<0.01$) or highly significant (***, $p<0.001$).

3.3: Results

3.3.1: CB-MSC Differentiation

3.3.1.1: Osteogenic Differentiation of Rat CB-MSCs

MSC osteogenic differentiation capacity was analysed by culturing cell populations in osteogenic induction media in normal (5.5mM) and high glucose (25mM) conditions. All the selected population doublings (PD) successfully attained osteogenic differentiation. However, each PD exhibited different levels of this differentiation. PD15 demonstrated the highest ability to form mineral, whereas PD50 exhibited the lowest. PD100 and PD200 showed decreased ability to differentiate, as described by results of Alizarin Red, mineral quantification, and expressions of mRNA osteogenic-specific markers (Figure 3.1; 3.2; 3.3).

3.3.1.2: Alizarin Red Staining

CB-MSCs cultured in osteogenic media were stained at day 28 with Alizarin Red and exhibited distinct red colour following MSC differentiation and mineral formation. Cells in control media demonstrated very minimally or no red staining. PD50 exhibited faint red colour in both normal and high glucose groups. Importantly, extending cell growth until day 35 exhibited deep red colour for PD50. PD100 and PD200 exhibited a darker staining compared to PD50, but they were still showing less red colour staining than PD15. Interestingly, there was a clear less red staining associated with high glucose groups at all PDs in comparison to the normal physiological glucose concentrations (Figure 3.1).

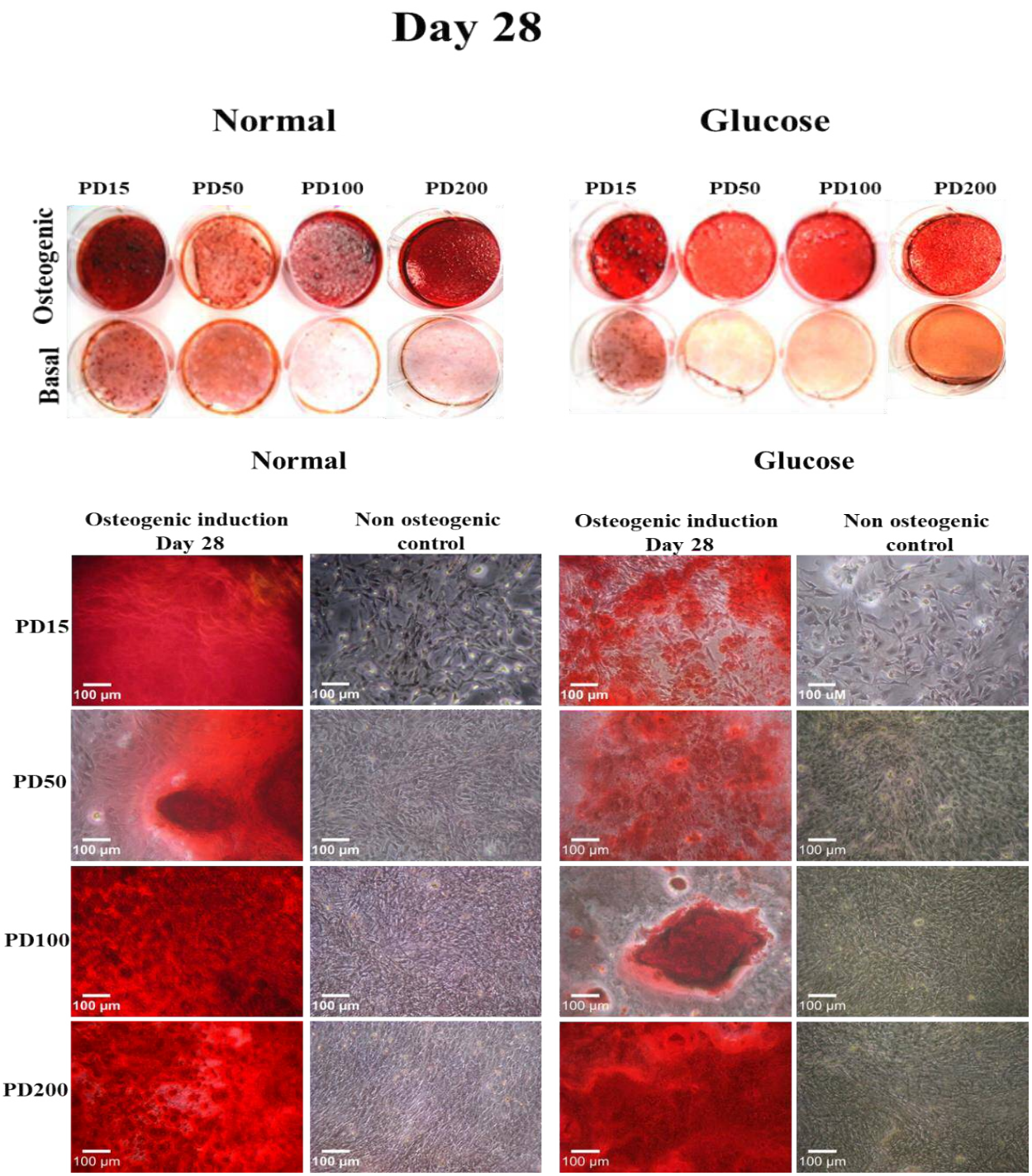

Figure 3.1 A: Alizarin Red staining of differentiation CB-MSCs at PD15,50, 100 and 200 at day 28 in normal and glucose conditions, in addition to day 35 for PD50. The red colour represents mineral deposition by extracellular matrix secreted by newly formed osteoblasts. Clear differences in the red colour can be noticed between normal and glucose conditions in all PD groups, which demonstrated that cells in glucose conditions had less osteogenic differentiation capacity. X10 magnification. Scale bar =100µm.

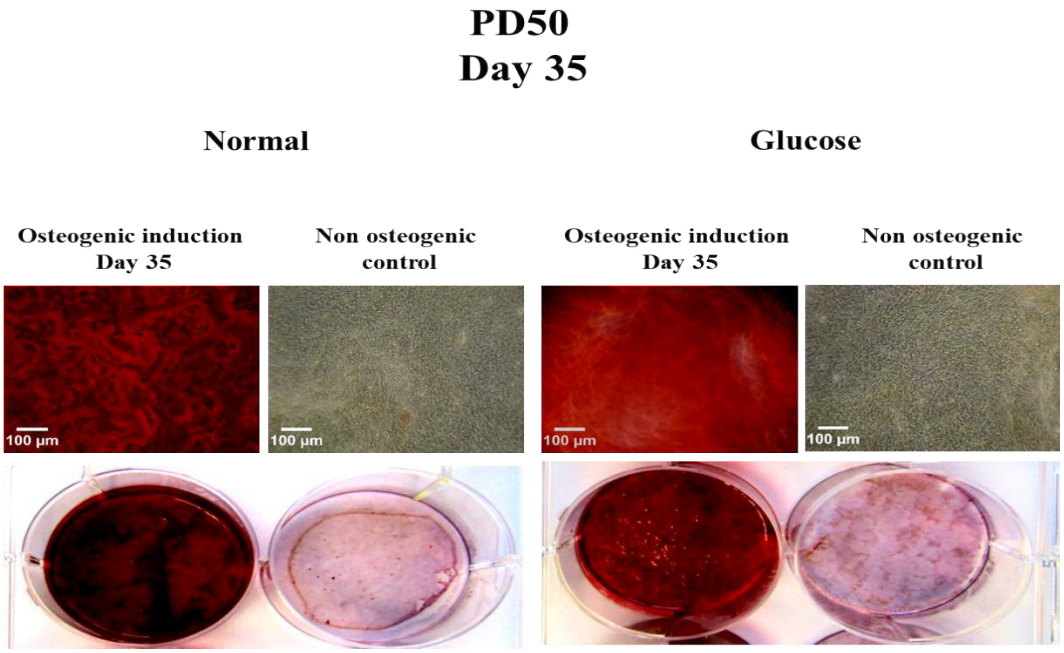

B. Extending PD50 until day 35 exhibited a deeper red colour, indicating osteoblast differentiation. X10 magnification. Scale bar =100µm.

3.3.1.3: Quantification of Mineral Formation after Alizarin Red Staining

PD15 normal (N) showed the highest mineral deposition, whereas PD50 had the least. PD50 N was significantly (p<0.001) lower than PD15 N. PD100 N was lower minerals than PD15 N, but not significant (p>0.05). PD200 N demonstrated significantly reduced mineral deposition, compared to PD15 N. Regarding high glucose, PD15 glucose (G) was significantly (p<0.05) lower than PD15 N. PD50 G exhibited higher mineral deposition compared to PD50 N, but not significant (p>0.05). PD100 N and PD200 N were significantly (p<0.05) higher compared to their high glucose counterparts (Figure 3.2).

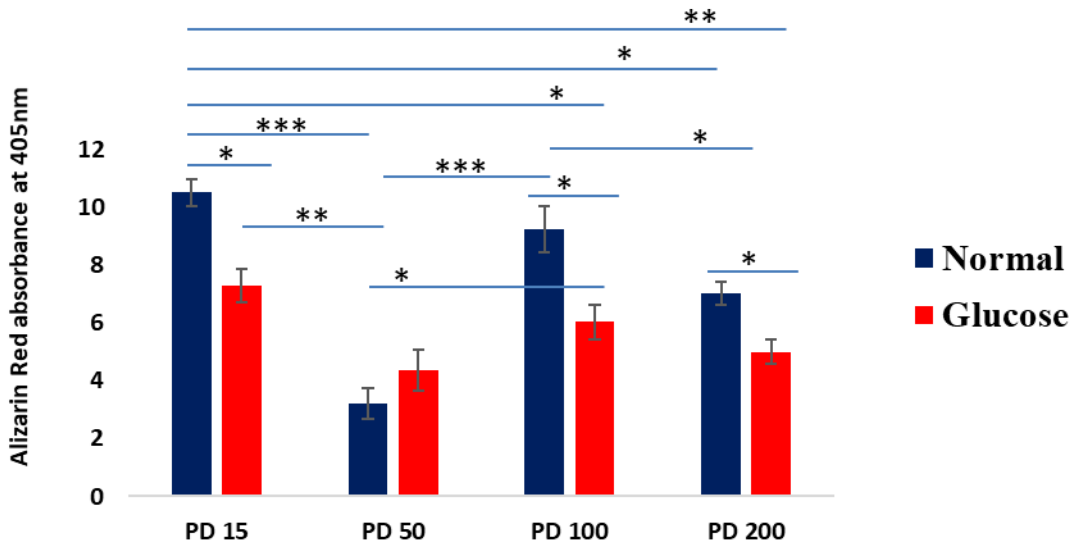

Figure 3.2: The quantification of the mineral formation after CB-MSC differentiation at different PDs. PD15 demonstrated the highest mineral formation, while PD50 was the lowest. Glucose conditions exhibited a significant impact on mineral deposition at all PD groups, except PD50. Error bars represent ± Standard error of the mean. n=3, * = p<0.05, ** = p<0.01, *** = p<0.001.

3.3.1.4: Quantitative and Analysis of mRNA Levels of Osteogenic mRNA Markers Using qPCR

The mRNA expression of osteogenic markers was investigated at different time points. OSX is considered as an early expression gene during osteogenic differentiation, thus it was examined at day 2 and day 7. PD15 exhibited a significant increase in expression (p<0.001) at day 2 compared to PD50, PD100 and PD200, which showed downregulation of OSX at day 2 and day 7. OPN was investigated on day 7, day 14 and day 21. PD15 demonstrated significantly higher mRNA expression of OPN (p<0.001) at day 21 glucose, compared to normal conditions. At PD50, OPN mRNA expression revealed significantly higher expression (p<0.001) normal compared to high glucose conditions, on day 7 and day 14. OPN was then downregulated at day 21. At PD15 mRNA expression for OCN was exhibited significant upregulated (p<0.001) in high glucose at day 21, whereas OCN mRNA expression in high glucose showed significantly downregulated (p<0.05) at day 28. PD100 revealed significant differences (p<0.05) between normal and high glucose groups at day 28. At PD200, day 28 OCN mRNA expression under normal conditions was higher than high glucose group but was not significantly different (p>0.05) (Figure 3.3).

Early Osteogenic Marker Osterix

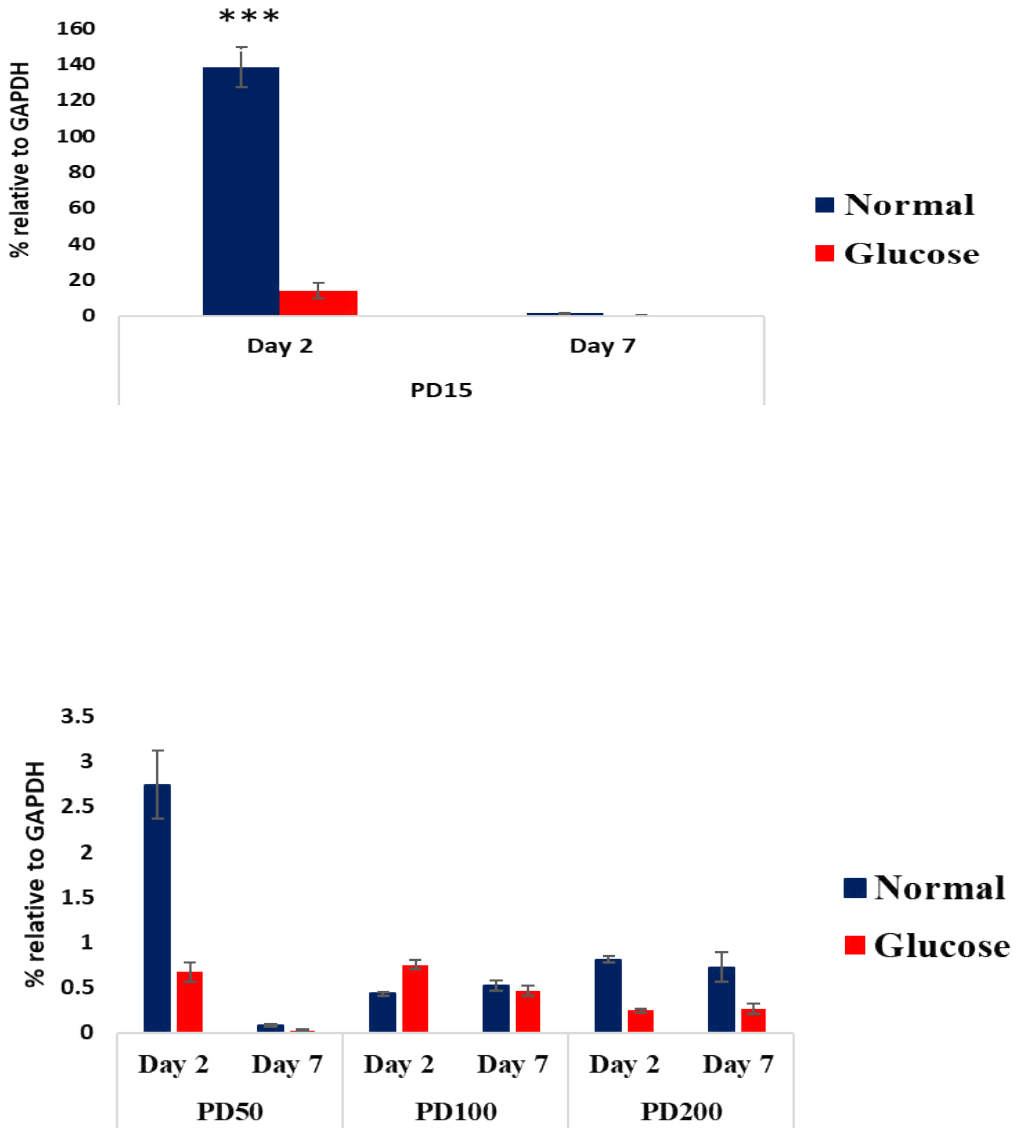

Figure 3.3: The bar chart shows mRNA level of osteogenic marker expression, early OSX, Mid OPN, and late OCN, using qPCR. Cells were induced for osteogenesis in normal and high glucose osteogenic conditions for 28 days. The values were normalized as a percentage expression of the endogenous gene (GAPDH). n=3. Error bars represent ± Standard error of the mean, * = p<0.05 and *** = p<0.001.

Mid Osteogenic Marker Osteopontin

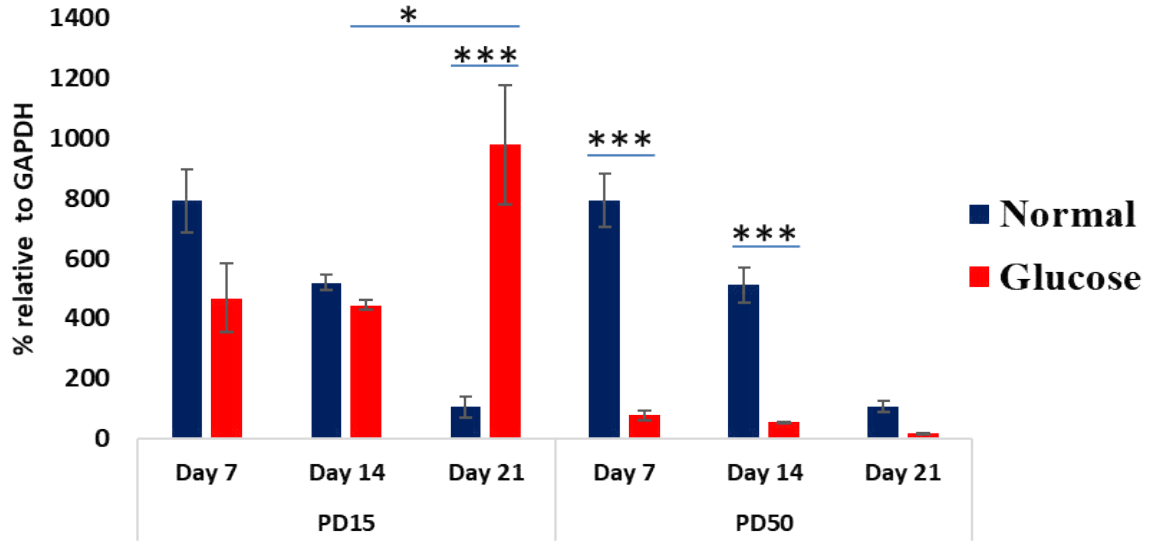

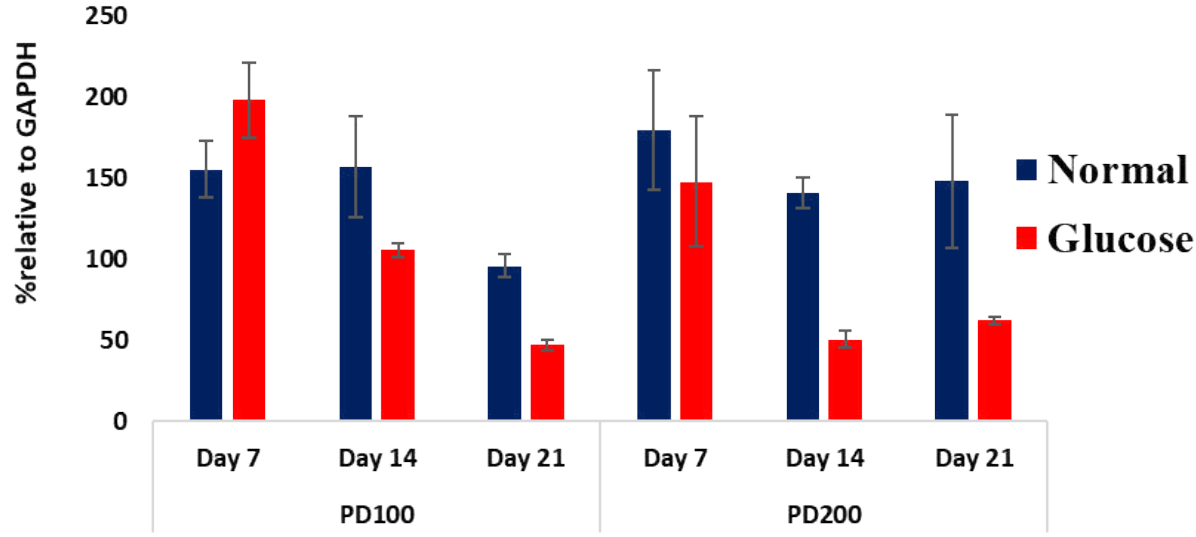

Late Osteogenic Marker Osteocalcin

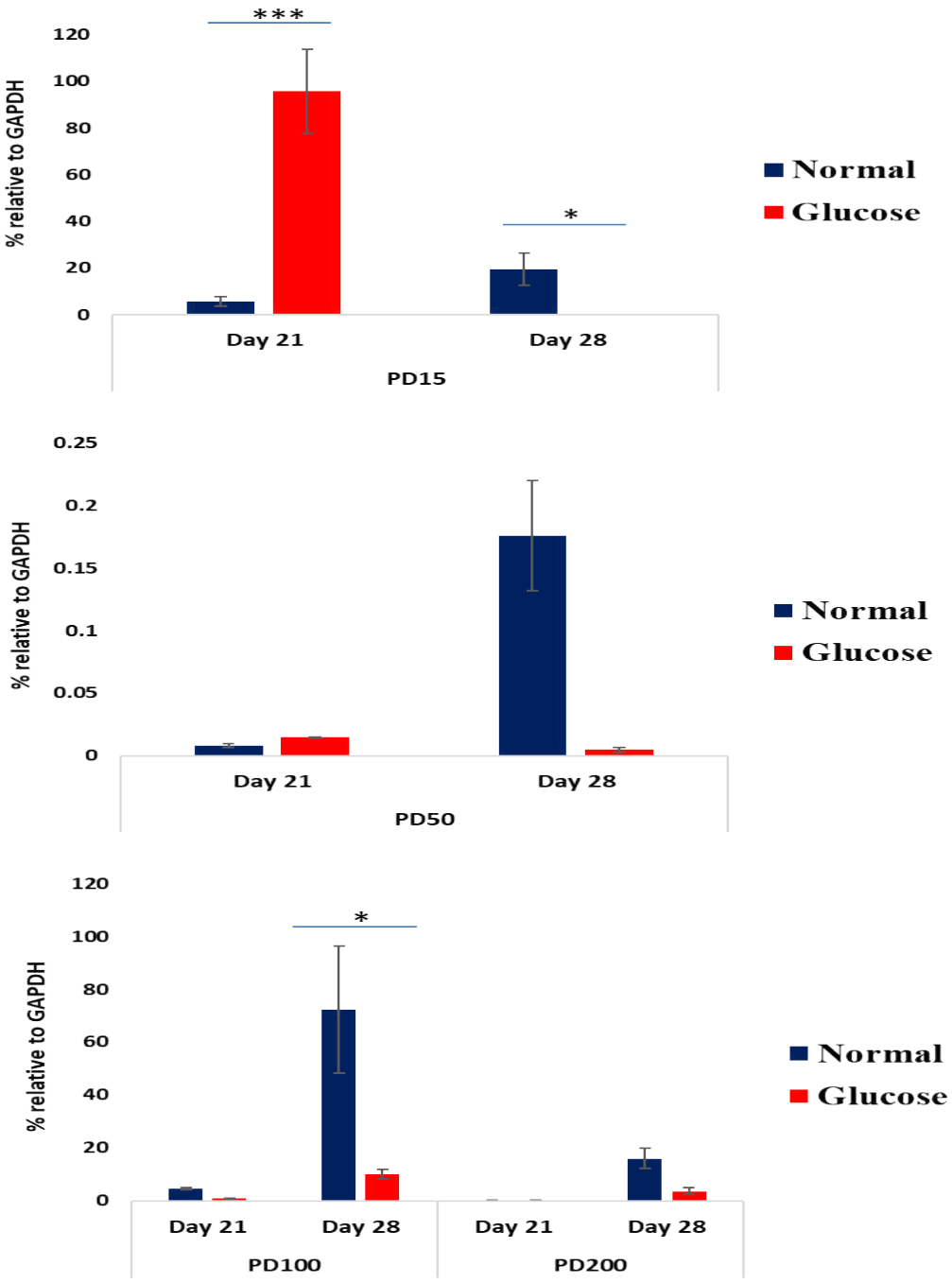

3.3.1.5: Adipogenic Differentiation and Lipid TOX™ Green Neutral Lipid Stain

CB-MSCs adipogenic differentiation capacity was investigated and showed cells were successfully transformed into adipocytes with large lipid droplets noted. Lipid TOX™ Green neutral lipid stain was examined at day 21 to confirm adipogenic differentiation and lipid vacuoles stained by a green colour appeared like clusters mostly at PD15 and PD50, whereseas there were fewer lipid vacuoles at PD100 and PD200 (Figure 3.4).

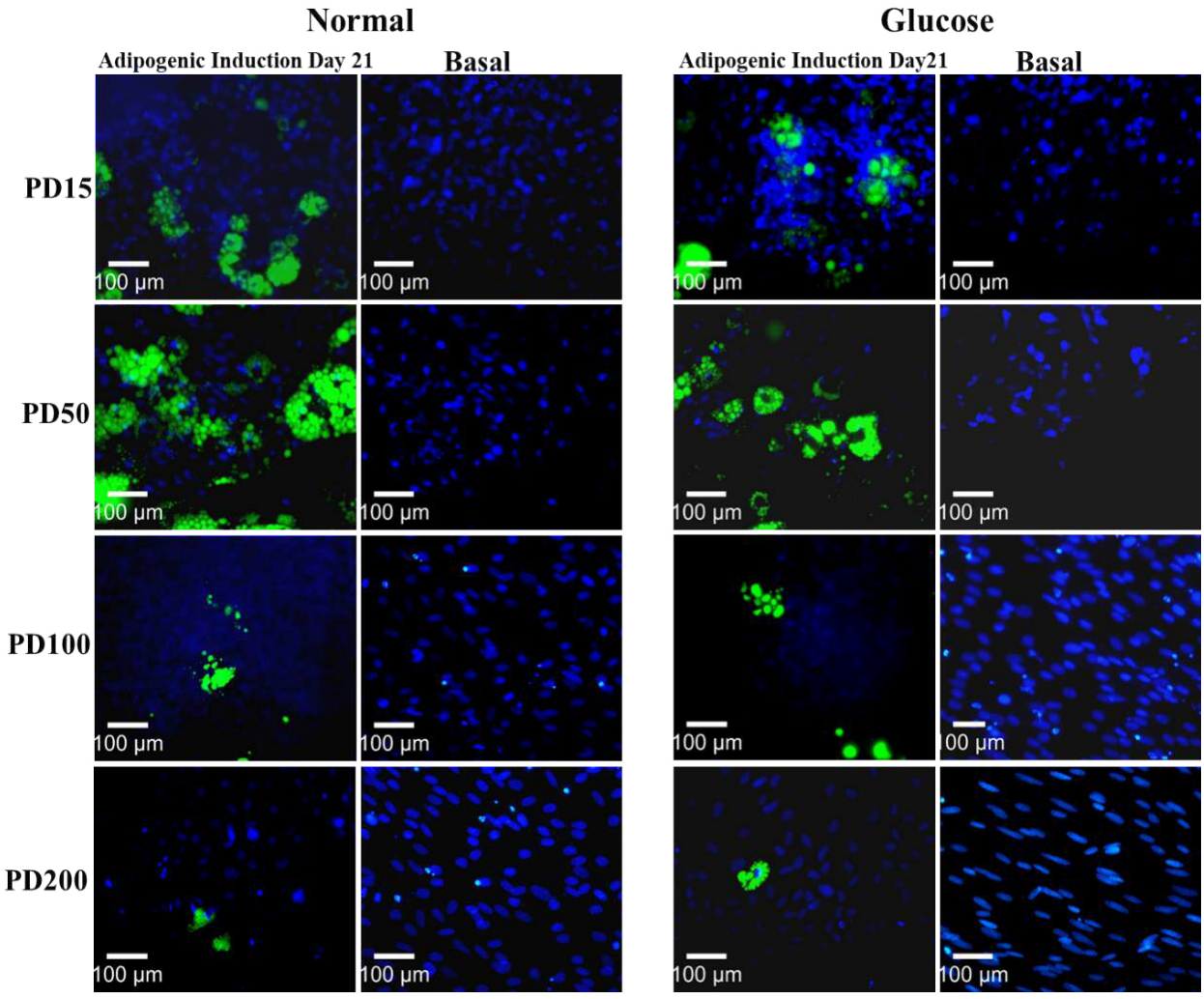

Figure 3.4: Lipid TOX™ staining of CB-MSCs at day 21 of adipogenic induction. Lipid vacuoles appeared green with cluster forming shapes at PD15 and PD50. As cells were further grown in culture (PD100, PD200), CB-MSCs exhibited a reduced capacity to differentiate into adipocytes. 20X magnification. Scale bar =100µm.

3.3.1.6: Quantitative Analysis of mRNA Levels of Adipogenic Markers Using qPCR

PPARγ and adiponectin mRNA expression were chosen, as late adipogenic-differentiation markers to investigate CB-MSCs adipogenesis differentiation capacity. Day zero was considered as a baseline and day 21 considered the day of adipocytes formation. Both markers showed significant upregulation ($p<0.001$) at day 21 at PD15 and PD50. However, almost no mRNA expression of PPARγ and adiponectin were observed in either PD100 and PD200. In high glucose media at day 21, PPARγ and adiponectin were significantly down-regulated ($p<0.001$), in comparison to the cells in normal adipogenic induction media (Figure 3.5).

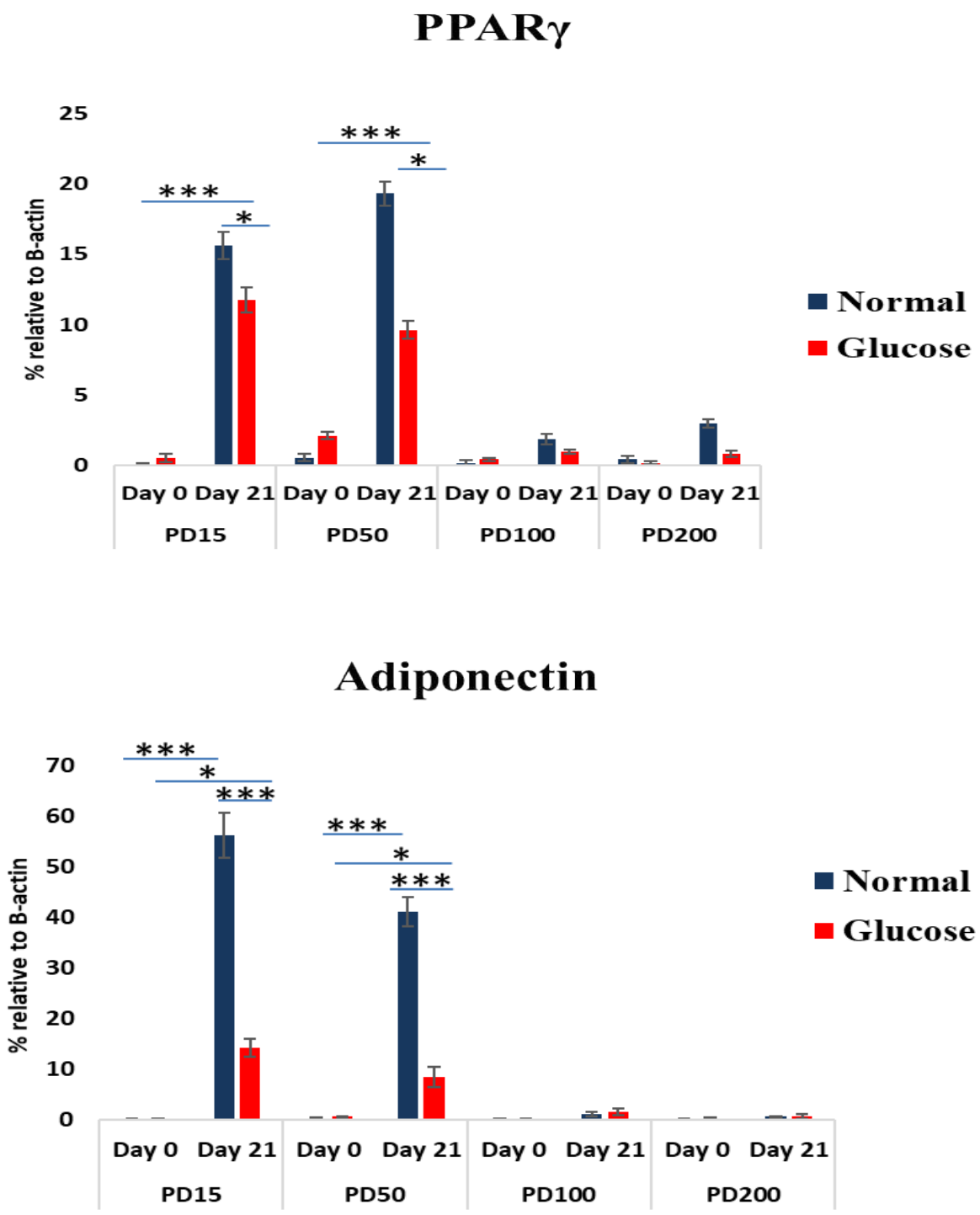

Figure 3.5: The bar chart shows mRNA levels of adipogenic markers PPARγ and adiponectin of CB-MSCs grown in adipogenic induction media at day 0 and day 21. Cells were induced for adipogenesis at normal and glucose conditions. Values were normalized as a percentage expression of the endogenous gene (β-actin). Error bars represent ± Standard error of the mean. n=3. * = $p<0.05$ and *** = $p<0.001$.

3.3.2: Investigation of Osteopontin Protein Content

3.3.2.1: Western Blot Analyses of Osteopontin in Cell Lysate

OPN was detected in cell lysates in both normal and high glucose supplemented osteogenic induction media at day 7, 14 and 21. OPN immuno-detected bands appeared at 55kDa at both PD15 and PD50. At PD15, the general protein profile started at day 7 with increasing protein levels at day14 and day 21. At PD50, OPN bands demonstrated increasing levels at day 14, then declined at day 21. Interestingly, the high glucose groups in both PD15 and PD50 exhibited more intense bands compared to normal control (Figure 3.6).

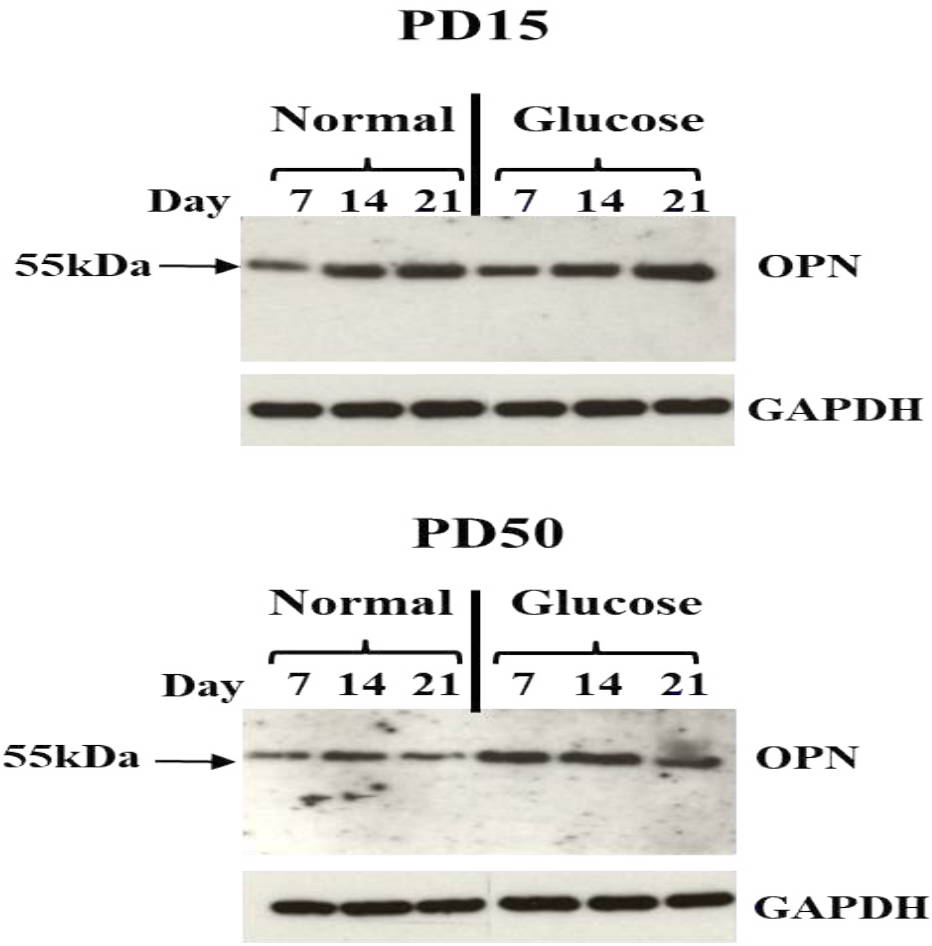

Figure 3.6: Western blot analysis of OPN immuno-detected bands in cell lysate of CB-MSCs grown in osteogenic induction media at PD15 and PD50, under normal and high glucose conditions. OPN bands were identified at 55kDa. The high glucose groups exhibited more intense bands. Western blots were repeated twice.

3.3.2.2: Western Blot Analyses of OPN in Culture Media

OPN was investigated in osteogenic culture media at day 7, 14 and 21. OPN was immuno-detected at three molecular weights. The main immuno-detected bands were at 55kDa, whereas there were 2 other bands at 120kDa and 25kDa. These features demonstrated potential post-translational modifications of the protein in the extracellular region. At PD15 normal samples, OPN bands were the highest level and more intense at day 7 compared to day 14 and then gradually decrease at day 21. PD50 demonstrated a different protein profile when there were small bands at day 7 and day 14, while showing intense bands at day 21. The high glucose bands, interestingly, were more intense than normal samples (figure 3.7).

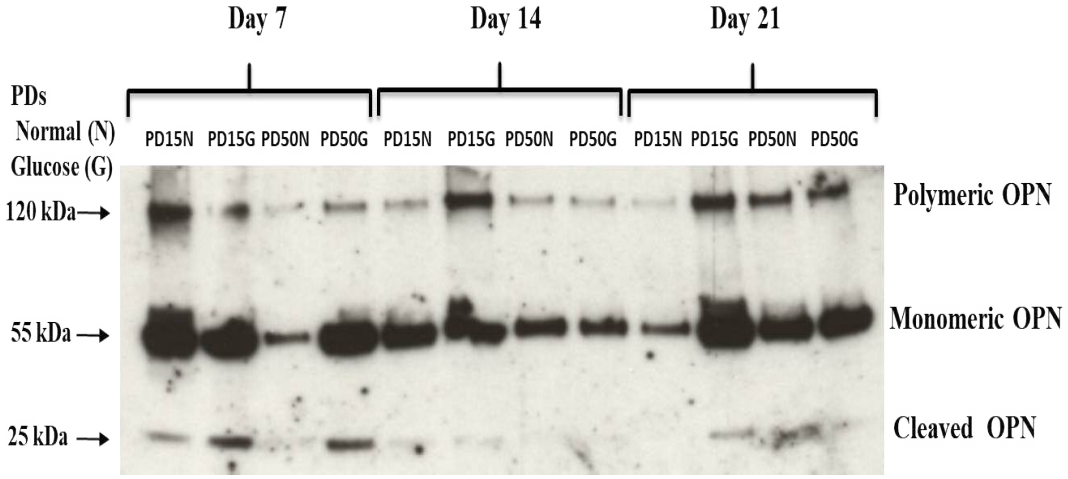

Figure 3.7: Western blot analysis of OPN immuno-detection in normal and high glucose osteogenic induction media. PD15 and PD50 were investigated in normal and glucose conditions. Three levels of immuno-detected bands were identified for OPN at 55kDa, 120kDa and 25kDa. The high glucose samples exhibited more intense bands. Western blots were repeated twice.

3.3.2.3: Enzyme Linked-Immunosorbent Assay (ELISA) Analyses of OPN in Culture Media

Quantification of OPN levels revealed that OPN was significantly (p<0.001) highest at PD15 compared to all other groups. OPN levels gradually declined at day 14 and day 21 at PD15. PD50 demonstrated less than half fold level, compared to PD15 at day 7. This level was low at both day 14 and day 21. In respect to the high glucose groups, OPN was expressed at higher levels at all

groups except PD15 day 7 and PD50 day 14 compared to normal samples, but were not significant (* = P>0.05) (Figure 3.8).

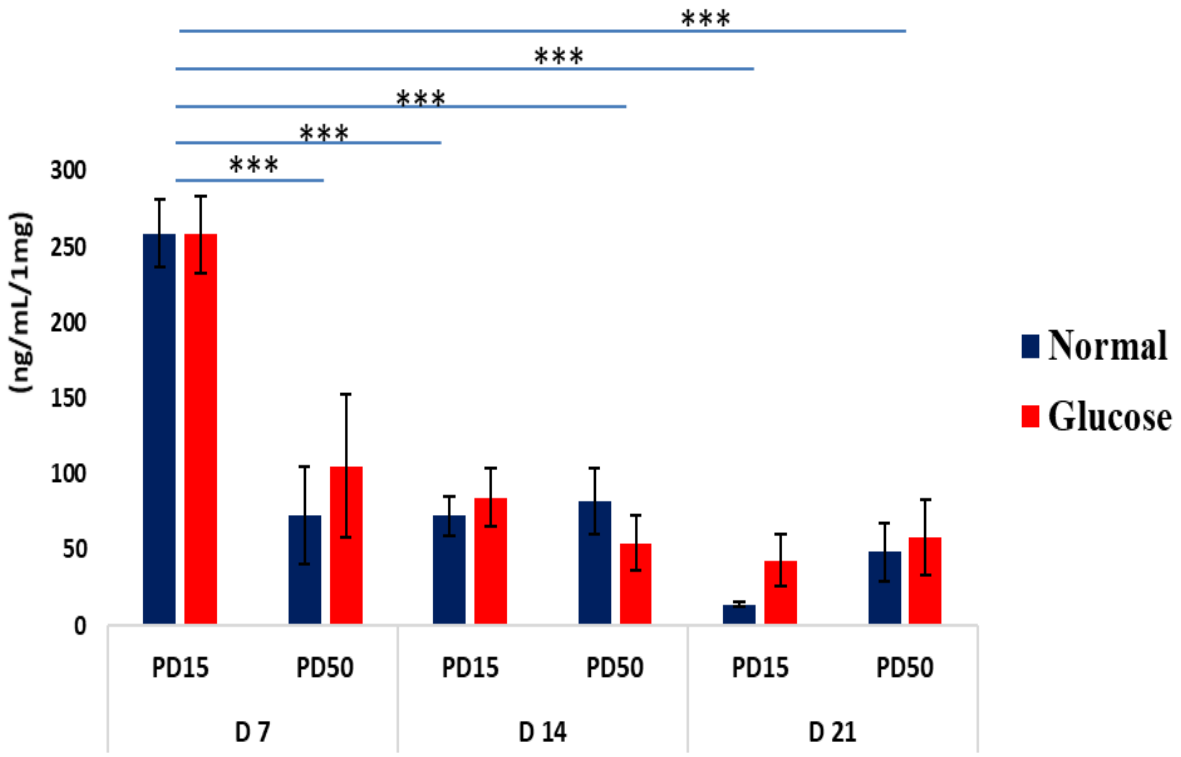

Figure 3.8: Quantification of OPN levels in osteogenic culture media using ELISA. OPN was measured on day 7, day 14 and day 21 for both PD15 and PD50 in normal and high glucose conditions. Error bars represent ± Standard error of the mean. n=3. *** = p<0.001.

3.3.3: Detection of Phosphorylated OPN

Western blot was performed to detect the phosphorylation status of OPN released in osteogenic culture media. The protein profile revealed that all samples had phosphorylated OPN at two molecular weights of the immuno-detected protein 55kDa and 120kDa (Figure 3.9).

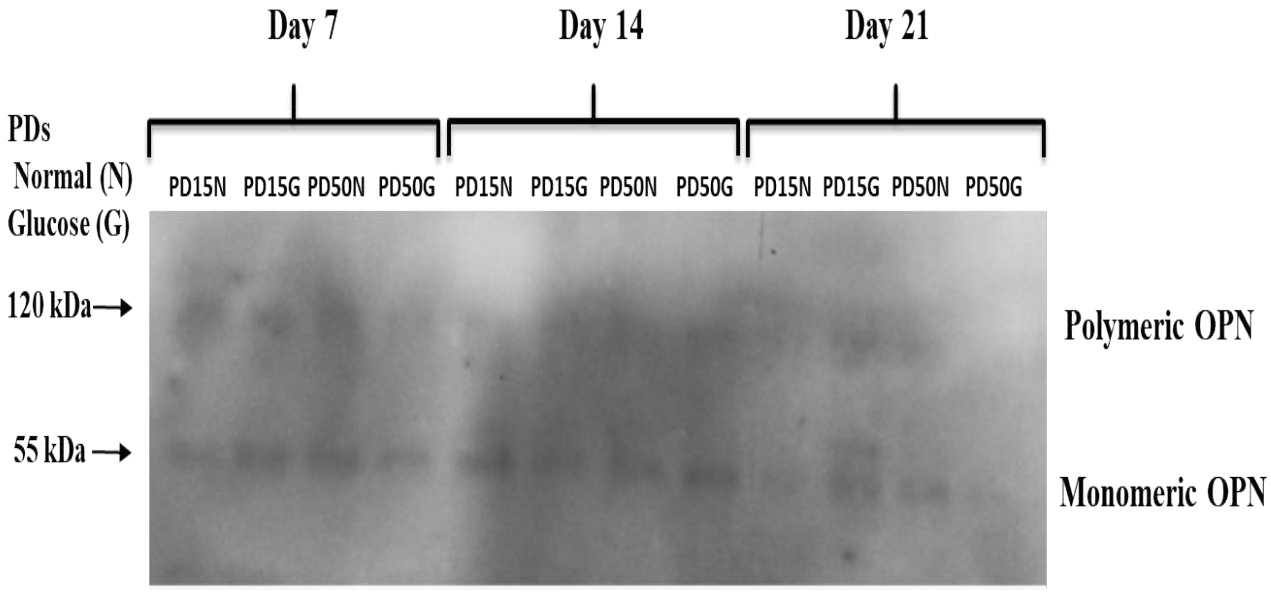

Figure 3.9: Western blot analysis by targeting anti-phosphoserine side of phosphorylated OPN from osteogenic induction culture media of CB-MSCs. PD15 and PD50 were analysed in normal and glucose conditions. Two immune-detected bands were identified for phosphorylated OPN at 55 kDa and 120 kDa. Western blots were repeated twice.

3.4: Discussion

This Chapter focused on the assessment of the bi-potential capacity of different populations of CB-MSCs to differentiate into osteoblasts and adipocytes under culture in normal and high glucose conditions. CB-MSCs successfully attained osteogenic differentiation at committed population PD15. This differentiation capacity was found to decrease in later populations. Regarding adipogenic differentiation, both committed and immature populations exhibited a better capacity to adipogenic differentiation, compared to the later populations. The high glucose microenvironment significantly affected osteogenesis in all populations except with the immature PD50. High glucose conditions reduced adipogenesis at committed and immature CB-MSCs populations. OPN was demonstrated to increase levels in cell lysates in high glucose conditions, regardless whether they were committed or immature populations.

Within this study, various investigated heterogeneous populations showed a different capacity to osteogenic differentiation. PD15 was the population selected to investigate after CB-MSCs passed the lag phase in culture, as previously described in Chapter 2; and proposed to consist of predominantly committed osteoprogenitor cells. This PD demonstrated the highest ability to differentiate into osteoblasts and deposition of minerals among all the population doublings. This high capacity of PD15 would be referred to as the committed osteoprogenitor and pre-osteoblastic stromal cells, which have been described to be present within the bone marrow stroma, namely the endosteal and perivascular niche (To et al. 2011). PD15 in high glucose microenvironment, however, exhibited a significant decrease in this mineral deposition capacity, which may be attributed to the detrimental effects of exposure to high glucose during the differentiation period. These results come in line with those of (Sugimoto et al. 2005; Liu et al. 2015; Zhang et al. 2016). However, Weil et al. (2009) have shown no effects of high glucose on cell proliferation and differentiation capacity. Thus, different cell mechanisms have been described to explain the effects of high glucose on bone formation, although, the exact cause is still inconclusive. Osteogenic-specific gene markers represented the osteogenic differentiation process. Herein, OSX is an essential osteogenic marker for the commitment of pre-osteoblasts to differentiate into mature osteoblasts (Iohara et al. 2009; Chi 2012). At PD15, OSX demonstrated significantly highest expression, supporting the characteristic findings in Chapter 2, describing the PD15 population as containing a mature/committed MSC phenotype. This outcome aligns with previous findings (Nakashima et al.

2002; Liu et al. 2015). OPN is known to inhibit hydroxyapatite crystal formation and regulate the size of newly formed crystals (Hunter et al. 1996). It was considered as a mid-osteogenic specific marker so that within this study, it was investigated at day 7, day 14 and day 21 during the osteogenic induction period. The interesting finding here was the significant increase in OPN expression at day 21 at PD15 under high glucose conditions. This important finding came in accordance with that of Colombo et al. (2011), who reported an increased OPN level in diabetic healing rat bone. Thus, this outcome sheds light on OPN having a possible role in delaying healing in diabetic bone. Regarding OCN, this is a late expressed osteogenic marker and always considered to be associated with mature osteoblasts, as it is tightly bound to the hydroxyapatite of the mineralised bone matrix (Hoang et al. 2003). PD15 normal at day 28, demonstrated a significantly higher expression of OCN compared to high glucose groups. These results are in agreement previous studies (Wang et al. 2010a, Kanazawa 2015; Liu et al. 2015). The commitment of PD15 to osteogenic lineage, however, does not expect to negate that committed cells were able to adipogenic differentiation. PPARγ can induce transdifferentiation of osteoblast MC3T3-E1 cells into mature adipocytes, as described by Kim et al. (2005). With this in mind, this heterogeneous population is proposed to have a subpopulation of immature cells which are already able to become adipogenic, when induced by PPARγ. Thus, PD15 successfully differentiated into adipocytes confirmed by Lipid TOX fluorescent staining, when cells showed a cluster of lipid droplets. Adipogenic-specific gene markers, PPARγ and adiponectin, were also upregulated indicating a presence of an adipose lineage.

On the other hand, PD50 has shown a change in the heterogenous population and has been described to have predominantly immature cells (as shown at Chapter 2). Herein, there was a delay in osteogenic differentiation, compared to other populations. Nevertheless, when CB-MSCs were maintained for a further 7 days in osteogenic induction media, they exhibited good differentiation into osteoblasts. This finding confirmed the outcomes of the previous characterization procedures and led to the proposal that this population contained immature MSCs. Alizarin Red staining supported this suggestion with a less intense red stain. Furthermore, this population revealed the lowest mineral deposition among all investigated populations, confirmed by Alizarin Stain and mineral quantification. Interestingly, in terms of mineral formation, high glucose exhibited no significant effects on immature cells. As far as possible, this is the first study to identify this novel result, which may need further research to assist in elucidation the real causative factors after the delay bone healing in a diabetic patient. Osteogenic specific markers confirmed these findings, OSX

and OCN at mRNA levels demonstrated very low expression, confirming the idea of immature MSCs phenotypes, which have been observed to spend a longer time to differentiate into pre-osteoblasts and then osteoblasts. OPN at the molecular level, exhibited upregulation in normal group and downregulation in high glucose samples, whereas OPN at protein level increased in the extracellular compartment in high glucose which is considered the place for OPN function (Nomiyama et al. 2007; Berezin and Kremzer 2013). Although this delay in osteogenesis process occurred, adipogenic induction of CB-MSCs within this population showed a higher capacity. Adipogenic-specific markers PPARγ and adiponectin were upregulated promoting adipogenesis. This tendency to adipogenesis may be due to the absence of committed osteoprogenitor cells so that the immature cells were easily driven to differentiate into adipocytes, unlike PD15, which contained committed osteoprogenitor cells. Herein, high glucose conditions exhibited significant effects on the adipogenic differentiation process as adipogenic-specific markers (PPARγ and adiponectin) demonstrated by significant downregulations them at day 21. However, these results did not concur with other studies (Chuang et al. 2007, Wang et al. 2010a), whereas Shilpa et al. (2013) have shown a significant decrease in adipogenesis due to long-term exposure to a very high glucose (105mM). These differences may be attributed to the different cell niche origin of the MSCs, which might express contradictory results.

PD100 revealed a better osteogenic differentiation ability than PD50. This population was reported to have the shortest telomere lengths in the previous Chapter (Chapter 2). This would infer that there is a mature subpopulation present within this heterogeneous population, which would be able to achieve osteogenic differentiation. These findings were confirmed by Alizarin Red staining and the amount of mineral deposition detected. Additionally, upregulation of osteogenic-specific marker expression, OCN, supported this notion. CB-MSCs, nonetheless, in this population failed to attain adipogenic differentiation. This outcome was also reported in other studies, when cells are no longer able to differentiate into adipocytes *in vitro* culture with increasing passage number (Ntambi and Kim 2000; Sethe et al. 2006; Ali et al. 2013).

In case of continuing cell growing in culture to PD200, the cells exhibited a decreased capacity to differentiation not only of osteogenesis and mineral deposition but also adipogenesis, which could be attributed to MSCs 'losing' their stemness characters as cells continue to grow in culture (Ntambi and Kim 2000). Nevertheless, the decreased ability for bone formation associated with age was

suggested to be owing to lower cell numbers rather than decreased cell proliferative capacity or loss of function (Stenderup et al. 2003). Regarding osteogenic-specific markers, OSX, OPN and OCN, there were all downregulated in this population, in addition to adipogenic-specific markers, PPARγ and adiponectin. These findings infer that this population would not be useful in bone repair process or assist in cell therapy research.

High glucose effects on bone regeneration have been studied by many researchers. However, a high number of contradictory results have found. Botolin and Mccabe (2006), Li et al. (2007) and García-hernández et al. (2012), have demonstrated an increase in cell proliferation and biomineralisation under hyperglycemic conditions. On the contrary, other studies have shown deleterious effects of high glucose on MSCs differentiation into osteoblasts and consequently affected their functions (Zayzafoon et al. 2000; Gopalakrishnan et al. 2006; Kim et al. 2006; Wang et al. 2010b). These contradictory results from different groups, investigating high glucose effects on bone biominerelisation might be due to several causes. Firstly, the heterogeneous nature of the cells, which is a common feature of the MSCs. This was well noted at PD15 and PD50 in this study. Secondly, the source of the cells from different species and cell-lines may give different responses. Thirdly, the different glucose concentrations were applied to various studies. Furthermore, the relative difference in the setting of the experiment and cell seeding density depending on different labratory protocols. All these inconsistent results would propose a mandatory investigation of cell response to any new condition, such as high glucose and its effects on the newly isolated CB-MSCs.

Chronic hyperglycemia, however, undeniably induces detrimental effects on MSCs. These cells would normally differentiate into osteoblasts, adipocytes and chondrocytes, which if associated with high glucose could alter the cellular differentiation of the bone marrow. Bone remodelling and repair depend on a balance between two activities; bone resorption and bone formation. In case of any change to this equilibrium, it may lead to bone loss (Botolin et al. 2005; Botolin and Mccabe 2007). High glucose has been reported to inhibit osteoblast differentiation in favour of adipocytes. This process is proposed to be governed by PPARγ, which does not only drive MSCs to differentiate into adipocytes, but guides committed osteoprogenitor cells to transdifferentiate into adipocytes (Kim et al. 2005). This pathological impact of high glucose may be behind osteoporosis and delay bone healing associated with diabetes (Keats et al. 2014). Within this study, it has been observed that high glucose reduces adipogenic-specific markers, however, for long-term cultures in diabetic

microenvironment could also accumulate more oxidative stress, which has been reported to induce adipogenesis a the expense of osteogenesis (Botolin et al. 2005; Botolin and McCabe 2007; Wang et al. 2010a).

Within this study, OPN was detectable at 55kDa and 120kDa with additional bands at 25kDa. This may be due to the functional post-translational modifications. OPN monomeric protein always appeared at 50-60kDa, whereas it has been reported to be cross-linked to transglutaminase 2 (TG2) at 120kDa. Both protein profiles were described to play important roles in mineral regulation (Kaartinen et al. 1999; Nishimichi et al. 2009). Interestingly, OPN was upregulated at day 21 at PD15 glucose. This dramatic increase in OPN expression suggests that there might be a relation between upregulated OPN and high glucose, which demonstrated a reduction in mineral deposition. OPN has also been deeply investigated at a protein level. Interestingly, this significant upregulation of OPN level revealed at the committed cells (PD15) in high glucose, whereas immature cells (PD50) showed lower levels. This information would assist in understanding the pathological bone loss in diabetes. Colombo et al. (2011) reported OPN upregulation in diabetic bone. Subsequently, herein, we can claim that this upregulated OPN came from committed osteoprogenitor cells. Taken together, these findings open the door to further investigating OPN role in diabetic bone.

This Chapter has shown that CB-MSCs at different PDs have different capacity for osteogenic and adipogenic differentiation. PD15 committed progenitor cells have demonstrated the highest capacity for osteogenic differentiation and mineral deposition. However, the change in cell heterogeneity at PD50 (immature cells) has clearly shown a reduction in this osteogenic ability. On the other hand, committed and immature cells demonstrated good ability to adipogenic differentiation. Intriguingly, high glucose has been observed to exhibit a significant decrease in osteogenic differentiation process in committed cells (PD15), but not immature (PD50), such a novel finding is yet to be mentioned as far as we are aware. OPN was reported to be increased at committed osteoprogenitor cells in high glucose samples. Obtaining this information about increased OPN levels supports the future investigation of the effects of *Porphyromonas gingivalis*-lipopolysaccharide, which has been described as a causative factor for periodontal disease and impaired bone osteogenesis.

Chapter 4: Effects of *Porphyromonas Gingivalis* Lipopolysaccharide on CB-MSC Osteogenesis under Normal and High Glucose Conditions

4.1: Introduction

Periodontal disease is an inflammatory pathologic state of the supporting structures of the periodontium, including the gingiva, alveolar bone, periodontal ligament and cementum. The etiology of the disease is of complex bacterial origin. Between the 1930s-1970s, researchers were unable to identify specific etiological agents of periodontal disease and hypothesized that it was due to a consortium of micro-organisms as the "non-specific theory" (Theilade 1986). Nevertheless, after the 1970s, more specific microorganisms were isolated and proposed to be the etiological factors of periodontitis (Tanner et al. 1979; Slots et al. 1986; Moore and Moore 1994). Intensive studies have now confirmed that the prime periodontopathic bacterial species among these etiological factors is *Porphyromonas gingivalis (Pg),* (Marcotte and Lavoie 1998; Maiden et al. 2003; Paster et al. 2006; Hajishengallis et al. 2012). *Pg* was found in 86% of subgingival plaque samples from patients affected by chronic periodontitis (Datta et al. 2008). This periodontopathic species is known to produce a plethora of virulence factors, including fimbriae, capsules and lipopolysaccharide (LPS) (Holt et al. 1999; Hajishengallis and Lamont 2014). LPS has been investigated in many studies and found to be involved in specific deleterious effects on bone formation and immunoglobulin proteases (Roberts et al. 2008; How et al. 2016).

Pg-LPS is a complex glycolipid forming an important part of the outer membrane of this Gram-negative bacterium. It plays critical roles in maintaining the cellular and structural integrity and controlling the entry of hydrophobic molecules and toxic chemicals (Silhavy et al. 2010). In terms of virulence, it is found to be the most significant pathogenic factor among other periodontopathic bacteria. *Pg*-LPS consists of a relatively large size molecule of at least 10kDa (Hamada et al. 1994) and a polysaccharide (O-antigen), the core oligosaccharide and the hydrophobic domain known as lipid A, which attaches the LPS to the bacterial cell membrane (Ogawa and Yagi 2010). Lipid A is the biologically active region of LPS, that could trigger both Toll-Like Receptors 2 and 4 (TLR2,TLR4), causing deregulation of the innate immune system in mammals (Darveau et al. 2004). Al-Qutub et al. (2006) have reported that lipid A has heterogeneous acylation patterns, which would be changed, depending on the microenvironmental conditions, to facilitate bacterial survival inside the host. Furthermore, Díaz et al. (2015) have observed that *P. gingivalis* isolated from periodontally involved subjects produced modified lipid-A molecules, unlike that from healthy subjects. It is worth

noting that the virulence and roles of the other components of *pg*-LPS are still poorly understood (How et al. 2016).

A number of studies have described the ability of LPS to activate the host inflammatory responses through TLR2 and TLR4, which in turn induce the production of proinflammatory cytokines, interleukin-1β (IL-1β), IL-6, IL-8 and tumor necrosis factors-α (TNF-α), disrupting bone remodelling and repair processes (Jiang et al. 2002; Graves et al. 2011; Herath et al. 2011; Kato et al. 2014). Understanding these mechanisms may be a prime step for the treatment of periodontal disease. Li et al. (2014) have demonstrated that blockage of TLR4-mediated NF-kB signaling pathway, prevented alveolar bone destruction by *E. coli*-LPS. Little is known, however, about the mechanisms of bone loss induced by *pg*-LPS. Despite the various research, investigating different concentration effects of *pg*-LPS on the osteogenic capacity of bone, overall findings have been contradictory. A growing number of studies have shown that 0.1, 0.2, 1 and 10µg/mL concentrations of *pg*-LPS could affect osteogenic differentiation (Roberts et al. 2008; Kato et al. 2014; Xing et al. 2015). On the contrary, Albiero et al. (2017) demonstrated that 0.1, 1 and 10µg/mL concentrations of *pg*-LPS have no effects on cell proliferative capacity and the osteogenic differentiation of periodontal ligament stem cells (PDLSCs). Tang et al. (2015), nevertheless, reported that concentration of 0.1µg/mL of *pg*-LPS induced bone formation, but they showed 10µg/mL would inhibit bone regeneration in bone marrow mesenchymal stem cells (BM-MSCs). These contradictory results may be due to the different cell origins assessed, which would produce various responses, in addition to the experimental settings in different studies. Roberts et al. (2008) reported that *pg*-LPS reduced osteogenic differentiation in rat alveolar bone osteoblasts through alteration of the extracellular matrix proteoglycans, decorin, and biglycan, which have been ascribed roles in bone formation. However, a limited number of studies have further investigated the effects of *pg*-LPS on the synthesis of extracellular matrix protein OPN. Kadono et al. (1999) demonstrated that *pg*-LPS inhibited OPN and OCN production in rat calvaria cells. OPN has a pivotal role in bone formation and remodelling when it binds to mineral crystals, inhibiting their growth to assist in the bone remodelling process (McKee et al. 2011). OPN levels have been found to be increased at the extracellular matrix of the bone in diabetic rats, which could have detrimental effects on bone regeneration (Colombo et al. 2011). Therefore, this study has focused on assessing OPN in high glucose conditions, aggravated by different concentrations of *pg*-LPS, to investigate the combined effects of these two factors on the osteogenic process and how they may affect the bone repair.

With a view to addressing the contradictory studies, this Chapter aims to investigate the effect of *pg*-LPS on the osteogenic differentiation of both committed and immature compact bone mesenchymal stem cell populations, under normal and high glucose conditions. In addition, investigation of the effects of *pg*-LPS on OPN levels, which are described to be increased in high glucose conditions and how this may affect or delay bone remodelling and repair. This study would assist in further understanding and elucidate the bone destruction during periodontitis associated with T2DM.

4.2: Materials and Methods

All the subsequent analyses were performed on CB-MSCs at the PD15 and PD50 populations, under normal and high glucose conditions, focusing on these well-defined populations while neglected PD100 and PD200.

4.2.1: Characterisation of *Porphyromonas Gingivalis* Lipopolysaccharide (*pg*-LPS)

Pg-LPS was purchased from InvivoGen, USA. It came as a lyophilized protein within a vial containing 1mg and provided with 1mL of distilled water for dilution. *Pg*-LPS were prepared according to the manufacturer's instructions to give a concentration of 1000µg/mL. A concentration of 10µg/10µL of *pg*-LPS was loaded on a pre-casted gel (Bio-Rad, Laboratories Ltd.), to conduct SDS-PAGE. An equal amount of *E. coli*-LPS (Sigma-Aldrich, UK) was also analyzed for comparison.

4.2.1.1: Coomassie Blue Staining

SDS-PAGE was conducted according to Chapter 3 (see Section 3.2.2.2). The gel was then submerged in a working solution of Coomassie Blue stain for 1h, with gentle agitation at room temperature [50mL Coomassie stock solution, 88mL methanol (Thermo Fisher Scientific, UK), 24mL glacial acetic acid (Thermo Fisher Scientific) and 88mL ddH_2O], [Coomassie Blue stock consisted of 250mL Methanol, 250mL ddH_2O and 1.25g of Coomassie Blue (Sigma-Aldrich)]. The gel was destained overnight at 4^oC with constant agitation, using destaining solution (5% methanol, 7.5 % glacial acetic acid, and 87.5% ddH_2O). The gel was finally rinsed with ddH_2O to remove excess Coomassie Blue stain and imaged by GelDoc™ Scanner using Doc™ EZ Imaging System with Image Lab™ version5 (Bio-Rad, Laboratories Ltd.).

4.2.1.2: Silver Staining

Silver staining was conducted using Silver Stain Plus™ Kit (Bio-Rad, Laboratories Ltd.). SDS-PAGE was conducted as above. The gel was submerged in a dish filled with fixative enhancer solution (50% reagent-grade methanol, 10% reagent-grade acetic acid, 10% fixative enhancer concentrate; and 30% ddH_2O) for 20min at room temperature, with gentle agitation. The gel was rinsed twice with ddH_2O for 10min each time, meanwhile the staining solution was prepared with thorough mixing (35% ddH_2O, 5% silver complex solution, 5% reduction moderator solution; and

5% image development reagent and immediately before use, adding 50% of accelerating solution at room temperature). The gel then placed in a dish filled with freshly prepared staining solution for 20min, or at least until the O-antigen polysaccharide bands became visible with gentle agitation. To stop the reaction, 5% acetic acid was added for 15min, followed by washing with ultrapure water (18.2MΩ H2O) and imaged by GelDoc™ Scanner using Doc™ as previously described.

4.2.1.3: Gel Electrophoresis for Nucleic Acid Detection

Gel electrophoresis was conducted according to Chapter 2 (Section 2.2.5.1.3). 10µg/mL of *pg*-LPS was loaded into the gel to investigate the purity, with *E. coli*-LPS for comparison.

4.2.2: Cell Proliferation and Viability Assay

Cells were seeded in 96-well plate at 4000/cm^2 in osteogenic induction culture media (see Chapter 3, Section 3.2.1.1), supplemented with *pg*-LPS at concentrations of 10µg/mL, 1µg/mL, 0.1µg/mL and 0µg/mL (negative control); and investigated at day 1, 3,5 and day 7. Briefly, media were gently removed and replaced with fresh culture media included 20µL of thiazolyl blue tetrazolium blue (MTT) assay reagent [5mg/mL MTT (Sigma-Aldrich) in phosphate buffered saline (PBS)]. The plates were incubated at 37ºC, 5% CO_2 for 5h. Culture media were removed and replaced with 100µL of dimethyl sulfoxide DMSO (ThermoFisher Scientific) and incubated at 37ºC, 5% CO_2 for 30min. The colorimetric absorbance was read at 570nm, using a FluoSTAR Omega Plate Reader (BMG Labtech, UK). Blank reading wells (empty wells) were incubated with MTT and the culture media only but without cells. The assay was conducted on three separate occasions.

4.2.3: Apoptosis Activity Assay

4.2.3.1: Positive Control for Apoptotic Assay

Four concentrations (0, 100, 200 and 500µM) of hydrogen peroxide (H_2O_2) (Sigma Aldrich) were analyzed to choose a positive control for Caspase-Glo® 3/7 Assay (Promega, UK). We found that 200µM concentration was the most suitable for all the PDs of the experiment (Figure 4.1).

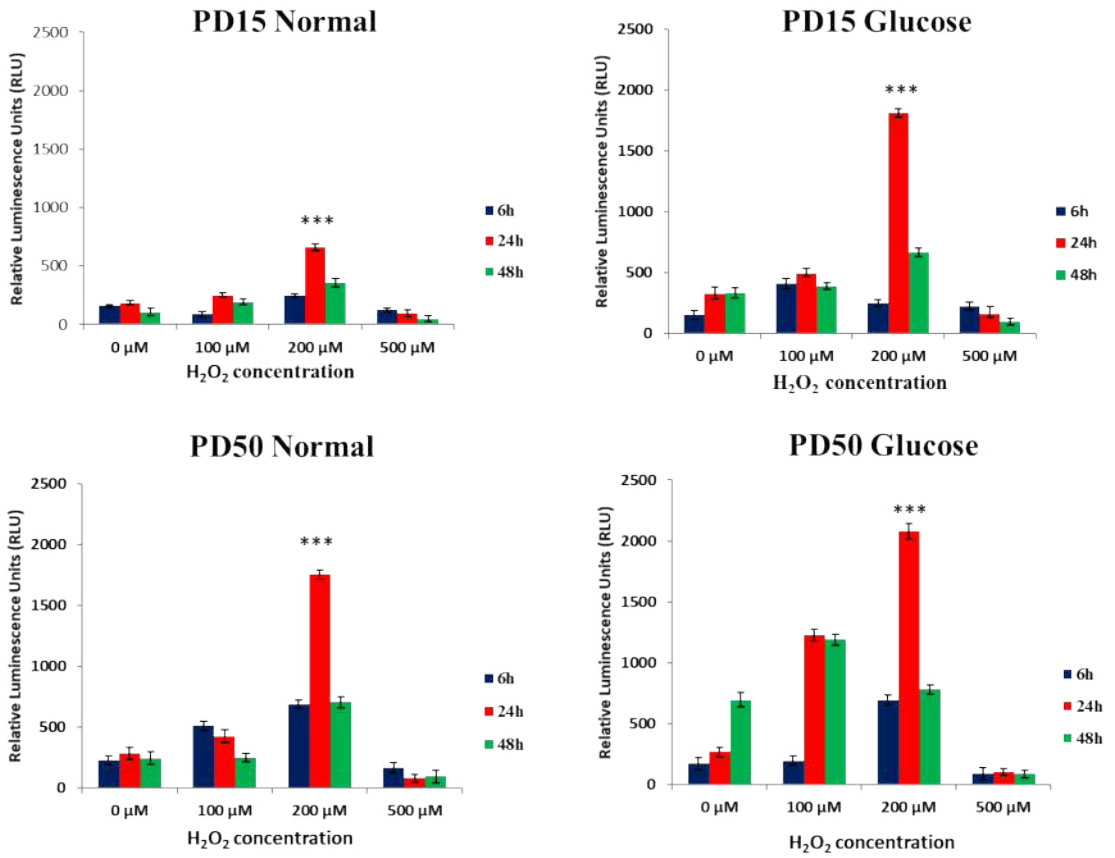

Figure 4.1 CB-MSCs were investigated with 0, 100, 200, and 500µM H_2O_2, to select a positive control for the Caspase Activity Assay. 200µM concentration appeared to be the most suitable for all PDs. Error bars represent ± SEM of the mean (n=3). ***=p<0.001.

4.2.3.2: Caspase Activity Assay

The Caspase-Glo® 3/7 Assay (Promega) was used to quantify the apoptotic activity of CB-MSCs cultured with different concentrations of *pg*-LPS in osteogenic induction media, under normal and glucose conditions. Caspase-Glo® 3/7 reagent was prepared by thawing the Caspase-Glo® 3/7 Buffer and mixing the entire contents with Caspase-Glo® 3/7 substrate, with gentle agitation to ensure a complete mixture of the reagents. Prepared Caspase-Glo® 3/7 reagent was stored for up to 1 week at 4°C. Before use, it was warmed to room temperature. MSCs were seeded in white-walled optically clear 96-well plates (GBO, UK), at 4,000/cm^2 in 10% FBS culture media supplemented with *pg*-LPS at three concentrations; 0.1µg/mL, 1µg/mL, 10µg/mL and 0µg/mL (negative control). Caspase activity was investigated at three-time points 6, 24 and 48h at 37ºC, 5% CO_2. The plate was removed from the incubator and acclimatised to the room temperature. 50µL of Caspase-Glo® 3/7 reagent was added to each well. The plates were then shaken on a plate shaker at 300rpm for 30s, followed by 1h incubation at room temperature, wrapped with aluminum foil to protect from light. Optical

emission was measured by using a FluoSTAR Optima plate reader, which was set to the maximum optical gain settings and arbitrary relative luminescence units (RLUs). Blank readings were obtained from wells that were incubated with Caspase-Glo® 3/7 reagent and osteogenic induction media containing no cells. The experiment was conducted on three separate occasions.

4.2.4: Investigation of CB-MSCs Osteogenic Differentiation Capacity Under Various *pg*-LPS concentrations

4.2.4.1: Osteogenic Conditioned with *pg*-LPS

CB-MSCs were plated at 4000/cm^2 in 6-well plates in osteogenic differentiation media for 28 days, in normal, high glucose and *pg*-LPS conditions. *Pg*-LPS was added to the media along the 28 days of osteodifferentiation at two concentrations; 0.1µg/mL and 1µg/mL. 10µg/mL *pg*-LPS was neglected as it was cytotoxic to CB-MSCs. For osteogenic medium compositions, refer to Chapter 3, (Section 3.2.1.1).

4.2.4.2: Alizarin Red Staining and Mineral Quantification

Cells were stained with Alizarin Red staining at day 28 and images taken. Quantification of mineral formation was also performed at day 28. All the procedures were discussed in detail, refer to Chapter 3, (Section 3.2.1.2).

4.2.4.3: Quantification of Osteogenic mRNA Markers Using qPCR

Cells were investigated at day 2, 7,14, 21 and day 28. Osteogenic mRNA markers Runx2, OSX, OPN and OCN expression were quantified using qPCR. Refer to Chapter 2 (Section 2.2.8).

4.2.5: Osteopontin Extraction and Analysis

CB-MSCs were plated in osteogenic media, in normal, high glucose and *pg*-LPS conditions; and grown for 21 days. Total protein was extracted at days 7, 14 and day 21; and dialyzed for 5 days (Chapter 3, Section 3.2.2). Protein contents were then quantified (Chapter 3, Section 3.2.2.1). Total protein was purified (Chapter 3, Section 3.2.2.4). Immuno- and electro-blotting detection was performed to assess OPN (Chapter 3, Section 3.2.2.2 and Section 3.2.2.3). OPN levels were quantified by ELISA (Chapter 3, Section 3.2.2.5).

4.2.6: Detection of Phosphorylated OPN through Targeting Anti-Phosphoserine Antibody

OPN phosphorylation status was immunodetected using anti-phosphoserine antibody (Chapter 3, Section 3.2.3).

4.2.7: Statistical Analyses

Statistical analyses were performed using One-Way ANOVA with a post-hoc Tukey test to determine the statistical differences between sample groups, using the software GraphPad InStat 3 (v3.06). Statistical significance of differences was defined as significant (*, $p<0.05$), very significant (**, $p<0.01$) or highly significant (***, $p<0.001$).

4.3: Results

4.3.1: Characterisation of *pg*-LPS

4.3.1.1: Coomassie and Silver Staining for Bacterial Protein detection, and Gel Electrophoresis for Nucleic Acid Detection

Pg-LPS showed no staining when investigated with Coomassie Blue stain, while with Silver staining, *pg*-LPS demonstrated a classical heterogeneous pattern which may be attributed to O-chain moiety, similar to that obtained from *E. coli*-LPS, which was used for comparison, but with lower molecular weight material that appeared with *pg*-LPS, which may be owing to structural differences between the two species (Figure 4.2 A, B). *Pg*-LPS assessed by agarose gel electrophoresis revealed very low levels of nucleic acid, compared to *E. coli*-LPS, which demonstrated a trace amount nucleic acid (Figure 4.2 C). These results proved that the *pg*-LPS were free from bacterial protein components, whereas the *E. coli*-LPS exhibited multiple bands indicated of a significant amount of different bacterial proteins.

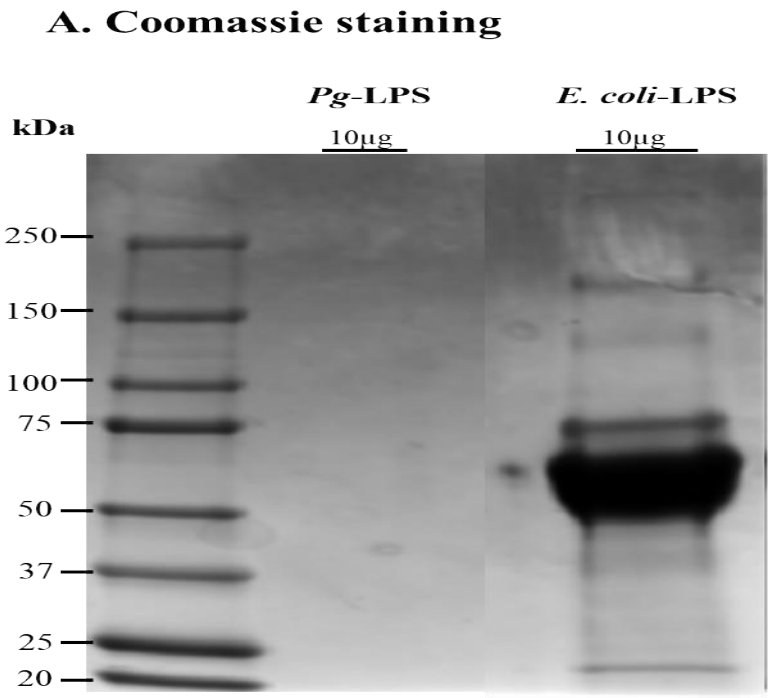

Figure 4.2: SDS-PAGE to characterise *pg*-LPS, by staining with **A.** Coomassie Blue stain showed no protein stain for *pg*-LPS and *E*. Coli-LPS for comparison.

B. Silver staining

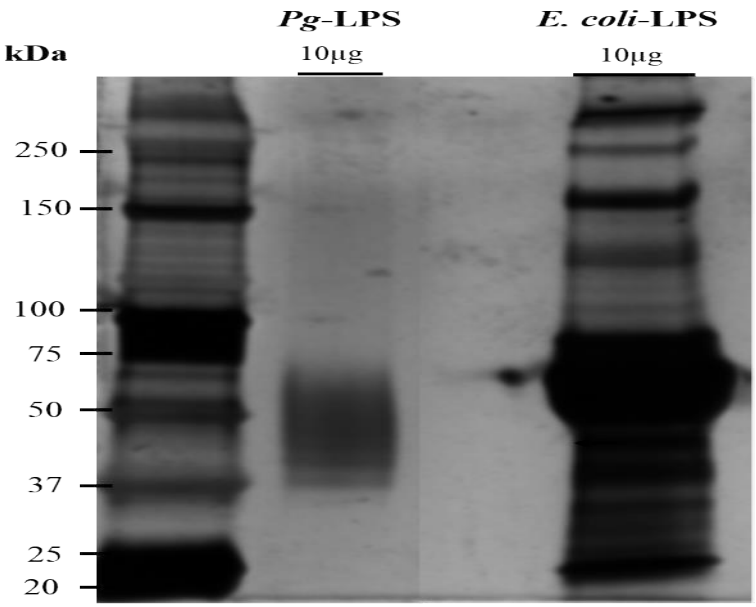

C. Gel Electrophoresis

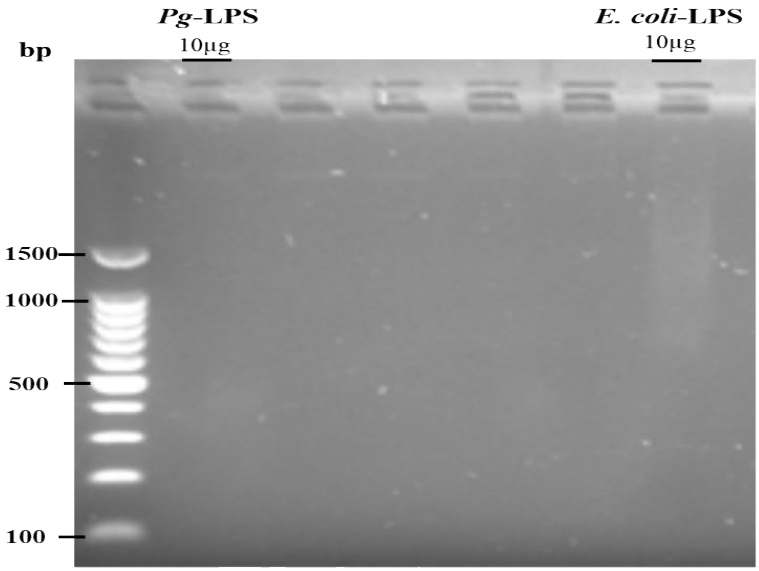

B. Silver stain demonstrated clear bands of O-chain moiety of *pg*-LPS, whereas *E. coli*-LPS exhibited multiple bands indicated of bacterial proteins. **C.** Gel electrophoresis to investigate the nucleic acid purity of the *pg*-LPS which revealed very low amounts. *E. coli*-LPS exhibited trace amount of nucleic acid impurities.

4.3.1.2: Effects of *pg*-LPS on Cellular Proliferation and Viability

Over 7 days in culture, 0.1µg/mL and 1µg/mL *pg*-LPS increased cell proliferation, but were not significant ($p>0.05$) compared to controls (concentration 0 µg/mL). *pg*-LPS at a concentration of 10µL/mL evoked a reduction of CB-MSC proliferation and viability mainly at day 7. At PD15 N, cell expansion developed gradually with no significant difference among various *pg*-LPS concentrations versus the control, until day 7. There were significant differences ($p<0.01$) between concentration 0.1µg/mL and 1µg/mL, compared to concentrations at 10µg/mL. In high glucose, PD15 exhibited similar growth trend as PD15 N. At day 7 in high glucose, there were significant differences ($p<0.001$) between 10µg/mL *pg*-LPS, compared to 0.1µg/mL, 1µg/mL and the controls. PD50 N day 7 exhibited a significant reduction ($p<0.01$) in cell proliferation compared to 1µg/mL *pg*-LPS and ($p<0.001$) compared to 0.1µg/mL *pg*-LPS concentrations. PD50 G demonstrated significant reduction at 10µg/mL compared to control ($p<0.01$), and significant reduction ($p<0.001$) compared to both concentrations 0.1 µg/mL and 1 µg/mL *pg*-LPS. Ultimately, 10µg/mL *pg*-LPS was neglected, considering it was cytotoxic to CB-MSCs (Figure 4.3).

4.3.1.3: Apoptotic Activity of CB-MSCs Treated with *pg*-LPS

There was low caspase activity in all samples except PD50 G, which demonstrated significant increase ($p<0.001$). PD15 N exhibited significant increased ($p<0.001$) at the concentration 1µg/mL *pg*-LPS at 48h compared with 0.1 and 10µg/mL concentrations and 0 µg/mL (negative control). At 0.1µg/mL *pg*-LPS of PD15 N, 48h showed significant increase in caspase activity ($p<0.001$) compared to 6h and 24h. At PD15 G, there were no significant differences between all concentrations in comparison to 0 µg/mL negative control. PD50 N demonstrated no significant differences among all concentrations, in comparison with the 0µg/mL control. However, there was significant increased at concentration of 1µg/mL at 48h, compared to 0.1 and 10µg/mL *pg*-LPS. At PD50 G, the caspase activity showed no significant differences at all concentrations, in comparison with the 0 µg/mL control, but demonstrated higher levels of Luminescence Units at 48h in comparison to 6h and 24h (Figure 4.4).

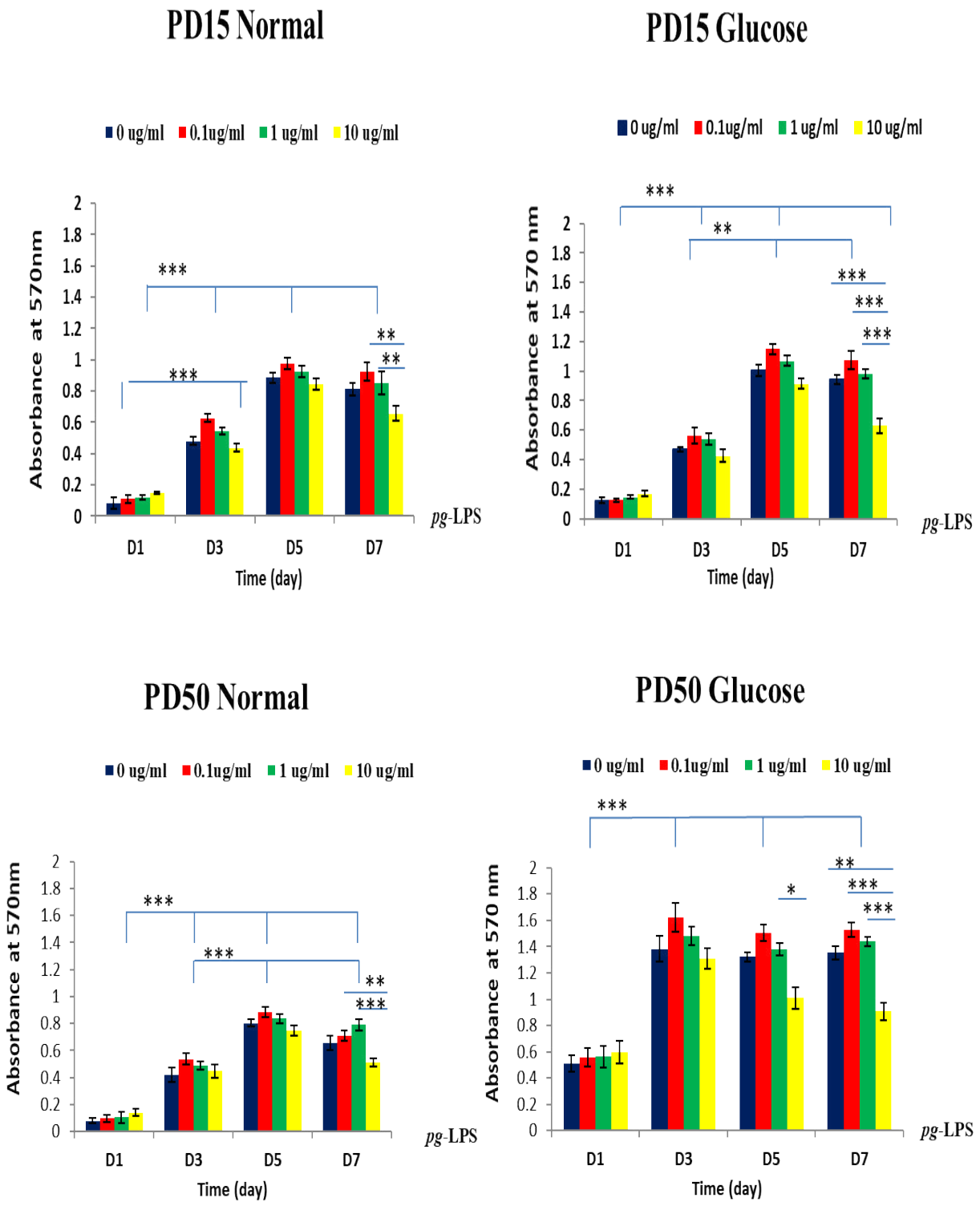

Figure 4.3: Monitoring cell proliferation and viability with various concentration of *pg*-LPS (0, 0.1, 1 and 10 µL/mL of *pg*-LPS) using the MTT assay. A marked reduction in CB-MSC expansion was noticed at day 7 with 10 µL/mL *pg*-LPS in comparison to 0.1 and 1 µL/mL concentrations. There were no significant differences between 0.1µL/mL and 1µL/mL of *pg*-LPS concentrations with the controls over 7 days ($p>0.05$). Error bars represent ± SEM of the mean (n=3). *=$p<0.05$, **=$p<0.01$, ***=$p<0.001$.

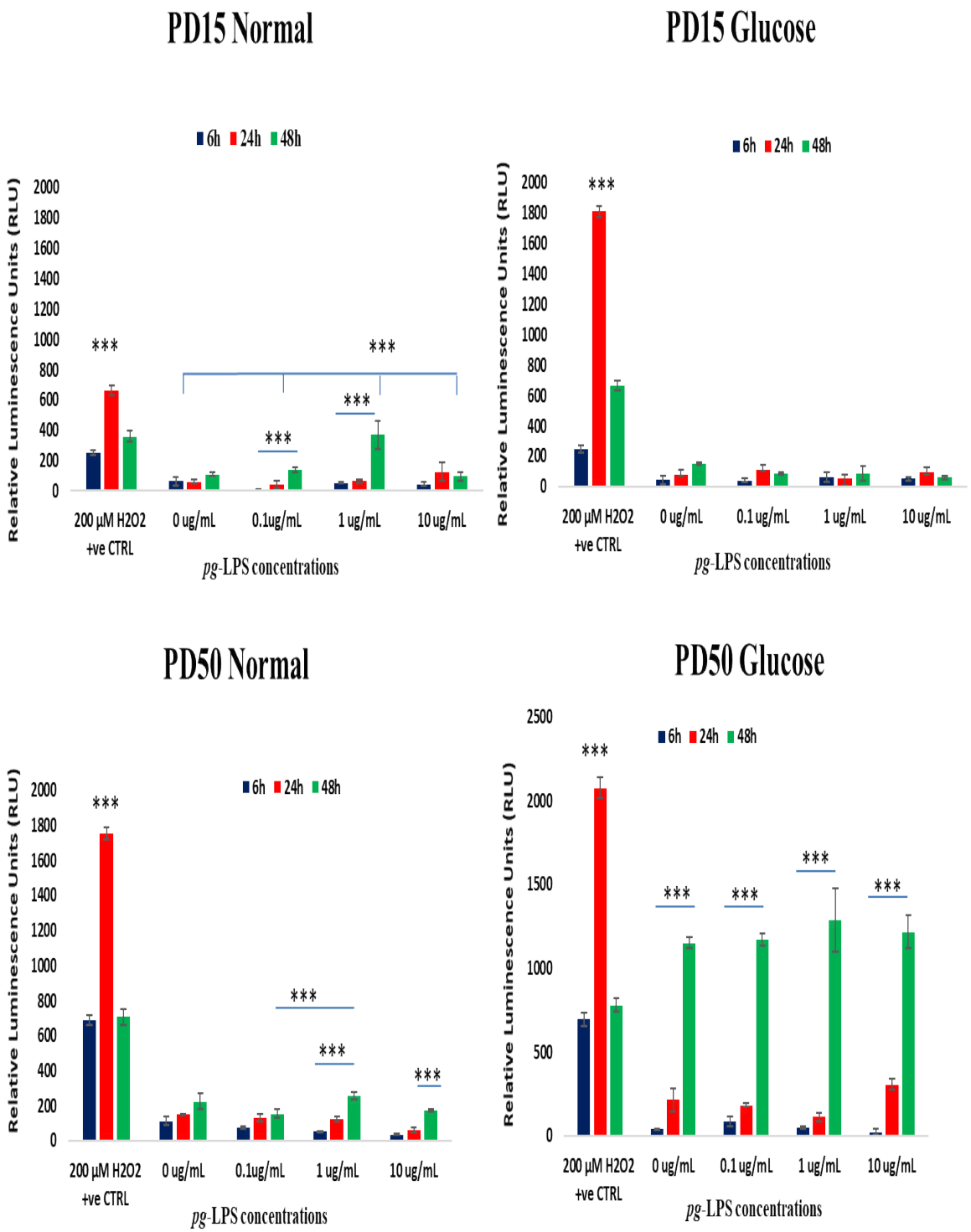

Figure 4.4: Caspase Activity Assay investigating the apoptotic activity of CB-MSCs cultured with various concentrations of *pg*-LPS (0, 0.1, 1 and 10 µg/mL). 200µM H_2O_2 were used as a positive control. Error bars represent ± SEM of the mean (n=3). ***=p<0.001.

4.3.2: Osteogenic Differentiation and Mineral Tissue Formation by CB-MSCs Treated with Normal and High Glucose and *pg*-LPS

CB-MSCs were cultured with osteogenic induction media and treated with 0, 0.1, and 1 µg/mL concentrations of *pg*-LPS. Alizarin Red staining and qPCR results for mRNA expression of osteogenic markers (Runx2, OSX, OPN and OCN), revealed that PD15 committed cells demonstrated a better capacity of osteogenic differentiation into osteoblasts than PD50 immature cells. High glucose demonstrated a reduction in osteogenic differentiation mainly at PD15, but not PD50. *Pg*-LPS revealed a reduction in osteogenic differentiation at both PD15 and PD50. However, more pronounced effects were observed on PD50 when combined with high glucose (Figure 4.5).

4.3.2.1: Alizarin Red Staining and Mineral Quantification

Alizarin red staining was conducted on day 28, when the CB-MSCs underwent differentiation. For PD15, there was a marked deep red colour with the 0 µg/mL (control) N. Alizarin staining became gradually less staining at 0.1 and 1 µg/mL concentrations of *pg*-LPS. The high glucose control appeared less stained than the N control. Adding *pg*-LPS revealed no further change. PD50 showed less staining at 0 µg/mL concentration in N and G controls, compared to PD15. Adding *pg*-LPS demonstrated less staining red colour in G groups (Figure 4.5). Regarding mineral quantification PD15 N, 0µg/mL concentration of *pg*-LPS (control) demonstrated the highest mineral formation and significantly different ($p<0.001$), compared to all other PD15 *pg*-LPS concentrations. High glucose exhibited a reduction in the mineral deposition in the control group. Interestingly, adding *pg*-LPS exerted further reductions in mineral formation in N groups. PD50 showed a different response, there were no significant differences ($p>0.05$) in mineral formation between N and G (0 µg/mL) controls. At 0.1 and 1 µg/mL *pg*-LPS, there was a significant decline in mineral formation in G groups, compared to controls (0 µg/mL). *Pg*-LPS appeared to only affect mineral formation at 0.1 µg/mL concentrations at N group (Figure 4.6).

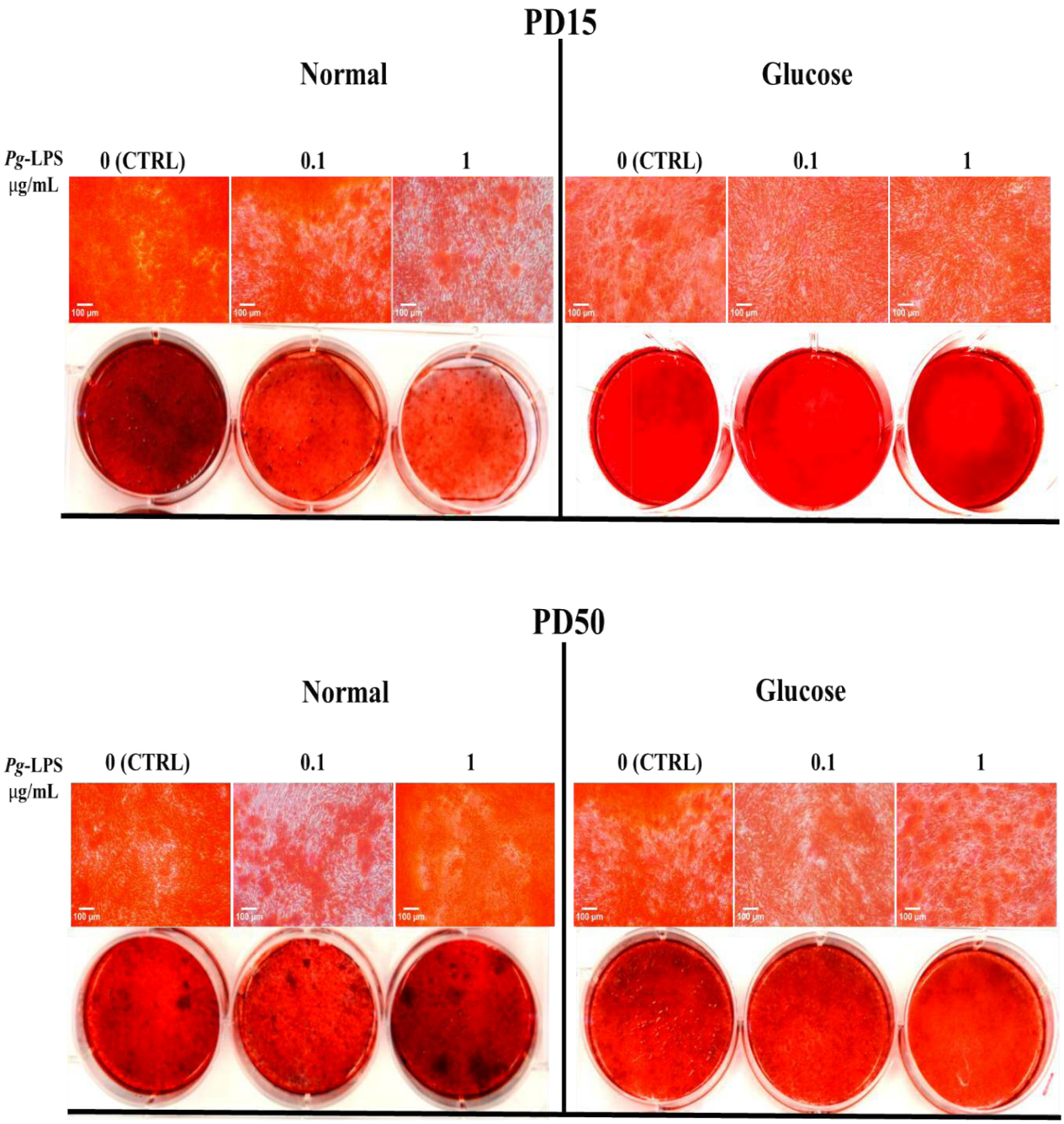

Figure 4.5: Alizarin Red staining for differentiated CB-MSCs, treated with various concentrations of *pg*-LPS (0, 0.1 and 1 µg/mL) in both N and G media at day 28. The red colour represents the mineral deposition by extracellular matrix secreted by newly formed osteoblasts. Differences in the red colour can be noticed between N and G and various concentration of *pg*-LPS in both population PD15 and PD50. Scale bar =100µm.

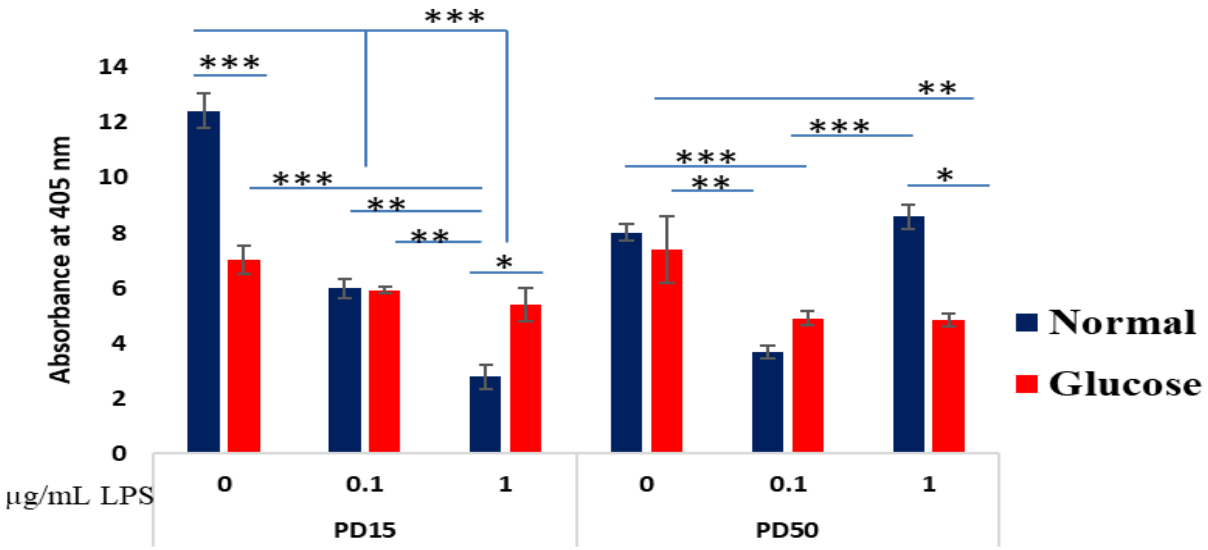

Figure 4.6: Bar chart represents the quantification of the mineral formation after osteogenic differentiation process of CB-MSCs. These cells were treated with various concentrations of *pg*-LPS (0, 0.1 and 1 µg/mL) in both N and G media. PD15 mineralisation appeared highly affected by G, whereas PD50 affected by combined effects of *pg*-LPS and glucose. Error bars represent ± SEM of the mean (n=3). **=p<0.01, ***=p<0.001

4.3.2.2: Quantitative Analysis of Osteogenic mRNA Marker Expressions

Runx2 is an early mRNA expression transcription factor for osteogenic differentiation. mRNA expression of Runx2 was upregulated at an early stage (day 2) in all groups and then downregulated at day 7. In PD15 glucose conditions, mRNA expression of Runx2 revealed a significant decrease in expression (p<0.05). Adding concentrations 0.1 and 1 µg/mL *pg*-LPS, downregulated Runx2 expression but was not significant (p>0.05). Combined high glucose with *pg*-LPS concentrations demonstrated non-significant differences (P>0.05). For PD50, the expression profile of mRNA expression of Runx2 was lower than PD15N. PD50 G was significant downregulated mRNA expression of Runx2 in 0 µg/mL and 0.1 µg/mL concentration (*=p<0.05) (Figure 4.7 A).

Osterix (OSX) proposed to be downstream to Runx2. mRNA expression of OSX exhibited the same profile of Runx2, upregulation at an early stage of day 2 and then downregulated at day 7. Its expression in PD15 was higher than PD50. In high glucose condition, there was significant (p<0.001), (p<0.05) downregulation of mRNA of OSX expression in both PD15 and PD50 respectively. Adding of 0.1 and 1 µg/mL of *pg*-LPS exerted no further downregulation (Figure 4.7 A).

OPN is considered as a mid-marker of osteogenic differentiation. mRNA expression of OPN showed upregulation at day 7 and continued downregulation through day 14 and 21 in PD15 and PD50.

Under high glucose condition, interestingly, there was upregulation of OPN at PD15 at day 21. In PD50 glucose conditions, however, there was downregulation of all mRNA expressions of OPN (Figure 4.7 B). Adding of 0.1 and 1 µg/mL of *pg*-LPS revealed no further significant effects. OCN is a late marker of osteogenic differentiation. mRNA expression of OCN was upregulated at day 28 for both PD15 and PD50, however, the expression in PD50 was very low. In high glucose conditions, mRNA expression of OCN was upregulated earlier at day 21, while significantly (p<0.05) downregulated at day 28. Adding *pg*-LPS revealed no significant effects (Figure 4.7 C).

A) Early Osteogenic Markers

Runx2

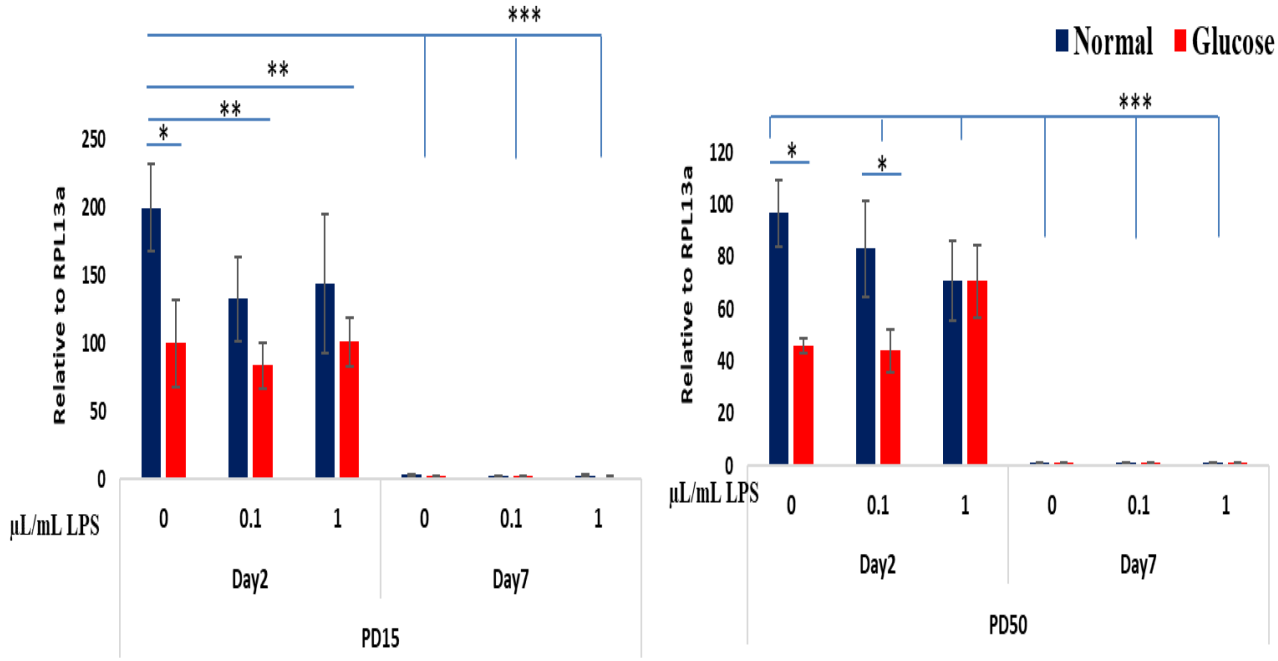

Figure 4.7: Investigation of osteogenic mRNA markers (Runx2, OSX, OPN, and OCN) in normal, high glucose and *pg*-LPS conditions using qPCR. **A)** Early osteogenic markers, Runx2 and OSX were considered as early expressed osteogenic markers and analyzed at day 2 and day 7. Error bars represent ± SEM of the mean (n=3). *=p<0.05, **=p<0.01, ***=p<0.001.

Osterix

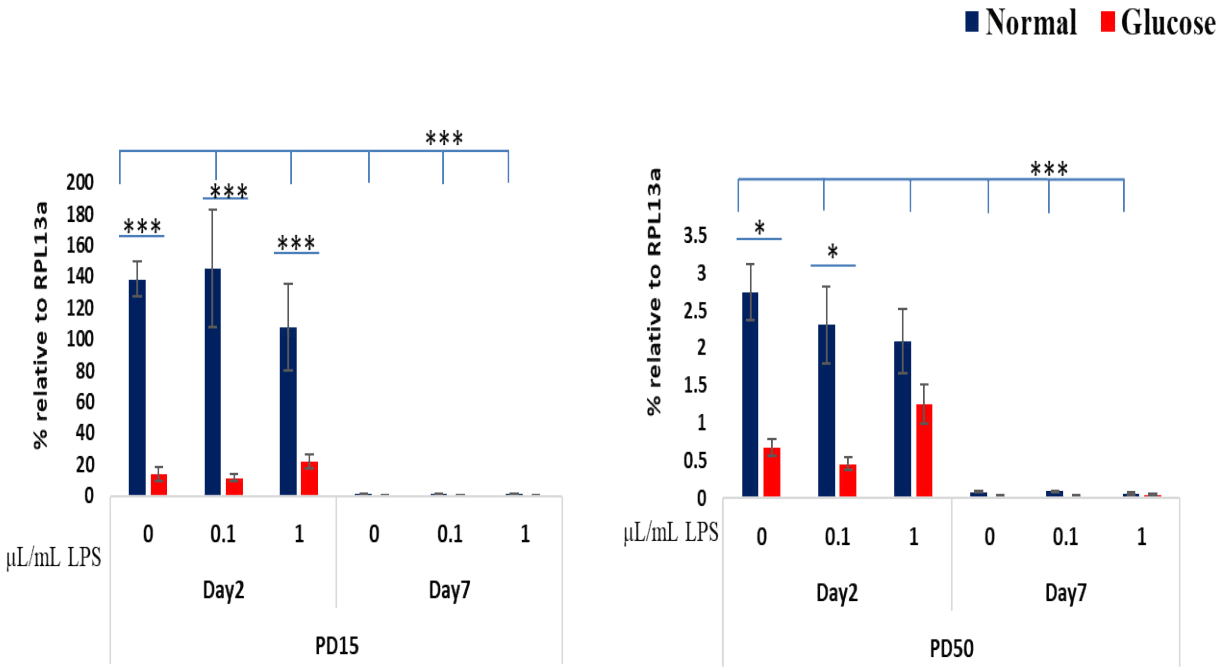

B) Mid Osteogenic Marker

Osteopontin

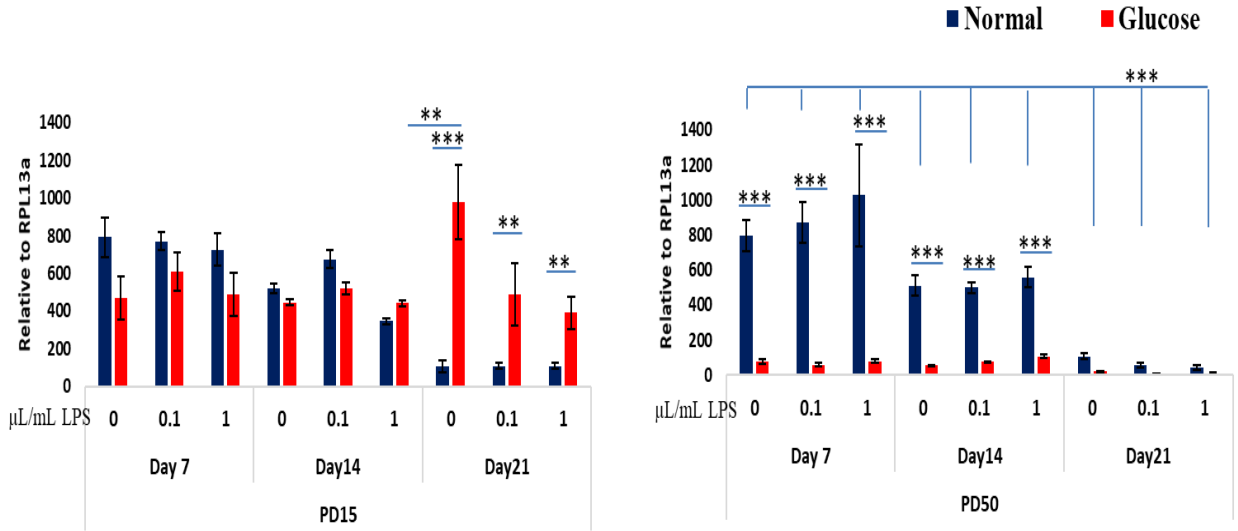

B) Mid osteogenic marker, OPN was considered as a mid-expressed osteogenic marker and investigated at day 7, 14 and day 21. Error bars represent ± SEM of the mean (n=3). *=p<0.05, **=p<0.01, ***=p<0.001.

C) Late Osteogenic Marker

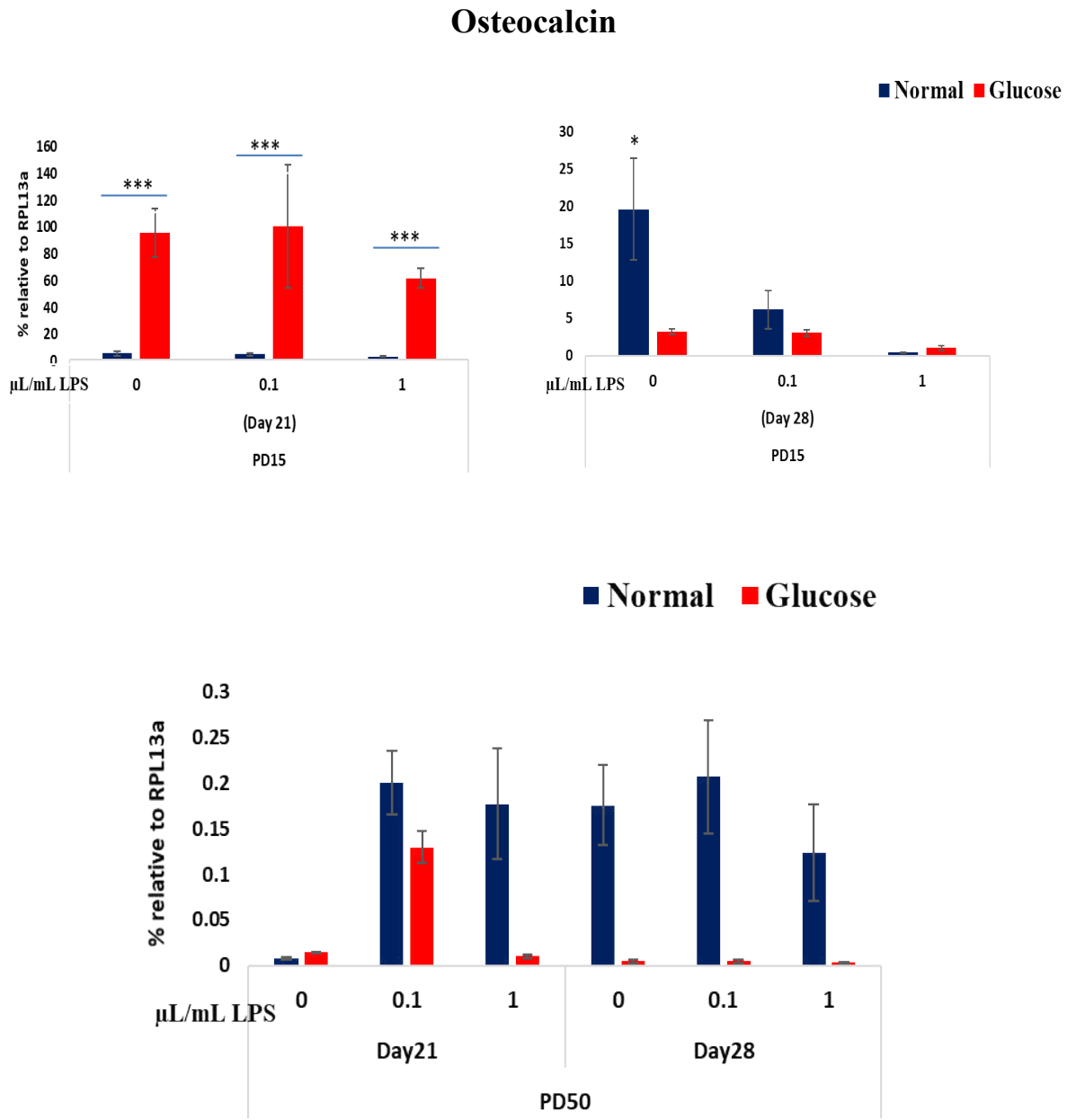

C) Late osteogenic marker, OCN considered late expression during osteogenesis and investigated at day 21 and day 28. Error bars represent ± SEM of the mean (n=3). *=p<0.05, **=p<0.01, ***=p<0.001.

4.3.3: Investigation of the Effects of *pg*-LPS on Osteopontin

4.3.3.1: Western Blot Analyses of Osteopontin in Cell Lysates and Extracellular Matrix (ECM)

As cultures continued, OPN synthesis and its incorporation into the extracellular matrix was detected at days 7,14 and 21(Figure 4.8). The main immunodetected bands were found at 55kDa molecular weight at all time-points, considered as monomeric OPN. Polymeric OPN appeared as faint bands at 120kDa on day 14 and day 21. At day 7, PD15 N and PD50 N showed denser bands, compared to G groups. At day 14, PD15 N *pg*-LPS concentrations (0, 0.1 and 1 µg/mL) demonstrated denser bands, compared to PD50 N. PD15 G control (0 µg/mL) exhibited dense bands and then became gradually less dense at 0,1 and 1 µg/mL. PD50 N and G demonstrated the same trend with less dense bands. At day 21, PD15 and PD50 G exhibited denser bands at all groups compared to normal (Figure 4.8).

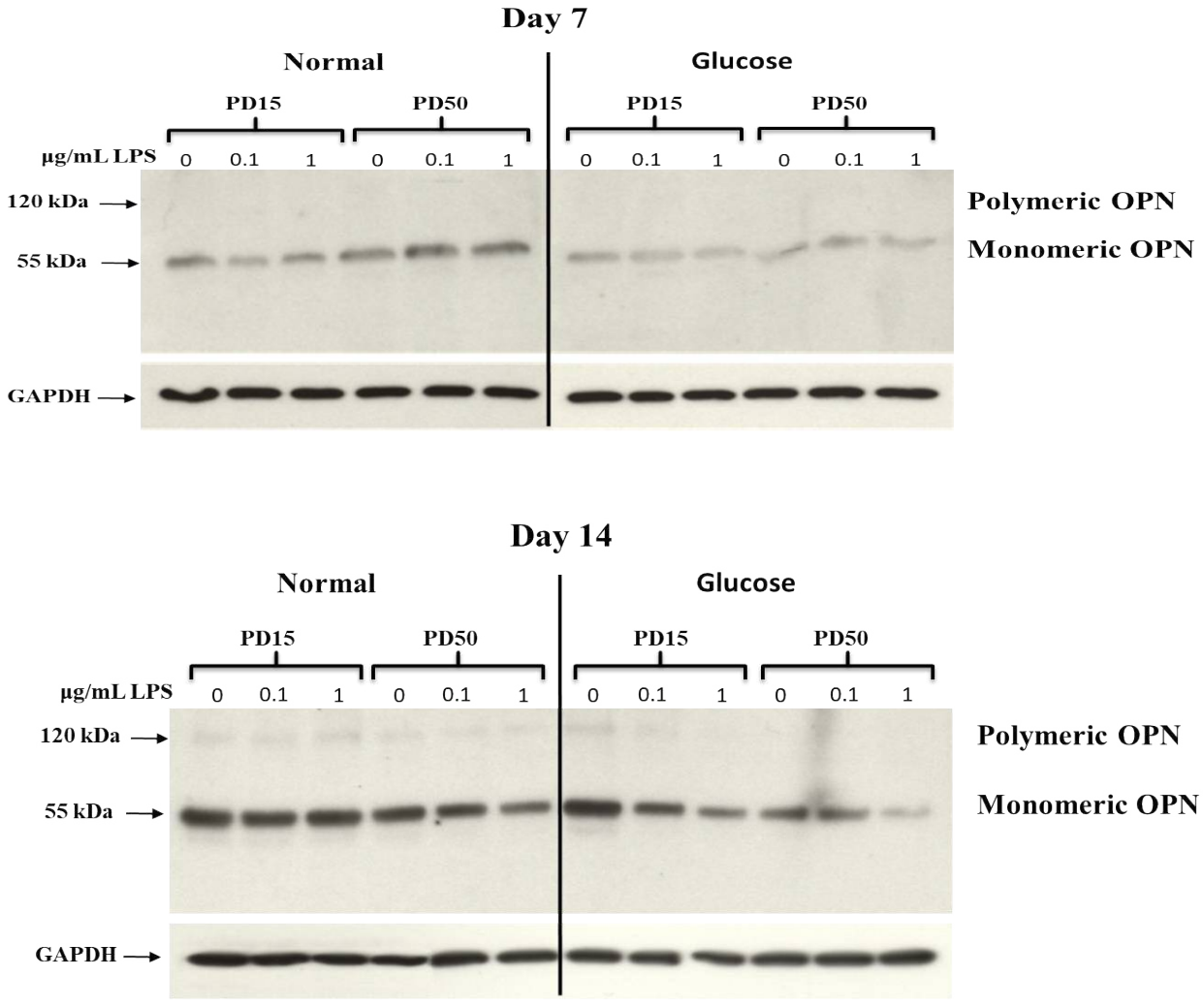

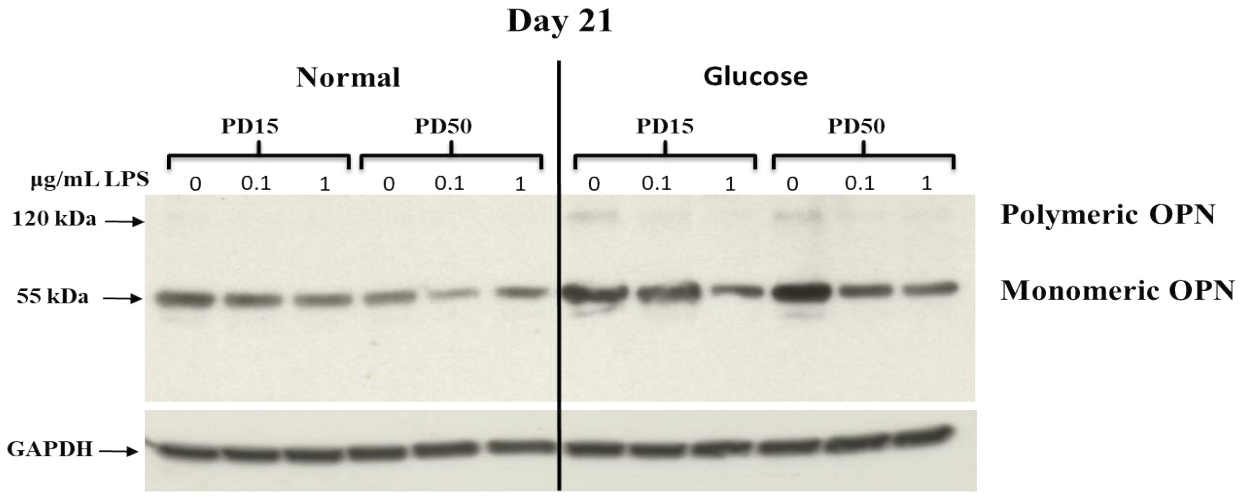

Figure 4.8: Western blot analysis of OPN levels in cell lysates and extracellular matrix of CB-MSCs grown in osteogenic media under normal and high glucose conditions. Cells were treated with 0, 0.1 and 1 µg/mL *pg*-LPS concentrations. Samples were investigated on day 7, 14 and 21. OPN bands were identified at 55kDa with some bands at 120 kDa. Western blots were repeated twice.

4.3.3.2: Western Blot Analyses of Osteopontin in Culture Media

OPN was also detected in culture media and identified of a post-translational modification at 120kDa and 55kDa in all samples. Cleaved OPN at 25kDa appeared mostly at day 7. At day 7, PD15 OPN exhibited a dense 55kDa bands in control groups, whereas adding 0.1 and 1 µg/mL *pg*-LPS reduced OPN levels. At PD50, however, a dense band occur with 0.1 µg/mL *pg*-LPS. In high glucose, it seems that combined effects of glucose and *pg*-LPS caused a gradual increase in OPN levels according to *pg*-LPS concentrations at PD15, while no further effects were evidenced at PD50 (Figure 4.9).

At day 14, control groups for both PD15 and PD50 showed dense OPN bands, which gradually became smaller in the presence of *pg*-LPS. In high glucose and in the presence of *pg*-LPS, there were smaller bands due to combined effects of both glucose and *pg*-LPS (Figure 4.9).

Day 21 revealed different OPN profiles, in PD15 and PD50 under normal conditions. OPN bands became denser with gradual increase of *pg*-LPS concentrations. In the presence of high glucose, denser OPN bands appeared. However, adding *pg*-LPS exerted inhibitory effects on OPN levels (Figure 4.9).

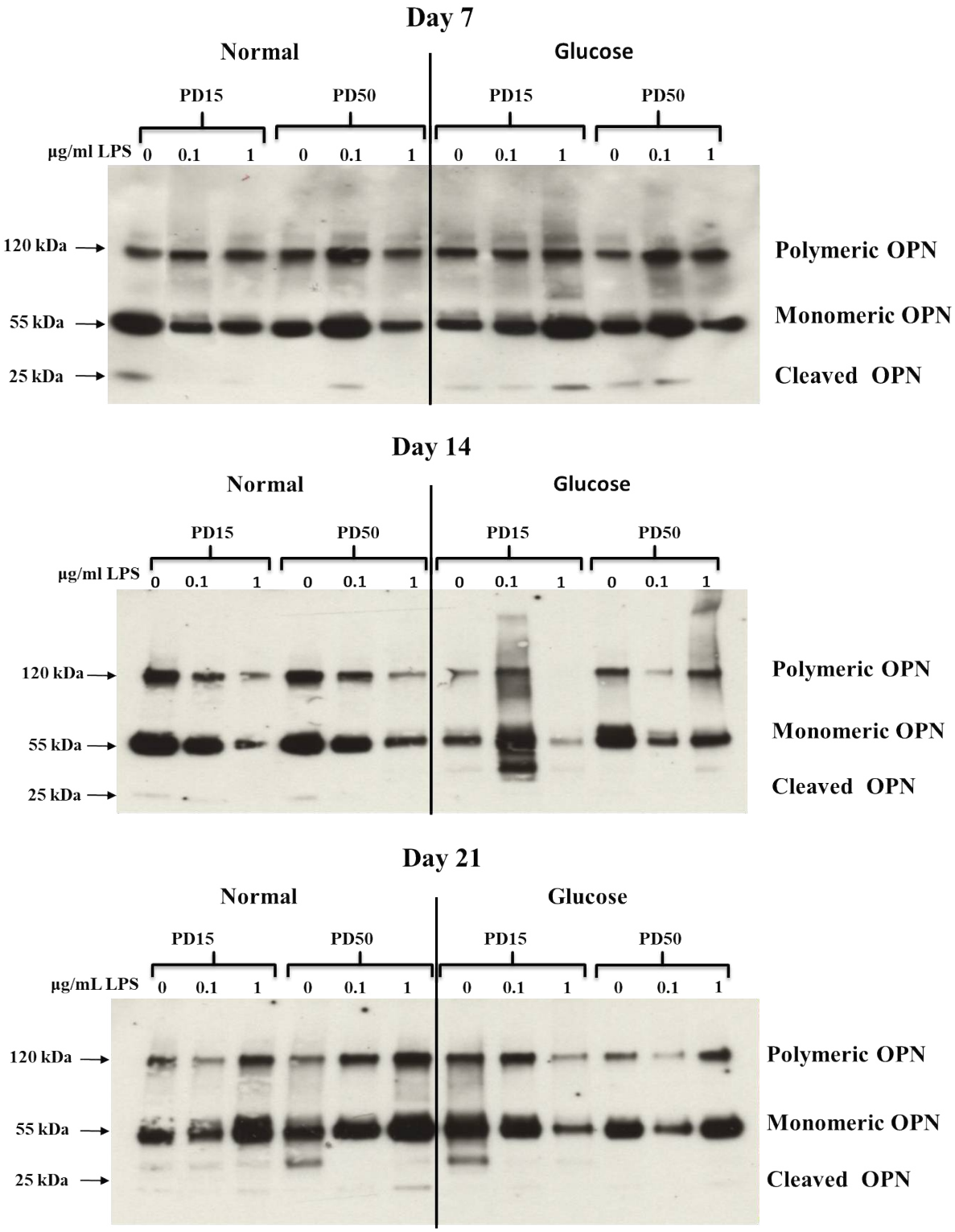

Figure 4.9: Western blot analysis of OPN levels in culture media of CB-MSCs grown in osteogenic media under normal and high glucose. Cells were treated with 0, 0.1 and 1 µg/mL *pg*-LPS. Samples were analysed on day 7, 14 and 21. OPN bands were identified at 55kDa, 120kDa and 25kDa. Western blots were repeated twice.

4.3.3.3: ELISA Quantification and Analyses of OPN in Culture Media

Quantification of OPN revealed that OPN levels in PD15 were about one-fold higher than PD50 at day 7. PD15 N, 0µg/mL *pg*-LPS, demonstrated significantly highest OPN levels ($p<0.001$). Addition of high glucose, OPN level was significantly reduced ($p<0.001$). In the presence of 0.1 and 1µg/mL *pg*-LPS, OPN levels was significantly reduced ($p<0.001$). PD50 N day 7, however, there was no significant differences under normal and high glucose conditions. Addition of 0.1 and 1µg/mL *pg*-LPS exerted no significant differences. In the presence of high glucose, however, 0.1 µg/mL and 1 µg/mL *pg*-LPS exhibited significant differences (*=$p<0.05$) compared to normal control. At day 14 and day 21, OPN levels decreased gradually in both PD15 and PD50 N and G groups without any significant differences (*=$p>0.05$) (Figure 4.10).

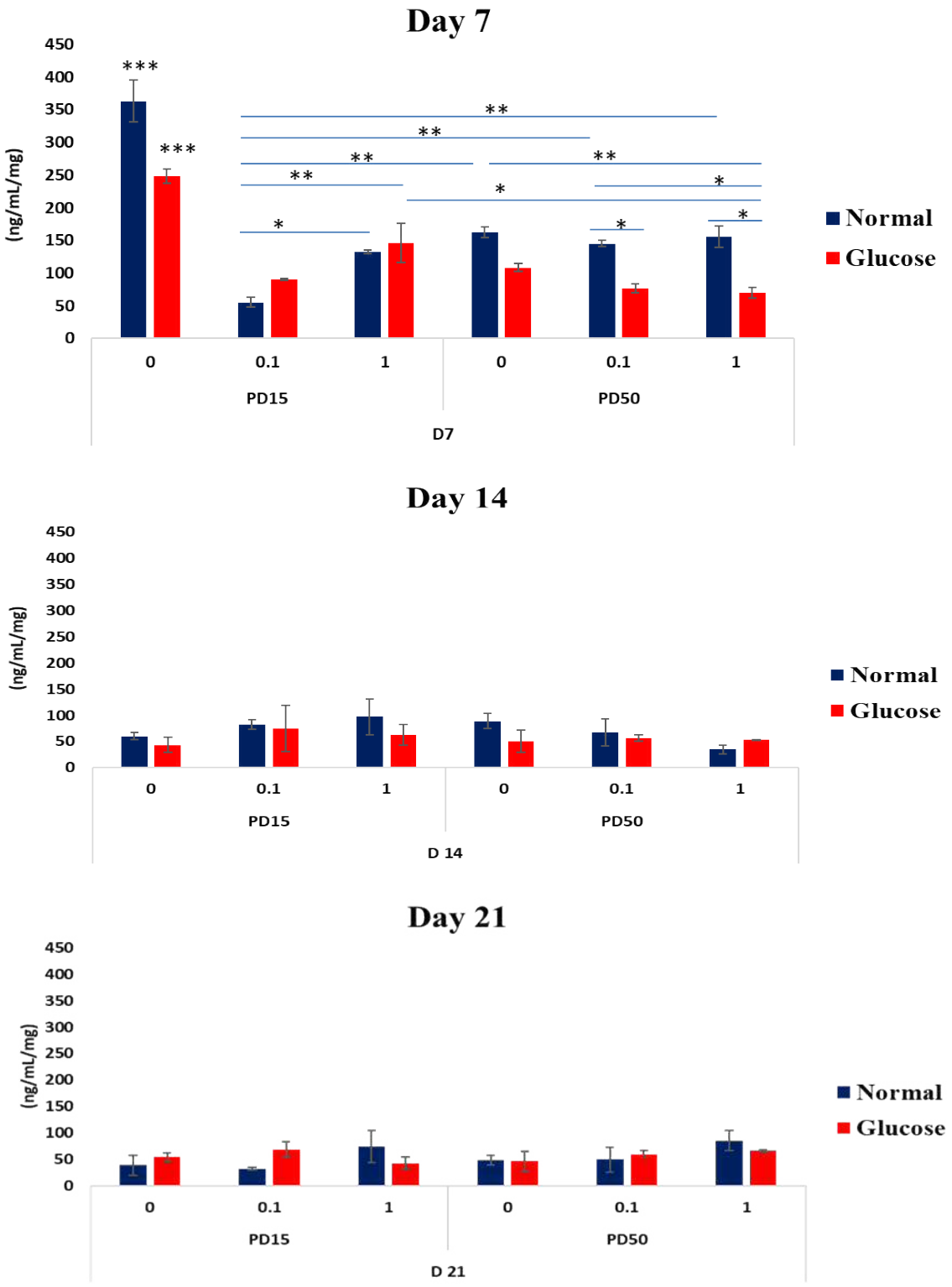

Figure 4.10: Quantification of OPN levels osteogenic induction media conditioned with high glucose and 0, 0.1, 1 µg/mL of *pg*-LPS concentrations using ELISA. OPN levels were measured on day 7, day 14 and day 21 for both PD15 and PD50. Error bars represent ± Standard error of the mean (SEM). * = $p<0.05$ and *** = $p<0.001$. ELISA repeated 3 times.

4.3.4: Phosphorylated Osteopontin Detection

Western blot was conducted to detect the phosphorylation status of OPN released to the osteogenic culture media. It revealed that all samples had phosphorylated OPN associated with the polymeric and monomeric forms at 120kDa and 55kDa. In high glucose conditions, extra bands appeared at 0.1 and 1µg/mL *pg*-LPS in PD15 at around 70-80 molecular levels. In addition, high glucose samples revealed denser bands specially at PD50 (Figure 4.11).

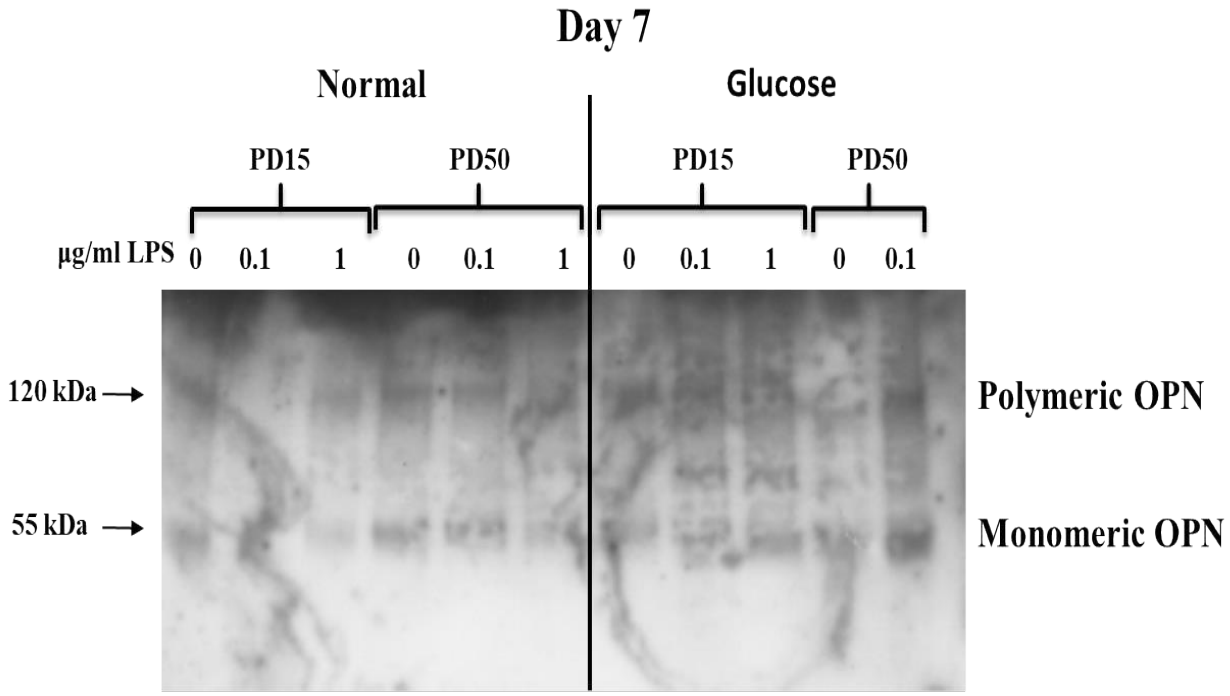

Figure 4.11: Western blot analysis by targeting anti-phosphoserine side of phosphorylated OPN in osteogenic induction media of CB-MSCs. The media were conditioned with 0.1, 1 µg/mL *pg*-LPS concentrations under normal and high glucose conditions. Two bands were identified for phosphorylated OPN at 55kDa, 120kDa. Western blots were repeated twice.

4.4: Discussion

This Chapter focused on the respective impacts of high glucose and *pg*-LPS on the osteogenic potential of CB-MSCs in two different populations, PD15 containing a high proportion of committed osteoprogenitor cells and PD50, which were previously characterised as immature MSCs. In *pg*-LPS condition, The PD15 population revealed a dose-dependent reduction in osteogenic differentiation under normal condition. However, in the presence of *pg*-LPS and high glucose, there were no further osteogenic reductions. For the PD50 population, adding *pg*-LPS reduced osteogenic differentiation at 0.1µg/mL *pg*-LPS concentrations only, whereas the combined effects of *pg*-LPS and high glucose caused further reductions at 1µg/mL *pg*-LPS. OPN revealed a peak level at day 7 and declined gradually through the culture period. Its levels were significantly higher for PD15 than PD50. In high glucose conditions, OPN demonstrated increased levels in cell lysates and matrix in both populations, while the addition of *pg*-LPS showed further inhibitory effects.

Within this study, characterisation of the commercial *pg*-LPS was conducted to evaluate its purity from bacterial proteins and nucleic acids, using electrophoresis techniques. The presence of the O-antigen polysaccharide was found attached to the lipid A-core; an important virulent component of *pg*-LPS, assisting in its detection by oxidation and reaction with silver nitrate staining (Tsai and Frasch 1982). The observed picture following silver staining (Figure 4.2 B) could be attributed to the variable of the O-antigen polysaccharide side chain (Tsai and Frasch 1982). Interestingly, similar patterns have been reported in other studies, where their own purified *pg*-LPS, rather than commercial sources (Kadono et al. 1999; Roberts et al. 2008). The commercial *E. coli*-LPS was also characterised and utilised as a comparative control. Characterisation showed that *E. coli*-LPS contained significant amounts of bacterial proteins and trace amounts of nucleic acids. These contaminates would be expected to affect the cellular activities of MSCs. On the contrary, we found that the commercial *pg*-LPS is pure, providing a more clinically relevant scenario to examine the direct effect of *pg*-LPS on the CB-MSCs *in vitro*.

MSCs of different origins have shown increases in proliferative capacity, but decreases in osteogenic differentiation by treating MSCs with certain concentrations of *pg*-LPS, namely 0.1, 1 and 10µg/mL (Roberts et al. 2008; Kato et al. 2014; Xing et al. 2015). It is well-documented that the severity of periodontal disease is positively related to the concentration of *pg*-LPS in the local

microenvironment (Socransky and Haffajee 2005). Thus, for a better understanding of this different concentrations of *pg*-LPS were used to observe the biological response of CB-MSCs involved in bone repair, in order to choose the sub-lethal dose. Within this study, *pg*-LPS at concentrations 0.1 and 1µg/mL demonstrated no inhibitory effects, whereas 10 µg/mL of *pg*-LPS concentration exhibited a reduction in the viability of CB-MSCs. This result is in agreement with Albiero et al. (2017) although they showed 10µg/mL concentrations causing an increase in proliferative capacity. Based on the results of both MTT and caspase activity, 10µg/mL concentrations have been excluded from the study and focussed on 0.1 and 1 µg/mL *pg*-LPS concentrations.

The osteogenic capacity and mineral formation of PD15 committed CB-MSCs has been observed to be significantly reduced by *pg*-LPS at both 0.1 and 1µg/mL concentrations, in a dose-dependent manner. Accordingly, Alizarin staining and mineral quantification confirmed these results by revealing different staining and mineral deposition among the treated groups. These results are in line with other studies, which also reported reductions in bone formation (Roberts et al. 2008; Kato et al. 2014; Xing et al. 2015). Albiero et al. (2017), however, reported that similar concentrations of *pg*-LPS had no effects on the osteogenesis of periodontal ligament stem cell (PDLSCs). These contradictory results may reflect contrasting biological responses to *pg*-LPS stimuli, depending on the source or the MSC status in the heterogeneous cell populations. Additionally, the relative difference in the setting of the experimental conditions and the source of the *pg*-LPS would also have an impact whether being commercially sourced or isolated and purified locally. More importantly, the heterogeneous nature of *pg*-LPS has been reported to be structurally different in a healthy individual, which is resistant to polymyxin B and exhibited low aggregation ability and is associated with low molecular weight O-antigen moieties (Díaz et al. 2015). *Pg*-LPS from a periodontally involved patient, however, produces modified lipid-A molecules, which are the most virulent factor (How et al. 2016). In the presence of high glucose, there was a reduction in mineral formation. However, no further reduction was seen by adding either *pg*-LPS concentrations. These findings point out that high glucose even modulates *pg*-LPS mineral reducing effects specifically at 1µg/mL concentration. These results were also confirmed by Alizarin Red staining. Intriguingly, this is the first study to investigate the combined effects of high glucose and *pg*-LPS on osteogenic mineralisation. However, García-Hernández et al. (2012) investigated the effects of high glucose and *pg*-E.Coli on the mineralisation of MSCs separately, but not in combination.

Osteogenic markers in PD15 showed greater reductions in the presence of high glucose more than the addition of *pg*-LPS. Runx2, which is a transcription factor for osteogenic differentiation, was negatively affected by high glucose. This result, however, was in partial agreement with Tang et al. (2015), who reported that Runx2 was upregulated at 0.1µg/mL concentrations, but downregulated at 1µg/mL of *pg*-LPS. OSX, which is downstream to Runx2, demonstrated a similar pattern as high glucose induced downregulation of this marker, whereas *pg*-LPS did not significantly affect OSX. Regarding OPN, at day 21, it was upregulated by high glucose which is similar to those findings of Colombo et al. (2011). *Pg*-LPS has an inhibitory effect on OPN. This very important finding would need further research to be explained. OCN was reported to be tightly bound to the hydroxyapatite within the mineralised bone matrix and found within mature osteoblasts (Hoang et al. 2003). Within this study, OCN was upregulated by high glucose at day 21. García-Hernández et al. (2012) and Liu et al. (2015) reported similar findings. This could be explained that high glucose proposed to assist in the formation of reactive oxygen species (ROS) (Evans et al. 2003), which in turn can activate phospholipase C, causing a release of calcium reserves inside the cells. This calcium may activate pathways, such as calmodulin kinase II, which allowed some osteogenic transcriptive molecules, for example Runx2 and OSX, to translocate into the nucleus and could assist in the transcription of biomineralisation molecules, namely OCN and OPN (Liu et al. 2015). This mineral formation, however, was found to be different than normal and with a low quality compared to control (García-Hernández et al. 2012). The cumulative increase in ROS levels for long-term, nonetheless, reported contributing to the inhibition of osteogenic differentiation through PI3K/Akt pathway (Zhang and Yang 2013). At day 28 and in the presence of *pg*-LPS, however, OCN expression was downregulated at 0.1 and 1µg/mL *pg*-LPS concentrations. These results were in agreement with previous findings (Kadono et al. 1999; Kato et al. 2014). In the case of combined high glucose and *pg*-LPS, the situation was exacerbated and OCN was downregulated.

The PD50 immature population, however, revealed a completely different response to osteogenic induction with high glucose and *pg*-LPS. This population exhibited a delay in osteogenic differentiation. Nevertheless, when the cells were cultured for a week further in osteogenic induction culture (until day 35), they successfully transformed into osteoblasts. Interestingly, high glucose demonstrated no effects in terms of mineral formation on the immature population, unlike the committed cells at PD15. Upon adding *pg*-LPS to the cells, only 0.1µg/mL *pg*-LPS showed a significant inhibition to mineral formation. The combined effects of high glucose and *pg*-LPS,

however, reduced the mineral formation at both 0.1µg/mL and 1µg/mL concentrations. Alizarin Red staining confirmed this result and mineral quantification demonstrated low mineral deposition of this population, compared to the committed cell population. Osteogenic specific markers, Runx2, OSX and OCN, exhibited downregulation, supporting the notion of a lower osteogenic capacity of immature cells. OPN showed significant downregulation in high glucose, while *pg*-LPS revealed no effects on OPN level. This gave a suggestion that there are no pronounced inhibitory effects of *pg*-LPS on OPN level within the PD50 population.

High glucose has been reported to have deleterious effects on osteogenesis to form bone (Juncheng et al. 2013; Liu et al. 2015). Within this study, we observed that high glucose exhibited significantly inhibitory effects on committed cell population (PD15), whereas it did not show any significant effect on immature cell population (PD50) as described previously. This profile has been observed to show different effects when adding *pg*-LPS. It has been noticed that committed cells (PD15) response to *pg*-LPS exposure can be described as dose-dependent effects on osteogenesis process, where 1µg/mL *pg*-LPS exerted more effect than 0.1µg/mL. However, in the presence of high glucose, the effect seemed no further amplified. On the contrary, this profile appeared differently in the immature population (PD50). High glucose revealed no effects on the immature cells, but the addition of *pg*-LPS to high glucose groups caused combined effects on osteogenesis at both concentrations, while 1µg/mL *pg*-LPS exerted no significant effects on the normal group. This may be a modulatory effect of high glucose on *pg*-LPS in the committed cells. On the other hand, *pg*-LPS affected immature MSCs when combined with high glucose, which may reflect a more complicated response of the heterogeneous population to different stimuli. In addition, it would explain the contradictory outcome of various studies in this field. Furthermore, these results represent the novelty finding of this study, which as far as we are aware, did not mention by previous studies.

The influence of *pg*-LPS on the synthesis of OPN protein was investigated. OPN is one of the earlier secreted proteins by (pre)-osteoblasts and it has been reported to be accumulated against resorbed bone surfaces forming a “OPN rich cement line”. OPN is proposed to act as an adhesion and cell signalling protein, to recruit the mature osteoblasts to the bone surface, regulating early stages of bone mineralisation and assisting in the bonding of old bone to new one forming an OPN cement line. However, OPN binds to mineral crystals to inhibit their growth assisting in bone remodelling

and therefore, increased expression might inhibit bone formation (McKee et al. 2011). OPN has been reported to act as a substrate for the covalent cross-linking activity of transglutaminase 2 (Kaartinen et al. 2002), proposed to contain several integrin-binding motifs (Lund et al. 2009); and acts as a potent regulator of mineralisation (Boskey 1995; Pampena et al. 2004). Colombo et al. (2011) reported an upregulation of OPN in diabetic healing bone. Within this study, OPN levels within the committed population were initially high and then fell in the presence of *pg*-LPS. This profile, however, was different in the immature population, when OPN appeared not to be affected by the presence of *pg*-LPS. In other words, the combination of those two factors; high glucose and *pg*-LPS did not seem to aggravate OPN levels. This trend is not in accordance with our hypothesis stated that OPN level supposed to be increased because of high glucose and in the presence of *pg*-LPS, proposing to impede bone regeneration and exacerbate the bone loss in the periodontally involved diabetic patient.

This Chapter has demonstrated that *pg*-LPS exerts different inhibitory effects on the osteogenesis of CB-MSC populations. PD15 committed cell population demonstrated the highest response to high glucose levels, rather than *pg*-LPS. On the contrary, the PD50 immature population was profoundly affected by *pg*-LPS, when combined with high glucose. Such novel findings have not been reported by previous studies, but it is important to elucidate the role of *pg*-LPS in the inhibition of bone repair. *Pg*-LPS was reported to have inhibitory effects on OPN levels in the committed population. On the other hand, *pg*-LPS demonstrated no effects on OPN levels in the immature population. Taken together, these findings were not consistent with the hypothesis that OPN would be upregulated in high glucose conditions, which leads us to consider macrophages as an alternative source of increased OPN during diabetic bone repair. Thus, the next Chapter will investigate macrophages derived from rat femur hematopoietic cells and their roles in secreting OPN under high glucose and *pg*-LPS conditions, which may perpetuate high levels of OPN, as a causative factor for impairment of bone regeneration under diabetic conditions.

Chapter 5: Investigating the Effects of High Glucose Microenvironment and *Porphyromonas Gingivalis*-Lipopolysaccharides (*Pg*-LPS) on Macrophage Phenotype and Osteopontin Synthesis

5.1: Introduction

Macrophages have a central role in response to pathogens as part of innate and adaptive immunity, acting as critical mediators of inflammatory processes, controlling tissue homeostasis, in addition to regulating various stages of wound and bone healing. Recently, two main populations of macrophages have been described; resident macrophages and circulating monocytes. The resident macrophages are proposed to be derived during early hematopoiesis from the embryonic yolk sac, which populate the tissues and have the capacity of self-renewal (Schulz et al. 2012; Sieweke and Allen 2013). These are present in all tissues of adult mammals, taking various nomenclatures according to their tissue location and may differentiate into osteoclasts in bone, Kupffer cells in liver and microglia in the brain. These specific populations have been proposed to have such highly different transcriptional profiles, they considered as unique classes of macrophages (Gautier et al. 2012). Circulating macrophages are described to originate from hematopoietic stem cells (HSCs) in bone marrow and consequently differentiate into macrophages (Akashi et al. 2000; Fogg et al. 2005; Liu et al. 2009; Hettinger et al. 2013). It has been described that both resident and circulating monocytes have the ability to differentiate into macrophages, M1 macrophages by means of granulocyte-macrophage colony stimulating factors (GM-CSF) and M2 macrophages by macrophage colony stimulating factor (M-CSF) (Burgess and Metcalf 1980; Gasson 1991). M1 cells are involved in the inflammatory state and phagocytosis in response to pathogenic stimuli. Consequently, inflammation is associated with deleterious effects and needs to be repressed by other type of cells, such as M2. M2 cells are reported to play a major role in the resolution of inflammation by producing anti-inflammatory cytokines and chemokines; and eliminating tissue debris (Tushinski et al. 1982; Bartocci et al. 1987; Hamilton 2008). The most acceptable theory of the function of macrophage phenotypes is the same in all tissue. However, although circulating macrophages, which mostly stay for 1-2 days in the circulation, assist in supporting the function of resident macrophage phenotypes. If they have not been recruited to fight a pathogenic infection, they undergo apoptosis and are removed (Italiani and Boraschi 2014).

Adipose tissue accumulation represents one of the important causes of the insulin resistance in type 2 diabetes mellitus (T2DM), (Olefsky and Glass 2010). Bone marrow-derived macrophages have been reported to be recruited in adipose tissue and initiate a low-grade chronic inflammation, which

has been described to comprise 40% of the total adipose tissue cells in obese rodents (Xu et al. 2003; Heilbronn and Campbell 2008). On the other hand, macrophages have been observed to consist of 10% of adipose tissue in counterpart lean mice (Weisberg et al. 2006). Free fatty acid (FFA) can be recognized by the Toll-Like Receptors 2 and 4 (TLR-2, TLR-4) of macrophages, which can switch macrophage polarity from M2 to more M1 regulated by peroxisomal proliferator-activated receptor gamma (PPARγ) transcription factor. In this case, the inflammatory response can be amplified, promoting the development of insulin resistance and consequently exacerbating T2DM (Shi et al. 2006; Davis et al. 2008). Interestingly, Espinoza-Jim´enez et al. (2012), have reported that using helminth parasites to induce M2, has been found to be effective in reducing hyperglycemia, obesity and decreased the incidence of T2DM.

Porphyromonas gingivalis- lipopolysaccharide (*pg*-LPS) is known to be the prime virulence factor of periodontal disease. It plays a pivotal role in triggering the immune response, through inducing macrophage TLR2 and TLR4 and aggravating the inflammatory process. This induction has been described to release inflammatory mediators, such as tumour necrosis factor (TNF-α), interleukin (IL)-1, IL-6, which are reported to perpetuate inflammation (Rittling 2011). These immune mediators, namely TNF-α and IL-1β, result in attracting more macrophages to the infected area and enhance activated macrophages to be pro-inflammatory (M1 phenotype), to be ready for killing and phagocytosis activities. This situation is strongly apparent, when the symptoms of periodontal disease have clinically appeared (Yang et al. 2017). The balance between M1/M2, however, has been associated with inflammation at the gingivitis stage, yet to progress into periodontitis (Yu et al. 2016; Yang et al. 2017). With this in mind, hyperglycemia has also been described to exhibit high levels of TNF-α in the circulation of affected individuals, which result in insulin resistance. *Pg*-LPS and hyperglycemia may thus act synergistically in individuals with periodontal disease and diabetes, resulting in rapid attachment loss and alveolar bone resorption (Lo 2005).

A prime functional protein in the recruitment and regulation of the macrophage function is osteopontin (OPN). Strong evidence has suggested that OPN may act as an opsonin to facilitate macrophage adhesion and engulf the newly formed mineral crystals, which may hinder bone biomineralisation at the healing site (Pedraza et al. 2008; McKee et al. 2011). In the case of inflammation, macrophages secrete pro-inflammatory cytokines, TNF-α, IL-1, IL-6, and interferon-γ (INF-γ), which in turn increase OPN levels (Rittling 2011). Colombo et al. (2011) demonstrated an increase in OPN levels as well as an increase in macrophages in diabetic healing bone.

Furthermore, in the case of LPS, Gao et al. (2005) reported that LPS induced S-nitrosylation of heterogeneous nuclear ribonucleoprotein A/B (hnRNP-A/B), which was described as RNA-binding proteins with chromatin-associated and can bind with RNA polymerase II, forming a complex. This, in turn, can inhibit OPN transcription through repressing its DNA binding activity. However, recent research suggested that secreted OPN is not regulated by LPS in RAW264.7 and mouse peritoneal macrophages (Zhao et al. 2010). Moreover, Nares et al. (2009) observed that OPN expression was not increased in macrophages in the presence of LPS as confirmed by Microarray analysis. Taken all together, more experiments are required to elucidate the real effects of LPS in regulating OPN in macrophages from different species. This knowledge would assist in understanding the role of this protein in bone loss, complicated by hyperglycemia.

Against this background, it is valuable to investigate the effects of high glucose in the presence of *pg*-LPS on circulating macrophages, which have a pivotal role in defending the body against this prime virulence factor of periodontal pathogens. This Chapter aims to investigate the role of M1 and M2 macrophages in OPN production under high glucose, *pg*-LPS or both conditions. These two factors are proposed to increase OPN levels, which in turn act as detrimental factors, resulting in delayed bone healing and remodelling in diabetic individuals with periodontal disease.

5.2: Materials and Methods

5.2.1: Isolation and Characterization of Rat Bone Marrow-Derived Macrophages

Rats were handled and sacrificed, according to the Code of Practice for the Human Killing of Animals Under Schedule 1 of the Animals Scientific Procedures Act (1986). Four-week old male Wistar rats were bought from Charles River UK Ltd., (Margate, UK). Femurs and tibias were taken from sacrificed rats, the ends were cut off and bone marrow flushed with ice-cold phosphate buffer saline (PBS) into containers, using a syringe with a 21-gauge needle. The PBS containing cells was centrifuged at 1800rpm for 5min. Supernatants were discarded and the cell pellets were suspended in 2mL of collagenase dispase (4µg/mL) (Sigma-Aldrich, Poole, UK) and incubated at 37ºC, 5% CO_2 incubator for 45min with gentle agitation every 15min. Cells were passed through a 70µm cell strainer (Sigma-Aldrich, UK) and collected into universal tubes. The collected cells were then centrifuged at 1800rpm for 5min, discarding the supernatants and the cell pellets were re-suspended with 2mL of Lysing Buffer (BD Biosciences, UK) with gentle agitation for 2min at room temperature. The universal tube containing cells were then filled with an isolation medium [RPMI 1640 (Invitrogen, UK) 1% antibiotics-antimycotics (Sigma-Aldrich, UK)], centrifuged and the supernatants discarded. The cell pellets were washed once again, re-suspended in 1mL of the isolated medium, counted and seeded at a density of $1x10^6$ cells/cm^2 in T-25 flasks (Sarstedt Ltd., UK). The cells were cultured in a standard culture medium [isolation medium containing 10% fetal bovine serum (FBS)], supplemented with either granulocyte-macrophage colony-stimulating factor (GM-CSF, 10ng/mL) to drive the monocyte cells to differentiate into M1 macrophages, or a combination of macrophage colony-stimulating factor (M-CSF, 10ng/mL) and interleukin-4 (IL-4, 10ng/ml) to allow the differentiation of monocytes into M2 macrophages. All the stimulating factors were bought from (PeproTech, USA). The monocytes were incubated in the culture medium for 7 days. The medium was changed every two days. Some cells were incubated in BD Falcon™ glass chamber slides (BD Biosciences, UK) for detection F4/80 a specific macrophage marker.

The culture media were collected at day 1 and day 7 to perform Enzyme Linked-Immunosorbent Assay (ELISA), to confirm the successful cell differentiation into macrophages by investigating specific cytokines; TNF-α, IL-6, TGF-β_1 and IL-12p40, in addition, to analysing OPN at protein

levels. Cells were recovered at day 1 and day 7 to quantify mRNA expression of OPN, using quantification polymerase chain reaction (qPCR).

5.2.1.1: Detection F4/80 Specific Macrophage Marker Using Immunocytochemistry

Cells were investigated on day 1 and day 7, using BD Falcon™ glass chamber slides (BD Biosciences, Oxford, UK). Culture media were removed, cells were washed twice with PBS, fixed in ethanol for 30min and cell non-specific binding was blocked with 1% Bovine Serum Albumin (BSA) diluted in Tris Base Saline (TBS). F4/80 primary rabbit polyclonal IgG antibody (Insight Biotechnology, UK) was added at 1:50 dilution in 1% BSA/TBS and incubated overnight at 4ºC. Normal rabbit IgG (Insight Biotechnology, Wembley, UK) was used as isotype control at 1:50 dilution in BSA/TBS in place of F4/80 antibody. Another control was antibody exclusion with 1% BSA/TBS only. Cells were rinsed twice with TBS for 5min and then incubated in secondary antibody goat anti-rabbit IgG-FITC (Insight Biotechnology, UK) with 1:200 dilution in 1% BSA/TBS for 1h at room temperature. Cells were rinsed twice with TBS for 5min. The chambers were removed, slides were stained with DAPI Vectashield Hard-Set Mounting Medium (Vector Laboratories Ltd, Peterborough, UK) and covered with cover slips (Thermo Scientific, UK). Nuclear DAPI and green-lipid fluorescence were observed using an Olympus Provis AX70 Microscope, with Nikon ACT-1 v.2.63 software.

5.2.1.2: Detection of M1 and M2 Specific Markers from Supernatant Using ELISA

5.2.1.2.1: Detection of Rat TNF-α

Cell culture medium samples were collected on day 1 and day 7. Secreted TNF-α in the supernatant was quantified using Rat TNF-α Quantikine® ELISA Kit (R&D Systems®, UK). The assay was conducted according to the manufacturer's instructions. Briefly, samples were centrifuged to remove particulates, diluted 3-fold with calibrator diluent, prior to loading 50µL into the wells of the plate which were pre-coated with TNF-α monoclonal antibodies. 50µL of the TNF-α standards were loaded in duplicate to separate wells in descending order of concentration, samples were incubated for 2h at room temperature, with gentle shaking. Each well content was removed and wells were washed five times with washing buffer. 100µL of rat TNF-α conjugate was added to each well, incubated for 2h and washed, as described previously. 100µL of the substrate solution was added to each well, incubated for 30min at room temperature and protected from light. The enzyme activity was terminated by addition of 100µL of stop solution and the plate was measured by

spectrophotometer at 450nm. The amount of TNF-α in the samples was calculated from reference standards of known concentrations of TNF-α. Experiments were performed in triplicate of two independent experiments and results were expressed as pg/mL.

5.2.1.2.2: Detection of Rat IL-6

This assay was conducted using Quantikine® ELISA Kit (R&D Systems®, UK) with the same steps as TNF-α and the plate was measured by spectrophotometer at 450nm. The amount of IL-6 in the samples was calculated from reference standards of known concentrations of IL-6. Experiments were performed in triplicate of two independent experiments and results were expressed as pg/mL.

5.2.1.2.3: Detection of Rat TGF-β_1

Cell culture medium samples were collected on day 1 and day 7. The secreted TGF-β_1 in the supernatants was quantified using Rat TGF-β_1 Quantikine® ELISA Kit (R&D Systems®, UK). The assay was conducted according to the manufacturer's instructions. Samples were centrifuged to remove particulates. 20µL of 1N HCl was added to 100µL of samples, which were then mixed well, incubated for 10min at room temperature, for activation then neutralized with 1.2 N sodium hydroxide (NaOH)/0.5M HEPES. 50µL of assay diluent (provided by the Kit) was added to each well prior to loading 50µL volume of duplicate standards in ascending order concentrations, control and activated samples (wells were already coated with TGF-β_1 monoclonal antibodies); and incubation for 2h at room temperature with gentle shaking. Well contents were removed and washed five times with washing buffer (provided with the Kit). 100µL of rat TGF-β_1 conjugate was added to each well, incubated for 2h and washed, as above. 100µL of substrate solution was added to each well, incubated for 30min at room temperature and protected from light. The enzyme activity was terminated by adding 100µL of stop solution. The plate was measured by spectrophotometer at 450nm. The amount of TGF-β_1 in the samples was calculated from reference standards of known concentrations of TGF-β_1. Experiments were performed in triplicate of two independent experiments and results were expressed as pg/mL.

5.2.1.2.4: Detection of Rat IL-12p40

Cell culture medium samples were collected on day 1 and day 7. The secreted IL-12p40 in the supernatant was quantified using Rat IL-12p40 ELISA Kit (Origene, USA). The assay was conducted according to the manufacturer's instructions. Briefly, 100µL of the samples, control, and standards were loaded into each well. A 50µL working solution of Biotin-Conjugate was added and

incubated for 2h at room temperature with a gentle agitation. Each well content was removed and the wells were washed 5 times with washing buffer (provided with the Kit). 100µL of rat IL-12p40 Conjugate was added to each well, incubated for 2h and washed, as above. 100µL of working solution of Streptavidin-HRP was added to each well, incubated for 30min at room temperature and protected from light. The washing steps were repeated, as before. 100µL of substrate solution was added to each well and incubated for 20min at room temperature with light protection. The enzyme activity was terminated by adding 100µL of stop solution. The plate was measured by spectrophotometer at 450nm. The amount of IL-12p40 in the samples was calculated from reference standards of known concentrations of IL-12p40. Experiments were performed in triplicate of two independent experiments and results were expressed as pg/mL.

5.2.2: Quantification of Osteopontin Expression in M1 and M2 Macrophages by qPCR

5.2.2.1: RNA Extraction and qPCR

RNA was extracted from the adherent cells at day 1 and day 7 and utilised for qPCR analysis. Total RNA was extracted using the RNeasy® Mini Kit (Qiagen, UK). cDNA Reverse transcription was obtained from RNA by reverse transcription, as described in Chapter 2 (Section 2.2.5.1.1). OPN expression was quantified using qPCR, described in Chapter 2 (Section 2.2.8). OPN forward and reverse primers were as stated in Chapter 3 (Table 3.1).

5.2.3: Quantification of Osteopontin Protein Levels in the Culture Media of M1 and M2 Macrophages by ELISA

Media were collected from cells at day 1 and day 7. ELISA was conducted according to methods described in Chapter 3 (Section 3.2.2.5) using Osteopontin (Rodent) ELISA Kit (Enzo Life Science, UK). Experiments were performed in triplicate of two independent experiments and results were expressed as ng/mL.

5.2.4: Statistical Analyses

Statistical analyses were performed using One-Way ANOVA with a post-hoc Tukey test to determine the statistical differences between sample groups, using the software GraphPad InStat 3 (v3.06). Statistical significance of differences was defined as significant (*, $p<0.05$), very significant (**, $p<0.01$) or highly significant (***, $p<0.001$).

5.3: Results

5.3.1: Morphological Observation of Macrophages During 7 Days in Culture

Monocytes treated with either GM-CSF or M-CSF/IL-4 are proposed to form M1 and M2 macrophages, respectively. After 24h in culture, all cells exhibited a homogenous small round morphology. At day 3, all cells appeared almost the same size with short processes. At day 5, the monocytes demonstrated considerable changes in their morphology and increase in cell size. Cells treated with GM-CSF exhibited rounded morphology with some spindle-like shape and possessed long cytoplasmic processes. On the other hand, cells stimulated with M-CSF and IL-4 revealed larger round and more spindle-shaped cells, with shorter processes. At day 7, monocytes showed further differentiation with their morphological populations, indicating different shapes depending on the stimulated cytokines treatment. M1 cells were round, oval with longer processes with very little spindle-like and heterogenous cell shape. M2 demonstrated mostly spindle-like and oval morphology (Figure 5.1).

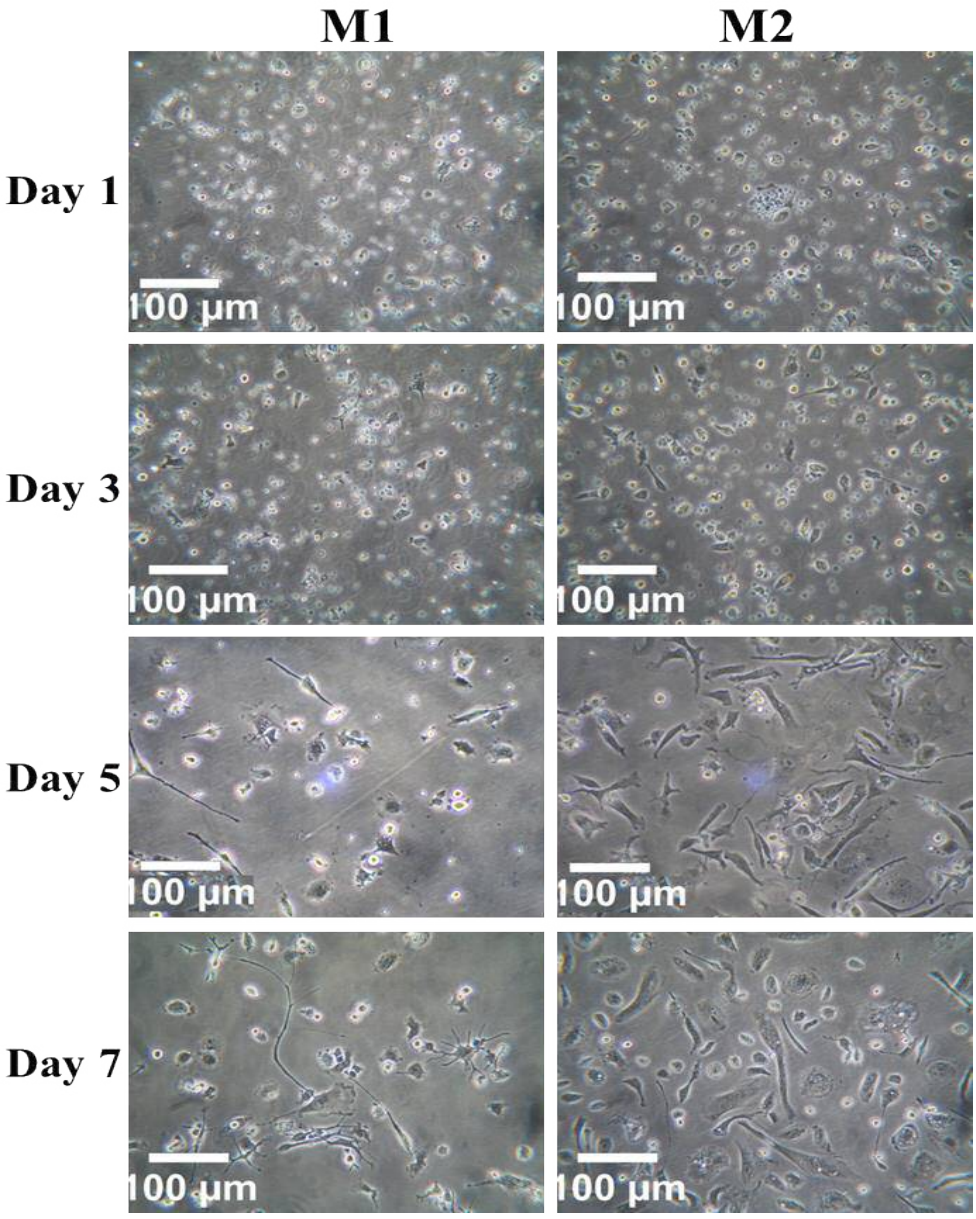

Figure 5.1: Images of monocyte cells stimulated by either GM-SCF or M-CSF and IL-4 for 7 days to differentiate into M1 and M2 macrophages respectively. Images were taken at days 1, 3, 5 and 7. Magnification of 20X, scale bar 100µm.

5.3.2: Characterisation of Identified Macrophages

5.3.2.1: Immunocytochemistry for F4/80 Identification

F4/80 specific marker for macrophages were clearly seen at day 7, as indicated by green FITC staining in both M1 and M2 populations. This indicated that monocytes stimulated by either GM-SCF or M-CSF and IL-4 were successfully differentiated into macrophages (Figure 5.2).

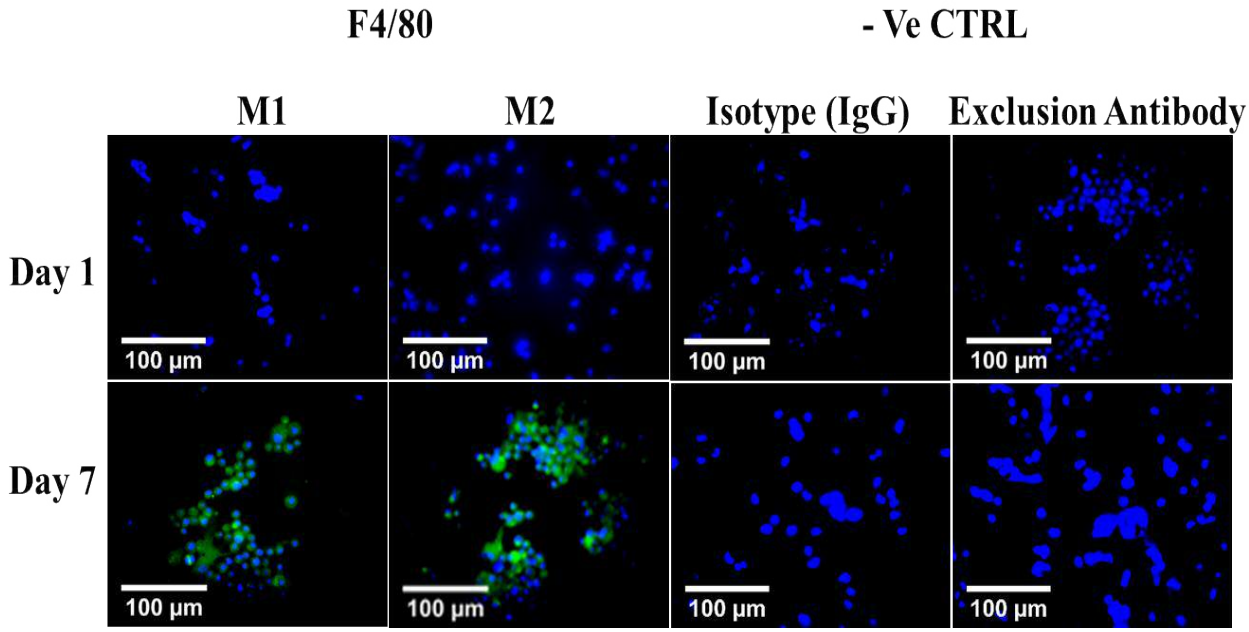

Figure 5.2: Immunocytochemistry identification of activated macrophages at day1 and day 7. F4/80 was confirmed by green-FITC colour at day 7. The control isotype (IgG) antibody and exclusion antibody were both negative. DAPI nuclei stain blue. Magnification of 40X, scale bar 100µm.

5.3.2.2: Quantification of M1 and M2 Macrophage Cytokines by ELISA

TNF-α exhibited higher levels in M1 compared to M2 macrophages, in normal glucose (N) conditions. In high glucose (G) conditions, TNF-α exhibited significantly increased levels in M1 compared to N condition (p<0.01). Addition of 0.1µg/mL concentration of *pg*-LPS to the media, caused TNF-α levels significantly decreases in M1 macrophages N condition (p<0.01). Increase in *pg*-LPS concentrations from 0.1µg/mL to 1µg/mL exhibited different response profiles. TNF-α levels increased significantly again in N condition (p<0.001) for M1 macrophages. Interestingly, in G conditions adding 0.1µg/mL of *pg*-LPS decreased TNF-α levels in M1 macrophages, whereas 1µg/mL caused increased TNF-α levels by 2-fold but still significantly less when comparing to G condition alone in M1 macrophages (Figure 5.3A).

IL-6 levels in M1 demonstrated higher by about 2-fold compared to M2 macrophages, in N condition. G conditions caused no significant differences. Addition of 0.1µg/mL concentration of *pg*-LPS revealed significant increase in IL-6 levels in M1 macrophages (p<0.01) in N conditions. Whereas 1µg/mL *pg*-LPS led to significant decrease in IL-6 levels in both M1 and M2 macrophages in N condition (p<0.001). In G conditions, 0.1µg/mL *pg*-LPS demonstrated a significant increase in

IL-6, however, adding 1µg/mL *pg*-LPS, leading to significant decrease in IL-6 levels in both M1 and M2 macrophages (Figure 5.3 B).

TGF-β_1 levels showed a different profile, it was higher by about 1.5-fold in M2 compared to M1 macrophages. G conditions caused slight increase in TGF-β_1 levels in M2 macrophages but was not significant. Addition of 0.1µg/mL concentration of *pg*-LPS resulted in significant increase in TGF-β_1 levels at both M1 and M2 macrophages accordingly ($p<0.05$), ($p<0.01$) compared to N conditions. While 1µg/mL concentration *pg*-LPS exhibited a significant increase in TGF-β_1 levels at both M1 and M2 macrophages ($p<0.05$) compared to N conditions. In G conditions, adding 0.1µg/mL concentration showed significant increase in TGF-β_1 levels ($p<0.05$), ($p<0.001$) in M1 and M2 macrophages. 1µg/mL concentration caused significant increase of TGF-β_1 levels ($p<0.001$) compared to G conditions alone (Figure 5.3 C).

IL-12p40 expressed 1.5-fold higher levels in M2 compared to M1 macrophages in N conditions. Addition of G caused significantly increased levels in M2 macrophages ($p<0.01$) compared to N conditions. 0.1µg/mL concentration of *pg*-LPS exhibited significant increase IL-12p40 levels ($p<0.001$), ($p<0.01$) at both M1 and M2 macrophages respectively compared to N conditions. Addition of 1µg/mL *pg*-LPS exerted significant increase at M1 only ($p<0.01$) compared to N conditions. In G conditions, interestingly, 0.1µg/mL concentration demonstrated significantly elevation of IL-12p40 levels ($p<0.001$) in M1 macrophages, whereas it was inhibited in M2 macrophages ($p<0.01$). 1µg/mL concentration revealed significant increase in IL-12p40 levels ($p<0.001$) in M1 and a significant decrease in M2 macrophages ($p<0.001$) (Figure 5.3 D).

A) TNF-α

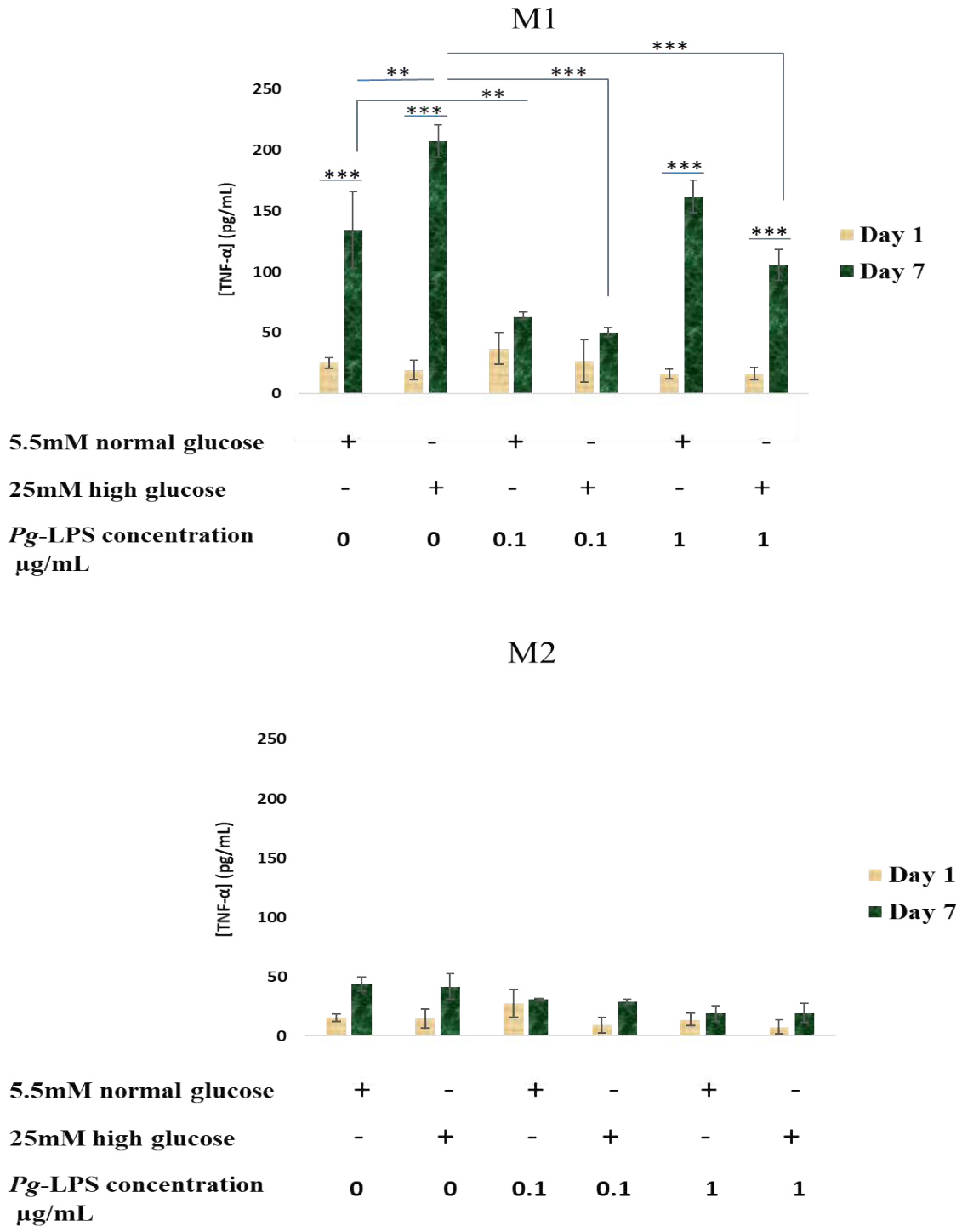

Figure 5.3: Bar charts represent quantifications of **A)** TNF-α, **B)** IL-6, **C)** TGF-β_1 and **D)** IL-12p40 levels using ELISA. TNF-α and IL-6 levels were higher in M1, whereas TGF-β_1 and IL-12p40 were higher in M2 control groups. Addition of 0,1 and 1 µg/mL concentrations of *pg*-LPS caused variable effects, increasing or decreasing the level of these cytokines. Error bar represents standard error of mean ±. n=3. (* = $p<0.05$) (** = $p<0.01$) (*** = $p<0.001$).

B) IL-6

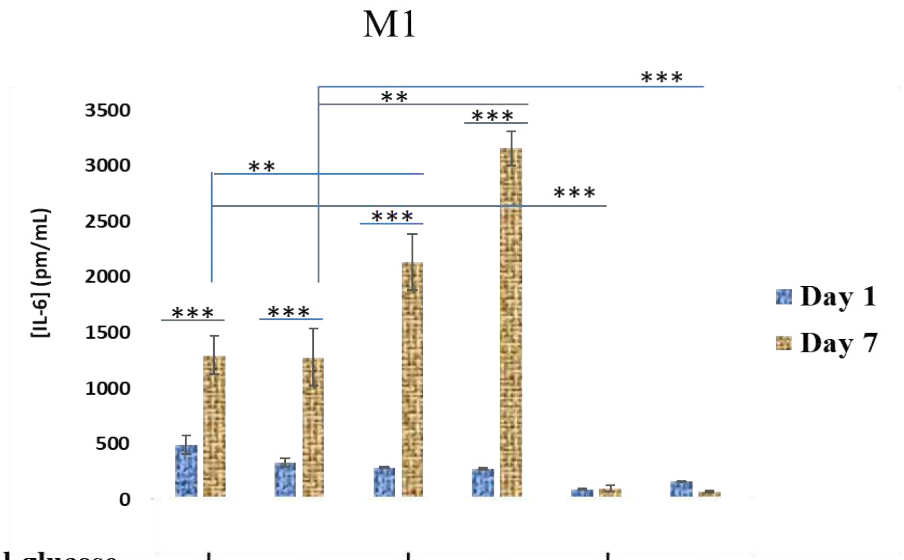

5.5mM normal glucose	+	-	+	-	+	-
25mM high glucose	-	+	-	+	-	+
***Pg*-LPS concentration µg/mL**	**0**	**0**	**0.1**	**0.1**	**1**	**1**

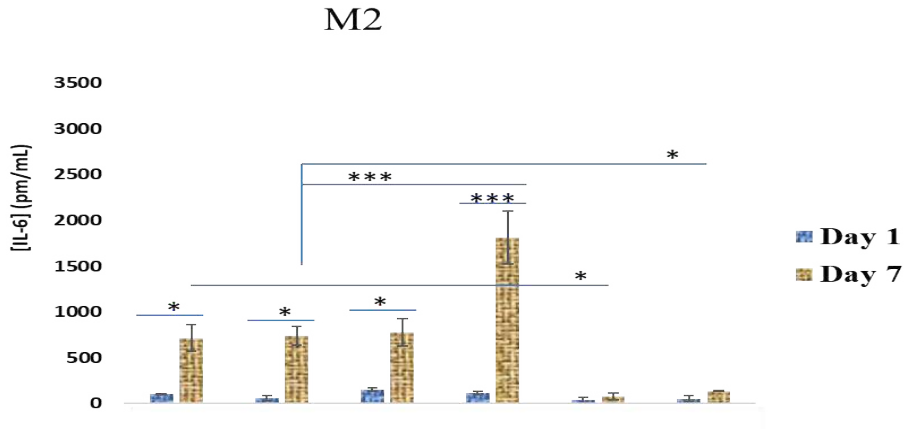

5.5mM normal glucose	+	-	+	-	+	-
25mM high glucose	-	+	-	+	-	+
***Pg*-LPS concentration µg/mL**	**0**	**0**	**0.1**	**0.1**	**1**	**1**

C) TGF-β_1

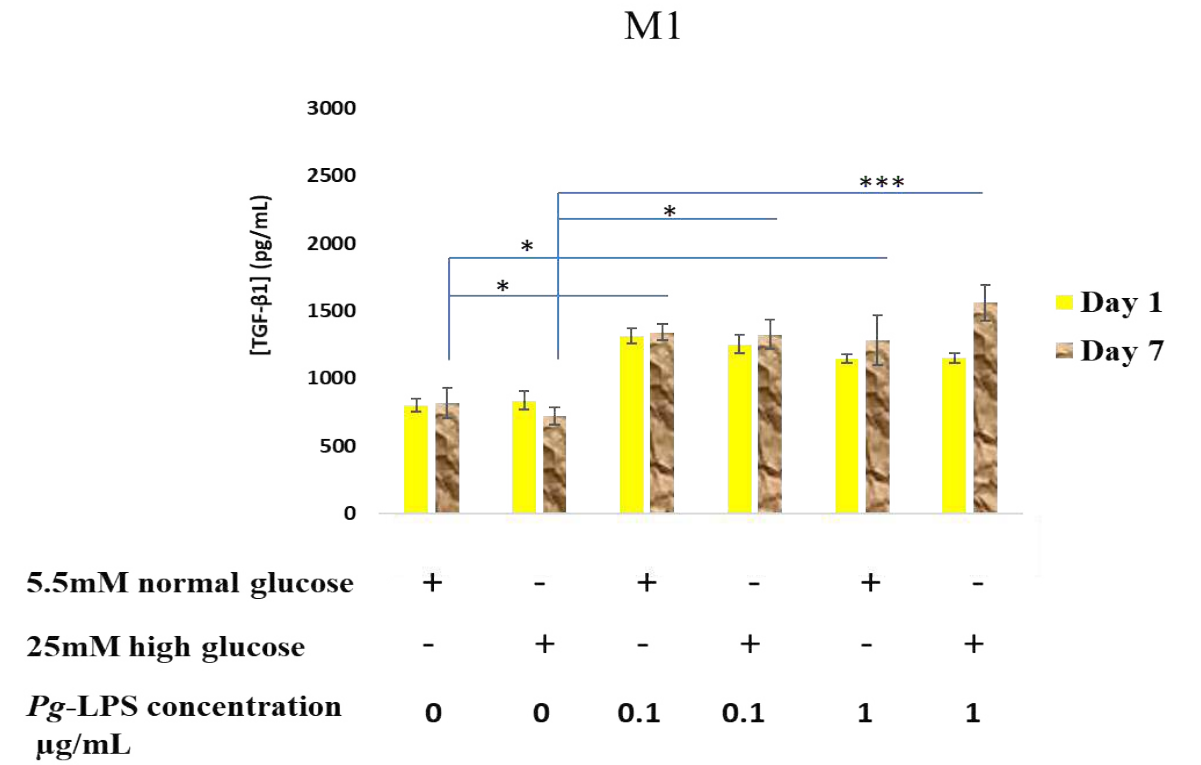
M1
[TGF-β1] (pg/mL)
3000
2500
2000
1500
1000
500
0
*
*
*
***
Day 1
Day 7
5.5mM normal glucose + - + - + -
25mM high glucose - + - + - +
Pg-LPS concentration µg/mL 0 0 0.1 0.1 1 1

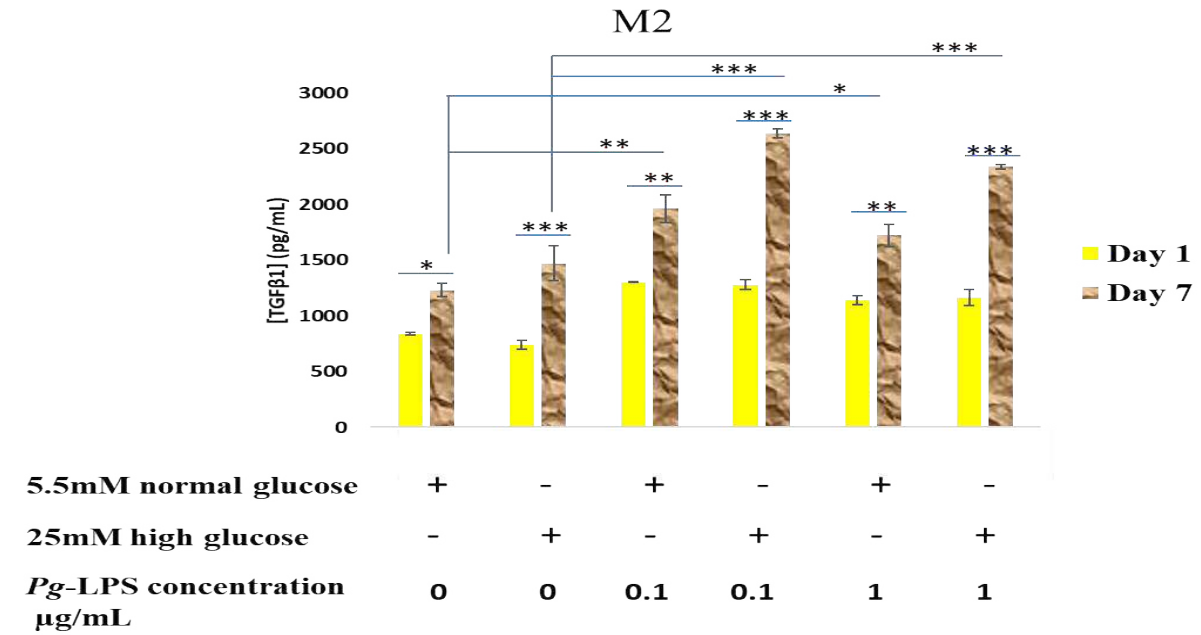
M2
[TGFβ1] (pg/mL)
3000
2500
2000
1500
1000
500
0
*
***
**
***
**
***
***
***
*
**
Day 1
Day 7
5.5mM normal glucose + - + - + -
25mM high glucose - + - + - +
Pg-LPS concentration µg/mL 0 0 0.1 0.1 1 1

D) IL-12p40

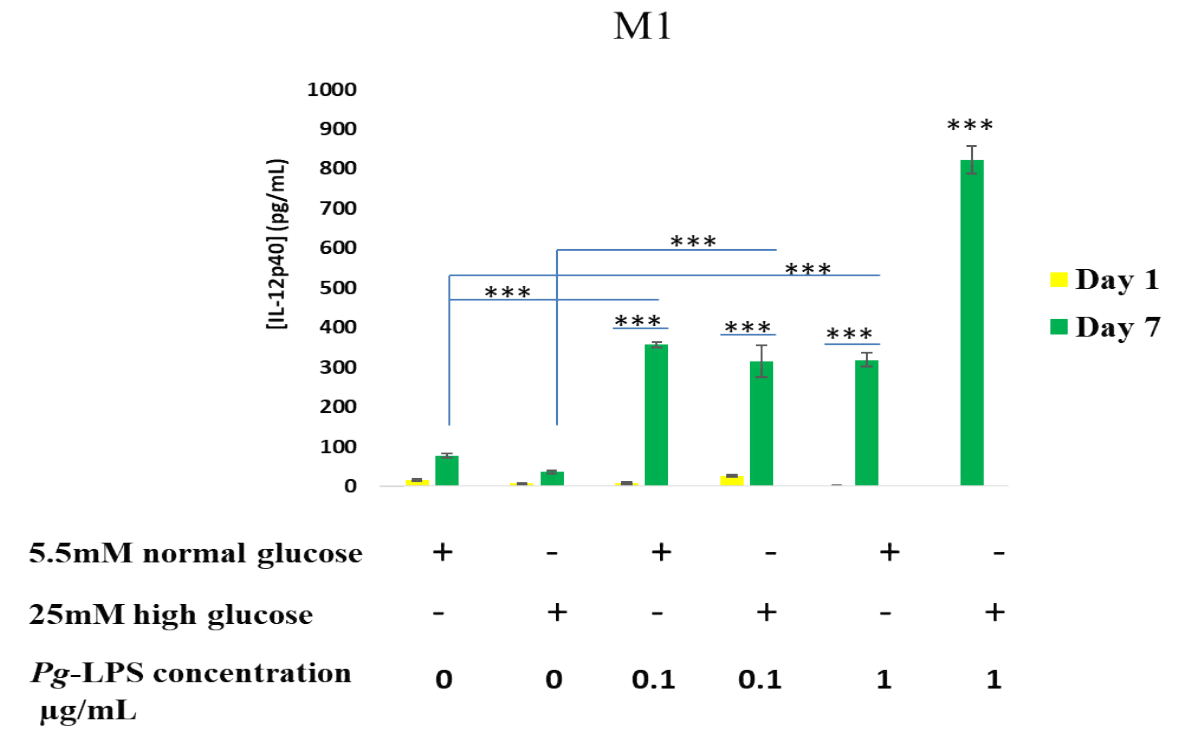
M1
[IL-12p40] (pg/mL)
1000
900
800
700
600
500
400
300
200
100
0
***
***
***
***
***
***
Day 1
Day 7
5.5mM normal glucose + - + - + -
25mM high glucose - + - + - +
Pg-LPS concentration µg/mL 0 0 0.1 0.1 1 1

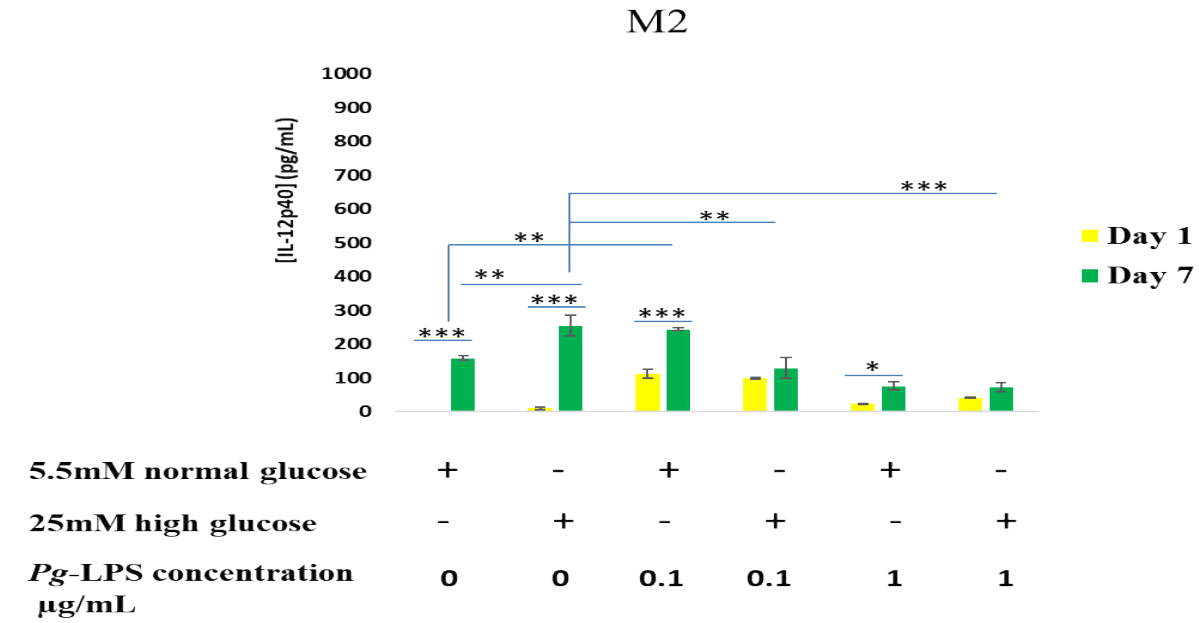
M2
[IL-12p40] (pg/mL)
1000
900
800
700
600
500
400
300
200
100
0
***
**
**
***
***
***
**
*
Day 1
Day 7
5.5mM normal glucose + - + - + -
25mM high glucose - + - + - +
Pg-LPS concentration µg/mL 0 0 0.1 0.1 1 1

5.3.3: Detection of Osteopontin in M1 and M2 Macrophages

5.3.3.1: Quantification of Osteopontin Expression by qPCR

OPN expression indicated no significant differences between day 1 and day 7 in N conditions for both M1 and M2 macrophages. In the case of G, there was also no significant differences between day 1 and day 7 in M1 and M2 macrophages. Adding 0.1µg/mL concentration of *pg*-LPS to the normoglucose condition resulted in an increase in OPN expression in M2 macrophages, but this was not significant. At the 1µg/mL concentration in N conditions, there was a significant increase in OPN expression in M2 macrophages ($p<0.01$). Adding 0.1µg/mL concentration to G conditions, caused a significant increase in OPN expression for M2 macrophages ($p<0.001$), whereas addition of 1µg/mL concentration resulted in a significant increase in OPN expression ($p<0.01$), but lower expression than 0.1µg/mL concentration (Figure 5.4).

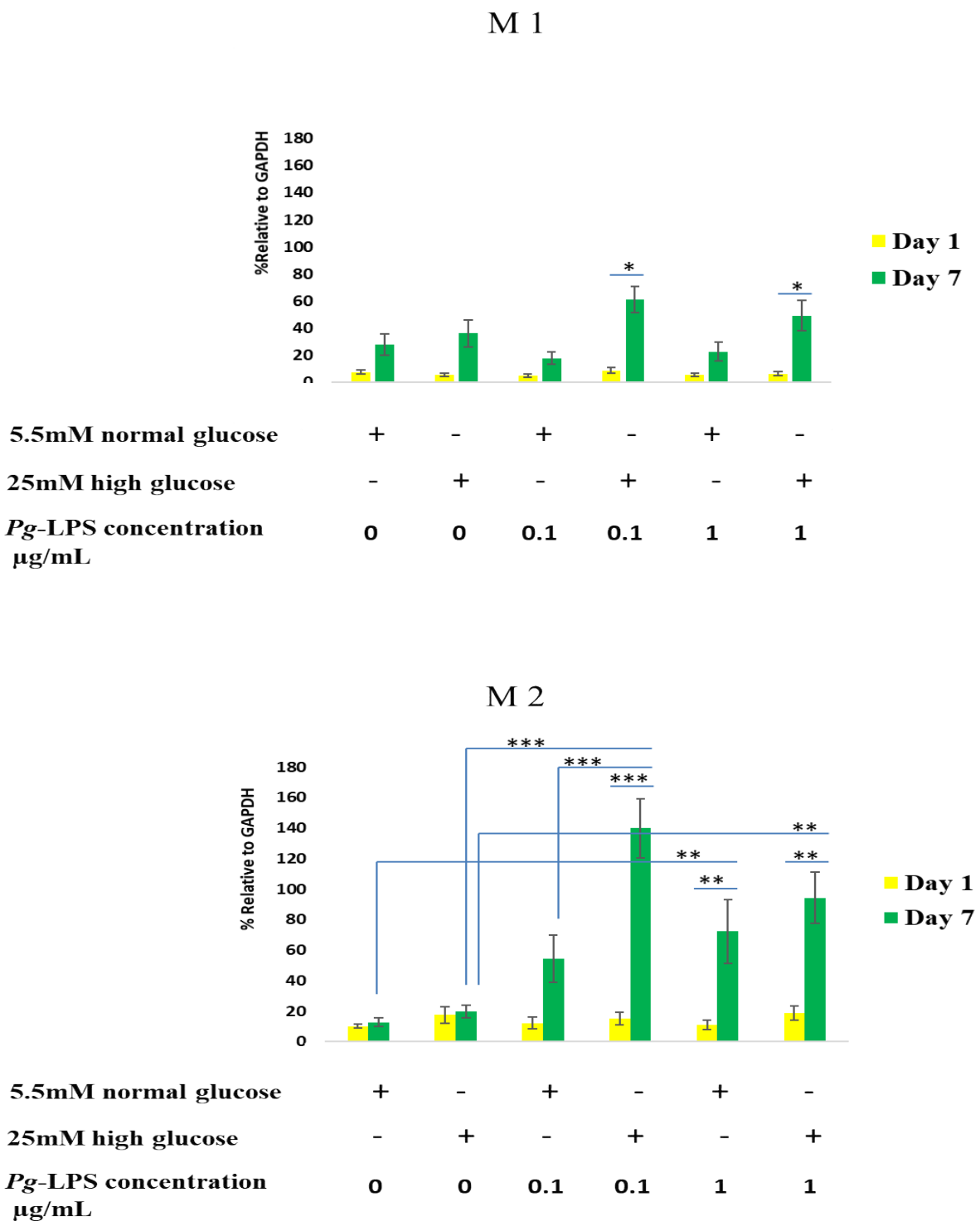

Figure 5.4: Bar charts represent mRNA OPN expression of M1 and M2 macrophages treated with glucose and 0,1 and 1 µg/mL concentrations of *pg*-LPS by qPCR. Error bar represents standard error of mean ±. n=3. (* = $p<0.05$), (** = $p<0.01$) and (*** = $p<0.001$).

5.3.3.2: Quantification of Osteopontin Levels in Culture Media for M1 and M2 Macrophages by ELISA

OPN levels in normoglucose groups were very low at day 1 and day 7, in both M1 and M2 macrophages. Addition of high glucose caused no significant differences in OPN levels for both M1 and M2. Addition of 0.1 and 1µg/mL of *pg*-LPS to the normoglucose conditions, resulted in significant increase in OPN levels in M2 macrophages ($p<0.001$). In the case of combining the effects of glucose and *pg*-LPS, it was found that 0.1 and 1µg/mL concentrations significantly increased OPN levels in both M1 and M2 ($p<0.001$, Figure 5.5).

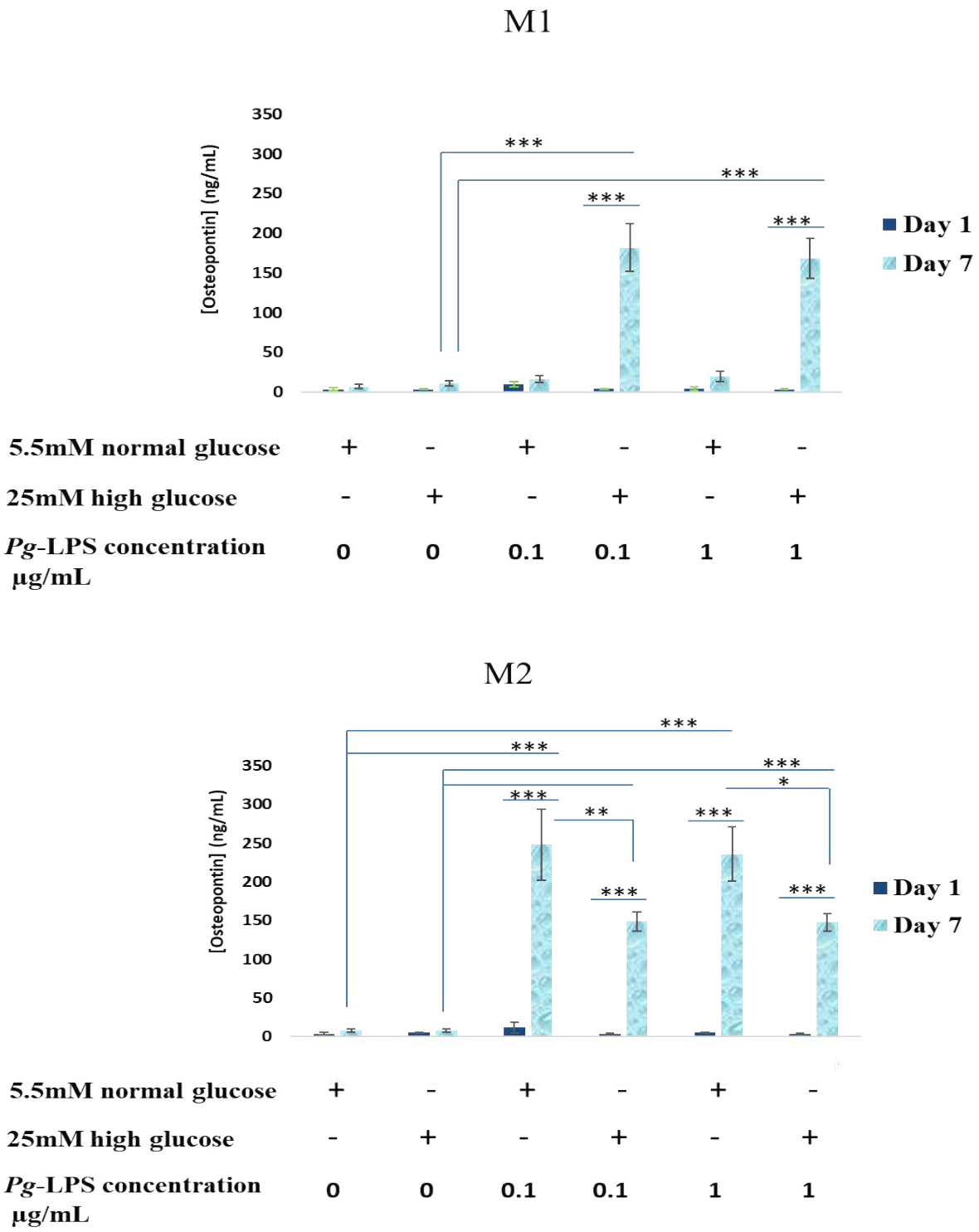

Figure 5.5: Bar charts represent OPN levels in the culture media of activated M1 and M2 macrophages treated with glucose and 0,1 and 1 µg/mL concentrations of *pg*-LPS by ELISA. Error bar represents standard error of mean ±. (n=3), (* = p<0.05), (** = p<0.01) and (*** = p<0.001).

5.4: Discussion

This Chapter has investigated OPN secreted by bone-marrow derived macrophages under normal, high glucose and *pg*-LPS conditions. In addition, studies analysed OPN levels after the combined application of high glucose and *pg*-LPS. These two factors may potentiate bone loss in periodontal disease, however, the mechanisms have remained unclear to date. This study has hypothesized that increased OPN level could be the causative factor of this delayed bone healing. The study findings revealed that the isolated monocytes successfully differentiated into M1 and M2 macrophages according to their stimuli, GM-CSF and M-CSF with IL-4 respectively and expression of related cytokines, TNF-α, IL-6, TGF-β_1 and IL12p40. OPN levels in M1 and M2 either in normal or in high glucose conditions alone did not increase. *Pg*-LPS increased OPN levels in M2 macrophages only. The combined conditions, however, in both high glucose and *pg*-LPS, demonstrated a significant elevation of OPN levels in M1 and M2 macrophages.

The first aim of this study was to confirm monocyte differentiation in normal culture media. The isolated monocytes demonstrated round-shaped cells mostly homogenous with no distinct morphological appearances at day one. The cell-shape exhibited morphological changes at day 5, when there were distinct morphological differences between GM-CSF and M-CSF and IL-4 stimulated cells. M1 cells revealed round and oval cells with long process cells. M2 demonstrated mostly spindle-like shaped and little number of round cells with shorter processes. These findings are partly in line with Gordon and Taylor (2005) who described the cells as heterogeneous, variable size, granular and nuclear morphology. In addition, Rey-Giraud et al. (2012) reported that the majority of cells are elongated and fibroblast-like. The heterogeneity was described to be highly dependent on various factors, for example, cell origin, the level of differentiation and the variation of the stimulated microenvironmental cytokines (Chakraborty et al. 2005).

The isolated monocytes were characterised throughout the induction period to differentiate into M1 and M2 macrophages. F4/80 is considered as a specific surface marker of macrophages. Within this study, the fully differentiated macrophages expressed this marker at day 7. This result is in line with the studies of (Nguyen et al. 2007; Zhang et al. 2008), who showed F4/80 in differentiated macrophages. Although F4/80 revealed some expression in bone-derived cell phenotypes, Schulz et al. (2012) have reported that resident macrophages derived from yolk sac, such as microglia cells in

the brain, Langerhans cells in the skin and Kupffer cells in the liver, exhibited brighter F4/80 macrophages than the bone-derived macrophages, which are hematopoietic in origin and would demonstrate lower F4/80 expression.

Macrophages which were driven to differentiate into inflammatory M1 cells were characterised and found to secrete more pro-inflammatory cytokines. These pro-inflammatory mediators play a prime role in phagocytosis of pathogens. TNF-α represents the most important cytokine in this process. Within this study, the secreted TNF-α and IL-6 were estimated in the culture medium. M1 revealed significant levels of TNF-α and IL-6, which confirms the inflammatory nature of M1 phenotypes, stimulated by GM-CSF. These results are in accordance with other studies (Lund et al. 2009; Rittling 2011; Wang et al. 2013; Italiani and Boraschi 2014). On the other hand, M2 stimulated by M-CSF and IL-4 exhibited significant levels of TGF-β_1 and IL-12p40. TGF-β_1 was described as a very important anti-inflammatory factor and with pivotal roles in starting the healing process (Mohammad et al. 2006; Lund et al. 2009; Rittling 2011). It is worth stating that Dr. Norhayati Yusop from our laboratory group, had precisely completely characterised these cells by investigating TNF-α, IL-6, iNOS related to M1 and TGF-β_1, IL12p40, CD163, Arginase1 (Arg1), MRC1 and VEGF related to M2 ; both cells have been isolated by the same protocol (unpublished data).

This study then continued to consider the effects of high glucose on the developing M1 and M2 phenotypes. There was a significant increase in the secretion of TNF-α by M1 macrophages in high glucose, compared to M1 cultured in normal conditions. TNF-α has been described to be related to insulin resistance and aggravates diabetes (Hotamisligil et al. 1993; Engebretson et al. 2006). This result may confirm the Colombo et al. (2011) findings, who reported a prolonged high level in TNF-α in diabetic rat alveolar bone at week 3-6. Prolonged expression of TNF-α was described to have an established role in inhibiting osteoblast differentiation (Gowen et al. 1988) and stimulating osteoclast bone resorption (Nanes 2003), which appears to significantly correlate with periodontal disease severity (Tunes et al. 2010). However, other studies have shown a decrease in TNF-α and other pro-inflammatory cytokines secreted by peritoneal-derived macrophages, when investigated under high glucose conditions at day 1 and day 5 (Doxey et al. 1998). Taken collectively, TNF-α demonstrated a prolonged expression from macrophages under hyperglycemic condition, leading to dysregulation of immune response, which may result in destruction of periodontal tissue in the presence of subgingival Gram-negative bacteria, such as *Porphyromonus gingivalis* (Graves et al. 2007; Tunes et al. 2010). Interestingly, inhibition of TNF-α by using a recombinant TNF-α receptor

immunoglobulin G protein was found to improve insulin sensitivity (Hotamisligil et al. 1993). In the present study, however, IL-6 under high glucose condition did not reveal any differences compared with the normal conditions.

Within this study, TGF-β_1 the anti-inflammatory cytokines from M2, exhibited an increased level in the presence of high glucose. This result may explain the findings of Colombo et al. (2011), who reported a delayed expression, but a significant increase in TGF-β_1 in diabetic healing bone. In addition, macrophages derived from adipose tissue of insulin-resistant individuals indicated that macrophages expressed anti-inflammatory M2 cell characterisation, but with a higher susceptibility to produce pro-inflammatory cytokines, that tend to develop more insulin resistance and higher rates of fibrosis (Zeyda et al. 2007; Spencer et al. 2010).

In the presence of *pg*-LPS, TNF-α was more affected by *pg*-LPS in a dose-dependent manner. This may explain that the severity of periodontal disease depends on the dose of the virulent bacterial *pg*-LPS, which was mentioned to be a predominantly high constituent of subgingival plaque of diabetic individuals (Preshaw et al. 2012; How et al. 2016). IL-6, which is reported to activate TNF-α by means of IL-1β, demonstrated to be increased by 0.1µg/mL *pg*-LPS. These findings came partially in line at a concentration of 1µg/mL with that of Belfield et al. (2017), who reported that TNF-α secretion, increased in M1 and decreased in M2 macrophages. However, they reported no effects of *pg*-LPS on IL-6 in both M1 and M2 macrophages.

The combined effects of high glucose and *pg*-LPS indicated change in the profile of cytokines synthesized by M1 and M2 populations. Hung et al. (2013) studied this synergistic effect, however, they investigated macrophages from cell line (U937) without specifying the effects on M1 or M2 macrophages. Within this study, low concentration of *pg*-LPS (0.1µg/mL) under high glucose decreased TNF-α levels in M1 by one-fold, compared to *pg*-LPS under normal conditions. In contrast, increased *pg*-LPS concentrations to 1µg/mL, resulted in an almost one-fold higher level of TNF-α. This may suggest that low concentration of *pg*-LPS may be able to modulate the inflammatory process, unlike 1µg/mL concentration, which increased TNF-α levels. These results again suggest the dose-dependent manner of *pg*-LPS, described to play a pivotal role in the inflammatory process within periodontium and can induce more tissue destruction. IL-6 levels in the combined effects of high glucose and *pg*-LPS, showed high secretion at 0.1µg/mL

concentrations of *pg*-LPS. These findings agree partially with Hung et al. (2013), who also demonstrated dose-dependent increases in TNF-α and IL-6 levels, in high glucose and 0.1 and 1μg/μL of *pg*-LPS. The synergistic effects from this data suggest that the doses of both high glucose and *pg*-LPS play an important factor in increasing the inflammatory process, however, the amount of periodontal tissue destruction depends on the host response.

Herein, combined high glucose and *pg*-LPS increased TGF-β_1 and IL-12p40 levels, as evidence proposed that IL-12p40 may upregulate TGF-β_1 (Sindrilaru et al. 2011; Zhang et al. 2013). Thus, overexpression caused by combined high glucose and *pg*-LPS suggests an important role in periodontal disease progression. It is worth mentioning, that differences in cytokine responses to high glucose and LPS were reported in various research studies and might be attributed to the diversity in differentiation protocols of macrophages, concurrent with different sources and antigenic structures of *pg*-LPS used.

OPN protein is proposed to regulate different aspects of macrophage function; migration to the site of infection, phagocytosis and bacterial cell killing. Pedraza et al. (2008) and McKee et al. (2011) proposed that OPN may act as an opsonin to facilitate macrophage adhesion and then engulf the newly formed bone mineral crystals, which may hamper the biomineralisation process at the healing site. Colombo et al. (2011) reported OPN upregulation in diabetic bone concomitantly with an increased number of macrophages. This result could lead to an inference that the source of accumulated OPN could be from the accumulated macrophages at sites of diabetic healing bone. However, this was still not conclusive. Within this study, it is suggested that this increase in OPN could be derived mainly from M2 macrophages, although M1 macrophages also showed increased OPN levels, but they were statistically not significant. The synergistic conditions of high glucose and *pg*-LPS were found to significantly elevate OPN levels. These findings support the hypothesis that OPN might be the causative factor, which targets newly formed bone crystals and inhibits their growth, which potentially occurs in T2DM patient with periodontal disease. This information has not been previously described.

This Chapter has successfully demonstrated the differentiation of monocytes derived from bone marrow into GM-CSF activated (M1) and M-CSF and IL-4 activated (M2) macrophages. Cell characterisation was performed and inflammatory macrophages (M1) revealed to secrete TNF-α and IL-6 more than M2 macrophages. On the other hand, anti-inflammatory (M2) secreted higher levels of TGF-β_1 and IL12p40. High glucose or *pg*-LPS have exhibited certain effects on the pro-

inflammatory mediators, however, the combined effects of these aforementioned factors revealed significant effects on these cytokines, whether inducing or inhibiting their levels. Importantly, the novelty of this study is the identification that OPN is mainly secreted by M2, in addition to M1 macrophages under synergistic effects of both high glucose and *pg*-LPS conditions. This result, as far as we are aware, has not been reported in previous studies. This valuable piece of information could be the key point to continue studies to track the role of OPN in the progression of bone loss in periodontal disease, especially when associated by T2DM.

Chapter 6: General Discussion

The aims of this Thesis were to elucidate the effects of high glucose levels on compact bone mesenchymal stem cells (CB-MSCs) during cell culture expansion and in terms of osteogenic and adipogenic differentiation. This would help elucidate some of the harmful effects of high glucose (HG) on the healing and repair processes. These detrimental effects may be worsened by the role of lipopolysaccharides (LPS) derived from *Porphyromonas gingivalis* (*Pg*), resulting in exacerbation of the situation in periodontal disease. This study attempted to develop an understanding of these effects, to elucidate more the proposed link between type 2 diabetes mellitus (T2DM) and periodontal disease, which may assist in offering a better management for periodontal individuals with T2DM.

Initially there was a need to develop and characterise a cell culture model system, which enabled examination of cell populations, where differentiation status of the CB-MSCs differed. Within this Thesis, a primary rat cell-line from the endosteal region was used to develop such a model. Upon isolation, the cells showed a slow-growing lag phase at the beginning of culture until around PD10. This lag phase may be an attempt of the CB-MSCs to adapt to the new culture environment, as it is already different from their *in vivo* stem cell niche. Such a cell growth trend has also been observed with MSCs from dental pulp (Harrington et al. 2014; Lee et al. 2015). Therefore, cells were investigated at PD15, considering that they had started to proliferate and adapt to their new environment. CB-MSCs here demonstrated to be a heterogenous population and as expansion continued, two distinct populations were established. The first one was at PD15, where the cells demonstrated heterogenous phenotypes with predominant mature committed osteoprogenitor cells with large spindle cells and a proportion of stellate cells. As growth continued, there was a change in this heterogeneity, the committed cells appeared to be lost, leaving smaller stellate-shaped, high proliferative immature cells at PD50. Thorough characterisations were performed to identify these CB-MSC populations. It is worth mentioning that CB-MSCs expressed the classical stem cell markers endoglin (CD105), 5'-ectonucleotidase (CD73) and Thy-1 (CD90) concomitantly, but no expression of hematopoietic stem cell markers, CD45 or CD34 in all investigated populations, which confirmed almost pure MSC populations. Moreover, CB-MSCs expressed CD146, Snail, Slug, Tert and Terc (TR), whereas they were negative for the expression of Nanog and Oct4, indicating adult CB-MSC phenotypes, having multipotency rather than pluripotency, as associated with embryonic stem cells.

PD15 demonstrated various cell shapes, ranging from large spindle, stellate and flat-shaped cells. Those cells exhibited low ability to proliferate with low colony forming efficiency (CFE), which reflect that the cells may reach the lineage-committed stage or a number of them could have approached a terminal proliferative stage. Telomere restriction fragment (TRF) length analysis, revealed shorter average telomere length, compared to PD50. The protein expression of $p16^{INK4a}$ and cell cycle marker was seen to be elevated, in addition to an expression of $p21^{wafl}$, which have both been detected by Zhang et al. (2010) in fully-differentiated osteoblasts derived from MC3T3 cells. This may support our notion that their presence may represent a subpopulation of committed and mature osteoblasts. The protein expression of $p21^{wafl}$, however, was downregulated, considering its increase, when cells enter the G0 quiescent phase (Spencer et al. 2013). Thus, it is suggested a presence of a subpopulation of highly proliferative capacity within this heterogenous population. Furthermore, β-galactosidase staining (SA β-gal) exhibited a relatively low number of senescent cells. This predominantly committed population exhibited the highest capacity for osteogenic differentiation and mineral formation among other assessed populations, confirmed by the expression of osteogenic markers, Runx2, Osterix (OSX) and osteocalcin (OCN); and mineral crystal formation. Furthermore, although this population was described to consist mainly of committed osteoprogenitor stem cells, it successfully achieved adipogenic differentiation. Kim et al. (2005), reported that the committed cells can be induced to transdifferentiate into adipocytes by peroxisomal proliferator-activated receptor gamma (PPARγ).

Conversely, PD50 showed a change in this heterogeneous profile, where most of the spindle cells vanished, leaving smaller cell surface areas and predominantly stellate-like cells. Herein, this would suggest that 'the lost cell' from the PD50 profile could be linked to the large committed cells. This conclusion was reasonably based on the characteristic outcomes exemplified by long average telomere lengths, increases in CFEs, high proliferative capacity and a significant decrease in the cell surface areas. Increase in the mean of telomere length may indicate the cells are actively proliferating, and took a longer period to achieve osteogenic differentiation, which underpins the notion of a predominantly young population emerging. Furthermore, cell cycle marker expression of $p16^{INK4a}$ demonstrated a decline, informing that the cells were not senescent, in addition to the low expression of $p21^{wafl}$ (Spencer et al. 2013). Furthermore, SA β-gal staining showed a relatively very low number of senescent cells. The capacity of this population to undergo osteogenic differentiation was clearly less than PD15. However, by extending the time in culture a week longer, it showed a successful osteogenic differentiation into osteoblasts. This trend supported the suggestion of the immature

profile of this population. In terms of adipogenic differentiation, PD50 revealed a high capacity for adipocytes formation. Although both mature and immature cell populations were able to differentiate into adipocytes, Lipid TOX fluorescent staining showed more cluster of lipid droplets associated with immature cells, which would suggest that immature cell population was easily driven to differentiate into adipocytes. Importantly, after successful osteogenic and adipogenic differentiation of CB-MSCs, this confirmed their bi-potent capacity and was considered as a sound foundation to continue this work, assisting in investigating their role in bone repair.

High glucose conditions appeared not to affect the classical and other assessed surface marker expression for CB-MSCs. However, the glucose did appear to cause a reduction in MSC regenerative capacity, as the CFE decreased and a marked shortening of the mean telomere lengths in PD50. The response of the CB-MSCs populations to osteogenic differentiation, however, was different. PD15, the predominantly mature cells, under high glucose conditions were observed to exhibit a significant decrease in osteogenic differentiation. Interestingly, PD50 the predominantly immature cells, demonstrated that osteogenic differentiation was not affected by high glucose conditions. Such a finding has not previously been reported in the literature, as far as we are aware. High glucose microenvironments also exhibited a significant decrease in adipogenesis in cells both PD15 and PD50 through decline in the expression of PPARγ and adiponectin markers. Although some other studies identified an increases in adipogenesis under high glucose conditions (Chuang et al. 2007; Wang et al. 2010a), Shilpa et al. (2013) reported that long-term exposure to very high glucose conditions demonstrated also decreased adipogenesis. These controversial results may be a reflection of different MSC origins assessed (endosteal and bone marrow); and variation in the protocols for assessing cell differentiation. We extended cell expansion to more than 300 days and investigated PD100 and PD200, where osteogenesis, but not adipogenesis was achievable. This has also been mentioned in other studies, that after long-term cell expansion, cells were no longer able to undergo adipogenic differentiation in culture (Ntambi and Kim 2000; Sethe et al. 2006; Ali et al. 2013).

Pg-LPS is known to have inhibitory effects on bone formation, as it can activate the host cells, such as macrophages through TLR2 and TLR4 receptors. These, in turn, induce secretion of proinflammatory cytokines, interleukin (IL) IL-1β, IL-6, IL-8 and tumour necrosis factor (TNF) TNF-α, resulting in disturbing bone remodelling and repair processes (Graves et al. 2011; Herath et al. 2011; Kato et al. 2014). However, little is known about this mechanism. Within this study, two

concentrations of *pg*-LPS (0.1 and 1µg/mL) were assayed to evaluate their effects on osteogenesis process within the mature and immature CB-MSC populations. In terms of mineral formation, *pg*-LPS was found to inhibit the osteogenic differentiation of committed cells in a dose-dependent manner, where 1µg/mL *pg*-LPS concentration showed more detrimental effects on mineral formation than 0.1µg/mL *pg*-LPS. The protein expression of osteocalcin (OCN) was downregulated at both concentrations of *pg*-LPS. These results were in line with other studies (Kadono et al. 1999; Kato et al. 2014). This profile, nonetheless, was different in immature cells, as this population appeared to be affected by 0.1µg/mL concentrations of *pg*-LPS, which exerted detrimental effects on the mineral formation. This again revealed the differences between the mature and immature MSC responses, which have consequential effects on the bone healing process.

When studying the combined effects of high glucose and *pg*-LPS on CB-MSCs, by trying to mimic the diabetic individual with periodontal disease, this Thesis suggested that immature cells were more affected by *pg*-LPS in the presence of high glucose, in terms of the ability of the MSCs to form mineral containing bone matrix nodules. This important finding opens the door for a deeper understanding of the detrimental effects of combined *pg*-LPS and high glucose, especially on immature cells. In this case, the turnover of MSCs during their life cycle through maturation from transit amplifying (TA) stage, until becoming committed and mature osteoprogenitor cells, will be affected. This outcome is also supported by the finding of decreasing CFEs due to high glucose conditions. Thus, bone formation may decline due to this harmful effect on immature population, resulting in greater bone resorption versus bone formation. Therefore, this might explain the delay in healing and repair process in periodontal disease, leading to a net bone loss. This valuable outcome about the role of *pg*-LPS and high glucose on immature cells is of great importance and needs further research.

Interestingly, OPN has been described to bind to the mineral crystals during bone mineralisation, which inhibit their growth, assisting in the remodelling process (Pedraza et al. 2008; McKee et al. 2011). OPN was observed to be increased in the diabetic healing bone within an *in vivo* model (Colombo et al. 2011). In the present Thesis, it has been proposed that increased OPN in diabetic healing bone could be the causative factor, especially when associated with *pg*-LPS, resulting in an increased net bone loss in T2DM. Herein, OPN was found to be elevated under high glucose conditions in both PD15 and PD50, but reported decrease, where combined with *pg*-LPS conditions at both concentrations. Although this important finding required more studies to be interpreted

further, it meant that the source of OPN, which is proposed to inhibit the mineral formation, was not from the CB-MSCs. Thus, this finding led us to consider macrophages as an alternative source of OPN.

Macrophages are known to play a pivotal role in defending the body against pathogens as part of innate, as well as adaptive, immunity. They act as critical mediators of inflammatory processes by controlling tissue homeostasis and by regulating different phases of wound and bone healing. In the present study, macrophages were derived from monocytes by stimulating them using granulocyte macrophage-colony stimulating factor (GM-CSF) and macrophage-colony stimulating factor and interleukin 4 (M-CSF/IL-4), to drive cells to differentiation into M1 (pro-inflammatory) and M2 (anti-inflammatory) macrophages, respectively. The cells were previously fully characterised by Dr. Norhayati Yusop from our laboratory (Norhayati Yusop PhD Thesis 2015). Various cytokines were investigated: TNF-α, IL-6 and iNOS expression related to M1 macrophages; and TGF-β_1, IL12p40, CD163, Arginase1 (Arg1), MRC1 and VEGF expression related to M2 macrophages. TNF-α, IL-6, TGF-β_1 and IL12p40 were assessed, looking at the effects of high glucose or *pg*-LPS alone; and when combined together. M1 macrophages revealed higher secretion levels of TNF-α and IL-6, whereas M2 macrophages secreted higher levels of TGF-β_1 and IL-12p40. High glucose exhibited a significant increase in TNF-α in M1 macrophages, which implies an increase in the pro-inflammatory process, but at the same time, TGF-β_1 was also elevated in M2 macrophages, which is known to induce healing and repair (Hamilton 2008; Italiani and Boraschi 2014). The combined effects of these two factors, HG and *pg*-LPS, however, revealed significant effects on these cytokines. TNF-α was affected in a dose-dependent manner, which was described to play a central role in periodontal disease, by inducing more tissue destruction. IL-6 levels were significantly elevated at 0.1µg/mL. Combined high glucose and *pg*-LPS was also found to increase TGF-β_1 and IL-12p40 levels, when recent evidence proposed that IL-12p40 may upregulate TGF-β_1 (Sindrilaru et al. 2011; Zhang et al. 2013). Thus, the changes in cytokine profile expression owing to the combined effects of HG and *pg*-LPS, suggested an important role in periodontal disease progression. In normal healing conditions, there is a balance between M1/M2 macrophage activities. Nevertheless, when this balance is disrupted and becomes more in favour of proinflammatory M1 macrophages, this can result in more tissue destruction, than healing and repair. This has been reported by a significant increase in TNF-α owing to high glucose effects (Davis et al. 2008; Kraakman et al. 2014). Although Hung et al. (2013), reported this synergistic effect on cytokines, they investigated macrophages from a cell line (U937). Within this study, the effects of HG and *pg*-LPS on M1 or M2 macrophages have been identified. The synergistic

effects from this data suggested that *pg*-LPS concentrations play an important role in elevating inflammatory events in addition to, HG. However, the amount of periodontal tissue destruction evident would depend on individual variations in the host response.

One of the important proteins secreted by macrophages is OPN. In normal or high glucose conditions, OPN revealed low expression levels at the molecular and protein levels. Intriguingly, the synergistic effects seen where adding *pg*-LPS at both concentrations, caused significant increases in OPN levels in both M1 and M2 macrophages. In addition, *pg*-LPS alone also elevated OPN levels in M2 macrophages. Such a significant increase in OPN levels could be linked to severe bone resorption, which is typically observed in periodontal disease with T2DM, when the pro-inflammatory phase predominantly consists of M1 macrophage activities. On the other hand, OPN levels registered a higher secretion from M2 macrophages, due to combined effects of *pg*-LPS and high glucose; and even in the case of *pg*-LPS alone. This led to speculation that OPN could cause detrimental effects when host conditions become more anti-inflammatory. These findings as far as we are aware, are novel and unveil a new mechanism of bone resorption at the expense of bone formation, in the case of patients with periodontal disease concurrently with T2DM.

It is worthy to mention one limitation in this study, that it was better to use freshly isolated MSCs from aged Goto-Kakizaki (GK) rats, which already had T2DM for 12 weeks. However, difficulties in isolation of these MSCs from old animals led to the performance of long-term CB-MSCs culture under high glucose conditions.

6.1: Future Work

The outcomes of this Thesis have been successful in identifying that the macrophage secretion of OPN is higher under the combined effects of *pg*-LPS and high glucose conditions, especially from M2 macrophages. This finding would assist in solving the complicated profile of periodontal disease associated with T2DM. However, there is still a lack of knowledge about mechanisms by which these changes happen and how the signalling pathways increase OPN levels. Despite the interesting outcomes of this Thesis, it would be advantageous for future work to use three-dimension culture model, instead of two-dimensions *in vitro*. This may reflect the real profile of *in vivo* conditions, which is more complicated by other factors, such as a plethora of subgingival bacterial biofilm formation, rather than *pg*-LPS alone. In addition to various immune cells and signalling pathways,

which all need to be considered when trying to make a precise conclusion about the underlying mechanisms of bone loss. If this understanding could translate into a therapeutic intervention, one suggestion is to investigate OPN levels in an *in vivo* model, such as GK rat with experimental periodontitis through a ligature on central teeth. In this case, we would obtain a translatable model to the human. By blocking OPN according to (Walker et al. 2010; Saito et al. 2016; Foster et al. 2018) and then assessing the mineral formation to evaluate the differences between the presence and absence of OPN, this may assist in identifying the proposed role of OPN in enhancing detrimental effects on bone formation in such circumstances. Interestingly, knock out of OPN may give an increase in tissue density, dental pulp and periodontal ligaments as mentioned by Foster et al. (2018). However, OPN was assayed in healthy knock out OPN mice. With this proposed model, it would be possible to observe the progression of periodontal disease. In addition, identifying the phosphorylated status of OPN is quite important as it is proposed that phosphorylated OPN is needed for mineral function, whereas dephosphorylated OPN may play a pivotal role in signalling and chemotactic activities. This will assist in better understanding the role of OPN in periodontium, which may aid to identify some of the potential therapeutic options in promoting the repair process in periodontal disease individuals with T2DM. Another suggestion related to the finding is that the immature cell population (PD50) was seen to be more affected by synergistic effects of HG and *pg*-LPS. Therefore, it would be worthwhile to isolate clonal cells from this population, in order to perform characterisation; investigating proliferative ability, multi-potency and unipotency under aforementioned synergistic conditions to confirm present findings. With a view to addressing T2DM with periodontitis, however, it is worth to state that proper oral hygiene and good HbA1c of blood glucose control, still remain to be the best approach to solve this complicated problem as evidenced by “prevention is better than cure”.

7.0: References

Aathira, R. and Jain, V. 2014. Advances in management of type 1 diabetes mellitus. *World Journal of Diabetes* 5(5), pp. 689–96.

Abbas, S. et al. 2003. Tumor necrosis factor-α inhibits pre-osteoblast differentiation through its type-1 receptor. *Cytokine* 22(1–2), pp. 33–41.

Abdalla, B. and Kassem, M. 2008. Human Mesenchymal Stem Cells : From Basic Biology to Clinical Applications Human mesenchymal stem cells : from basic biology to clinical applications. *Gene Therapy* 15, pp. 109–116.

Acosta, J.C. et al. 2008. Chemokine Signaling via the CXCR2 Receptor Reinforces Senescence. *Cell* 133(6), pp. 1006–1018.

Addison, W.N. et al. 2007. Pyrophosphate Inhibits Mineralisation of Osteoblast Cultures by Binding to Mineral , Up-regulating Osteopontin , and Inhibiting Alkaline Phosphatase Activity. *The Journal of Biological Chemistry* 282(21), pp. 15872–15883.

Agnihotri, R. et al. 2001. Osteopontin , a Novel Substrate for Matrix Metalloproteinase-3 (Stromelysin-1) and Matrix Metalloproteinase-7 (Matrilysin). *The Journal of biological chemistry* 276(30), pp. 28261–28267.

Ahlqvist, E. et al. 2013. Link between GIP and osteopontin in adipose tissue and insulin resistance. *Diabetes* 62(6), pp. 2088–94.

AI-Aql, Z.S. et al. 2008. Molecular mechanisms controlling bone formation during fracture healing and distraction osteogenesis. *Journal of Dental Research* 87(2), pp. 107–18.

Akashi, K. et al. 2000. A clonogenic common myeloid progenitor that gives rise to all myeloid lineages. *Nature* 404, pp. 193–197.

Al-Mashat, H. et al. 2006. Diabetes enhances mRNA levels of proapoptotic genes and caspase activity, which contribute to impaired healing. *Diabetes* 55(February), pp. 487–495.

Al-Qutub, M.N. et al. 2006. Hemin-Dependent Modulation of the Lipid A Structure of Porphyromonas gingivalis Lipopolysaccharide. *Infection and Immunity* 74(8), pp. 4474–4485.

Al-Zube, L. et al. 2009. Recombinant human platelet-derived growth factor BB (rhPDGF-BB) and beta-tricalcium phosphate/collagen matrix enhance fracture healing in a diabetic rat model. *Journal of Orthopaedic Research* 27(8), pp. 1074–1081.

Albiero, M. et al. 2011. Defective recruitment , survival and proliferation of bone marrow-derived progenitor cells at sites of delayed diabetic wound ective recruitment , survival and proliferation of bone marrow-derived progenitor cells at sites of delayed diabetic wound. *Diabetologia* 54(4), pp. 945–953.

Albiero, M.L. et al. 2017. Osteogenic potential of periodontal ligament stem cells are unaffected after exposure to lipopolysaccharides. *Brazilian Oral Research* 31, pp. 1–10.

Ali, A.T. et al. 2013. Adipocyte and adipogenesis. *European Journal of Cell Biology* 92, pp. 229–236.

Alikhani, Z. et al. 2005. Advanced glycation end products enhance expression of pro-apoptotic genes and stimulate fibroblast apoptosis through cytoplasmic and mitochondrial pathways. *The Journal of Biological Chemistry* 280(13), pp. 12087–95.

Andrews, S. et al. 2012. Knockdown of osteopontin reduces the inflammatory response and subsequent size of postsurgical adhesions in a murine model. *The American Journal of Pathology* 181(4), pp. 1165–72.

Armas, L. and Recker, R. 2012. Pathophysiology of Osteoporosis: New Mechanistic Insights. *Endocrinology and Metabolism Clinics of North America* 41(3), pp. 475–486.

Arvidson, K. et al. 2011. Bone regeneration and stem cells. *Journal of Cellular and Molecular Medicine* 15(4), pp. 718–746.

Ashton, B.A. et al. 1980. Formation of bone and cartilage by marrow stromal cells in diffusion chambers in vivo. *Clinical Orthopaedics and Related Research* (151), pp. 294–307.

Asnaghi, V. et al. 2003. A Role for the Polyol Pathway in the Early Neuroretinal Apoptosis and Glial Changes Induced by Diabetes in the Rat. *Diabetes* 52, pp. 506–511.

Asou, Y. et al. 2001. Osteopontin facilitates angiogenesis, accumulation of osteoclasts, and resorption in ectopic bone. *Endocrinology* 142(3), pp. 1325–32.

Asumda, F.Z. and Chase, P.B. 2011. Age-related changes in rat bone-marrow mesenchymal stem cell plasticity. *BMC Cell Biology* 12(44), pp. 1–11.

Atashi, F. et al. 2015. The Role of Reactive Oxygen Species in Mesenchymal Stem Cell Adipogenic and Osteogenic Differentiation : *Stem Cells and Development* 24(10), pp. 1150–1163.

Aubert, G. et al. 2013. assessment of the available technologies and tools. 730(604), pp. 59–67.

Autréaux, B.D. and Toledano, M.B. 2007. ROS as signalling molecules : mechanisms that generate specificity in ROS homeostasis. *Nature Review Molecular Cell Biology* 8, pp. 813–824.

Aybar, M.J. et al. 2003. Snail precedes Slug in the genetic cascade required for the specification and migration of the Xenopus neural crest. *Development* 130, pp. 483–494.

Baird, D.M. et al. 2003. Extensive allelic variation and ultrashort telomeres in senescent human cells. *Nature Genetics* 33, pp. 203–207.

Baker, N. et al. 2014. Characterization of bone marrow-derived mesenchymal stem cells in aging. *Bone* 70, pp. 37–47.

Balduino, A. et al. 2012. Molecular Signature and *In Vivo* Behavior of Bone Marrow Endosteal and Subendosteal Stromal Cell Populationa and their Relevance to Hematopoiesis. *Experimental cell research* 318(19), pp. 2427–2437.

Bargonetti, J. and Manfredi, J. 2002. Multiple roles of the tumor suppressor p53. *Current Opinion in Oncology* 14(1), pp. 86–91.

Bari, C. De et al. 2001. Multipotent Mesenchymal Stem Cells From Adult Human Synovial Membrane.

Arthritis and Rheumatism 44(8), pp. 1928–1942.

Bari, C. De et al. 2006. Mesenchymal Multipotency of Adult Human Periosteal Cells Demonstrated by Single-Cell Lineage Analysis. *Arthritis and Rheumatism* 54(4), pp. 1209–1221.

Bartocci, A. et al. 1987. Macrophages specifically regulate the concentration of their own growth factor in the circulation. *Cell Biology* 84, pp. 6179–6183.

Batlle, R. et al. 2013. Snail1 controls TGF-β responsivness and differentiation of Mesenchymal Stem Cells. *Oncogene* 32(28), pp. 3381–3389.

Belfield, L. et al. 2017. Exposure to Porphyromonas gingivalis LPS during macrophage polarisation leads to diminished in flammatory cytokine production. *Archives of Oral Biology* 81, pp. 41–47.

Bennett, J.H. et al. 1991. Adipocytic cells cultured from marrow have osteogenic potential. *Journal of Cell Science* 99, pp. 131–139.

Bensidhoum, M. et al. 2004. Homing of in vitro expanded Stro-1- or Stro-1+ human mesenchymal stem cells into the NOD/SCID mouse and their role in supporting human CD34 cell engraftment. *Blood* 103(9), pp. 3313–9.

Berezin, A.E. and Kremzer, A.A. 2013. Circulating osteopontin as a marker of early coronary vascular calcification in type two diabetes mellitus patients with known asymptomatic coronary artery disease. *Atherosclerosis* 229, pp. 475–81.

Bertola, A. et al. 2009. Elevated expression of osteopontin may be related to adipose tissue macrophage accumulation and liver steatosis in morbid obesity. *Diabetes* 58(1), pp. 125–33.

Bianco, P. 2014. Stem cells and bone: A historical perspective. *Bone* S8756-3282(14), pp. 322–6.

Bielby, R. et al. 2007. The Role of Mesenchymal Stem Cells in Maintenance and Repair of Bone The role of mesenchymal stem cells in maintenance and repair of bone. *Injury* 38(1), pp. 27–33.

Blasco, M.A. 2005. Telomeres and human disease: Ageing, cancer and beyond. *Nature Reviews Genetics* 6(8), pp. 611–622.

Blondet, J.J. and Beilman, G.J. 2007. Glycemic control and prevention of perioperative infection. *Current Opinion in Critical Care* 13(4), pp. 421–427.

Bongso, A. and Lee, E.H. 2005. Stem Cells: Their Definition, Classification and Sources. *Biology of Blood and Marrow Transplantation*, pp. 1–13.

Borst, S.E. 2004. The role of TNF-alpha in insulin resistance. *Endocrine* 23(2–3), pp. 177–82..

Bos, T. van den and Beertsen, W. 1999. Alkaline phosphatase activity in human periodontal ligament: age effect and relation to cementum growth rate. *Journal of Periodontal Research* 34(1), pp. 1–6.

Boskey, A.L. 1995. Osteopontin and Related Phosphorylated Sialoproteins: Effects on Mineralisation. *Annals of the New York Academy of Sciences* 760, pp. 249–256.

Boskey, A.L. et al. 2002. Osteopontin deficiency increases mineral content and mineral crystallinity in mouse bone. *Calcified Tissue International* 71, pp. 145–154.

Boskey, A.L. et al. 2013. Post-Translational Modification of Osteopontin: Effects on in Vitro Hydroxy apatite Frmation. *Biochem Biophys Res Commun* 419(2), pp. 1–13.

Bosshardt, D.D. et al. 1998. Developmental appearance and distribution of bone sialoprotein and osteopontin in human and rat cementum. *Anatomical Record* 250(1), pp. 13–33.

Botolin, S. et al. 2005. Increased Bone Adiposity and Peroxisomal. *Endocrinology* 146(8), pp. 3622–3631.

Botolin, S. and Mccabe, L.R. 2006. Chronic Hyperglycemia Modulates Osteoblast Gene Expression Through Osmotic and Non-Osmotic Pathways. *Journal of Cellular Biochemistry* 99, pp. 411–424.

Botolin, S. and Mccabe, L.R. 2007. Bone Loss and Increased Bone Adiposity in Spontaneous and Pharmacologically Induced Diabetic Mice. *Endocrinology* 148(1), pp. 198–205.

Bouillon, R. 1991. Diabetic bone disease. *Calcified Tissue International* 49(3), pp. 155–60.

Boxall, S. a and Jones, E. 2012. Markers for characterization of bone marrow multipotential stromal cells. *Stem Cells International* 975871, pp. 1–12.

Boyden, L.M. et al. 2002. High Bone Density Due to a Mutation in LDL-Receptor–Related Protein 5. *New England Journal of Medicine* 346(20), pp. 1513–1521.

Brem, H. and Tomic-Canic, M. 2007. Cellular and molecular basis of wound healing in diabetes. *J Clin Invest* 117(5), pp. 1219–1222.

Bronckers, A.L.J.J. et al. 1994. Immunolocalization of Osteopontin, Osteocalcin, and Dentin Sialoprotein During Dental Root Formation and Early Cementogenesis in the Rat. *Journal of Bone and Mineral Research* 9(6), pp. 833–841.

Brownlee, M. 2005. The pathobiology of diabetic complications: A unifying mechanism. *Diabetes* 54, pp. 1615–1625.

Burgess, A.W. and Metcalf, D. 1980. The Nature and Action of Granulocyte-Macropage Colony Stimulating Factors. *Blood* 56(6), pp. 947–959.

Buse, M.G. 2006. Hexosamines, insulin resistance, and the complications of diabetes: current status. *AJP: Endocrinology and Metabolism* 290(1), pp. E1–E8..

Byon, C.H. et al. 2008. Oxidative Stress Induces Vascular Calcification through Modulation of the Osteogenic Transcription Factor Runx2 by AKT Signaling. *The Journal of Biological Chemistry* 283(22), pp. 15319–15327.

Byun, M.R. et al. 2014. FGF2 stimulates osteogenic differentiation through ERK induced TAZ expression. *Bone* 58, pp. 72–80.

Cai, L. et al. 2002. Hyperglycemia-induced apoptosis in mouse myocardium: mitochondrial cytochrome C-mediated caspase-3 activation pathway. *Diabetes* 51(6), pp. 1938–48.

Campisi, J. and d'Adda di Fagagna, F. 2007. Cellular senescence: when bad things happen to good cells. *Nature Reviews. Molecular cell biology* 8, pp. 729–740.

Canalis, E. and Gabbitas, B. 1994. Bone morphogenetic protein 2 increases insulin-like growth factor I

and II transcripts and polypeptide levels in bone cell cultures. *Journal of Bone and Mineral Research* 9(12), pp. 1999–2005.

Caplan, A.I. 1991. Mesenchymal Stem Cells. *Journal of Orthopaedic Research* 9(5), pp. 641–650.

Carnevale, V. et al. 2014. Bone damage in type 2 diabetes mellitus. *Nutrition, metabolism, and cardiovascular diseases : NMCD* xx, pp. 1–7.

Chakraborty, D. et al. 2005. Leishmania donovani Affects Antigen Presentation of Macrophage by Disrupting Lipid Rafts. *The Journal of Immunology* 175(5), pp. 3214–3224.

Chan, R.W.S. et al. 2004. Clonogenicity of Human Endometrial Epithelial and Stromal Cells. *Biology of Reproduction* 70, pp. 1738–1750.

Chan, R.W.S. et al. 2004. Clonogenicity of human endometrial epithelial and stromal cells. *Biology of Reproduction* 70(6), pp. 1738–50.

Chau, B.N. and Wang, J.Y.J. 2003. Coordinated regulation of life and death by RB. *Nature Review Cancer* 3, pp. 130–138.

Chavarry, N.G. et al. 2009. The relationship between diabetes mellitus and destructive periodontal disease: a meta-analysis. *Oral health & Preventive Dentistry* 7(2), pp. 107–127.

Chen, A.L. et al. 2004. Expression of bone morphogenetic proteins, receptors, and tissue inhibitors in human fetal, adult, and osteoarthritic articular cartilage. *Journal of orthopaedic research* 22(6), pp. 1188–92.

Chen, F. and Jin, Y. 2010. Periodontal Tissue Engineering and Regeneration : Current Approaches and Expanding Opportunities. *Tissue Engineering: Part B* 16(2), pp. 219–253.

Chi, Z. 2012. Molecular mechnasims of osteoblast-specific transcription factor Osterix effects on bone formation. *Journal of Peking University (Health Sciences* 44(5), pp. 659–665.

Chiquette, E. and Chilton, R. 2002. Cardiovascular disease: much more aggressive in patients with type 2 diabetes. *Current Atherosclerosis Reports* 4(2), pp. 134–42.

Cho, M.-L. et al. 2006. Transforming growth factor-β1(TGF-β1) down-regulates TNFα-induced RANTES production in rheumatoid synovial fibroblasts through NF- κB-mediated transcriptional repression. *Immunology Letters* 105(2), pp. 159–166.

Choi, Y.H. et al. 2011. Osterix is regulated by Erk1/2 during osteoblast differentiation. *Biochem Biophys Res Commun* 415(3), pp. 472–478.

Chow, A. et al. 2010. promote the retention of hematopoietic stem and progenitor cells in the mesenchymal stem cell niche. *Journal of Experimental Medicine* 208(2), pp. 261–271.

Christensen, B. et al. 2010. Osteopontin Is Cleaved at Multiple Sites Close to Its Integrin-binding Motifs in Milk and Is a Novel Substrate for Plasmin and Cathepsin D. *The Journal of Biological Chemistry* 285(11), pp. 7929–7937.

Christensen, B. et al. 2012. C-terminal modification of osteopontin inhibits interaction with the -integrin. *Journal of Biological Chemistry* 287(6), pp. 3788–3797.

Chuang, C.C. et al. 2007. Hyperglycemia Enhances Adipogenic Induction of Lipid Accumulation : Involvement Hyperglycemia Enhances Adipogenic Induction of Lipid Accumulation : Involvement of Extracellular Signal-. *Endocrinology* 148(9), pp. 4267–4275.

Clément-Lacroix, P. et al. 2005. Lrp5-independent activation of Wnt signaling by lithium chloride increases bone formation and bone mass in mice. *Proceedings of the National Academy of Sciences of the United States of America* 102, pp. 17406–11.

Colombo, J.S. et al. 2011. Delayed osteoblast differentiation and altered inflammatory response around implants placed in incisor sockets of type 2 diabetic rats. *Clinical Oral Implants Research* 22(6), pp. 578–86.

Colter, D.C. et al. 2000. Rapid expansion of recycling stem cells in cultures of plastic-adherent cells from human bone marrow. *Proceedings of the National Academy of Sciences* 97(7), pp. 3213–3218.

Cooper, L. et al. 2005. Wound healing and inflammation genes revealed by array analysis of 'macrophageless' PU.1 null mice. *Genome Biology* 6(1), p. R5.

Coppé, J.-P. et al. 2010. The Senescence-Associated Secretory Phenotype: The Dark Side of Tumor Suppression Jean-Philippe. *Annual Revision Pathology* 5, pp. 99–118.

Costa, K.L. et al. 2017. Influence of Periodontal Disease on Changes of Glycated Hemoglobin Levels in Patients With Type 2 Diabetes Mellitus: A Retrospective Cohort Study. *Journal of Periodontology* 88(1), pp. 17–25.

Cui, C. Bin et al. 2003. Transcriptional coactivation of bone-specific transcription factor Cbfa1 by TAZ. *Molecular and Cellular Biology* 23(3), pp. 1004–1013.

D'Souza, D.R. et al. 2009. Hyperglycemia regulates RUNX2 activation and cellular wound healing through the aldose reductase polyol pathway. *Journal of Biological Chemistry* 284(27), pp. 17947–17955.

Darby, I.A. et al. 1997. Apoptosis is increased in a model of diabetes-impaired wound healing in genetically diabetic mice. *The International Journal of Biochemistry & Cell biology* 29(1), pp. 191–200.

Darveau, R.P. et al. 2004. Porphyromonas gingivalis Lipopolysaccharide Contains Multiple Lipid A Species That Functionally Interact with Both Toll-Like Receptors 2 and 4. *Infection and Immunity* 72(9), pp. 5041–5051.

Datta, H.K. et al. 2008. The Cell Biology of Bone Metabolism. *Journal of Clinical Pathology* 61, pp. 577–587.

Davis, J.E. et al. 2008. Tlr-4 Deficiency Selectively Protects Against Obesity Induced by Diets High in Saturated Fat. *Obesity* 16(6), pp. 1248–1255.

Day, T.F. et al. 2005. Wnt/β-catenin signaling in mesenchymal progenitors controls osteoblast and chondrocyte differentiation during vertebrate skeletogenesis. *Developmental Cell* 8, pp. 739–750.

Delorme, B. et al. 2009. Specific lineage-priming of bone marrow mesenchymal stem cells provides the molecular framework for their plasticity. *Stem cells (Dayton, Ohio)* 27(5), pp. 1142–51.

Demmer, R. et al. 2010. Periodontal Status and A1c Change. *Diabetes Care* 33(5), pp. 1037–1043.

Denham, M. et al. 2005. Stem cells: an overview. *Current Protocols in Cell Biology* 5, pp. 1–12.

Denu, R.A. and Hematti, P. 2016. Effects of Oxidative Stress on Mesenchymal Stem Cell Biology. *Oxidative Medicine and Cellular Longevity*, pp. 1–9.

Díaz, L. et al. 2015. Changes in lipopolysaccharide profile of Porphyromonas gingivalis clinical isolates correlate with changes in colony morphology and polymyxin B resistance. *Anaerobe* 33, pp. 25–32.

Dickson, L.M. and Rhodes, C.J. 2004. Pancreatic beta-cell growth and survival in the onset of type 2 diabetes: a role for protein kinase B in the Akt? *American Journal of Physiology, Endocrinology and metabolism* 287(2), pp. E192-8.

Dimitriou, R. et al. 2005. Current concepts of molecular aspects of bone healing. *Injury* 36(12), pp. 1392–404.

Dimri, G. et al. 1995. A biomarker that identifies senescent human cells in culture and in aging skin *in vivo*. *Proceedings of the National Academy of Sciences* 92(September), pp. 9363–9367.

Ding, C. et al. 2013. Adiponectin Increases Secretion of Rat Submandibular Gland via Adiponectin Receptors-Mediated AMPK Signaling. *PloS one* 8(5), p. e63878.

Dominici, M. et al. 2006. Minimal criteria for defining multipotent mesenchymal stromal cells. The International Society for Cellular Therapy position statement. *Cytotherapy* 8(4), pp. 315–7.

Donovan, J. et al. 2013. Platelet-derived growth factor signaling in mesenchymal cells. *Frontiers in Bioscience* 18, pp. 106–119.

Doxey, D.L. et al. 1998. Diabetes-induced impairment of macrophage cytokine release in a rat model: Potential role of serum lipids. *Life Sciences* 63(13), pp. 1127–1136.

Ducy, P. et al. 1997. Osf2/Cbfa1: A transcriptional activator of osteoblast differentiation. *Cell* 89, pp. 747–754.

Edwards, J.R. and Mundy, G.R. 2011. Advances in osteoclast biology: old findings and new insights from mouse models. *Nature Reviews Rheumatology* 7, pp. 235–243.

Eghbali-Fatourechi, G. et al. 2005. Circulating osteoblast-lineage cells in humans. *N Engl J Med* 352(19), pp. 1959–66.

Ehnert, S. et al. 2010. TGF-β1 as possible link between loss of bone mineral density and chronic inflammation. *PLoS ONE* 5(11), p. e14073.

Engebretson, S. et al. 2006. Plasma levels of tumour necrosis factor- a in patients with chronic periodontitis and type 2 diabetes. *Journal of Clinical Periodontology* 34, pp. 18–24.

Erik Holm, J.S. et al. 2014. Osteopontin mediates mineralisation and not osteogenic cell devel- opment in vitro. *Biochemical Journal* 464(3), pp. 355–364.

Espinoza-Jim´enez, A. et al. 2012. Alternatively Activated Macrophages in Types 1 and 2 Diabetes. *Mediators of Inflammation* 2012, pp. 1–10.

Evans, J.L. et al. 2002. Oxidative stress and stress-activated signaling pathways: A unifying hypothesis of type 2 diabetes. *Endocrine Reviews* 23(5), pp. 599–622.

Evans, J.L. et al. 2003. Are Oxidative Stress-Activated Signaling Pathways Mediators of Insulin Resistance and B-Cell Dysfunction? *Diabetes* 52, pp. 1–8.

Fenga, Y.-F. et al. 2013. Feng, Y. F. et al. 2013. Effect of reactive oxygen species overproduction on osteogenesis of porous titanium implant in the present of diabetes mellitus. *Biomaterials* 34(9), pp. 2234–2243.

Fiorina, P. et al. 2010. The mobilization and effect of endogenous bone marrow progenitor cells in diabetic wound healing. *Cell Transplantation* 19(11), pp. 1369–1381.

Fisher, L.W. and Fedarko, N.S. 2003. Six genes expressed in bones and teeth encode the current members of the SIBLING family of proteins. *Connective Tissue Research* 44(1), pp. 33–40.

Fogg, D.K. et al. 2005. A Clonogenic Bone Marrow Progenitor Specific for Macrophages and Dendritic Cells. *Science* 311, pp. 83–87.

Foster, B.L. 2012. Methods for studying tooth root cementum by light microscopy. *International Journal of Oral Science* 4, pp. 119–128. Available at: http://dx.doi.org/10.1038/ijos.2012.57.

Foster, B.L. et al. 2018. Osteopontin regulates dentin and alveolar bone development and mineralisation. *Bone* 107, pp. 196–207.

Fox, C. 1992. New considerations in the prevalence of periodontal disease. *Curr Opin Dent* 2, pp. 5–11.

Fox, C.H. et al. 1994. Periodontal disease among New England elders. *Journal of periodontology* 65(7), pp. 676–684.

Franzén, A. and Heinegård, D. 1985. Isolation and characterization of two sialoproteins present only in bone calcified matrix. *The Biochemical Journal* 232, pp. 715–24.

Friedenstein, A.J. et al. 1968. Heterotopic of bone marrow. Analysis of precursor cells for osteogenic and hematopoietic tissues. *Transplantation* 6(2), pp. 230–47.

Friedenstein, A.J. et al. 1987. Bone marrow osteogenic stem cells: in vitro cultivation and transplantation in diffusion chambers. *Cell and Tissue Kinetics* 20(3), pp. 263–72.

Fujisaka, S. et al. 2009. Regulatory Mechanisms for Adipose Tissue M1 and M2 Macrophages in Diet-Induced Obese Mice. *Diabetes* 58, pp. 2574–2582.

Fujita, K. and Janz, S. 2007. Attenuation of WNT signaling by DKK-1 and -2 regulates BMP2-induced osteoblast differentiation and expression of OPG, RANKL and M-CSF. *Molecular Cancer* 6, p. 71.

Gabbay, K. 1973. The sorbitol pathway and the complications of diabetes. *N Engl J Med* 288, pp. 831–836.

Gafni, Y. et al. 2004. Stem cells as vehicles for orthopedic gene therapy. *Gene Therapy* 11(4), pp. 417–426.

Gallagher, K.A. et al. 2007. Diabetic impairments in NO-mediated endothelial progenitor cell

mobilization and homing are reversed by hyperoxia and SDF-1α. *Journal of Clinical Investigation* 117(5), pp. 1249–1259.

Gandhi, A. et al. 2005. The effects of local insulin delivery on diabetic fracture healing. *Bone* 37(4), pp. 482–490.

Gao, C. et al. 2005. Transcriptional Regulatory Functions of Heterogeneous Nuclear Ribonucleoprotein-U and -A/B in Endotoxin-Mediated Macrophage Expression of Osteopontin. *Journal of Immunology* 175, pp. 523–530.

García-hernández, A. et al. 2012. High glucose concentrations alter the biomineralisation process in human osteoblastic cells ☆. *Bone* 50(1), pp. 276–288.

Gasson, J.C. 1991. Molecular Physiology of Granulocyte-Macrophage Colony-Stimulating Factor. *Blood* 77(6), pp. 1131–1145.

Gatto, M. et al. 2008. Insulin-like growth factor-1 isoforms in rat hepatocytes and cholangiocytes and their involvment in protection aganist cholestatic injury. *Gene Expression* 88(9), pp. 986–994.

Gaudio, A. et al. 2012. Sclerostin Levels Associated with Inhibition of the Wnt/β-Catenin Signaling and Reduced Bone Turnover in Type 2 Diabetes Mellitus. *The Journal of Clinical Endocrinology & Metabolism* 97(10), pp. 3744–3750.

Gaur, T. et al. 2005. Canonical WNT signaling promotes osteogenesis by directly stimulating Runx2 gene expression. *The Journal of Biological Chemistry* 280(39), pp. 33132–40.

Gautier, E.L. et al. 2012. Gene expression profiles and transcriptional regulatory pathways underlying mouse tissue macrophage identity and diversity. *Nature Immunology* 13(11), pp. 1118–1128.

Gemmell, E. et al. 2002. Destructive periodontitis lesions are determined by the nature of the lymphocytic response. *Critical Reviews in Oral Biology and Medicine* 13(1), pp. 17–34.

Georgiou, K.R. et al. 2012. Methotrexate Chemotherapy Reduces Osteogenesis but Increases Adipogenic Potential in the Bone Marrow. *Journal of Cellular Physiology* 227, pp. 909–918.

Gerstenfeld, L.C. et al. 2001. Impaired intramembranous bone formation during bone repair in the absence of tumor necrosis factor-alpha signaling. *Cells Tissues Organs* 169, pp. 285–294.

Giacinti, C. and Giordano, A. 2006. RB and cell cycle progression. *Oncogene* 25(38), pp. 5220–5227.

Goncharova, E.A. et al. 2012. Differential effects of formoterol on thrombin- and PDGF-induced proliferation of human pulmonary arterial vascular smooth muscle cells. *Respiratory Research* 13(109), pp. 1–12.

Good, J. et al. 1998. Protein kinase C isotypes controlled by phosphoinositide 3- kinase throught the protein kinase PDK1 1998; 281: *Science* 281, pp. 2042–2045.

Gopalakrishnan, V. et al. 2006. Effects of streptozotocin-induced diabetes mellitus on some bone turnover markers in the vertebrae of ovary-intact and ovariectomized. *Biochemistry and Cell Biology* 84, pp. 728–736.

Gordon, S. and Taylor, P.R. 2005. Monocyte and Macrophage Heterogeneity. *Immunology* 5(December), pp. 953–964.

Goshima, J. et al. 1991. The origin of bone formed in composite grafts of porous calcium phosphate ceramic loaded with marrow cells. *Clinical Orthopaedics and Related Research* 269, pp. 274–283.

Góth, L. 2008. Catalase deficiency and type 2 diabetes. *Diabetes Care* 31(12), pp. 8–9.

Gowen, M. et al. 1988. Actions of Recombinant Human gamma-Interferon and Tumor Necrosis factor-alpha on the Proliferation and Osteoblastic Characteristics of Human Trabecular Bone Cells *in Vitro*. *Arthritis and Rheumatism* 31(12), pp. 1500–1507.

Graves, D.T. et al. 2006. Diabetes-enhanced Inflammation and Apoptosis: Impact on Periodontal Pathology. *Journal of Dental Research* 85(1), pp. 15–21.

Graves, D.T. et al. 2007. Diabetes-enhanced inflammation and apoptosis: impact on periodontal pathosis. *Periodontology 2000* 45, pp. 128–37. Available at:

Graves, D.T. et al. 2007. Diabetes-enhanced inflammation and apoptosis – impact on periodontal pathosis. *Periodontology 2000* 45, pp. 128–137.

Graves, D.T. et al. 2011. Review of osteoimmunology and the host response in endodontic and periodontal lesions. *Journal of Oral Microbiology* 3, pp. 1–15.

Graves, D.T. and Kayal, R.A. 2011. Diabetic complications and dysregulated innate immunity. *Front Bioscience* 13, pp. 1227–1239.

Greenberg, A.S. and Obin, M.S. 2006. Obesity and the role of adipose tissue in inflammation and metabolism. *The American Journal of Clinical Nutrition* 83, p. 461S–465S.

Greeneand, D. and Stevens, M. 1996. The sorbitol-osmotic and sorbitor-redox hypotheses. *Diabetes Mellitus Lippinocott Raven*, pp. 801–809.

Gregory, C.A. et al. 2004. An Alizarin red-based assay of mineralisation by adherent cells in culture : comparison with cetylpyridinium chloride extraction. *Analytical Biochemistry* 329(1), pp. 77–84.

Groeneveld, M.C. et al. 1995. Alkaline phosphatase activity in the peri- odontal ligament and gingiva of the ratmolar: its relation to cementumformation. *Journal of Dental Research* 74(7), pp. 1374–1381.

Gronthos, S. et al. 2003. Molecular and cellular characterisation of highly purified stromal stem cells derived from human bone marrow. *Journal of Cell Science* 116(9), pp. 1827–1835.

Gualillo, O. et al. 2007. The emerging role of adipokines as mediators of cardiovascular function: physiologic and clinical perspectives. *Trends in Cardiovascular Medicine* 17(8), pp. 275–83.

Hajishengallis, G. et al. 2012. The Keystone Pathogen Hypothesis. *Nat Rev Microbiology* 10(10), pp. 717–725.

Hajishengallis, G. and Lamont, R.J. 2014. Breaking bad: Manipulation of the host response by Porphyromonas gingivalis. *European Journal of Immunology* 44(2), pp. 328–338.

Halfon, S. et al. 2011. Markers Distinguishing Mesenchymal Stem Cells from Fibroblasts Are Downregulated with Passaging. *Stem Cells and Development* 20(1), pp. 53–66.

Hamada, N. et al. 1994. Construction and Characterization of a fimA Mutant of Porphyromonas gingivalis. *Infection and Immunity* 62(5), pp. 1696–1704.

Hamed, S. et al. 2010. Nitric oxide: a key factor behind the dysfunctionality of endothelial progenitor cells in diabetes mellitus type-2. *Cardiovascular Research* 91(1), pp. 9–15.

Hamilton, J.A. 2008. Colony-stimulating factors in inflammation and autoimmunity. *Nature Review Immunology* 8, pp. 533–544.

Harrington, J. et al. 2014. Quantification of clonal heterogeneity of mesenchymal progenitor cells in dental pulp and bone marrow. *Connective Tissue Research* 8207, pp. 62–67.

Hayflick, L. and Moorhead, P.S. 1961. The serial cultivation of human diploid cell strains. *Exp Cell Res* 25, pp. 585–621.

Hebert, L.F. et al. 1996. Overexpression of Glutamine : Fructose-6-Phosphate Amidotransferase in Transgenic Mice Leads to Insulin Resistance. *The Journal of Clinical Investigation* 98(4), pp. 930–936.

Heilbronn, L.K. and Campbell, L. V 2008. Adipose Tissue Macrophages , Low Grade Inflammation and Insulin Resistance in Human Obesity. *Current Pharmaceutical Design* 14, pp. 1225–1230.

Heldin, C.-H. and Westermark, B. 1999. Mechanism of Action and In Vivo Role of Platelet-Derived Growth Factor. *Physiological Reviews* 79(4), pp. 1283–1316.

Herath, T.D.K. et al. 2011. Heterogeneous LPS of Porphyromonas gingivalis differentially modulate the innate immune response of human gingiva. *BMC Proceeding* 5(1), p. 86.

Hettinger, J. et al. 2013. Origin of monocytes and macrophages in a committed progenitor Origin of monocytes and macrophages in a committed progenitor. *Nature Immunology* 14, pp. 821–830.

Hiramatsu, Y. et al. 2002. Diacylglycerol production and protein kinase C activity are increased in a mouse model of diabetic embryopathy. *Diabetes* 51, pp. 2804–2810..

Hirose, M. et al. 2012. Role of osteopontin in early phase of renal crystal formation: immunohistochemical and microstructural comparisons with osteopontin knock-out mice. *Urological research* 40, pp. 121–9.

Hiyama, E. and Hiyama, K. 2007. Telomere and telomerase in stem cells. *British Journal of Cancer* 96(7), pp. 1020–4.

Hoang, Q.Q. et al. 2003. Bone recognition mechanism of porcine osteocalcin from crystal structure. *Nature* 425, pp. 977–980.

Holmlund, A. et al. 2017. Oral health and cardiovascular disease risk in a cohort of periodontitis patients. *Atherosclerosis* 262, pp. 101–106.

Holt, S.C. et al. 1999. Virulence factors of porphyrornonas gingivalis. *Periodontology 2000* 20, pp. 168–238.

Hombach-Klonisch, S. et al. 2008. Adult stem cells and their trans-differentiation potential--perspectives and therapeutic applications. *Journal of Molecular Medicine* 86(12), pp. 1301–14.

Hong, J.H. et al. 2005. TAZ, a transcriptional modulator of mesenchymal stem cell differentiation. *Science* 309(5737), pp. 1074–1078.

Hotamisligil, G.S. et al. 1993. Adipose Expression of Tumor Necrosis Factor-x : Direct Role in

Obesity-Linked Insulin Resistance. *Science* 259, pp. 87–91.

How, K.Y. et al. 2016. Porphyromonas gingivalis: An Overview of Periodontopathic Pathogen below the Gum Line. *Frontiers in Microbiology* 7(53), pp. 1–14.

Hung, S.-L. et al. 2013. Stimulatory Effects of Glucose and Porphyromonas gingivalis Lipopolysaccharide on the Secretion of Inflammatory Mediators From Human Macrophages. *Journal of Periodontology* 85(1), pp. 140–149.

Hunter, G.K. et al. 1996. Nucleation and inhibition of hydroxyapatite formation by mineralised tissue proteins. *The Biochemical Journal* 317, pp. 59–64.

Hunter, G.K. 2013. Role of Osteopontin in Modulation of Hydroxyapatite Formation Role of Osteopontin in Modulation of Hydroxyapatite Formation. *Calcified Tissue International* 93, pp. 348–354.

Imano, M. et al. 2010. An immunohistochemical study of osteopontin in pigment gallstone formation. *The American Surgeon* 76, pp. 91–5.

Inoguchi, T. et al. 2000. High Glucose Level and Free Fatty Acid Stimulate Protein Kinase C – Dependent Activation of NAD (P) H Oxidase in Cultured Vascular Cells. *Diabetes* 49, pp. 1939–1945.

Iohara, K. et al. 2009. Regeneration of dental pulp after pulpotomy by cells from a canine tooth R esearch A rticle. *Regenerative Medicine* 4(3), pp. 377–385.

Italiani, P. and Boraschi, D. 2014. From monocytes to M1 / M2 macrophages : phenotypical vs . functional differentiation. *Frontiers in Immunology* 5(514), pp. 1–22.

Jackson, A. et al. 2005. Gene array analysis of Wnt-regulated genes in C3H10T1/2 cells. *Bone* 36(4), pp. 585–598.

James, L.R. et al. 2002. Flux through the hexosamine pathway is a determinant of nuclear factor κB-dependent promoter activation. *Diabetes* 51, pp. 1146–1156.

Janssens, K. et al. 2005. Transforming growth factor-beta1 to the bone. *Endocrine Reviews* 26(6), pp. 743–74.

Javed, A. 2001. Runx2-C/EBP molecular interactions and functional synergism support maximal expression of osteocalcin in osteoblasts. *Molecular Biology of the Cell* 12, p. 100a–100a.

Ji, Y. et al. 2009. PPAR g agonist , rosiglitazone , regulates angiotensin II-induced vascular inflammation through the TLR4-dependent signaling pathway. *Laboratory Investigation* 89(8), pp. 887–902.

Jiang, Y. et al. 2002. Bacteria Induce Osteoclastogenesis via an Osteoblast-Independent Pathway. *Infection and Immunity* 70(6), pp. 3143–3148.

Jiang, Z.L. et al. 2013. Study of TNF-α, IL-1β and LPS levels in the gingival crevicular fluid of a rat model of diabetes mellitus and periodontitis. *Disease Markers* 34, pp. 295–304.

Jones, E. et al. 2010. Large-scale extraction and characterization of CD271+ multipotential stromal cells from trabecular bone in health and osteoarthritis: implications for bone regeneration strategies

based on uncultured or minimally cultured multipotential stromal cells. *Arthritis and Rheumatism* 62(7), pp. 1944–54.

Jones, P.H. and Watt, F.M. 1993. Separation of human epidermal stem cells from transit amplifying cells on the basis of differences in integrin function and expression. *Cell* 73(4), pp. 713–24.

Junaid, A. et al. 2007. Osteopontin localizes to the nucleus of 293 cells and associates with polo-like kinase-1. *American journal of physiology. Cell Physiology* 292(2), pp. C919-26.

Juncheng, W. et al. 2013. High Glucose Inhibits Osteogenic Differentiation Through The BMP Signaling Pathway in Bone Mesenchymal Stem Cells In Mice. *EXCLI Journal* 12, pp. 584–597.

Jung, E. et al. 2011. Evidences for correlation between the reduced VCAM-1 expression and hyaluronan synthesis during cellular senescence of human mesenchymal stem cells. *Biochem Biophys Res Commun* 404(1), pp. 463–469.

Kaartinen, M.T. et al. 1999. Cross-linking of osteopontin by tissue transglutaminase increases its collagen binding properties. *Journal of Biological Chemistry* 274(3), pp. 1729–1735.

Kaartinen, M.T. et al. 2002. Tissue Transglutaminase and Its Substrates in Bone. *Journal of Bone and Mineral Research* 17(12), pp. 2161–2173.

Kadono, H. et al. 1999. Inhibition of Osteoblastic Cell Differentiation by Lipopolysaccharide Extract from Porphyromonas gingivalis. *Infection and Immunity* 67(6), pp. 2841–2846.

Kahles, F. et al. 2014. Osteopontin: A novel regulator at the cross roads of inflammation, obesity and diabetes. *Molecular Metabolism* 3, pp. 384–93.

Kahn, B.B. and Flier, J.S. 2000. Obesity and insulin resistance. *The Journal of Clinical Investigation* 106(4), pp. 473–481.

Kammoun, H.L. et al. 2014. Adipose tissue inflammation in glucose metabolism. *Reviews in Endocrine and Metabolic Disorders* 15(1), pp. 31–44.

Kanazawa, I. 2015. Osteocalcin as a hormone regulating glucose metabolism. *World Journal of Diabetes* 6(18), pp. 1345–1354.

Kato, H. et al. 2014. Porphyromonas gingivalis LPS inhibits osteoblastic differentiation and promotes pro-inflammatory cytokine production in human periodontal ligament stem cells . *Archives of Oral Biology* 59(2), pp. 167–175.

Kazanecki, C.C. et al. 2007. Control of osteopontin signaling and function by post-translational phosphorylation and protein folding. *Journal of Cellular Biochmistry* 102(4), pp. 912–924.

Keats, E.C. et al. 2014. Switch from canonical to noncanonical Wnt signaling mediates high glucose-induced adipogenesis Emily. *Stem Cells* 32(6), pp. 1649–1660.

Kerkis, I. et al. 2006. Isolation and Characterization of a Population of Immature Dental Pulp Stem Cells Expressing OCT-4 and Other Embryonic Stem Cell Markers. *Cells Tissues Organs* 184(3–4), pp. 105–116.

Khader, Y.S. et al. 2006. Periodontal status of diabetics compared with nondiabetics: a meta-analysis. *J Diabetes Complicat* 20(1), pp. 59–68.

Kiefer, F.W. et al. 2008. Osteopontin expression in human and murine obesity: extensive local up-regulation in adipose tissue but minimal systemic alterations. *Endocrinology* 149(3), pp. 1350–7.

Kiel, M.J. et al. 2005. Resource Hematopoietic Stem and Progenitor Cells and Reveal Endothelial Niches for Stem Cells. *Cell* 121(7), pp. 1109–1121.

Kim, H.S. et al. 2006. Effects of high glucose on cellular activity of periodontal ligament cells in vitro. *Diabetes Research and Clinical Practice* 74, pp. 41–47.

Kim, S.W. et al. 2005. Ectopic overexpression of adipogenic transcription factors induces transdifferentiation of MC3T3-E1 osteoblasts. *Biochemical and Biophysical Research Communications* 327, pp. 811–819.

Kim, S.Y. et al. 2013. Hesperetin alleviates the inhibitory effects of high glucose on the osteoblastic differentiation of periodontal ligament stem cells. *PloS one* 8(6), pp. 1–11.

Kimura, M. et al. 2010. Measurement of telomere length by the Southern blot analysis of terminal restriction fragment lengths. Nature Protocol 5(9), pp.1596-607.

Kingand, G. and Brownlee, M. 1996. The cellular and molecular mechanisms of diabetic complications. *Endocrinol Metab Clin North Am* 25, pp. 255–270.

Knight, M.N. and Hankenson, K.D. 2013. Mesenchymal Stem Cells in Bone Regeneration. *Advances in Wound Care* 2(6), pp. 306–316.

Kohler, A. et al. 2009. Altered cellular dynamics and endosteal location of aged early hematopoietic progenitor cells revealed by time-lapse intravital imaging in long bones. *Blood* 114(2), pp. 290–299.

Kokudo, T. et al. 2008. Snail is required for TGFβ-induced endothelial- mesenchymal transition of embryonic stem cell-derived endothelial cells. *Journal of Cell Science* 121(20), pp. 3317–3324.

Komori, T. 2006. Regulation of Osteoblast Differentiation by Transcription Factors. *J Cell Biochem* 1;99(5), pp. 1233–1239.

Korkalainen, M. et al. 2009. Dioxins interfere with differentiation of osteoblasts and osteoclasts. *Bone* 44, pp. 1134–1142.

Kornman, K.S. et al. 1997. The host response to the microbial challenge in periodontitis: assembling the players. *Periodontology 2000* 14, pp. 33–53.

Koyaand, D. and King, G. 1998. Protein kinase C activation and the development of diabetic complications. *Diabetes* 47, pp. 859–866.

Kraakman, M.J. et al. 2014. Macrophage polarization in obesity and type 2 diabetes: Weighing down our understanding of macrophage function? *Frontiers in Immunology* 5, pp. 1–6.

Kratchmarova, I. et al. 2005. Mechanism of divergent growth factor effects in mesenchymal stem cell differentiation. *Science* 308(5727), pp. 1472–1477.

Kumar, A. et al. 2010. Platelet-derived growth factor receptor signaling is not involved in osteogenic differentiation of human mesenchymal stem cells. *Tissue Engineering. Part A* 16(3), pp. 983–93.

Kuzyk, P.R. and Schemitsch, E.H. 2011. The basic science of peri-implant bone healing. *Indian*

Journal of Ortopaedics 45(2), pp. 108–115.

Kwon, D. et al. 2008. Treatment with bone marrow-derived stromal cells accelerates wound healing in diabetic rats. *International Wound Journal* 5(3), pp. 1–20.

Kwong, F. and Harris, M.B. 2008. Recent Developments in the Biology of Fracture Repair. *Journal of the American Academy of Orthopaedic Surgeons* 16(11), pp. 619–25.

Lalla, E. et al. 2000. Blockade of RAGE suppresses periodontitis-associated bone loss in diabetic mice. *The Journal of Clinical Investigation* 105(8), pp. 1117–24.

Lalla, E. et al. 2001. Receptor for Advanced Glycation End Products, Inflammation, and Accelerated Periodontal Disease in Diabetes: Mechanisms and Insights Into Therapeutic Modalities. *Annals of Periodontology* 6(113–118).

Lee, B.Y. et al. 2006. Senescence-associated β-galactosidase is lysosomal β -galactosidase. *Aging Cell* 5, pp. 187–195.

Lee, C.C.I. et al. 2010. Clonal analysis and hierarchy of human bone marrow mesenchymal stem and progenitor cells. *Experimental Hematology* 38, pp. 46–54.

Lee, C.P. et al. 2015. Elucidating the cellular actions of demineralised dentine matrix extract on a clonal dental pulp stem cell population in orchestrating dental tissue repair. *Journal of Tissue Engineering* 6.

Lee, M.-H. et al. 2003. BMP-2-induced Osterix expression is mediated by Dlx5 but is independent of Runx2. *Biochemical and Biophysical Research Communications* 309(3), pp. 689–694.

Levasseur, R. et al. 2005. LRP5 mutations in osteoporosis-pseudoglioma syndrome and high-bone-mass disorders. *Joint Bone Spine* 72(3), pp. 207–214.

Levesque, J.-P.& and Winkler, I. 2011. Hierarchy of immature hematopoietic cells related to blood flow and niche. *Current Opinion in Hematology* 18(4), pp. 220–225.

Li, C. et al. 2014. Lipopolysaccharide differentially affects the osteogenic differentiation of periodontal ligament stem cells and bone marrow mesenchymal stem cells through Toll-like receptor 4 mediated nuclear factor κB pathway. *Stem cell Research & Therapy* 5(67), pp. 1–13.

Li, Y. et al. 2007. Effects of high glucose on mesenchymal stem cell proliferation and differentiation. *Biomedical and Biophysical Research Communications* 363(1), pp. 209–215.

Lieberman, J.R.R. et al. 2002. The role of growth factors in the repair of bone - Biology and clinical applications. *Journal of Bone and Joint Surgery-American Volume* 84A(6), pp. 1032–1044.

Lin, N.-H. et al. 2008. Stem Cells and Periodontal Regeneration. *Australian Dental Journal* 53(2), pp. 108–21.

Lindsey, M.L. 2015. Osteopontin is proteolytically processed by matrix metalloproteinase 9. *Canadian Journal of Physiology and Pharmacy* 93(10), pp. 879–886.

Liu, K. et al. 2009. *In vivo* analysis of dendritic cell development and homeostasis. *Science* 324(5925), pp. 392–397.

Liu, X. et al. 2012. TNF- α and G-CSF induce CD62L and CD106 expressions on rat bone marrow-derived MSCs. *Asian Biomedicine* 6(3), pp. 453–458.

Liu, Z. et al. 2015. Different Concentrations of Glucose Regulate Proliferation and Osteogenic Differentiation of Osteoblasts Via the PI3 Kinase/Akt Pathway. *Implant Dentistry* 24(1), pp. 83–91.

Lo, C. 2005. Upregulation of Cyclooxygenase-II Gene and PGE 2 Production of Peritoneal Macrophages in Diabetic Rats 1. *Journal of Surgical Research* 125, pp. 121–127.

Lu, B. et al. 2008. Relationship of periodontal attachment loss to peripheral vascular disease: An analysis of NHANES 1999-2002 data. *Atherosclerosis* 200(1), pp. 199–205.

Lu, H. et al. 2003. Diabetes interferes with the bone formation by affecting the expression of transcription factors that regulate osteoblast differentiation. *Endocrinology* 144(1), pp. 346–52.

Lund, S.A. et al. 2009. The role of osteopontin in inflammatory processes. *Journal of Cell Communication and Signaling* 3(3–4), pp. 311–322.

Luo, G. et al. 1995. BMP-7 is an inducer of nephrogenesis, and is also required for eye development and skeletal patterning. *Genes & Development* 9(22), pp. 2808–20.

Macleod, R. et al. 1995. Regulation of DNA Methylation by the Ras Signaling Pathway. *The Journal of Biological Chemistry* 270(12), pp. 11327–11337.

Mafi, R. et al. 2011. Sources of adult mesenchymal stem cells applicable for musculoskeletal applications - a systematic review of the literature. *The Open Orthopaedics Journal* 5, pp. 242–248.

Mahanonda, R. and Pichyangkul, S. 2007. Toll-like receptors and their role in periodontal health and disease. *Periodontology 2000* 43(1), pp. 41–55.

Maiden, M.F.J. et al. 2003. Proposal to conserve the adjectival form of the specific epithet in the reclassification of Bacteroides forsythus Tanner et al . 1986 to the genus Tannerella Sakamoto et al . 2002 as Tannerella forsythia corrig ., gen . nov ., comb . nov . Request for an. *International Journal of Systematic and Evolutionary Microbiology* 53, pp. 2111–2112.

Majo, F. et al. 2008. Oligopotent stem cells are distributed throughout the mammalian ocular surface. *Nature* 456(7219), pp. 250–4.

Mansukhani, A. et al. 2000. Signaling by fibroblast growth factors (FGF) and fibroblast growth factor receptor 2 (FGFR2)-activating mutations blocks mineralisation and induces apoptosis in osteoblasts. *The Journal of Cell Biology* 149(6), pp. 1297–308.

Marcotte, H. and Lavoie, M.C. 1998. Oral Microbial Ecology and the Role of Salivary Immunoglobulin A. *Microbiology and Molecular Biology Review* 62(1), pp. 71–109.

Mareschi, K. et al. 2001. Isolation of human mesenchymal stem cells: bone marrow versus umbilical cord blood. *Haematologica* 86(10), pp. 1099–100.

Maruyama, K. et al. 2007. Decreased macrophage number and activation lead to reduced lymphatic vessel formation and contribute to impaired diabetic wound healing. *American Journal of Pathology* 170(4), pp. 1178–1191.

Mattila, K.J. et al. 1989. Association between dental health and acute myocardial infarction. *BMJ*

(Clinical research ed.) 298, pp. 779–81.

Mckee, M.D. et al. 1996. Extracellular matrix in tooth cementum and mantle dentin: Localization of osteopontin and other noncollagenous proteins, plasma proteins, and glycoconjugates by electron microscopy. *Anatomical Record* 245, pp. 293–312.

Mckee, M.D. et al. 2013. Compounded PHOSPHO1/ALPL deficiencies reduce dentinmin- eralization, J. Dent. Res. *Journal of Dental Research* 92(8), pp. 721–727.

McKee, M.D. et al. 2011. Osteopontin and wound healing in bone. *Cells Tissues Organs* 194(2–4), pp. 313–9.

Medina, J. et al. 2005. Evidence of angiogenesis in primary biliary cirrhosis: An immunohistochemical descriptive study. *Journal of Hepatology* 42, pp. 124–131.

Millán, J.L. and Whyte, M.P. 2016. Alkaline Phosphatase and Hypophosphatasia. *Calcified Tissue International* 98(4), pp. 398–416.

Mohammad, M.K. et al. 2006. Dysregulated Toll-like receptor expression and signaling in bone marrow-derived macrophages at the onset of diabetes in the non-obese diabetic mouse. *International Immunology* 18(7), pp. 1101–1113.

Moore, W.E.C. and Moore, H. 1994. The bacteria of periodontal diseases. *Periodontology 2000* 5, pp. 66–77.

Moseley, R. et al. 2004. Comparison of oxidative stress biomarker profiles between acute and chronic wound environments. *Wound Repair and Regeneration* 12(4), pp. 419–429.

Muraglia, A. et al. 2000. Clonal mesenchymal progenitors from human bone marrow differentiate in vitro according to a hierarchical model. *Journal of Cell Science* 113(7), pp. 1161–1166.

Naganawa, T. et al. 2008. Reduced expression and function of bone morphogenetic protein-2 in bones of Fgf2 null mice. *Journal of Cellular Biochemistry* 103(6), pp. 1975–88.

Naguib, G. et al. 2004. Diabetes prolongs the inflammatory response to a bacterial stimulus through cytokine dysregulation. *The Journal of Investigative Dermatology* 123(1), pp. 87–92.

Nakamura, T. et al. 1998. Recombinant human basic fibroblast growth factor accelerates fracture healing by enhancing callus remodeling in experimental dog tibial fracture. *Journal of Bone and Mineral Research* 13(6), pp. 942–9.

Nakamura, T. et al. 2004. Effect of low dose Actinobacillus actinomycetemcomitans lipopolysaccharide pretreatment on cytokine production by human whole blood. *Journal of Periodontal Research* 39(2), pp. 129–35.

Nakashima, K. et al. 2002. The novel zinc finger-containing transcription factor Osterix is required for osteoblast differentiation and bone formation. *Cell* 108(1), pp. 17–29.

Nanci, A. and Bosshardt, D.D. 2006. Structure of periodontal tissues in health and disease. *Periodontology 2000* 40, pp. 11–28.

Nanes, M.S. 2003. Nanes, M.S. (2003) Tumor necrosis factor-alpha: molecular and cellular mechanisms in skeletal pathology. *Gene* 321, pp. 1–15.

Nares, S. et al. 2009. Rapid Myeloid Cell Transcriptional and Proteomic Responses to Periodontopathogenic Porphyromonas gingivalis. *The American Journal of Pathology* 174(4), pp. 1400–1414.

Narisawa, S. et al. 2013. In vivo overexpression of tissue-nonspecific alkaline phosphatase increases skeletal mineralisation and affects the phosphorylation status of osteopontin. *Journal of Bone and Mineral Research* 28(7), pp. 1587–1598.

Neame, P.J. and Butler, W.T. 1996. Posttranslational modification in rat bone osteopontin. *Connective Tissue Research* 35(1–4), pp. 145–150.

Nguyen, M.T.A. et al. 2007. A Subpopulation of Macrophages Infiltrates Hypertrophic Adipose Tissue and Is Activated by Free Fatty Acids via Toll-like Receptors 2 and 4 and JNK-dependent Pathways. *The Journal of Biological Chemistry* 282(48), pp. 35279–35292.

Nishimichi, N., Higashikawa, F., Kinoh, H.H., et al. 2009. Polymeric osteopontin employs integrin as a receptor and attracts neutrophils by presenting a de Novo binding site. *Journal of Biological Chemistry* 284(22), pp. 14769–14776.

Nishimichi, N., Higashikawa, F., Kinoh, H.H., et al. 2009. Polymeric osteopontin employs integrin alpha9beta1 as a receptor and attracts neutrophils by presenting a de novo binding site. *The Journal of Biological Chemistry* 284(22), pp. 14769–76.

Nomiyama, T. et al. 2007. Osteopontin mediates obesity-induced adipose tissue macrophage infiltration and insulin resistance in mice. *The Journal of Clinical Investigation* 117(10), pp. 2877–88. Available at:

Noth, U. et al. 2002. Multilineage mesenchymal differentiation potential of human trabecular bone-derived cells. *Journal of Orthopaedic Research* 20, pp. 1060–1069.

Noto, H. et al. 2013. Latest insights into the risk of cancer in diabetes. *Journal of Diabetes Investigation* 4(3), pp. 225–232.

Ntambi, J.M. and Kim, Y. 2000. Adipocyte Differentiation and Gene Expression. *Journal Nutritional Sciences* 130, pp. 3122–3126.

O'Dowd, L.K. et al. 2010. Patients' experiences of the impact of periodontal disease. *J Clin Periodontol* 37, pp. 334–339.

Ogawa, T.O. and Yagi, T.A.Y. 2010. Bioactive mechanism of Porphyromonas gingivalis lipid A. *Periodontology 2000* 54, pp. 71–77.

Okabe, Y. and Medzhitov, R. 2014. Tissue-specific signals control reversible program of localization and functional polarization of macrophages. *Cell* 157, pp. 832–844.

Okazaki, R. et al. 1995. Transforming growth factor-beta and forskolin increase all classes of insulin-like growth factor-I transcripts in normal human osteoblast-like cells. *Biochemical and Biophysical Research Communications* 207(3), pp. 963–70.

Olefsky, J.M. and Glass, C.K. 2010. Macrophages, Inflammation, and Insulin Resistance. *Annual Revivion Physiology* 72, pp. 219–246.

Olieslagers, S. et al. 2011. TGF-β1/ALK5-induced monocyte migration involves PI3K and p38 pathways and is not negatively affected by diabetes mellitus. *Cardiovascular Research* 91(3), pp. 510–518.

Osborn, O. and Olefsky, J.M. 2012. The cellular and signaling networks linking the immune system and metabolism in disease. *Nature Medicine* 18(3), pp. 363–374.

Otto, F. et al. 1997. Cbfa1, a candidate gene for cleidocranial dysplasia syndrome, is essential for osteoblast differentiation and bone development. *Cell* 89(5), pp. 765–771.

Owen, W.F. et al. 1998. Beta 2-microglobulin modified with advanced glycation end products modulates collagen synthesis by human fibroblasts. *Kidney International* 53(5), pp. 1365–73.

Mafi, P. et al. 2011. Adult mesenchymal stem cells and cell surface characterization - a systematic review of the literature. *The Open Orthopaedics Journal* 5, pp. 253–60.

Page, R.. et al. 1997. Advances in the pathogenesis of periodontitis: Summary of development, clinical implications and future directions. *Periodontology 2000* 14, pp. 216–248.

Pampena, D.A. et al. 2004. Inhibition of hydroxyapatite formation by osteopontin phosphopeptides. *Biochemical Journal* 378(Pt3), pp. 1083–1087.

Paster, B.J. et al. 2006. The breadth of bacterial diversity in the human periodontal pocket and other oral sites. *Periodontology 2000* 42, pp. 80–87.

Patsouris, D. et al. 2008. Ablation of CD11c-Positive Cells Normalizes Insulin Sensitivity in Obese Insulin Resistant Animals. *Cell Metabolism* 8(4), pp. 301–309.

Pedraza, C.E. et al. 2008. Osteopontin functions as an opsonin and facilitates phagocytosis by macrophages of hydroxyapatite-coated microspheres: Implications for bone wound healing. *Bone* 43, pp. 708–716.

Peister, A. et al. 2004. Adult stem cells from bone marrow (MSCs) isolated from different strains of inbred mice vary in surface epitopes , rates of proliferation , and differentiation potential. *Blood* 103(5), pp. 1662–1668.

Pfeilschifter, J. et al. 1998. Concentration of transforming growth factor beta in human bone tissue: relationship to age, menopause, bone turnover, and bone volume. *Journal of Bone and Mineral Research* 13(4), pp. 716–30.

Phinney, D.G. 2012. Cellular Biochemistry. *Journal of Cellular Biochemistry* 113, pp. 2806–2812.

Pihlstrom, B.L. et al. 2005. Periodontal Diseases. *Lancet* 366(9499), pp. 1809–1820.

Pittenger, M.F. et al. 1999. Multilineage Potential of Adult Human Mesenchymal Stem Cells. *Science* 284, pp. 143–147.

Poole, N.M. et al. 2013. Prostaglandin E2 in tick saliva regulates macrophage cell migration and cytokine profile. *Parasites & Vectors* 6(261), pp. 2–11.

Porter, R.M. et al. 2003. Effect of Dexamethasone Withdrawal on Osteoblastic Differentiation of Bone Marrow Stromal Cells. *Journal of Cellular Biochmistry* 90, pp. 13–22.

Preshaw, P.M. 2009. Periodontal disease and diabetes. *Journal of Dentistry* 37, pp. s575–s577.

Preshaw, P.M. et al. 2012. Periodontitis and diabetes: a two-way relationship. *Diabetologia* 55(1), pp. 21–31.

Qin, C. et al. 2004. Post-translational modifications of SIBLING proteins and their roles in osteogenesis and dentinogenesis. *Critical Reviews in Oral Biology and Medicine* 15(3), pp. 126–136.

Rai, N.K. et al. 2005. Effect of glycaemic control on apoptosis in diabetic wounds. *Journal of Wound Care* 14(6), pp. 277–81.

Ramirez, P.T. et al. 2001. Expression of Cell-Cycle Mediators in Ovarian Cancer Cells. *Gynecologic Oncology* 83, pp. 543–548.

Rayess, H. et al. 2012. Cellular senescence and tumor suppressor gene p16. *International Journal of Cancer* 130(8), pp. 1715–1725.

Reinholt, F.P. et al. 1990. Osteopontin-a possible anchor of osteoclasts to bone. *Proceedings of the National Academy of Sciences of the United States of America* 87, pp. 4473–5.

Rey-Giraud, F. et al. 2012. In Vitro Generation of Monocyte-Derived Macrophages under Serum-Free Conditions Improves Their Tumor Promoting Functions. *PloS one* 7(8), p. e42656 (1-10).

Reya, T. et al. 2001. Stem cells, cancer, and cancer stem cells. *Nature* 414(6859), pp. 105–11.

Rickard, D.J. et al. 1996. Isolation and characterization of osteoblast precursor cells from human bone marrow. *Journal of Bone and Mineral Research* 11(3), pp. 312–324.

Riquelme, P.A. et al. 2008. Brain micro-ecologies: neural stem cell niches in the adult mammalian brain. *Philosophical Transactions of the Royal Society B: Biological Sciences* 363(1489), pp. 123–137.

Rittling, S.R. 2011. Osteopontin in macrophage function Osteopontin in macrophage function. *Expert Reviews in Molecular Medicine* 13(e15), pp. 1–21.

Roberts, H.C. et al. 2008. Lipopolysaccharide alters decorin and biglycan synthesis in rat alveolar bone osteoblasts: consequences for bone repair during periodontal disease. *European Journal of Oral Sciences* 116(3), pp. 207–16.

Rodier, F. et al. 2011. DNA-SCARS: distinct nuclear structures that sustain damage-induced senescence growth arrest and inflammatory cytokine secretion. *Journal of Cell Science* 124(1), pp. 68–81.

Rolo, A.P. and Palmeira, C.M. 2006. Diabetes and mitochondrial function: Role of hyperglycemia and oxidative stress. *Toxicology and Applied Pharmacology* 212(2), pp. 167–178.

Russell, K.C. et al. 2010. In vitro high-capacity assay to quantify the clonal heterogeneity in trilineage potential of mesenchymal stem cells reveals a complex hierarchy of lineage commitment. *Stem Cells* 28(4), pp. 788–98.

Russell, K.C. et al. 2011. Clonal Analysis of the Proliferation Potential of Bone Marrow Mesenchymal Stem Cells as a Function of Potency. *Biotechnol Bioeng* 108(11), pp. 2716–2726.

Sacchetti, B. et al. 2007. Self-Renewing Osteoprogenitors in Bone Marrow Sinusoids Can Organize a

Hematopoietic Microenvironment. *Cell* 131(2), pp. 324–336.

Saito, K. et al. 2016. Osteopontin Is Essential for Type I Collagen Secretion in Reparative Dentin. *Journal of Dental Research*.

Sakou, T. 1998. Bone morphogenetic proteins: from basic studies to clinical approaches. *Bone* 22(6), pp. 591–603.

Salabei, J.K. et al. 2016. Type 2 Diabetes Dysregulates Glucose Metabolism in Cardiac Progenitor Cells. *The Journal of Biological Chemistry* 291(26), pp. 13634–13648.

Salih, E. et al. 1996. Phosphorylation of purified bovine bone sialoprotein and osteopontin by protein kinases. *Journal of Biological Chemistry* 271(28), pp. 16897–16905.

Salpea, K.D. et al. 2010. Association of telomere length with type 2 diabetes , oxidative stress and UCP2 gene variation. *Atherosclerosis* 209, pp. 42–50.

Salpea, K.D. and Humphries, S.E. 2010. Telomere length in atherosclerosis and diabetes. *Atherosclerosis* 209, pp. 35–38.

Salvi, G. et al. 1997. Inflammatory mediator response as a potential risk marker for periodontal diseases in insulin- dependent diabetes mellitus patients. *Journal of Periodontology* 68, pp. 127–135.

Salvi, G.E. et al. 2008. Effects of diabetes mellitus on periodontal and peri-implant conditions: update on associations and risks. *J Clin Periodontol* 35, pp. 398– 409.

Samsonraj, R. et al. 2015. Establishing Criteria for Human Mesenchymal Stem Cell Potency. *Stem Cells* 33, pp. 1878–1891.

Saretzki, G. et al. 2010. Telomerase , mitochondria and oxidative stress. *Experimental Gerontology* 44(8), pp. 1-25.

Sarugaser, R. et al. 2009. Human mesenchymal stem cells self-renew and differentiate according to a deterministic hierarchy. *PloS one* 4(8), p. e6498.

Scherer, E.B.S. et al. 2012. Chronic mild hyperhomocysteinemia alters ectonucleotidase activities and gene expression of ecto-5′-nucleotidase/CD73 in rat lymphocytes. *Molecular and Cellular Biochemistry* 361(1–2), pp. 187–194.

Schulz, C. et al. 2012. A Lineage of Myeloid Cells Independent of Myb and Hematopoietic Stem Cells. *Science* 336, pp. 86–90.

Senn, J.J. et al. 2002. Interleukin-6 induces cellular insulin resistance in hepatocytes. *Diabetes* 51(12), pp. 3391–9.

Serakinci, N. et al. 2008. Telomere stability and telomerase in mesenchymal stem cells. *Biochime* 90, pp. 33-40.

Sethe, S. et al. 2006. Aging of mesenchymal stem cells. *Ageing Research Reviews* 5, pp. 91–116.

Seydoux, G. and Braun, R.E. 2006. Pathway to totipotency: lessons from germ cells. *Cell* 127(5), pp. 891–904.

Sharma, R.R. et al. 2014. Mesenchymal stem or stromal cells : A review of clinical applications and manufacturing practices Mesenchymal stem or stromal cells : a review of clinical applications and manufacturing practices. *Transfusion* 54(5), pp. 1418–1437.

Shi, H. et al. 2006. TLR4 links innate immunity and fatty acid – induced insulin resistance. *The Journal of Clinical Investigationrnal* 116(11), pp. 3015–3025.

Shilpa, K. et al. 2013. An In Vitro Model to Probe the Regulation of Adipocyte Differentiation under Hyperglycemia (Diabetes Metab J 2013 ; 37 : 176-80). *Diabetes and Metabolism Journal* 37, pp. 298–299.

Shipounova, I.N. et al. 2013. Hierarchy of mesenchymal stem cells: Comparison of multipotentmesenchymal stromal cells with fibroblast colony forming units. *Journal of Biomedical Science and Engineering* 6(8), pp. 66–73.

Shirakihara, T. et al. 2011. TGF-β regulates isoform switching of FGF receptors and epithelial-mesenchymal transition. *The EMBO Journal* 30, pp. 783–95.

Sieweke, M.H. and Allen, J.E. 2013. Beyond Stem Cells: Self-Renewal of Differentiated Macrophages. *Science* 342, p. 1242974.

Silhavy, T.J. et al. 2010. The Bacterial Cell Envelope. *Cold Spring Harbor Perspectives in Biology* 2(5), pp. 1–17.

da Silva, L. et al. 2006. da Silva ML , Chagastelles PC , Nardi NB. Mesenchymal stem cells reside in virtually all post-natal organs and tissues. *Journal of Cell Science* 119(11), pp. 2204–2213.

Sima, C. and Glogauer, M. 2013. Macrophage subsets and osteoimmunology: Tuning of the immunological recognition and effector systems that maintain alveolar bone. *Periodontology 2000* 63(1), pp. 80–101.

Simmons, P.J. and Torok-Storb, B. 1991. Identification of stromal cell precursors in human bone marrow by a novel monoclonal antibody, STRO-1. *Blood* 78(1), pp. 55–62.

Sindrilaru, A. et al. 2011. An unrestrained proinflammatory M1 macrophage population induced by iron impairs wound healing in humans and mice. *The Journal of Clinical Investigation* 121(3), pp. 985–997.

Slots, J. et al. 1986. The occurrence of Actinobacillus Bacteroides gingivalis and Bacteroides intermedius in destructive periodontal disease in adults. *Microbiology and Adult Periodontitis* 13, pp. 570–577.

Soardo, G. et al. 2011. Oxidative Stress Is Activated by Free Fatty Acids in Cultured Human Hepatocytes. *Metabolic Syndrome and Related Disorders* 9(5), pp. 397–401.

Socransky, S.S. and Haffajee, A.D. 2005. Periodontal microbial ecology. *Periodontology 2000* 38, pp. 135–187.

Sodek, J. et al. 2000. Osteopontin. *Critical Reviews in Oral Biology and Medicine* 11, pp. 279–303.

Solanas, G. et al. 2008. E-cadherin controls β -catenin and NF- κ B transcriptional activity in mesenchymal gene expression. *Journal of Cell Science* 121, pp. 2224–2234.

Spencer, M. et al. 2010. Adipose tissue macrophages in insulin-resistant subjects are associated with collagen VI and fibrosis and demonstrate alternative activation. *American Journal of Physiological Endocrinology and Metabolism* 299, pp. E1016–E1027.

Spencer, S.L. et al. 2013. The Proliferation-Quiescence Decision Is Controlled by a Bifurcation in CDK2 Activity at Mitotic Exit. *Cell* 155(2), pp. 369–383.

Standal, T. et al. 2004. Role of Osteopontin in Adhesion, Migration, Cell Survival and Bone Remodeling. *Experimental Oncology* 26(3), pp. 179–184.

Stenderup, K. et al. 2003. Aging is associated with decreased maximal life span and accelerated senescence of bone marrow stromal cells. *Bone* 33, pp. 919–926.

Stolzing, A. et al. 2011. Effect of Age and Diabetes on the Response of Mesenchymal Progenitor Cells to Fibrin Matrices. *International of Biometerials*, pp. 1–9.

Stolzing, A. et al. 2012. Suspension Cultures of Bone-Marrow-Derived Mesenchymal Stem Cells: Effects of Donor Age and Glucose Level. *Stem Cells and Development* 21(14), pp. 2718–2723.

Sugimoto, R. et al. 2005. High glucose stimulates hepatic stellate cells to proliferate and to produce collagen through free radical production and activation of mitogen-activated protein kinase. *Liver International* 25(5), pp. 1018–26.

Sugiyama, T. et al. 2006. Maintenance of the Hematopoietic Stem Cell Pool by CXCL12-CXCR4 Chemokine Signaling in Bone Marrow Stromal Cell Niches. *Immunity* 25(6), pp. 977–988.

Suzuki, S. et al. 2005. Enamel Matrix Derivative Gel Stimulates Signal Transduction of BMP and TGF-β. *Journal of Dental Research* 84, pp. 510–514.

Tadic, T. et al. 2002. Overexpression of Dlx5 in chicken calvarial cells accelerates osteoblastic differentiation. *Journal of Bone and Mineral Research* 17(6), pp. 1008–1014.

Tang, J. et al. 2015. Porphyromonas gingivalis lipopolysaccharides regulate functions of bone marrow mesenchymal stem cells. *Cell Proliferation* 48(2), pp. 239–248.

Taniguchi, C.M. et al. 2006. Critical nodes in signalling pathways: Insights into insulin action. *Nature Reviews Molecular Cell Biology* 7(2), pp. 85–96.

Taniyama, Y. and Griendling, K.K. 2003. Reactive Oxygen Species in the Vasculature: Molecular and Cellular Mechanisms. *Hypertension* 42(6), pp. 1075–1081.

Tanner, A.C.R. et al. 1979. A study of the bacteria associated with advancing periodontitis in man. *Journal of Clinical Periodontology* 6, pp. 278–307.

Taylor, G.W. et al. 1996. Severe periodontitis and risk for poor glycemic control in patients with non-insulin- dependent diabetes mellitus. *Journal of Periodontology* 67(10s), pp. 1085–1093.

Taylor, G.W. 2001. Bidirectional interrelationships between diabetes and periodontal diseases: an epidemiologic perspective. *Annals of Periodontology* 6(1), pp. 99–112.

Theilade, E. 1986. The non-specific theory in microbial etiology of inflammatory periodontal diseases. *Journal of Clinical Periodontology* 13, pp. 905–911.

To, L.B. et al. 2011. How I treat patients who mobilize hematopoietic stem cells poorly. *Blood* 118(17), pp. 4530–4541.

Tokunaga, A. et al. 2008. PDGF receptor β is a potent regulator of mesenchymal stromal cell function. *Journal of Bone and Mineral Research* 23, pp. 1519–1528.

Tsai, C. et al. 2002. Glycemic control of type 2 diabetes and severe periodontal disease in the US adult population. *Community Dent Oral Epidemiol* 30, pp. 182–92.

Tsai, T.-M. and Frasch, C. 1982. A sensitive silver stain for detecting lipopolysaccharides in polyacrylamide gels. *Journal of Dental Research* 119(1), pp. 115–119.

Tsiridis, E. et al. 2007. Molecular aspects of fracture healing: which are the important molecules? *Injury* 38 Suppl 1, pp. S11-25.

Tsubone, T. et al. 2006. Effect of TGF-b Inducible Early Gene Deficiency on Flexor Tendon Healing. *Journal of Orthopaedic Research* 24(3), pp. 569–575.

Tunes, S.R. et al. 2010. Impact of periodontitis on the diabetes-related inflammatory status. *Journal (Canadian Dental Association)* 76, p. a35.

Turinetto, V. et al. 2016. Senescence in human mesenchymal stem cells: Functional changes and implications in stem cell-based therapy. *International Journal of Molecular Sciences* 17(7), pp. 1–18.

Tushinski, R.J. et al. 1982. Survival of Mononuclear Phagocytes Depends on a Lineage-Specific Growth Factor That the Differentiated Cells Selectively Destroy of Adherent. *Cell* 28, pp. 71–81.

Valero, A.M. et al. 2007. Effects of diabetes on the osseointegration of dental implants. *Medicina Oral, Patología Oral y Cirugía Bucal* 12, pp. E38-43.

Veerababu, G. et al. 2000. Overexpression of glutamine:fructose-6-phosphate amidotransferase in the liver of transgenic mice results in enhanced glycogen storage, hyperlipidemia, obesity, and impaired glucose tolerance. *Diabetes* 49(12), pp. 2070–2078.

Verstappen, J. et al. 2009. A functional model for adult stem cells in epithelial tissues. *Wound Repair and Regeneration* 17(3), pp. 296–305.

Viereck, V. et al. 2002. Differential regulation of Cbfa1/Runx2 and osteocalcin gene expression by vitamin-D3, dexamethasone, and local growth factors in primary human osteoblasts. *Journal of Cellular Biochemistry* 86(2), pp. 348–356.

Vlassara, H. 1997. Recent Progress in Advanced Glycation End Products and Diabetic Complications. *Diabetes* 46, p. S19.

Vlassara, H. and Palace, M.R. 2002. Diabetes and advanced glycation endproducts. *Journal of Internal Medicine* 251(2), pp. 87–101.

Waddington, R.J. et al. 2000. Reactive oxygen species: a potential role in the pathogenesis of periodontal diseases. *Oral Diseases* 6(3), pp. 138–151.

Waddington, R.J. et al. 2003. Differential roles for small leucine-rich proteoglycans in bone formation. *European Cells & Materials* 6, pp. 12–21.

Waddington, R.J. et al. 2011. Characterization of oxidative stress status during diabetic bone healing. *Cells Tissues Organs* 194(2–4), pp. 307–312.

Wagner, W. et al. 2008. Replicative Senescence of Mesenchymal Stem Cells : A Continuous and Organized Process. *PloS one* 3(5), p. e2213.

Wakitani, S. et al. 1995. Myogenic cells derived from rat bone marrow mesenchymal stem cells exposed to 5-azacytidine. *Muscle & Nerve* 18(12), pp. 1417–26.

Walker, C.G. et al. 2010. Osteopontin is Required for Unloading-Induced Osteoclast Recruitment and Modulation of RANKL Expression during Tooth Drift-associated Bone Remodeling, but Not for Super-Eruption. *Bone* 47(6), pp. 1020–1029.

Walsh, S. et al. 2001. High concentrations of dexamethasone suppress the proliferation but not the differentiation or further maturation of human osteoblast precursors in vitro : relevance to glucocorticoid-induced osteoporosis. *Rheumatology* 40, pp. 74–83.

Wang, C. et al. 2013. Characterization of murine macrophages from bone marrow , spleen and peritoneum. *BMC Immunology* 14(6), pp. 1–10.

Wang, J. et al. 2013. Metagenomic sequencing reveals microbiota and its functional potential associated with periodontal disease. *Scientific Reports* 3, pp. 1–10.

Wang, L. et al. 2010. Activation of Protein Serine/Threonine Phosphatase PP2C a Efficiently Prevents Liver Fibrosis. *PLoS ONE* 5(12), pp. 12–15.

Wang, W. et al. 2010. High glucose stimulates adipogenic and inhibits osteogenic differentiation in MG-63 cells through cAMP/protein kinase A/extracellular signal-regulated kinase pathway. *Molecular and Cellular Biochemistry* 338(1–2), pp. 115–22.

Weil, B.R. et al. 2009. High glucose concentration in cell culture medium does not acutely affect human mesenchymal stem cell growth factor production or proliferation. *Am J Physiol Regul Integr Comp Physio*l, pp. 1735–1743.

Weisberg, S.P. et al. 2006. CCR2 modulates inflammatory and metabolic effects of high-fat feeding. *The Journal of Clinical Investigation* 116(1), pp. 115–124.

Wesson, J.A. et al. 2003. Osteopontin is a critical inhibitor of calcium oxalate crystal formation and retention in renal tubules. *Journal of the American Society of Nephrology* 14(1), pp. 139–147.

Westendorf, J.J. et al. 2004. Wnt signaling in osteoblasts and bone diseases. *Gene* 341, pp. 19–39.

Wilson, A. et al. 2008. Hematopoietic Stem Cells Reversibly Switch from Dormancy to Self-Renewal during Homeostasis and Repair. *Cell* 135(6), pp. 1118–1129.

Winkler, I.G. et al. 2010. Bone marrow macrophages maintain hematopoietic stem cell (HSC) niches and their depletion mobilizes HSC. *Blood* 116(23), pp. 4815–4828.

Würgler-Hauri, C.C. et al. 2007. Temporal expression of 8 growth factors in tendon-to-bone healing in a rat supraspinatus model. *Journal of Shoulder and Elbow Surgery* 16(5), pp. S198–S203.

Wynn, T.A. et al. 2013. Origins and Hallmarks of Macrophages: Development, Homeostasis, and Disease. *Nature* 496(7446), pp. 445–455.

Xiao, X. et al. 2014. M2 macrophages promote beta-cell proliferation by up-regulation of SMAD7. *Proceedings of the National Academy of Sciences* 111(13), pp. E1211–E1220.

Xie, Y. et al. 2009. Detection of functional hematopoietc stem cell niche using real-time imaging. *Nature* 457(7225), pp. 97–101.

Xing, H. et al. 2015. Effect of Porphyromonas gingivalis Lipopolysaccharide on Bone Marrow Mesenchymal Stem Cell Osteogenesis on a Titanium Nanosurface. *Journal of Periodontology* 86(3), pp. 448–455.

Xing, W. et al. 2009. Quantitative Evaluation and Selection of Reference Genes in a Rat Model of Extended Liver Resection. *Journal of Biomolecular Techniques* 20(2), pp. 109–115.

Xu, H. et al. 2003. Chronic inflammation in fat plays a crucial role in the development of obesity-related insulin resistance. *The Journal of Clinical Investigation* 112(12), pp. 1821–1830.

Yang, J. et al. 2017. Enhanced activity of macrophage M1/M2 phenotypes in periodontitis. *Archives of Oral Biology* 17, pp. 1–9.

Yang, Y. et al. 2011. Accumulation of β-catenin by lithium chloride in porcine myoblast cultures accelerates cell differentiation. *Molecular Biology Reports* 38, pp. 2043–2049.

Yu, T. et al. 2016. Enhanced Activity of the Macrophage M1/M2 Phenotypes and Phenotypic Switch to M1 in Periodontal Infection. *Journal of Periodontology* 87(9), pp. 1092–1102.

Yusop, N. 2015. Altered Biological Responsiveness of Cells Regulating Intramembraneous Bone Repair Associated with Type 2 Diabetes Mellitus. *PhD Thesis*, pp. 161–181.

Zayzafoon, M. et al. 2000. Extracellular Glucose Influences Osteoblast Differentiation and c – Jun Expression. *Journal of Cellular Biochemistry* 79, pp. 301–310.

Zeichner-David, M. 2006. Regeneration of periodontal tissues: cementogenesis revisited. *Periodontology 2000* 41, pp. 196–217.

Zeyda, M. et al. 2007. Human adipose tissue macrophages are of an anti-inflammatory phenotype but capable of excessive pro-inflammatory mediator production. *International Journal of Obesity* 31, pp. 1420–1428.

Zhang, B. et al. 2016. High glucose microenvironments inhibit the proliferation and migration of bone mesenchymal stem cells by activating GSK3 β. *Journal of Bone and Mineral Metabolism*, pp. 140–150.

Zhang, H. et al. 2010. Defects in Mesenchymal Stem Cell Self-Renewal and Cell Fate Determination Lead to an Osteopenic Phenotype in Bmi-1 Null Mice. *Journal of Bone and Mineral Research* 25(3), pp. 640–652.

Zhang, W. et al. 2013. Klf10 inhibits IL-12p40 production in macrophage colony-stimulating factor-induced mouse bone marrow-derived macrophages. *European Journal of Immunology* 43(1), pp. 258–269.

Zhang, X. et al. 2005. Periosteal Progenitor Cell Fate in Segment Cortical Bone Graft Transplantations: Implications for Functional Tissue Engineering. *Journal of Bone and Mineral Research* 20(12), pp.

2124–2137.

Zhang, X. et al. 2008. The Isolation and Characterization of Murine Macrophages. *Current Protocols in Immunology* 14, pp. 1–18.

Zhang, Y. and Yang, J.H. 2013. Activation of the PI3K/Akt pathway by oxidative stress mediates high glucose-induced increase of adipogenic differentiation in primary rat osteoblasts. *Journal of Cellular Biochemistry* 114(11), pp. 2595–2602.

Zhao, W. et al. 2010. Differential expression of intracellular and secreted osteopontin isoforms by murine macrophages in response to toll-like receptor agonists. *Journal of Biological Chemistry* 285(27), pp. 20452–20461.

Zimmermann, S. et al. 2003. Lack of telomerase activity in human mesenchymal stem cells. *Leukemia* 17(6), pp. 1146–9.

8.0: Appendix

The work of chapter 2, chapter 3 and Chapter 4 has been presented in the following conferences:

Chapter 2: in the British Society of Oral and Dental Research (BSODR) 2015, Cardiff, UK.

Chapter 3: in the Tissue and Cell Engineering Society (TCES) 2016, London, UK.

Chapter 4: in the British Society of Oral and Dental Research (BSODR) 2017, Plymouth, UK.